Sediment-hosted base metal deposits

Research results for 1998

AMIRA/ARC project P384A

Final Report
December 1998

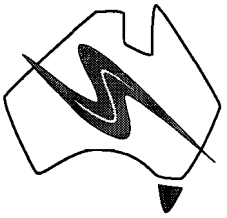

CODES SRC
Centre for Ore Deposit Research
University of Tasmania

CODES Special Research Centre
School of Earth Sciences
University of Tasmania
GPO Box 252-79
Hobart Tasmania
Australia 7001

A Special Research Centre established by the Australian Research Council.

another Pongratz & Hlaing Production 1998

Contents

Introduction

Project objectives P384A

There were four principal objectives of P384A as outlined in the original project proposal and in the November 1996 synopsis:

- To determine the primary geological, geochemical and structural controls on the location and timing of base metal mineral deposits in sedimentary basins, and to develop and refine ore deposit models applicable to exploration.

- To investigate the chemical processes controlling brine compositions and metal sulfide accumulation during fluid movements in sedimentary basins, including the relationships between copper and lead-zinc deposition

- To investigate the physical and hydrological processes involved in the evolution and movement of metalliferous fluids in sedimentary basins

- To develop geological and geochemical vectors to a variety of styles of sedimentary base metal mineralisation that may be used in the exploration for large tonnage deposits.

Research framework

This project utilised a multidisciplinary approach incorporating geophysics, sedimentology and structure, lithogeochemistry, and physical and chemical fluid modelling. For convenience, the research programme for the original P384 project and the P384A project extension, has been run as three separate, but related modules (see figure below). As the original P384 project progressed, this distinction began to break down, resulting in the presentation of several integrated studies in the final report. This integration of research disciplines has carried over into the P384A project extension, and the studies presented here in the final report routinely overlap more than one module.

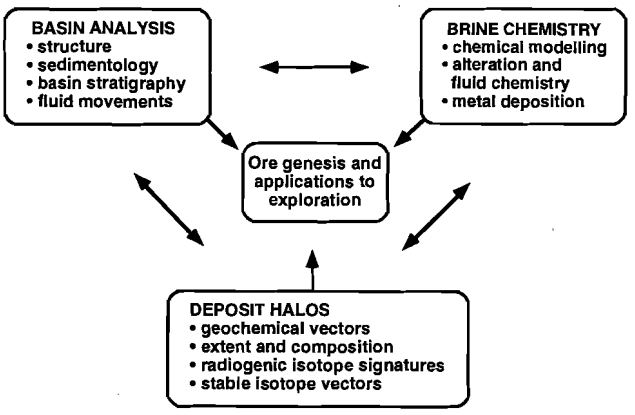

Achievements of the project

Module 1 : Basin Analysis

1. Interpretation of regional gravity and magnetic data has been extended through the Camooweal and Dobbyn 1:250,000 sheets to include 5 sections across the Mount Isa and Cloncurry region. Structures and sequences from the western Mount Isa Basin are consistent with those previously described from the Mt Drummond and Lawn Hill sheets. Indications are that the major mafic sequence interpreted across the region is a correlate or extension of the Eastern Creek Volcanics.

2. Interpretation of the gravity data in the southern McArthur Basin has been used to infer thickness of the dense, dolomite-dominated McArthur Group and revise the overall setting around HYC.

3. Detailed interpretation of the gravity, magnetic and radiometric data from around the Lady Loretta deposit has also been carried out. It indicates a WNW-oriented syndepositional structure extending from Lady Loretta to the Mount Gordon Fault Zone along the Redie Creek Fault trend, and a magnetic low beneath the ore body that could represent a sub-basin or zone of alteration.

4. Mapping and integrated structural and sedimentological analysis of key areas of McArthur Group in the southern McArthur Basin, has confirmed that the mineralised succession, comprising the Barney Creek Formation and adjacent units, was deposited during a period of tectonically-generated sub-basin formation. This is reflected by rapid lateral facies changes from depocentres to marginal areas that render the current layer cake stratigraphic scheme inadequate for detailed studies.

5. Structural mapping and sedimentological sectioning around the mineralised stratigraphic level along the sinuous Tawallah and Hot Springs Faults, using the Coxco Dolomite as a stratigraphic marker, indicates an apparently systematic structural control on sedimentation, and hence basin formation. Basinal facies deposits like those that host HYC occur in accommodation space generated adjacent to NNW-trending fault segments by extension and growth faulting on parallel structures. In contrast, there are often no basinal facies present in areas adjacent to N-NNE-trending fault segments, where sedimentation records sustained shallow water conditions indicating no accommodation space was generated.

6. Detailed mapping of the Myrtle Basin, an area situated some distance from the major N-NNW-trending structures where the original basin geometries have been masked by major wrenching and associated transpressional folding has provided the first constrained field evidence that E-W-trending faults and folds are syn-Barney Creek Formation structures. Sub-basin formation and deposition of potentially mineralised Basinal Facies deposits was optimised where these structures intersect the NNW-trending faults, and occurred in two distinct transgressional cycles. Work in this region has also given insight into the potential significance of spectacular heterolithic carbonate megabreccias similar to the breccias in the Barney Creek Formation around HYC.

7. In the Mount Isa Basin, integrated structural and sedimentological analysis of the basal McNamara Group units in the Kamarga Dome and Lady Loretta areas of the Lawn Hill Platform, indicates that they represent a phase of active tectonism (~rifting). This event established the structural template which controlled mineralisation in the overlying "sag" phase carbonates and clastics.

8. The Lady Loretta deposit occurs in the tectonically quiescent "sag" phase of the McNamara group, that is characterised by the deposition of peri-tidal platform carbonates. The host rocks are indistinguishable from the formation regionally, and there is no evidence that the mineralising event was associated with active tectonism and sub-basin formation. However, the mineralised site is located adjacent to a growth fault in the subsurface that was active at lower McNamara , illustrating the importance of understanding the rift-phase architecture of mineralised basin settings. This situation is similar in some respects to that of the Century deposit.

9. Sedimentological analysis concurs with geophysical interpretation that the growth fault adjacent to Lady Loretta was a northwestern continuation of the Redie Creek Fault. In the area of the deposit, this structure appears to have been cut/offset by a number of relatively

closely spaced, roughly orthogonal faults (?transfers). These were subsequently re-activated during the Isan Orogeny to produce the present day structural complexity of the Lady Loretta area, suggesting that other areas of equivalent structural complexity in the Lawn Hill Platform could be prospective for base metal mineralisation.

Module 2 : Brine Chemistry and Fluid Flow

10. Based on the results of chemical modelling, two brine types have been identified that are capable of precipitating stratiform sediment-hosted Pb-Zn mineralisation, which should form in distinct tectonostratigraphic environments. McArthur-type brines can form in basins dominated by oxidised sedimentary lithologies, such as the northern Australian Proterozoic basins. These oxidised brines can transport high concentrations of Pb, Zn, Cu and (depending on pH) Fe and Mn, but will not carry Ba, Au or Au. Selwyn type brines have reduced and acidic compositions, and form in reduced basinal environments. They can carry elevated Pb, Zn, Ba, Fe, Mn and in some cases Au or Sn, but are unlikely to carry high concentrations of Cu.

11. Numerical simulations of ore deposition have identified that fluid mixing is the most viable mechanism for Pb-Zn sulfide deposition in the Northern Australian basins. Mineralising brines can potentially mix with seawater or hydrocarbon reservoirs and precipitate their base metal loads. In general, water-rock interaction is predicted to precipitate base metal sulfides associated with complicated gangue assemblages, unless only one or two reactive components are present in the host lithology.

12. Several discrete episodes of alkali metasomatism have been documented in the sedimentary and volcanic lithologies of the McArthur and Tawallah Groups. Low-temperature alkali metasomatism resulted in leaching of base metals from the Tawallah Group dolerites, and the resultant metal-rich brines had potential to become involved in base metal mineralising processes elsewhere in the basin.

13. In parallel to P384A, a preliminary hydrogeological study of the southern McArthur Basin has been undertaken with funding from CODES SRC. This involved numerical modelling by Grant Garven, of an east-west section through the Batten Fault Zone in the area of the HYC deposit. The section was constrained using open file geophysical and field-based data from the Basin Analysis Module of the original P384 Project. The results confirm that large fault zones exert a major control on flow patterns in both density- and topography-driven hydrothermal systems, and that the upper Tawallah Group sandstones provide a significant strata parallel aquifer system for the focus of deep basinal brines.

14. Petrographic, lithogeochemical and FTIR studies in the McArthur Basin have defined a pattern of K-Al silicate distribution, which is considered to result from diagenesis and fluid evolution related to basin-wide fluid migration. This work, when integrated with hydrologic modelling, and structural/sedimentological studies, has the capacity to focus exploration into high priority fluid discharge sites related to stratiform mineralisation.

Module 3 : Deposit Halos

15. Detailed lithogeochemical halo models have been developed for the following seven Australian Proterozoic stratiform Zn-Pb-Ag deposits: Lady Loretta, HYC, Mt Isa, Century, Mt Novit, Walford Creek and Grevillea, and one strata-bound deposit (Kamarga). Lithogeochemical vectors for these deposits have been tested on samples from the Sullivan deposit in Canada.

    Each model includes a description of the geochemistry and mineralogy of the halo and a set of criteria and vectors that are useful for regional and mine scale exploration.

16. A basket of exploration indices has been developed which can be applied in the identification of favourable horizons for stratiform Zn-Pb-Ag deposits within carbonate-bearing sedimentary basins.

17. Specific studies of lithogeochemistry in the Lawn Hill region surrounding Century have identified the potential for several mineralised horizons within the Lawn Hill Formation. This research has shown that, in addition to unit Pmh 4, there are three other stratigraphic levels with potential for stratiform Zn-Pb-Ag mineralisation.

18. Carbon and oxygen isotope chemostratigraphy has been undertaken in a number of locations throughout the McArthur Basin to establish the background and anomalous isotope patterns. This work has identified an extensive C/O isotope halo surrounding the HYC deposit, of similar character to the isotope halo previously defined at Lady Loretta in P384. This work has also revealed that the isotope trends within the halos at HYC and Lady Loretta are unique, and very different to carbonate isotope patterns associated with other carbonate replacement deposits (MVT, skarn, carlin-type and Renison-style replacement deposits).

This report

The Final Report for P384A is divided into three volumes:

Volume 1: Summary of Outcomes

Volume 2: Research results for 1998

Volume 3: Publications from AMIRA P384 (1992 to 1995)

Acknowledgments

The project has been supported by the following companies and organisations:

Aberfoyle Limited
Australian Geological Survey Organisation
BHP Exploration
Billiton Exploration
Cominco Limited
Inco Exploration
MIM Exploration
Noranda
Normandy Poseidon Exploration
North Exploration
Pancontinental Mining
Pasminco
RGC Exploration

Thanks also to Buka and Brenton Grant for continued access to Lady Loretta. To Damien Nihil at McArthur River Mining for access to drill core and underground exposures at HYC. To Andrew Allen and Ian Matheison at North Limited for supporting honours projects and allowing access to their Bloodwood Bore prospect, and to Ian Garsed at MIMEX for allowing continued access to the Kamarga Dome area. To Coolgardie Gold and Andrew Allen again for allowing access to the Grevillea Prospect. To Dave Wallace and Tony Hespe at Aberfoyle for allowing access to their Lawn Hill drilling. To Cominco for allowing sampling of Sullivan and Sheep Creek. To Lesley Wyborn for access to the AGSO Rock Chem data base and for providing the delightful fruit cakes at the sponsors meetings. To John Dunster, Peter Winefield & Mark Duffett for unstinting contributions to the overall research program. To the NABRE team for fruitful discussions and access to gamma log data. To the NTGS for field equipment (sorry about the fridge Neils). To the high quality analysis team (Phil, Nilar and Katie) for the geochemical data. And last, but not least, to Mike Blake and June (Pongratz Productions), without whom the compilation of this report would have been impossible.

P. McGoldrick, S. Bull, D. Cooke, R. Large
Project Leaders

Primary geological, geochemical and structural controls on the location and timing of base metal deposits in sedimentary basins: A summary

Stuart Bull, Ross Large, David Cooke and Peter McGoldrick
Centre for Ore Deposit Research

Introduction

The following summary combines the research findings of P384 and 384A as outlined in the Final Outcomes Report (vol. 1). This addresses the first objective of AMIRA P384A, which was specifically *"to determine the primary geological, geochemical and structural controls on the location and timing of base metal mineral deposits in sedimentary basins, and to develop and refine ore deposit models applicable to exploration".*

Geological controls

Broad tectonic setting

For ***McArthur-type deposits*** formed from oxidised, near neutral brines:

- A multi-phase extensional regime developed on a basement of metamorphosed continental crust (ie. intra- or epi-cratonic setting).
- Significant basal thickness (kilometres) dominated by "rift" phase subaerial/marginal marine (oxidised), sandy clastic sediments and intercalated bimodal volcanics.
- Overlain by kilometres of dominantly "sag" phase marginal marine (evaporitic), fine-grained clastic- and carbonate-sediments. Intercalated volcanics not required.

For ***Selwyn-type deposits*** formed from reduced, acidic brines:

- Thick accumulation (kilometres) of reduced, deep-water (turbiditic) sediments.
- High heat flow, (>25°C) volcanism and/or high-level intrusions regionally associated with the host package required for base metal transport.

Favourable tectono-sedimentary trap sites

First order controls for ***McArthur-type deposits***:

- Are illustrated in terms of tectonics by the association of Zn-Pb-Ag deposits with major faults shown in Figure 1 (eg. Century with the Termite Range Fault; HYC with the Emu Fault). Where their early history can be established, these structures will have controlled episodes of "rift" phase sedimentation, and they may ultimately reflect basement discontinuities.
- In terms of sedimentology, first order controls are indicated by the restriction of economic mineralisation to reduced (carbonaceous) facies in the "sag" phase package.

Second/third order controls for ***McArthur-type deposits*** are dependent on the timing of the mineralising event:

- Large tonnage syngenetic Zn-Pb-Ag deposits (eg. HYC) are associated with anomalously active tectonic activity during "sag" phase sedimentation, which facilitates both the expulsion of metal-bearing fluids and the development of sub-basins to host brine pools (Fig 2a). This tectonism may manifest as mass flow deposits (breccias and turbidites) interbedded with the fine-grained, reduced carbonaceous host facies.
- Prospective intervals will be manifest in the basin stratigraphy as an abrupt change of environment/redox state, from shallow water (oxidised) to local

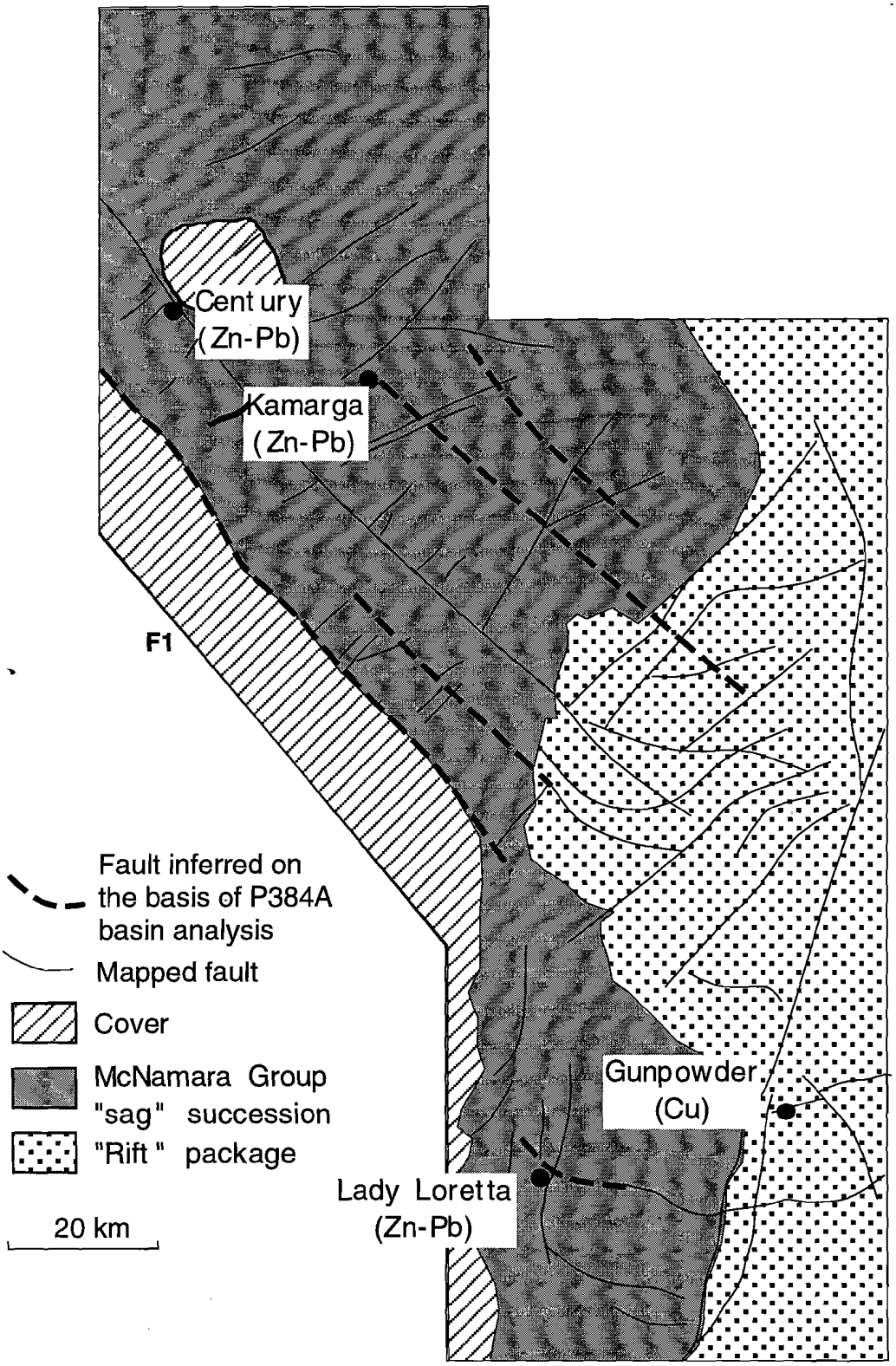

Figure 1. Relationship between mineral deposits and fault intersections in the western Mount Isa Basin. In some cases (Gunpowder and Century) the link is obvious on the basis of faults mapped on the 1:100,000 scale geology sheets. In others it is more obscure (Lady Loretta and Kamarga) and requires knowledge of the basin history provided by P384A basin analysis research.

deeper, sub-wave base (reduced basinal) conditions. This may be accompanied by a transitional facies unit with manganese carbonate enrichment.
- Potentially mineralised sub-basins will be controlled by syn-sedimentary faults (Fig. 2a) that are generally splays off reactivated first order-scale structures, and their formation is optimised in areas where faults intersect (Fig. 1).
- Smaller tonnage syngenetic Zn-Pb-Ag deposits (eg. Lady Loretta) may occur in normal tectonically quiescent "sag" phase sediments independent of active sub-basin formation and related sub-wave base sedimentation (Fig. 2b). These will be preferentially situated where suitably carbonaceous "trap" lithologies occur adjacent to subsurface syn-sedimentary fault intersections that were active during earlier "rift" cycles.
- Where significant subsequent basin inversion has occurred such sites may manifest as areas of relatively high strain (Fig. 1).
- Large tonnage epigenetic (~syn-inversion) Zn-Pb-Ag deposits (eg. Century) occur in similar sites where the subsurface growth faults are reactivated during basin inversion (Fig. 2c). This facilitates both pathways for the ascension of mineralised fluids, and the formation of anticlinal petroleum style traps in suitable carbonaceous host lithologies.
- There is potential for significant sediment-hosted Cu mineralisation to be genetically related to McArthur-type Zn-Pb-Ag deposits. Mafic volcanics can act as a metal source for Cu, Zn and to a lesser extent, Pb. Cu deposition may be spatially decoupled from Zn-Pb-Ag deposition, due to solubility controls. The "rift" phase clastics, or the contact between restricted haematitic clastics (aquifer) and reduced shales (aquiclude) in the "sag" phase package may be prospective for such mineralisation.

Although tectono-sedimentary trap sites for ***Selwyn-type deposits*** were not examined in detail in P384A, some observations can be made for one major example, the Sullivan deposit, based on published data and a reconnaissance visit to the Belt Basin.
- Large tonnage syngenetic deposits (eg. Sullivan) also appear to be associated with anomalous intra-basinal tectonic activity and sub basin formation facilitated at the intersection of regional faults.
- In this case prospective intervals will be manifest in the basin stratigraphy as an abrupt regional (?basin-wide) change in turbidite facies (eg. increase in bed thickness, change of provenance etc.).
- Evidence for anomalous high cross-stratal fluid flow may be present.

Geochemical controls and ore genesis

McArthur-type deposits

Fluid conditions and metal sources
- **McArthur type deposits** are hosted in carbonate-rich packages and are inferred to precipitate from oxidised ($SO^{=}_4 > H_2S$), acid to neutral, high salinity brines with relatively low temperature (90-200°C).
- Such fluids are most likely recycled hyper-saline marine waters that descend through the evaporitic carbonate stratigraphy and are focussed along sandstone aquifers at 2 to 10 km depth in the basin (Fig. 3).
- Recharge fluids, descending the stratigraphy, are low temperature, neutral to alkaline, in equilibrium with K-feldspar, and give rise to alteration characterised by high K_2O/Al_2O_3 ratios and light $\delta^{18}O$ carbonate values. Discharge fluids are high temperature, weakly acidic, in equilibrium with illite, and give rise to alteration characterised by low K_2O/Al_2O_3 ratios with heavy $\delta^{18}O$ carbonate values.
- Metals are derived by either (a) leaching of mafic and/or felsic volcanics within and adjacent to the aquifer system or (b) leaching of haematitic sandstones within the aquifer.
- A well-homogenous brine and metal reservoir is developed within the sandstone aquifer during long periods of density driven fluid convection. Prolonged mixing homogenises the Zn/Pb ratio and Pb isotopic composition of the basinal brine.

Metal and fluid transport
- Saline, oxidised (sulfate-bearing) fluids carry metals from the aquifer to the basin floor during periods of tectonic activity related to renewed rifting, or basin inversion.

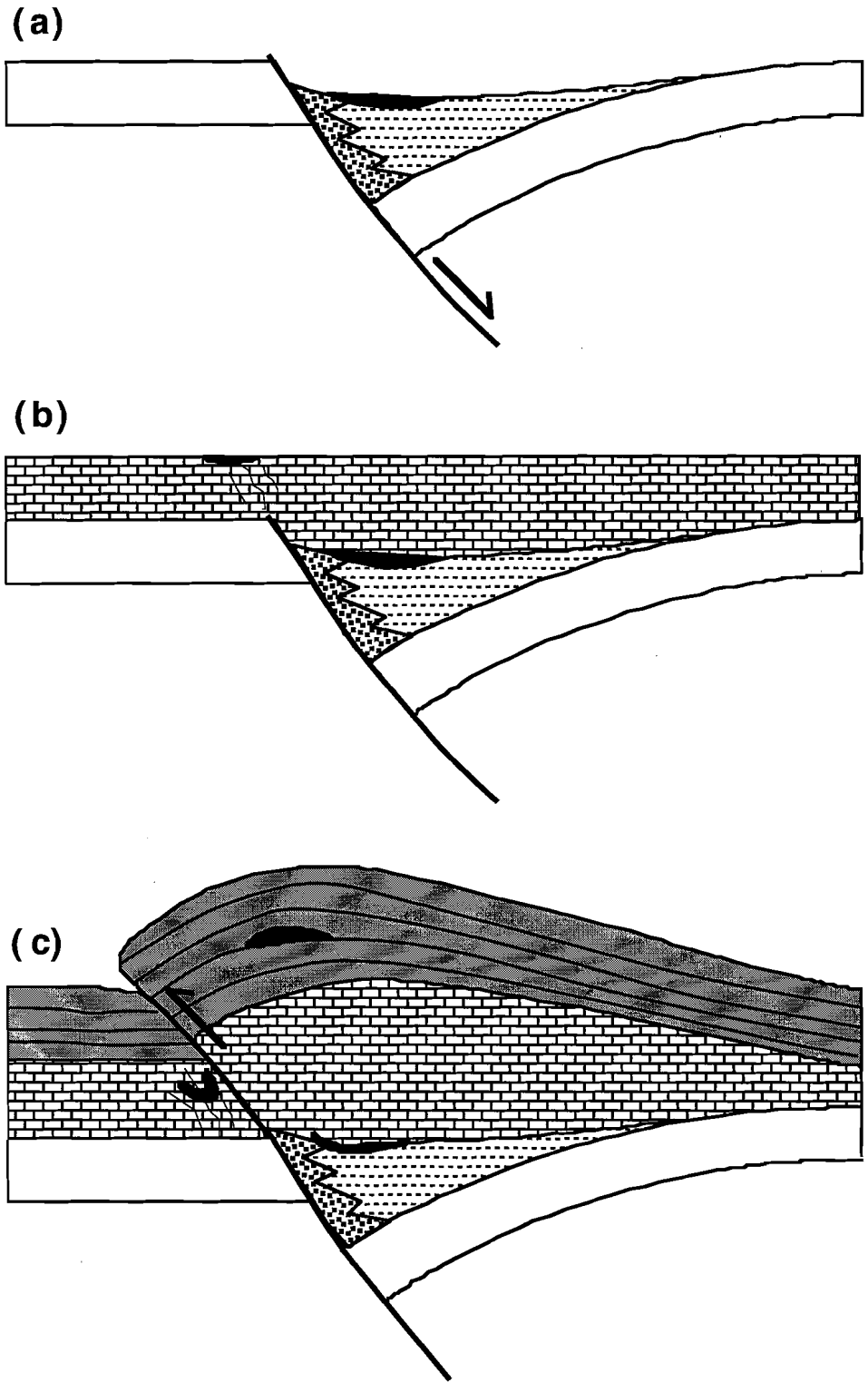

Figure 2. Schematic representation of the potential different settings/timing for base metal mineralisation in the Proterozoic of northern Australia (a) syngenetic exhalative during active subsidence (~HYC deposit) (b) syngenetic exhalative during passive subsidence (~Lady Loretta deposit) (c) epigenetic replacement during basin inversion (~Century deposit).

- The homogeneous, mineralised brine in the aquifer is "tapped" on a regular basis, leading to pulses of metalliferous brine moving upwards along the tapping structures.
- Brine ascent is sufficiently rapid and water-rock interaction of minimal effect in changing brine compositions during transport, allowing the Pb-Zn content of the brine to be retained to the trap site.
- Thousands of pulses of brine may be associated with the development of a single ore lens.

Metal deposition

- Interaction of the oxidised metalliferous brine with a reductant and/or reduced sulfur reservoir is the key to ore deposition, in both syngenetic and epigenetic environments. The trap may be carbonaceous shales, anoxic H_2S-bearing basin waters, liquid hydrocarbons and/or sour gas accumulations.
- Sites of base metal accumulation are often sites of intense (hydrothermally driven) microbial activity.
- Thermo-chemical and/or biogenic sulfate reduction commonly produces the reduced S involved in base metal sulfide precipitation.
- The mineralised brines may carry Pb, Zn, Ag, Cu, and possibly (depending on acidity) Fe and Mn towards the trap site. Ba can only be transported with base metals (e.g., Lady Loretta) if sulfate contents are low (<0.001 m) in the mineralising brine. Eu anomolies may develop at the trap site (depending on acidity), but the Au, Sn and Ba tenor of the ores should be low.
- McArthur-type brines have the potential to carry high concentrations of copper, lead and zinc. However, due to solubility relationships, copper will be spatially separated from lead and zinc. Copper may be deposited deeper in the basin, close to the aquifer system, whereas Zn-Pb may be transported greater distances before being trapped by organic-rich environments.

Geochemical halo

- Manganese deposition typically precedes the Zn-Pb mineralisation event leading to a footwall Mn-carbonate halo that extends along the favourable unit for several kilometres (Fig. 4).
- Fe-rich carbonates form an extensive halo around the ore zone which shows a zonation that may include some of the following minerals; ore → siderite → Mn-siderite → ankerite → ferroan dolomite → dolomite
- Both oxygen and carbon exhibit a broad isotope halo in carbonates surrounding some deposits. The heavy δ^{18} O signature, which is derived from the deep basinal brine, is unique to this type of deposit and unlike the light isotope halo patterns exhibited by MVT or other carbonate replacement systems.
- Thallium is commonly enriched within the Fe-carbonate alteration halo and may extend beyond this halo along the favourable unit.
- A series of alteration indices have been developed to characterise the favourable unit and provide vectors to ore in McArthur-type systems. These are Sedex AI, AI3, MnO_d and C/O isotopes of carbonates.

Timing

- Studies of sulfide-sediment relationships and textures indicate that some deposits (e.g., HYC) form principally by syn-sedimentary deposition on the basin floor with minor sub-surface syn-diagenetic mineralisation.
- Other deposits are considered to form during basin inversion and late diagenesis at a depth of 500 to 1000 m in the basin (e.g., Century).
- We have found no evidence during this study to support the concept that some stratiform Zn-Pb-Ag deposits form during late stage, post lithification, syn-tectonic replacement processes.

Selwyn-type deposits

The following comments on the characteristics of Selwyn-type deposits are more speculative than those for the McArthur-type systems. More detailed work is required to test our hypotheses on Selwyn-type deposits.

Fluid conditions and metal sources

- Reduced (H_2S-bearing or low sulfur), moderate salinity brines carry metals from aquifer(s) and/or the basement to the basin floor during tectonism.
- Cooling is a key depositional parameter (via quenching with cold seawater?). Pb-Zn deposition can also be driven by dilution, pH increase or

interaction with a solid, liquid or gaseous reduced sulfur reservoir. Reduction is unimportant.

- The mineralised brines can carry Pb, Zn, Ag, Fe, Mn and Ba towards the trap site. Eu anomolies may develop at the trap site (depending on acidity). There is potential for ore-grade or by-product gold at the trap site (e.g., DY, Vangorda), depending on the H_2S concentration of the brine. Tin may also occur in elevated concentrations if the brines are highly reduced (pyrrhotite-stable; e.g., Sullivan). Copper should not occur in economic concentrations, unless the mineralising solutions are highly acidic and/or deficient in H_2S.

Geochemical halo

The geochemical halo of Selwyn-type deposits remains untested. Further work is required.

Timing

Most of the documented Selwyn-type deposits appear to form predominantly via syn-sedimentary deposition on the basin floor, with minor sub-surface syn-diagenetic mineralisation. This may be an artefact of the genetic bias of the researchers who have documented these systems.

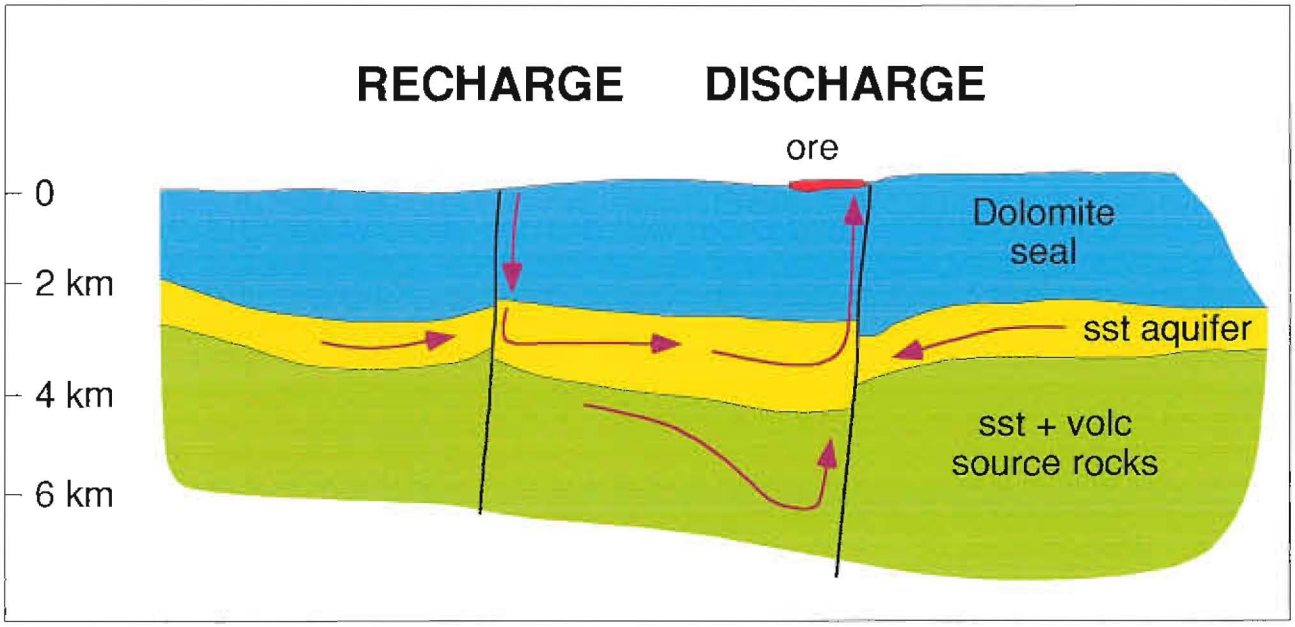

Figure 3. Potential paths for McArthur type fluids.

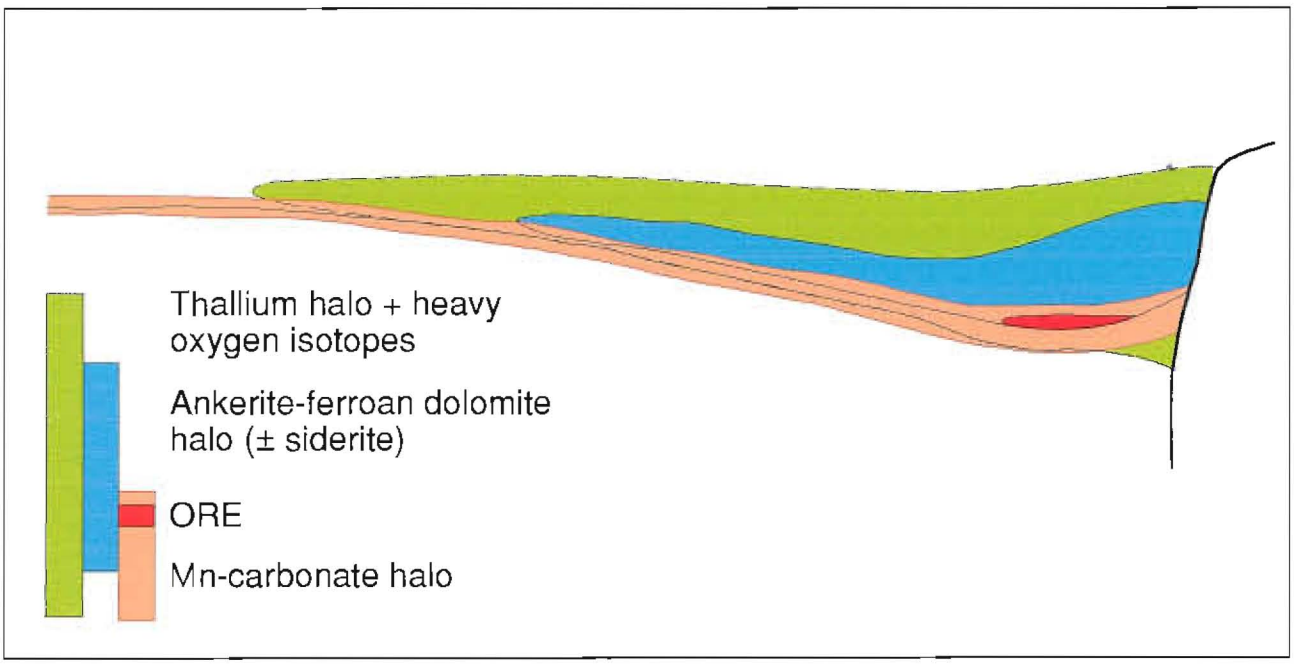

Figure 4. Lithogeochemical halos to McArthur type deposits.

Geology of the BCDC in the Myrtle Basin area, southern McArthur Basin, Northern Territory

Stuart Bull and Robert Scott
Centre for Ore Deposit Research

Introduction

P384A fieldwork in the southern McArthur Basin in the 1997 field season focussed on the relation between the sedimentology of the Barney Creek Formation and adjacent units and major faults (Winefield et al., 1997). Critical to this work was a stratigraphic marker provided by the recognition that the needle pseudomorphs that define the Coxco Dolomite Member are not after evaporitic gypsum, but represent aragonite precipitated due to a regional change in sea water chemistry (Winefield, 1997). Correlations across faults based on the Coxco marker horizon, indicate that lithofacies elements currently mapped as formations are absent at some localities, highlighting the inadequacy of the existing layer cake stratigraphic scheme. As a result, a new facies scheme was proposed for the stratigraphic interval above the Coxco Dolomite, that includes the Barney Creek Formation, Reward Dolomite and Lynott Formation, that is here termed the Barney Creek Depositional Cycle (BCDC). It consists of six facies associations that represent sub-environments developed in response to basin-formation, termed Basinal, Slope, Deep Subtidal, Shallow Subtidal Peritidal and Continental (Winefield et al., this report).

Documentation of the distribution of BCDC elements along the sinuous Tawallah and Hot Springs Faults, particularly the Basinal versus Shallow Subtidal/Peritidal Facies, indicated an apparently systematic structural control on sedimentation, and hence basin formation. In summary, it was proposed that Basinal Facies occur in accommodation space generated adjacent to NNW-trending fault segments by extension and growth faulting on parallel structures (Winefield et al., 1997; Fig. 1a). In contrast, areas of BCDC exposure adjacent to N-NNE-trending fault segments record sustained shallow water conditions, indicating no accommodation space was generated. It was proposed that this was consistent with transtension and transpression respectively, under a regional stress field involving NNW-SSE compression/ENE-WSW extension during accumulation of the BCDC (Fig. 1a). However, there are two marked inconsistencies between this interpretation and the current models for formation of this mineralised package.

(1) Both the regional stress field and the controlling structures are incompatible with models currently proposed for the McArthur Group in general (Etheridge and Wall, 1994), and the Barney Creek Formation in particular (Neudert and McGeough, 1996). These invoke regional N-S extension that generated E-W-trending syn-sedimentary growth faults that extended to the west from an area just north of HYC (Fig. 1b).

(2) In addition to being sites of low accommodation space during the BCDC, areas adjacent to N-NNE-trending fault segments (eg. Top Crossing; Winefield et al., 1997) are also sites of transpressional folding about N-NNE-trending axes (Fig. 2a). These folds are similar in geometry and scale to those documented through the same stratigraphy in an E-W cross section through HYC, which are interpreted to be the result of syn-Barney Creek Formation deformation (Hinman, 1995; Fig. 2b). However, in the Top Crossing example, this folding clearly affects stratigraphy considerably younger that the BCF, including the upper McArthur Group stratigraphy and the overlying Nathan Group (Fig. 2a). At this locality at least, this deformation may well therefore have occurred during the Isan Orogeny.

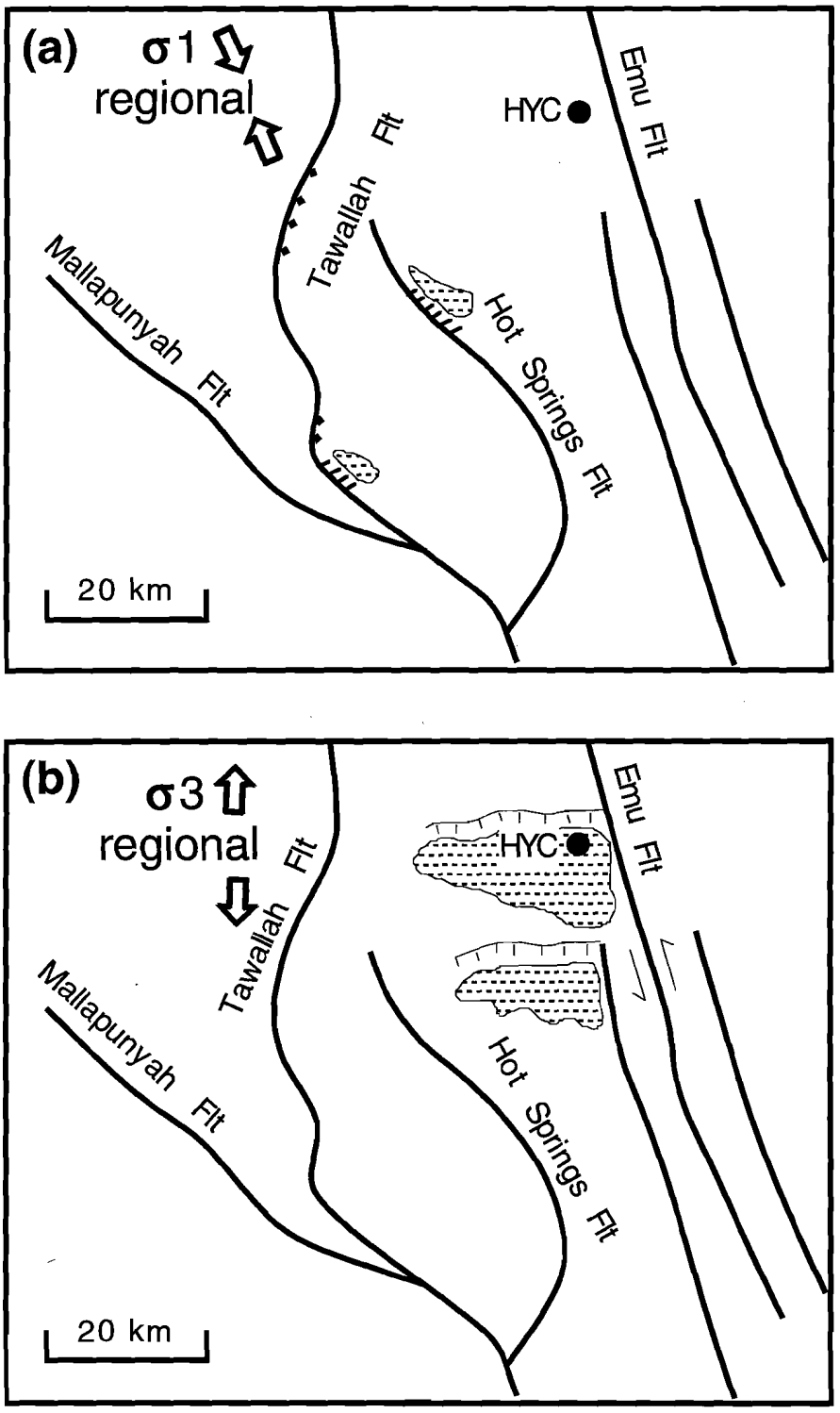

Figure 1. (a) Schematic representation of the distribution of Basinal Facies deposits along the sinuous Tawallah Fault, note the implied regional stress field. (b) Schematic representation of the structural configuration and implied regional stress field proposed by Etheridge and Wall (1994) and Neudert and McGeough (1996).

One factor that clearly contributes to the inconsistencies outlined above relates to the areas where the structural setting of the BCF and adjacent stratigraphy have been studied in detail. These are all adjacent to major N-NNW-trending faults (eg. the Emu Fault and associated structures at HYC, Hinman, 1995; and various localities along the Tawallah Fault, Winefield et al., 1997; Winefield, this volume). These structures have been interpreted as regional transfers during deposition of the McArthur Group (Etheridge and Wall, 1994). However, they have subsequently been sites of major wrench faulting and associated folding during the Isan Orogeny (eg. Rogers, 1996). As a result, unequivocal timing criteria, which are rarely preserved, are required to differentiate the Isan deformation from that generated during earlier, syn-sedimentary tectonism.

The Myrtle Basin is an area of outcropping BCDC situated 18 km SSW of HYC and 10 km west of the Emu Fault Zone (Fig. 3). It has been the focus of sporadic base metal exploration since an initial diamond drill hole, completed in 1967, intersected minor Zn-Pb mineralisation (35.7 m @ 0.6% Zn, 0.09% Pb and 0.2 oz/t Ag) in pyritic siltstone at the interpreted base of the Barney Creek Formation. By 1982 an additional four diamond drill holes had been completed. Although all of the holes intersected pyritic BCDC basinal facies (termed the Barney Creek Formation and the Upper Surprise Creek Dolomite Pyritic Shale), no further significant mineralisation was detected.

The Myrtle Basin area was chosen to clarify the structural controls on the BCDC because:

1. The BCDC, including the normally recessive Basinal Facies, crops out relatively well providing the opportunity to map an apparent depocentre.
2. The area is far enough away from the major NNW-trending structures (?transfers, eg. the Emu, Hot Springs and Tawallah Faults) to have escaped major Isan wrench faulting that could mask the original basin geometry, as may be the case at HYC.
3. A prominent E-W-trending fault separates the BCDC package from older McArthur Group stratigraphy (the Tooganinie Formation; Jackson et al., 1984) This fault could potentially represent a syn-BCDC structure in either proposed regional stress field; in the case of N-S extension (Neudert and McGeough, 1996) it could represent a normal (growth) fault; in the case of NNW-SSE compression (Winefield et al., 1997) it could represent a reverse (thrust) fault.
4. East-west-trending synclines are also developed in the BCDC in this area. These structures could represent syn-depositional drag folds developed in response to either normal or reverse movement on the adjacent E-W-trending faults, or younger structures unrelated to basin formation.

Methods

This study of the controls on the formation of the Barney Creek Formation and adjacent stratigraphy continues the approach outlined in the preceding report (Winefield et al., 1997). In summary, this consists of using the Coxco stratigraphic marker-based BCDC stratigraphic scheme (Winefield, this report; Fig. 1), in combination with integrated structural and sedimentological fieldwork, to overcome the limitations imposed on previous workers by scale (ie. restriction to the area of the HYC deposit) and drillcore based methods. In the Myrtle Basin area, sedimentological logs were measured and stratigraphic and structural data collected from two areas where the BCDC is exposed within ~E-W-trending synclines, termed the N Myrtle Basin and SW Myrtle Basin (Fig. 3). In the N Myrtle Basin the mapped stratigraphy comprises Teena Dolomite, Barney Creek Formation, Reward Dolomite, and the Caranbirini and Hot Springs Members of the Lynott Formation. The basal succession exposed in the SW Myrtle Basin is the same, however the uppermost mapped unit in this area is the Reward Dolomite. The stratigraphically lower Tooganinie Formation was also examined in the SW Myrtle area, where it occurs to the south of the E-W-trending fault that bounds the BCDC syncline (Fig. 3). This unit was investigated on the grounds minor structures within it may provide clues to the true nature (normal or reverse) of the adjacent E-W bounding fault, which is itself poorly-exposed.

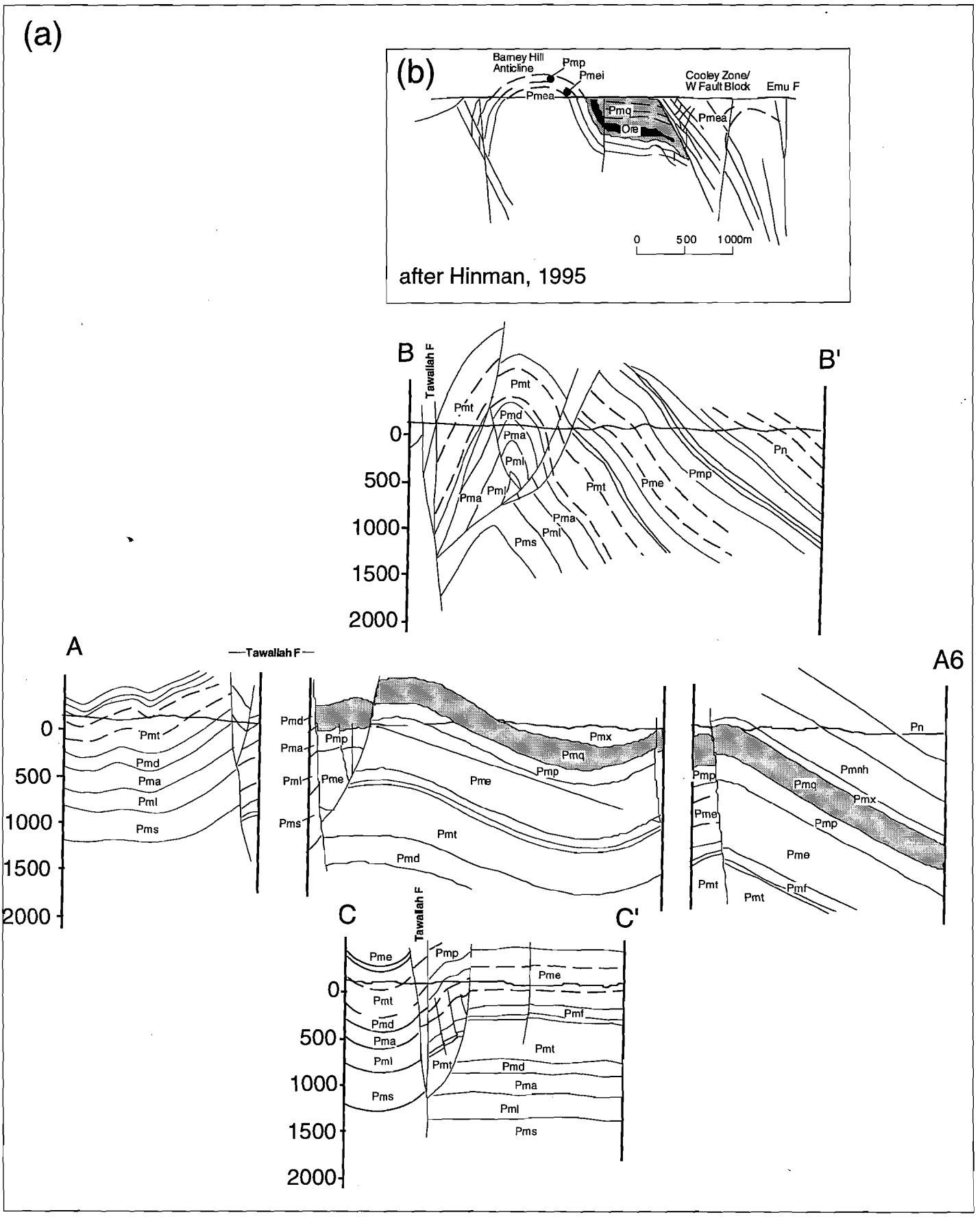

Figure 2. (a) Series of ~E-W cross-sections of the McArthur Group across the Tawallah Fault in the Top Crossing region (after Winefield et al., 1997; see Fig. 4 for locations). (b) E-W cross-section of the McArthur Group in the area of the HYC deposit (modified after Hinman, 1995).

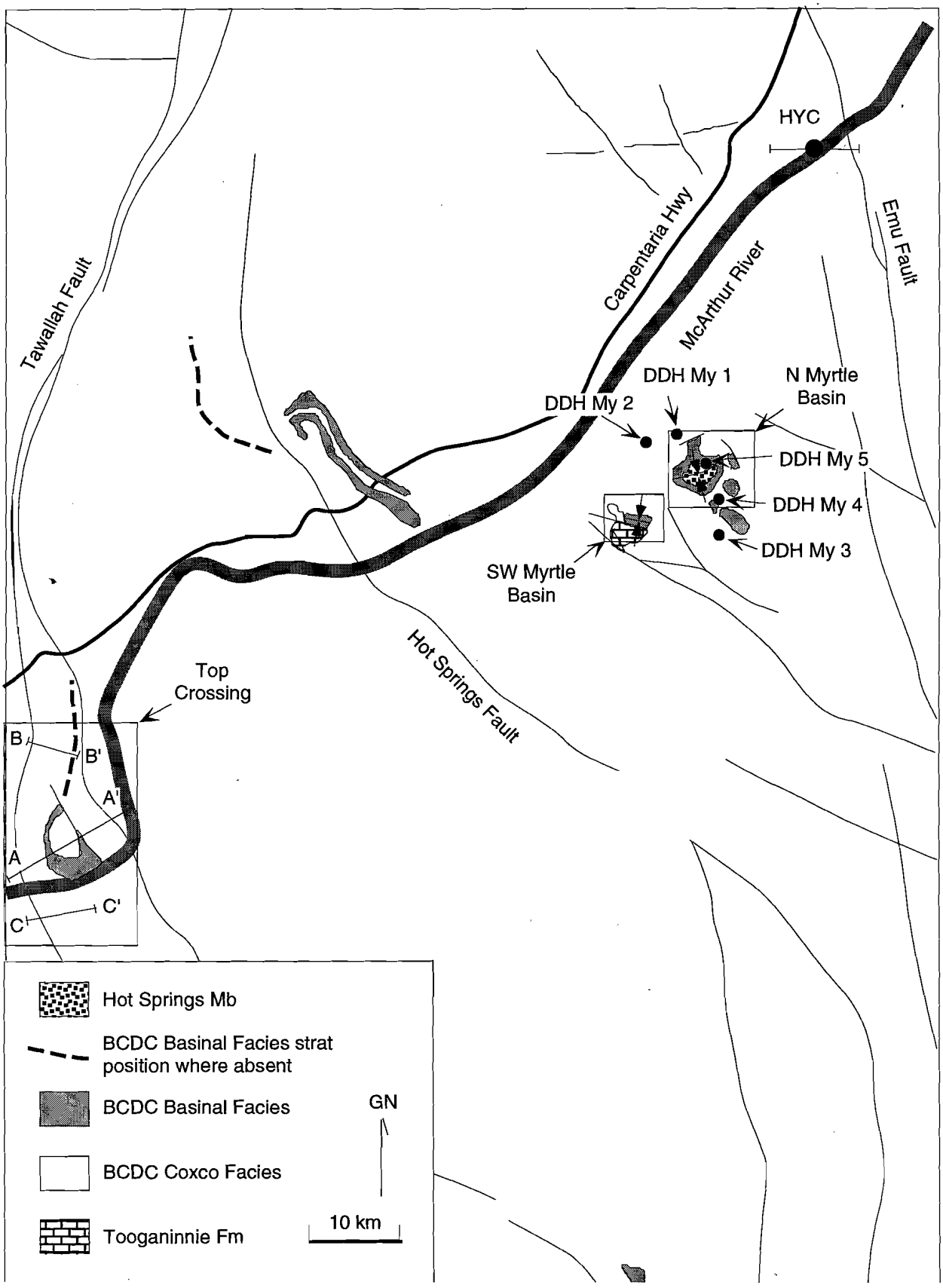

Figure 3. Locality diagram; geology modified after Pietsch et al., 1991 and Hinman, 1995.

Sedimentology of the BCDC in the Myrtle Basin

A detailed map and one representative sedimentary section were produced for each study area (SW Myrtle Basin Fig. 4 and 5 and N Myrtle Basin Fig 6 and 7). As at other localities studied (Winefield et al., 1997), the Coxco Dolomite (mapped as Teena Dolomite; Jackson et al., 1984) is taken to represent the basal cycle of BCDC sedimentation in each case. It is characterised by needle pseudomorph-bearing, massive to microbially laminated dolostone and locally dolomitic siltstone. Both sections focus on the BCDC overlying the Coxco Dolomite that records sub-basin development. This consists of the lowermost Basinal Facies element (~ the Barney Creek Formation) and the diverse range of overlying facies (ie. Slope, Deep Subtidal, Shallow Subtidal and Peritidal Facies) generally mapped as Reward Dolomite (Jackson et al., 1984). The upper units in the N Myrtle Basin area, consist of the Caranbirini Member (BCDC Basinal Facies) and the Hot Springs Member (BCDC Shallow Subtidal/Peritidal Facies), were mapped but not logged in detail.

SW Myrtle Basin

In the SW Myrtle area, the upper contact of the Coxco Dolomite is exposed and is immediately overlain by finely laminated, locally pyritic, carbonaceous dolomitic siltstone (Fig. 5a, b & c). These deposits are interpreted to represent the quiet, reduced, sub-wave base conditions that characterise the BCDC Basinal Facies. The abrupt nature of the contact between contrasting lithologies suggests that the accommodation space that led to basin formation was rapidly generated.

The other component of the Basinal Facies in the SW Myrtle Basin is bedded dolomitic breccia. In the area where the section was measured, three 1-2 m thick tabular beds of open framework pebble to boulder breccia are present (Fig. 5a & c). However, the lower two beds thicken rapidly to the south and east into breccia zones several metres in thickness (Fig. 4; Fig 8a). Clasts are generally sub-angular to sub-rounded cobbles and boulders of massive to microbially laminated and occasionally stromatolitic dolomite (Fig. 8b & c). They occur in an open framework arrangement within massive to laminated carbonaceous dolomitic siltstone matrix. Some clasts have the distinctive needle pseudomorphs characteristic of the Coxco Dolomite, and others silicified microbial/stromatolitic texture identical to that from Emmerugga Dolomite outcrops ~1 km NW of the section. Both low-sphericity (~tabular) and high-sphericity examples are present, and most of the larger clasts, including one > 7 m in length (Fig. 8d), are tabular and arranged with their long-axes parallel to bedding. Some of the larger clasts have well defined basal sags defined by plastic deformation of the laminated siltstone matrix (Fig. 8b) and siltstone draped tops (Fig. 8c). Occasional smaller tabular clasts have long axes at a high angle to bedding.

The characteristics of the breccia within the Basinal Facies described above, indicate that it formed by rockfall of clasts of dolomite sourced from adjacent areas of high relief, directly into the basinal siltstones. It is therefore interpreted as a true talus deposit. Thin laterally equivalent matrix-supported breccia beds with randomly oriented clasts are present to the north of the thickest rockfall deposits in the measured section (Fig. 5a & d), and where the talus apron thins to the east in an east-west section exposed at the back of the ridge (Fig. 4; Fig. 8a). These are interpreted as debris flows that travelled for a short distance beyond the area of rockfall. Their distribution suggests that the high-relief source for the main deposit was located to the southwest of the exposed section.

The upper contact of the Basinal Facies in the SW Myrtle Basin is defined by the initial transition from dolomitic siltstone to thin/medium bedded dolostone at ~ 50 m (Fig. 5a; Fig. 9a). The latter deposits are typical of the BCDC Deep Subtidal Facies (Winefield, this report). The intercalated plate breccias within a few metres of the contact (Fig. 5a; Fig. 9b) represent storm-wave reworking, and indicate that these deposits represent rapid regression to above-wave base conditions.

A facies repeat occurs in the SW Myrtle Basin section above ~ 50 m (Fig. 5a). A gap in outcrop between ~ 50 and 65 m probably corresponds to second interval of Basinal Facies dolomitic siltstone. It is also overlain by Deep Subtidal Facies thin/ medium bedded dolostone with intercalated plate breccias. This interval (Fig. 5a; ~ 51-75 m) could represent either a second upward shallowing

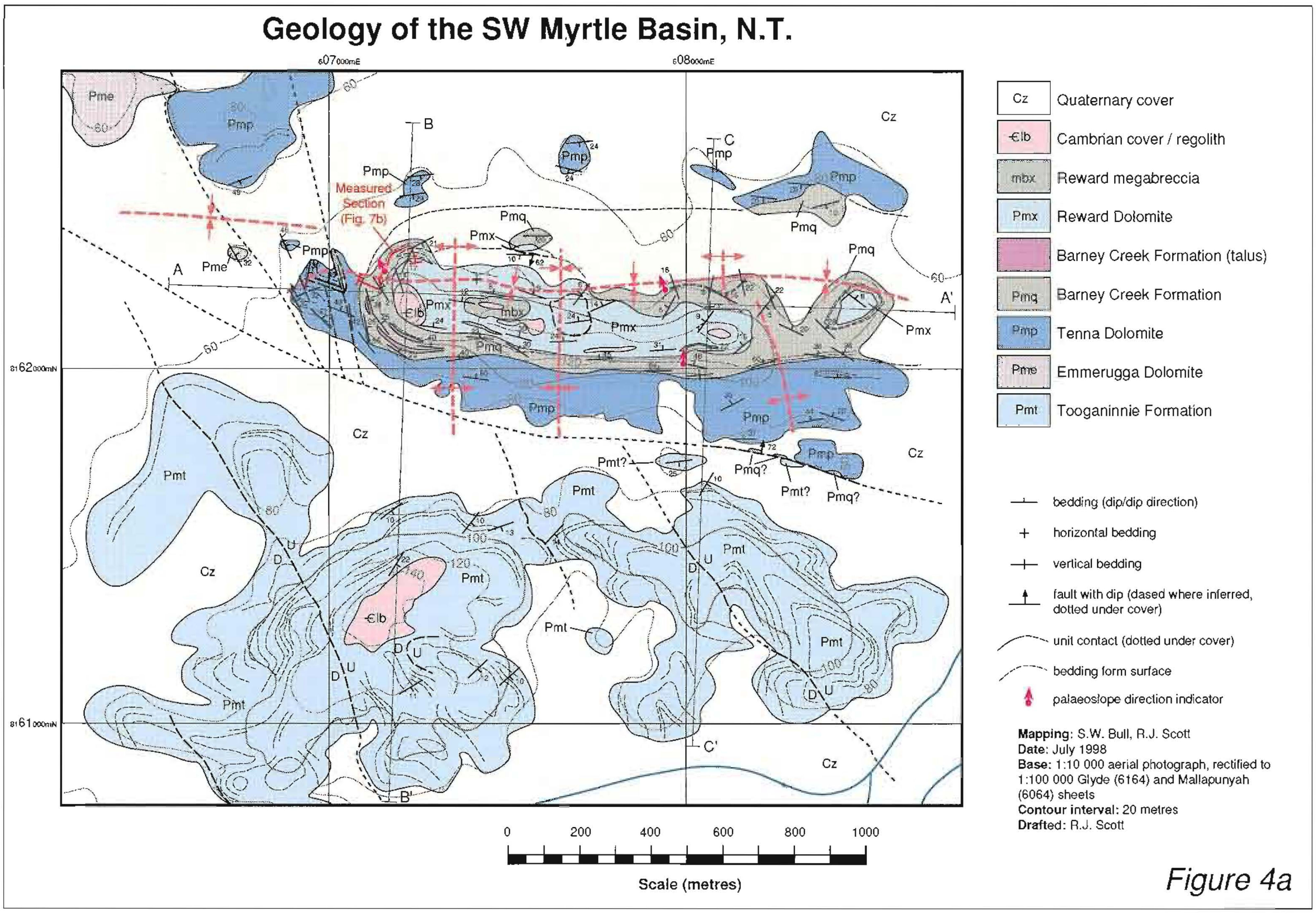

Figure 4a

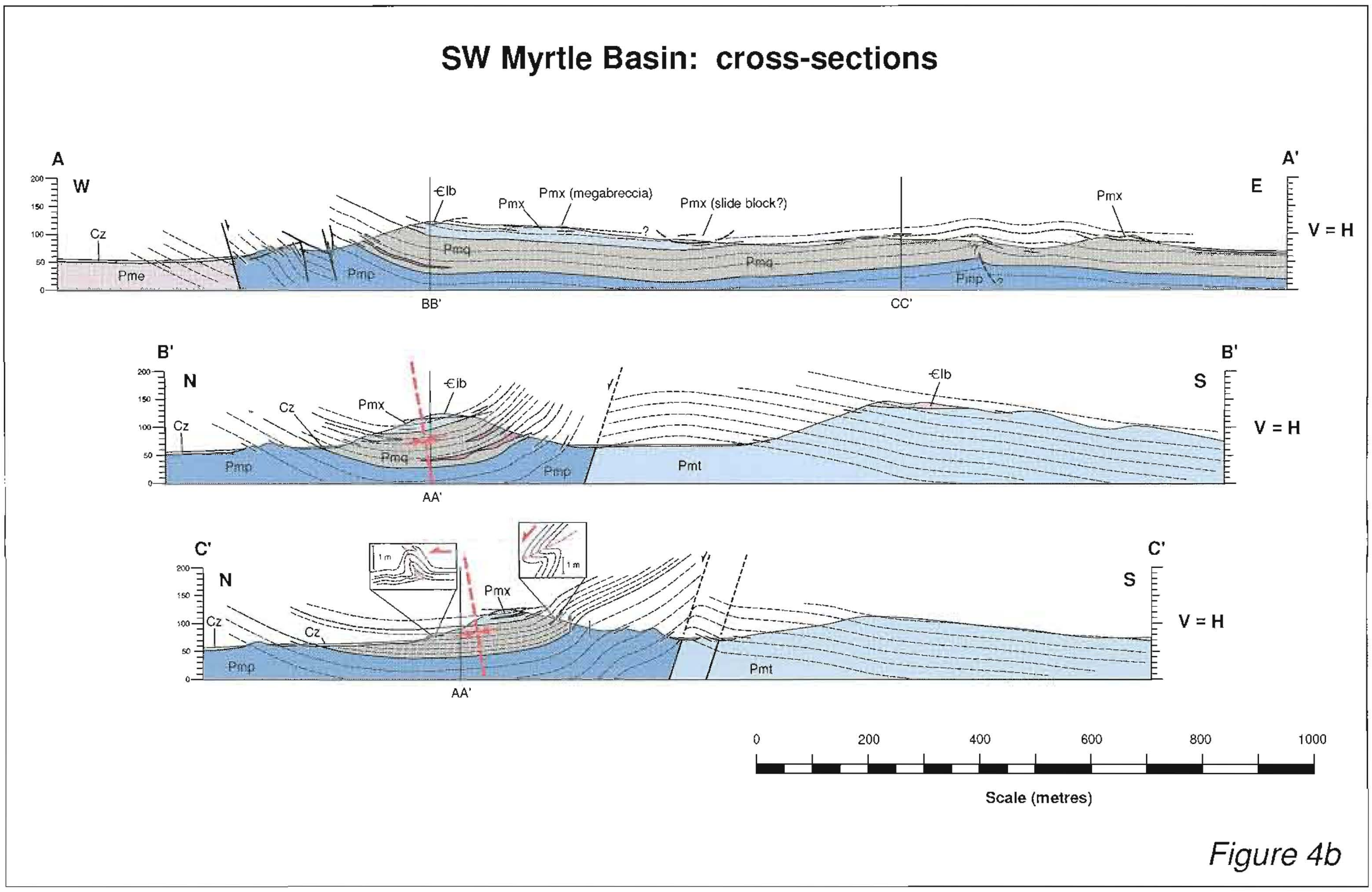

Figure 4b

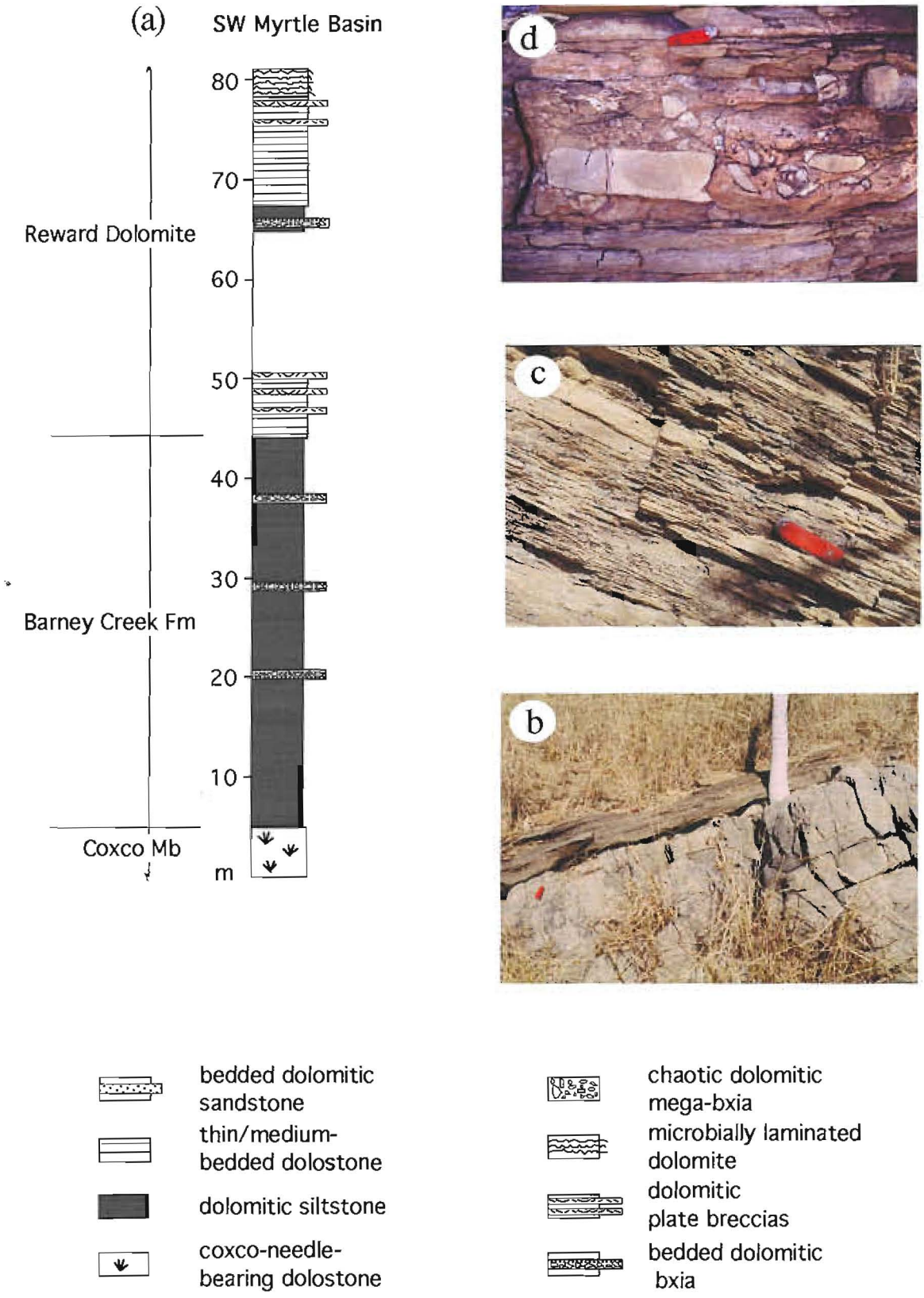

Figure 5 (a) Sedimentological log of the BCDC in the SW Myrtle Basin area (see Fig. 4 for location). (b) Sharp contact between Coxco Dolomite and Basinal Facies carbonaceous dolomitic siltstones. (c) Typical thinly-bedded/planar-laminated Basinal Facies carbonaceous dolomitic siltstones. (d) Dolomitic breccia bed within Basinal Facies siltstones.

Geology of the North Myrtle Basin, N.T.

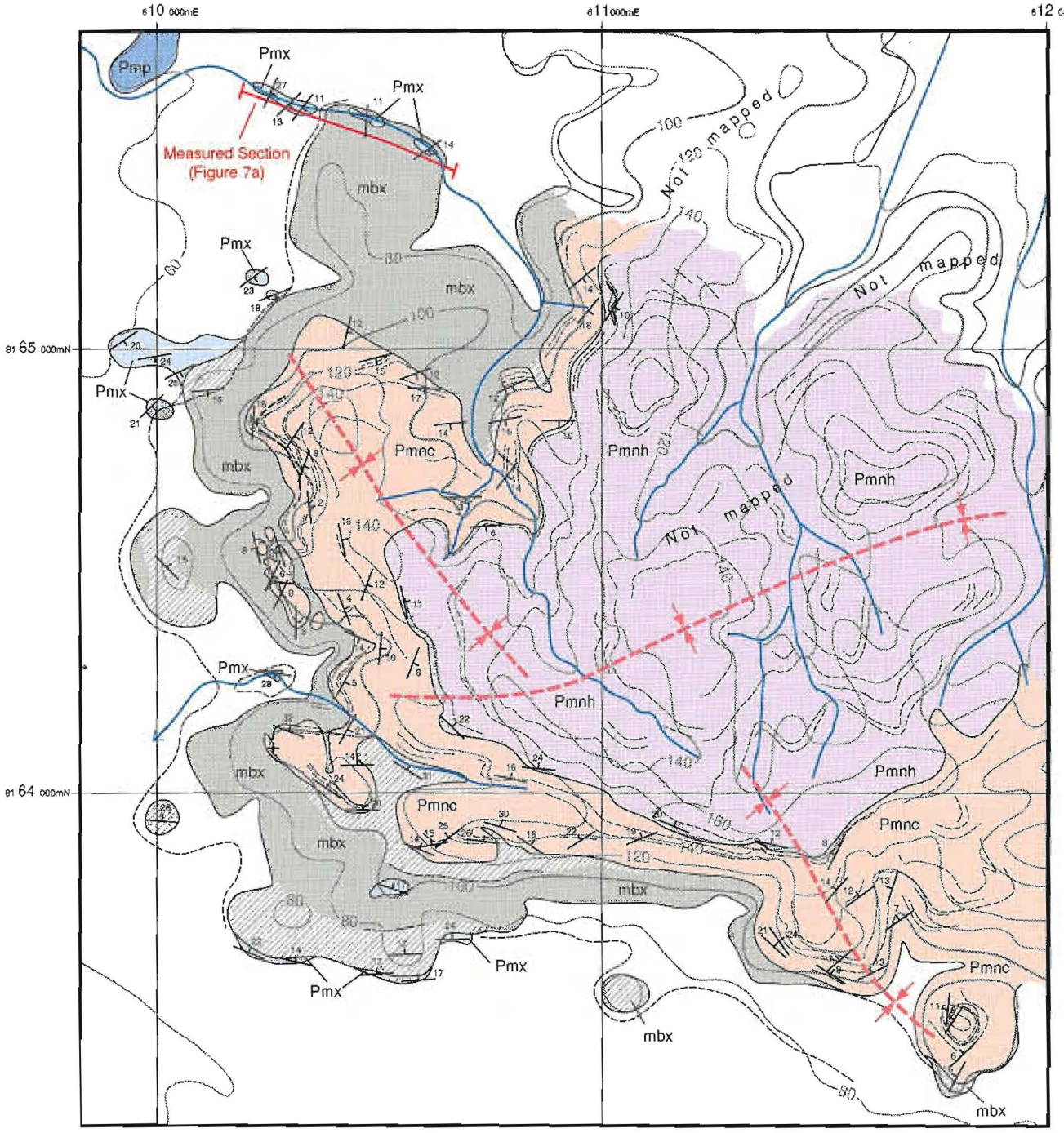

Cz	Alluvium, colluvial and aeolian deposits
Pmnh	Hot Springs Formation
Pmnc	Caranbirini Member
mbx	megabreccia (hatched where *in situ*)
Pmx	Reward Dolomite
Pmp	Teena Dolomite

- bedding (dip/dip direction)
- \+ horizontal bedding
- vertical bedding
- fault with dip (dased where inferred, dotted under cover)
- unit contact (dotted under cover)
- bedding form surface

Mapping: S.W. Bull, R.J. Scott
Date: July 1998
Base: 1:10 000 aerial photograph, rectified to 1:100 000 Glyde Sheet (6164)
Contour interval: 20 metres
Drafted: R.J. Scott

Figure 6

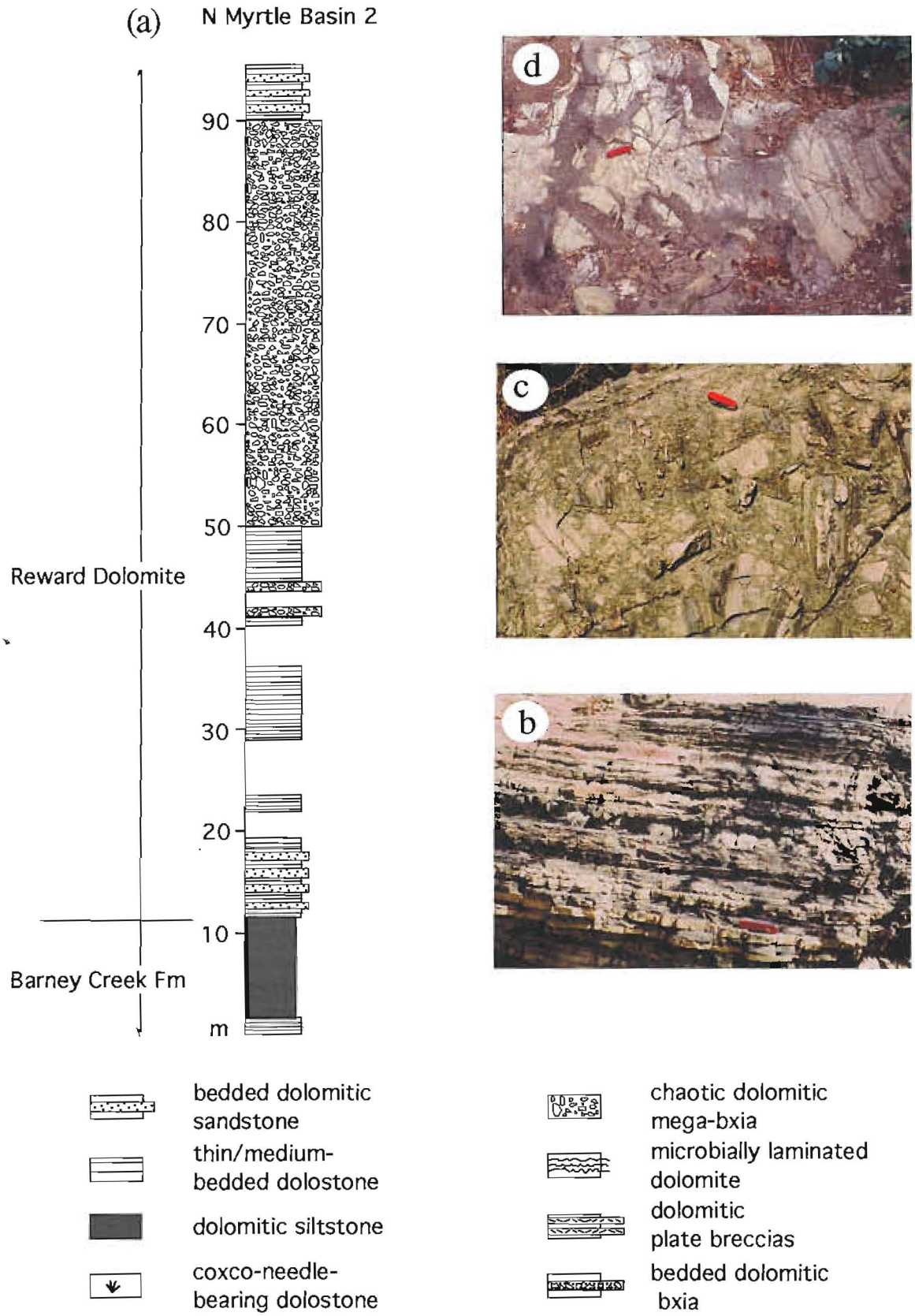

Figure 7 (a) Sedimentological log of the lower part of the BCDC in the N Myrtle Basin area (see Fig. 4 for location). (b) Thin/medium bedded dolostone typical of the BCDC Deep Subtidal Facies. (c) Massive megabreccia of tabular clasts of thinly bedded and microbially laminated dolomite. (d) Clastic dykes/sills of disaggregated Slope Facies dolomitic sandstone (pale material); note relict bedding at centre right.

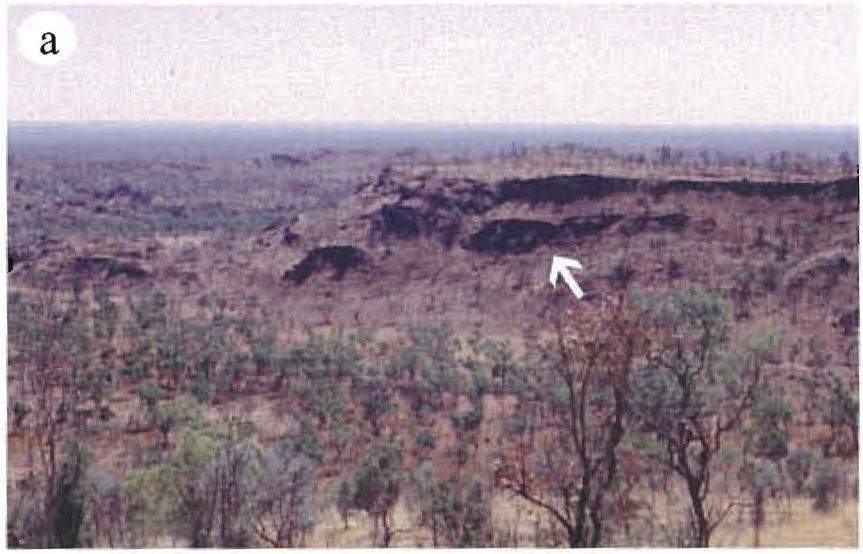

Figure 8 (a) View looking N across SW Myrtle Basin; dark E-tapering wedge-shaped outcrop below ridge line (arrowed) is talus deposit. (b) Typical sub-rounded dolomite talus clast; note well-developed basal sag. (c) Typical tabular sub-angular dolomite talus clast; not siltstone drapes over top. (d) Large (> 7 m) tabular Coxco Dolomite block (right of figure) in upper part of talus deposit.

sedimentation cycle, or a structural repeat of the lower cycle. The lack of outcrop in the critical area above 50 m makes it impossible to determine which interpretation is most likely. However, carbonate megabreccias that occur slightly higher in the stratigraphy 200 m east of the section (Fig. 4) attest to considerable post-depositional stratigraphic disruption (see below), and may indicate the latter scenario. In either case, the upper Deep Subtidal Facies interval is thicker, and ultimately passes upward into microbially laminated and evaporitic dolomite (Fig. 5a; Fig. 9c & d) typical of the BCDC Shallow Subtidal/Peritidal Facies. This is the highest stratigraphic level reached in the SW Myrtle Basin area.

N Myrtle Basin

In the N Myrtle area, the lowermost BCDC Basinal Facies element is poorly-exposed, but an area of no outcrop corresponding to ~ 80 m of section overlying outcropping Teena Dolomite (Fig. 6) probably represents the constituent recessive dolomitic siltstone. The measured section begins in the uppermost 10 m of dolomitic siltstone, which is overlain by a > 80 m thick package of thin/medium bedded dolostone (~ BCDC Deep Subtidal Facies; Fig. 7a & b). At this locality, the dolostone package includes a significant proportion of intercalated beds of dolomitic sandstone/gravel (Fig. 9e). These units are massive, up to 60 cm thick and consist of abundant well-rounded dolomitic lithic fragments, often with a minor proportion of clear quartz grains. They clearly record active erosion of lithified material in agitated environments upslope and are characteristic of the BCDC Slope Facies (Winefield, this report). Their presence, in combination with the absence of units characteristic of the Shallow Subtidal/Peritidal Facies (eg. microbial structures, evaporite pseudomorphs), suggest that the transition from BCDC Basinal to Deep Subtidal/Slope Facies at this locality is more a record of slope development than decreasing water depth.

A 10 m gap in outcrop occurs at the top of the N Myrtle Basin section, above which ~ 20 m of Basinal Facies dolomitic siltstones (mapped as Caranbirini Member) is exposed. These deposits are overlain by Shallow Subtidal/Peritidal Facies units (mapped as Hot Springs Member), consisting of thin/medium bedded and/or microbially laminated dolostone, synaeresis cracked and rippled fine-grained quartz sandstone (Fig. 9f) and cross-bedded coarse-grained quartz sandstone. These deposits have been documented in other BCDC localities (Winefield et al., 1997), and they are interpreted to represent sub- to inter-tidal environments developed in response to widespread shallowing See below).

The other facies represented in the in the N Myrtle Basin area is spectacular heterolithic dolomitic megabreccia (Fig. 6; Fig. 7a & c). Similar deposits are also present in the SW Myrtle Basin area along strike from the measured section (Fig. 4). They consist of gravel- to boulder-sized, often tabular clasts in a massive, clast-supported fabric (Fig. 7c; Fig. 10a & b). A range of clast types are present including massive dolostone, thin/medium bedded dolostone (Fig. 7c), microbial dolomite (Fig. 10a), evaporitic dolomite (Fig. 10b), dolomitic sandstone and quartz sandstone. Areas of apparent fine-grained and coarse-grained matrix generally consist of soft-sediment deformed siltstone (Basinal Facies) and dolomitic sandstone (Slope Facies) clasts (Fig. 7d) respectively.

The dolomite megabreccia occurs above the basal Basinal Facies interval in both study areas as a crudely bedding parallel discontinuous sheet. It is up to at least 80 m thick in the N Myrtle Basin area (Fig. 6). The margins of this thicker occurrence of megabreccia are highly irregular and locally difficult to constrain. Locally both the upper and lower contacts of the megabreccia transect stratigraphy (Fig. 6). At some localities the base of the unit consists of largely coherent to in-situ brecciated blocks of Deep Subtidal/Slope Facies units, that can be traced laterally over 5-10 m through jigsaw fit breccia to extensively disaggregated, clast-rotated polymict megabreccia. At others, such as the area of the measured section (Fig. 7a), brecciation is developed over at least 70 m of section, but includes > 10 m thick intervals of bedded Deep Subtidal/Slope Facies stratigraphy that have similar dips to the coherent stratigraphy in the same area. At its upper surface "dykes" of breccia a few to 10s of metres across penetrate the overlying stratigraphy. These occupy extensional "tears" in the overlying largely coherent Basinal Facies siltstones (mapped as Caranbirini Member). Locally along the western edge of the range, large blocks of the Basinal Facies are bound on all

sides by breccia dykes, to form apparently "floating" blocks up to several metres thick and 10s of metres in length (Fig. 6 & Fig. 10c). The upward penetrating breccia "dykes" locally affect the base of the upper Shallow Subtidal/Peritidal Facies interval (mapped as upper Caranbirini), but do not affect the main interval of Peritidal Facies (mapped as Hot Springs Member) in the present mapped area. At one locality, coherent upper Basinal Facies stratigraphy above the main megabreccia zone is apparently thrust over a large "floating" block (Fig. 10d), indicating local contraction during emplacement. These relations indicate the megabreccia deposit and the largely coherent sheet of upper Basinal Facies deposits overriding it were locally at least 100 m thick.

Breccia units similar to those described above have previously been recorded from the type section of the Caranbirini Member, located approximately 2.5 km to the south of the SW Myrtle Basin area (Jackson et al., 1987). They were termed "slump breccias" but were not mapped or interpreted in detail. Our work in the Myrtle Basin suggests that carbonate megabreccias also occur within stratigraphy outside the Caranbirini Member (including units mapped as Reward Dolomite), and are developed over a much larger area than was previously recognised.

The interpretation of carbonate megabreccias is a controversial subject in the recent sedimentological literature (eg. Spence and Tucker, 1997). These deposits have widely been interpreted as the result of catastrophic collapse of over-steepened (high-angle, metastable) carbonate seafloor slopes, and in particular reefs, where vertically growing organisms enable development of slope dips approaching 90°. If a steep slope is required for megabreccia formation, then Proterozoic examples have additional significance, indicating stromatolites were also efficient reef builders. As a result, carbonate platform development should be analogous to the better constrained models developed for the Phanerozoic. However, recent recognition of similar deposits formed on very gently-dipping slopes has forced a reappraisal of megabreccia formation, in which it has been proposed that they can be initiated by sudden release of overpressured pore fluids at some depth below shallow, previously stable slopes.

Although the megabreccia deposits in the Myrtle Basin area have not been studied in detail, provisional interpretation based on the following factors suggest the latter mode of formation;

- The megabreccia clasts are not restricted to potentially reef forming facies (ie. microbial dolomite) but represent the whole spectrum of BCDC Facies lithologies.
- Brecciation appears to have developed in-situ, as areas of megabreccia can be traced laterally and vertically into coherent stratigraphy.
- The upper Basinal Facies element (mapped as Caranbirini Formation) provides an obvious aquaclude, below which it would have been possible to develop high pore fluid pressures in the diverse BCDC Facies deposits that represent the main level of brecciation.
- Such overpressure is suggested by the fact that the most porous units present, the Slope Facies dolomitic sandstones, are often disaggregated into sediment dykes and sills within the megabreccia fabric (Fig. 7d).
- Initiation of megabrecciation appears to have occurred during the onset of the shallowing event at the end of the BCDC (as suggested by the age of the youngest units affected). Decreases in relative sea level have been implicated as important means of generating fluid overpressures and hence triggering megabreccia formation (Spence and Tucker, 1997).

Structure of the Myrtle Basin

SW Myrtle Basin

The general structure of the SW Myrtle Basin area as documented by Jackson et al. (1984), consists of an E-W-trending syncline developed in stratigraphy mapped as Emmerugga Dolomite to Barney Creek Formation (Fig. 3). This folded sequence is exposed for ~ 2 km along strike, and the N-dipping southern limb is separated from SE-dipping older stratigraphy (Tooganinie Formation) to the south by a WNW-trending fault that occupies the intervening valley. The western part of the area is also cut by a series of NW-trending faults, one of which truncates the E-W-trending syncline.

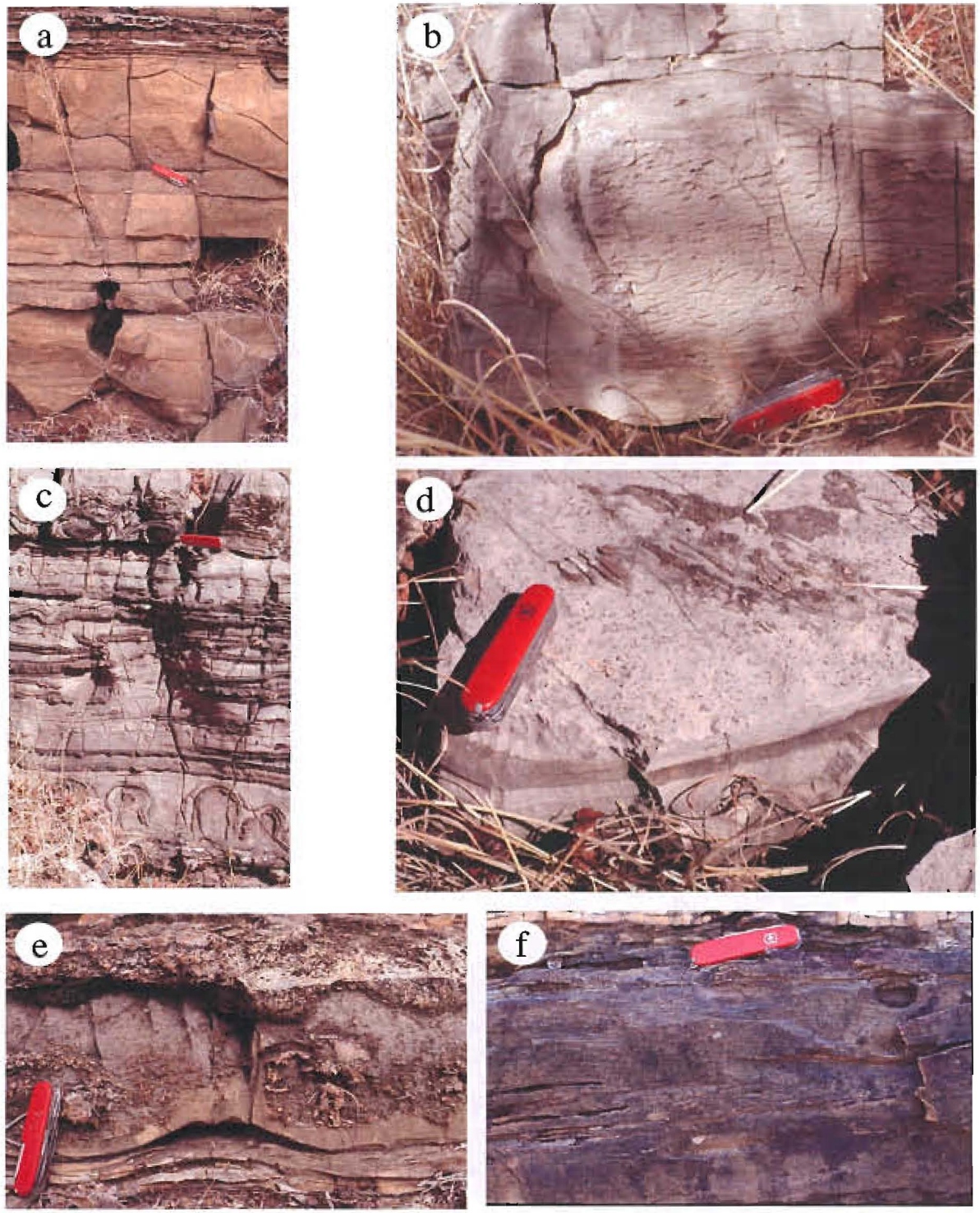

Figure 9 (a) BCDC Deep Subtidal Facies bedded dolostone deposits from the N Myrtle Basin. (b) Bedded plate breccia from the SW Myrtle Basin; represents storm-wave reworking of cemented dolomitic substrate typical of the BCDC Shallow Subtidal/Peritidal Facies. (c) Silicified microbially laminated dolomite typical of the BCDC Shallow Subtidal/Peritidal Facies from the SW Myrtle Basin; note the ? stromatolitic forms at lower right. (d) Shallow Subtidal/Peritidal Facies dolomite from the SW Myrtle Basin; dark spots to right of knife are pseudomorphs after evaporitic gypsum. (e) Bedded dolomitic gravel characteristic of the BCDC Slope Facies from the N Myrtle Basin; note flame structure in lower centre. (f) BCDC Shallow Subtidal/Peritidal Facies planar laminated and symmetrically (wave-) rippled fine-grained sandstone from the upper interval (~Hot Springs Member) in the N Myrtle Basin.

Figure 10 (a) Typical massive megabreccia from N Myrtle Basin; note angular microbially laminated dolomite clast in upper middle and pseudomatrix of diffuse soft sediment deformed Basinal Facies siltstone clasts evident surrounding it. (b) Massive megabreccia in the SW Myrtle Basin with clasts of dolomite that have abundant pseudomorphs after evaporitic gypsum (left of knife) derived from disaggregation of nearby BCDC Marginal/Platform deposits (see Fig. 9d). (c) Large crosscutting "dyke" of massive megabreccia (arrowed) penetrating the upper Basinal Facies deposits (~Caranbirini Member; bedded deposits right of centre) in the N Myrtle Basin. (d) Angular relationship due to overriding between two megaclasts of upper Basinal Facies in the N Myrtle Basin.

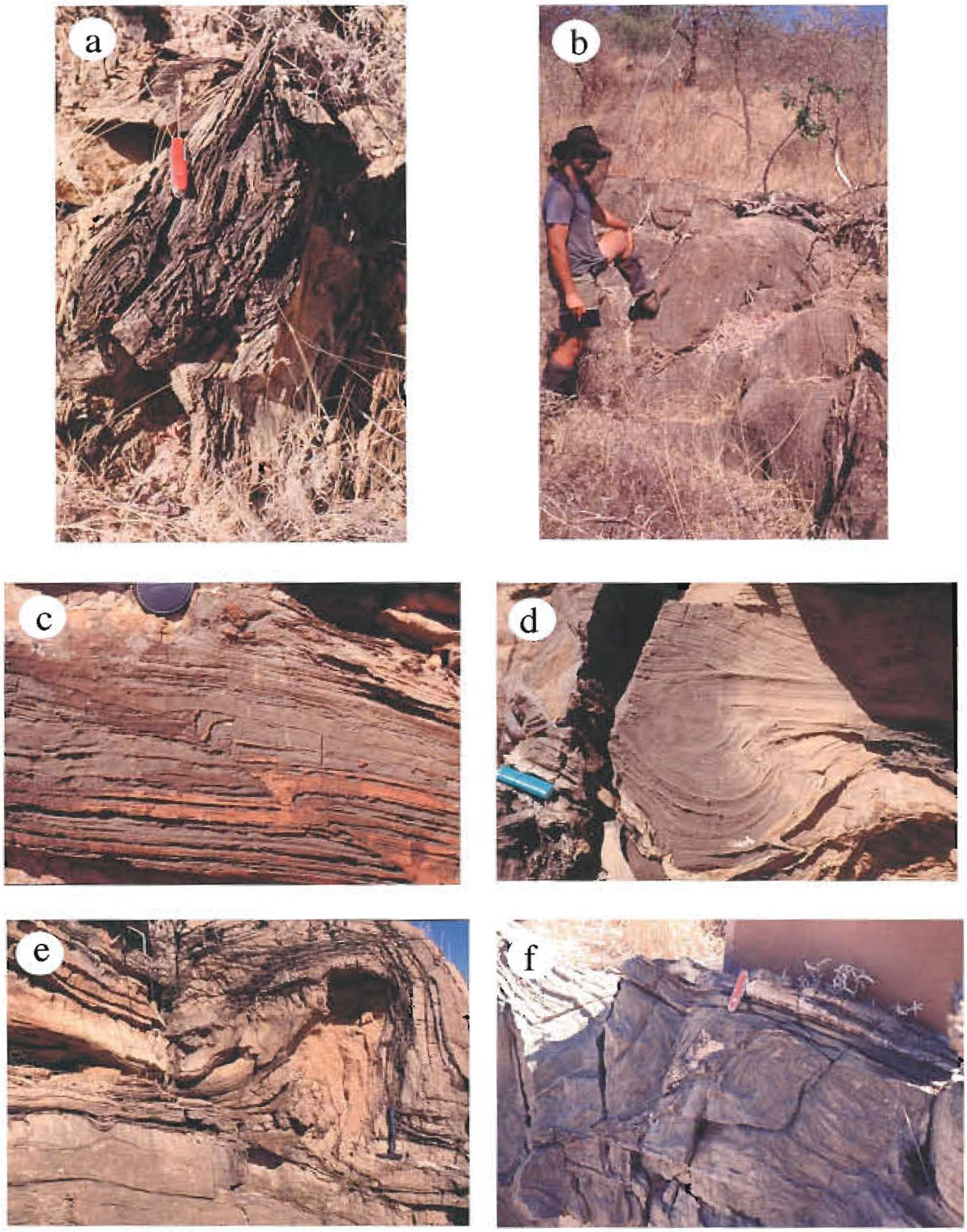

Figure 11 (a) Small upright isoclinal folds developed in the lowermost BCDC Basinal Facies deposits adjacent to the main NNW-trending fault at the western end of the SW Myrtle Basin area. (b) Large upright isoclinal fold hinge developed in the lowermost BCDC Basinal Facies deposits adjacent to a NNW-trending fault 3 km south of the SW Myrtle Basin area. (c) Small thrust fault and associated fold in BCDC Basinal Facies deposits in the SW Myrtle Basin area; ? soft-sediment or tectonic in origin. (d) Small thrusts and associated folds in BCDC Basinal Facies deposits in the SW Myrtle Basin area; ? soft-sediment or tectonic in origin. (e) Soft sediment fold in BCDC Basinal Facies deposits in the SW Myrtle Basin as evidenced by migration of dolomitic sandstone (pale bed left of hammer) into fold hinge; note also boudinage of nearest limb at lower left. (f) Slump in lower BCDC Basinal Facies deposits in the SW Myrtle Basin area as evidenced by the eroded fold hinges below planar contact to right of knife.

The detailed structure the SW Myrtle Basin as mapped for this study is presented in a map and accompanying cross-sections (Fig. 4). Important features to note are listed below.

- Deformation of the BCDC Basinal Facies is vertically inhomogeneous on either side of a high strain zone (?decollement) that locally defines the contact with the underlying Coxco Dolomite. A sliver of Basinal Facies preserved below this high strain zone, along the trace of the main NNW-trending fault at the western end of the mapped area (Fig. 5), is isoclinally folded about NNE-trending axes (Fig. 11a & b). However, the bulk of the Basinal Facies occur above the high strain zone where they occupy the open, E-W trending syncline (Fig. 4) originally mapped by Jackson et al. (1984).

- This main E-W-trending syncline is markedly assymetrical (Fig. 4), with dips on the southern limb of between 40 and 90° compared to dips on the northern limb of between 20 and 30°.

- The main E-W-trending syncline is overprinted by a series of open N-S-trending folds that have a wavelengths between 300 and 600 m (Fig. 4).

- The E-W-trending fault that separates the BCDC syncline from the older Tooganinie Formation to the south occupies a recessive valley. At one locality, poorly outcropping fault material gives a dip for the structure of 72° to the north (Fig. 4), which in combination with the current stratigraphic configuration, indicates a normal sense of movement. The fact that the high-relief source for the talus deposits appears to have been in the area where this structure intersected the zone of NNW-trending faults at the western end of the syncline, is interpreted to indicate that at least some of the normal displacement on this fault was syn-BCDC. Normal displacement on the NNW-trending fault was synchronous with that on the E-W fault from which they appear to splay.

- The geometry of the BCDC Basinal Facies package within the main E-W-trending syncline (Fig. 4) is as follows;

  In the western N-S cross-section it is thickest on the southern limb of the syncline and thins to the north.

  In the eastern N-S cross-section the thickness remains ~ the same from south to north.

  In the E-W cross-section it thins gradually from west to east.

- In terms of slope indicators, small scale thrusts and less commonly normal faults occur throughout the BCDC Basinal Facies (Fig. 11c & d). In general these are difficult to interpret, because in the absence of clear timing criteria, they could have been formed during the Isan Orogeny. However, unequivocal indicators of palaeoslope were observed at three localities;

  At the western end of the syncline, a flame structure at the base of a dolomitic mass flow in the lower middle part of the Basinal Facies section has a bent top indicating a current direction towards ~ 330°. Given the proximal setting the current direction is interpreted to represent the inclination of the palaeoslope.

  In the central part of the area, two areas of folding were documented, both within a few metres of the base of the Basinal Facies section. In both cases the deformation is clearly syn-sedimentary slumping, as indicated by the migration of dolomite sandstone into the fold hinge at the northern locality (Fig. 11e) and by erosion of the anticlinal fold hinge at the southern (Fig. 11f). These indicate a slope inclined to the N to NNW.

N Myrtle Basin

The general structure of the N Myrtle Basin consists of an ENE- to NE-trending syncline developed in stratigraphy mapped as Barney Creek Formation to the Hot Springs Member of the Lynott Formation (Jackson et al., 1984; Fig. 3). A NE-trending fault is mapped on the northern limb in an area of poor outcrop.

The detailed structure the N Myrtle Basin as mapped for this study is presented in a map (Fig. 6). Unfortunately the N Myrtle area does not much additional insight into basin development. This is because the Basinal Facies is recessive and poorly-outcropping and the other BCDC Facies are much more extensively brecciated than previously recognised. As a result, data such as unambiguous

slope indicators and the position and geometry of bounding (basin controlling) faults that is critical to the interpretation of basin-forming processes are not preserved. However, the area provides exposure to a higher stratigraphic level than the SW Myrtle Basin and has also provided considerable insight into the nature and origin of the spectacular megabreccia deposits. The interpretation of these deposits may have significant implications for the interpretation of the BCDC anywhere that breccias occur (eg. in the area of the HYC deposit) as discussed below.

Discussion

The Myrtle Basin area was chosen for study because E-W-trending structures are present at some distance from the major N-S-trending faults (?transfers; Etheridge and Wall, 1994), where Isan and possibly also earlier (?syn-BCDC; Hinman, 1995) wrench faulting complicate the structural history. As a result, the area was considered suitable to evaluate the E-W-trending folds and faults as syn-BCDC, basin-related structures. Detailed mapping of the SW Myrtle, and to a lesser extent the N Myrtle areas, has provided considerable constraints on the basin-forming process discussed below.

BCDC basin history

Integrated sedimentological and structural data from the SW Myrtle Basin indicate the following basin history during accumulation of the BCDC:

Initial subsidence controlling Coxco and subsequent Basinal Facies sedimentation occurred in the area where the main E-W-trending fault intersects NNW-trending faults.

Subsequent more widespread subsidence was controlled by the E-W-trending structure, which acted as a normal growth fault to the south of the developing depocentre. This resulted in the rapid development of a N-directed slope immediately adjacent to the fault, synchronous with the onset of more widespread Basinal Facies sedimentation. Syn-sedimentary slopes have also been documented from HYC, where deposition of the basal part of the HYC Pyritic Shale occurred on a substrate inclined to the NE (Hinman, 1995). This was interpreted to reflect tilting towards subsidence at the intersection of an E-W-trending growth fault and a NNW-trending transfer fault (~Emu Fault), situated to the NE of the deposit. In contrast, in the Myrtle Basin, the slope is inclined away from the main E-W-trending growth structure. In this case however, the slumped sediments occur effectively adjacent to the controlling fault. They are interpreted to represent the southern, probably steeper limb, of a hanging wall syncline developed at the edge of the subsiding tilt block in the general area of the present-day E-W-trending fault. Regionally, we would expect the situation to be similar to that at HYC, with the palaeoslope, in this case on the northern limb of the syncline, inclined towards the growth fault. However, no slope data was found from the northern limb to confirm this interpretation due to the poor outcrop on the more gently dipping N-limb of the syncline.

Subsidiary growth continued on the main NNW-trending cross-fault, as indicated by the fact that the talus, which must record maximum footwall relief, was sourced from the area where this structure intersects the main E-W-trending normal fault.

Following the first phase of Basin Facies sedimentation, generation of accommodation space on the controlling growth faults appears to have slowed for a period. This resulted in shallowing and the development of the complex facies mosaic mapped as the Reward Dolomite, that includes Deep and Shallow Subtidal and Peritidal Facies.

A renewed phase of subsidence resulted in the resumption of Basinal Facies sedimentation (~Caranbirini Member). These deposits appear to have acted as an aquaclude/seal, promoting the generation of high pore fluid pressures in the underlying units and ultimately carbonate megabreccia formation, although the timing of this event is uncertain. The significance of these deposits is discussed below.

The final phase of sedimentation once again records slowing of growth on the controlling faults with resultant shallowing to sub- to inter-tidal conditions. These units are mapped as Hot Springs Formation, and regionally they form the base of a thick package of sustained shallow water sedimentation (upper McArthur and Nathan Groups). They are therefore interpreted to represent infilling of the last of the tectonically formed accommodation space generated during the BCDC.

Effects of the Isan Orogeny

The Myrtle Basin was thought to be sufficiently far from the major N-NNW-trending structures that were subjected to wrench faulting and associated locally intense transpressional deformation during the Isan Orogeny. Nonetheless, Isan effects of are expressed in the BCDC Basinal Facies in the Myrtle Basin area, and the recorded strain shows a marked vertical inhomogeneity.

The most intense deformation is recorded in the lowermost laterally restricted Basinal Facies deposits that occur in the area where the main E-W-trending fault is cross-cut by NNW-trending faults. They are interpreted to represent depositional "sumps" formed during the initial subsidence of Coxco Dolomite blocks, and closed up during Isan shortening producing isoclinal folding and basin inversion (Winefield et al., 1997).

The more regionally extensive Basinal Facies blanket inferred to occupy a syn-sedimentary hanging-wall syncline, appears to have been separated from these more deformed underlying deposits by a decollement surface (Winefield et al., 1997). As a result, it was not deformed to the same degree during the Isan Orogeny. However, the steep dips of the basal Basinal Facies deposits on the southern limb (40 to 64°) are interpreted to be the result of significant tightening of the main syncline during the Isan event. This is because although there is significant syn-sedimentary slump folding of the partly-consolidated fine-grained sediments on this limb, there is no evidence of the large-scale gravitational collapse that would presumably have occurred if the steep dips were syn-sedimentary.

Significance of carbonate megabreccias

The only other area where breccias and megabreccias of the same scale as those developed in the Myrtle Basin have been described, is in the Barney Creek Formation in the area of the HYC deposit. At this locality, breccia units are mainly known from drillcore intersections in the immediate area of the mineralisation. In detail, three types of breccia have been identified (Walker et al., 1977) that have characteristic clast populations, stratigraphic distribution and isopach patterns indicating three different source areas in relation to the HYC deposit;

- Type I breccia beds occur in the lower half of the HYC Pyritic Shale Member and were interpreted to have been sourced from N-NE of HYC. This area has subsequently been implicated as the site of the intersection of the NNW-trending Emu Fault, with a major E-W-trending growth fault that has been proposed to extend to the west from the area immediately north of HYC, and which controlled sub-basin formation during accumulation of the Barney Creek Formation (eg. Hinman, 1995; Neudert and McGeough, 1996);
- Type II breccia beds are most common in the upper half of the HYC Pyritic Shale Member and were interpreted to have been sourced from an area SE of HYC;
- Type III breccia beds are confined to the uppermost part of the HYC Pyritic Shale Member and no definite source area was determined for these deposits.

Walker et al. (1977) interpret all three breccia types to "contain clasts characteristic of lithologies in formations of the McArthur Group below the Barney Creek Formation". Examples include;

The Type II breccia beds contain clasts of grey dololutite, some of which contain radiating acicular crystal pseudomorphs after gypsum. These are described as being similar to lithologies in the stratigraphically lower Emmerugga and Teena Dolomites, and on this basis are interpreted to have been derived from these units;

The type III breccia beds contain clasts of sandstone and quartzite, and K-feldspar-altered dolerite said to be characteristic of the Masterton Formation (now upper Tawallah Group). These units are therefore interpreted to have been sourced from erosion to a level below the base of the McArthur Group. The implication, if the entire McArthur and upper Tawallah Group stratigraphic package was present, is that by upper Barney Creek Formation time, > 2 km of stratigraphy had been uplifted and/or incised in the HYC area. This has undoubtedly contributed to the recent model for the formation of the sub-basin that hosts the mineralised Barney Creek Formation in the HYC area, that proposes relatively intense syn-sedimentary deformation (Hinman, 1995).

In terms of understanding the breccias in the Barney Creek Formation and adjacent units, the

Myrtle Basin area has two distinct advantages over the HYC area. Firstly, because the breccias are exposed at the surface, their nature and relationship to adjacent facies can be mapped and examined in detail. Secondly, the upper BCDC units (ie. those that overlie the Barney Creek Formation, usually mapped as Reward Dolomite and Lynott Formation) are preserved. In the HYC area the level of exposure is around the upper part of the Barney Creek Formation, and the upper units, if they were present, have been removed by erosion. As a result, the interpretation presented above of the Myrtle Basin breccia deposits may have significant implications for previous interpretations of the breccias at HYC.

It is evident from the talus deposits in the Myrtle Basin area that significant relief was generated during the BCDC basin-forming event, as has been implied at HYC. It has been proposed that the source for the talus blocks was an area of maximum relief to the SW of the exposed section. This corresponds to the site of intersection of an E-W-trending, north dipping growth fault and subsidiary NNW-trending growth structures that together controlled sub-basin formation. This is a virtual mirror image of the situation envisaged for the Type I breccia beds at HYC (Walker et al., 1977; Hinman, 1995; Neudert and McGeough, 1996), where the clasts are interpreted to come from a growth fault intersection N-NE of the deposit. In the case of the Myrtle Basin talus, the clast types present are sourced either from the BCDC itself, of from McArthur Group units immediately underling it (eg. Emmerugga Dolomite). This necessitates syn-sedimentary relief in the order of a few hundred metres.

In contrast, the stratigraphically higher megabreccia deposits in the Myrtle Basin comprise a diverse clast population. Overall, the megabreccia deposits include all of the lithologies described from the three types of breccia defined at HYC, except for the K-feldspar-altered dolerite clasts. In this case however, all of the clasts are demonstrably sourced from disaggregation of the complex mosaic of BCDC Facies deposits mapped as Reward Dolomite and the Caranbirini Member of the Lynott Formation. If these units were present in the HYC area, they have subsequently been removed by erosion. However, if the situation at BCDC time was in any way similar to that recorded in the Myrtle Basin area, then this potentially removes the need for the extreme amounts of uplift/incision currently envisaged to account for the derivation of the various clast types from the underlying stratigraphy. It follows that there may be no need to invoke the intense syn-sedimentary deformation proposed by Hinman (1995) to account for the current structural configuration of the HYC area. The latter may instead represent transpression during the Isan Orogeny, as has been documented to deform the same stratigraphy to a similar degree in the Top Crossing Region (Fig. 2).

Regional Stress Field

This Myrtle Basin study has produced the first detailed map of a BCDC depocentre away from the major ~N-S-trending (?transfer) faults. In terms of the implications for the regional stress field, at first pass, the apparent control of widespread Basin Facies sedimentation by an ~E-W-trending growth fault in the SW Myrtle area (Fig. 4) accords well with N-S extension models (Etheridge and Wall, 1994; Neudert and McGeough, 1996; Fig. 12a). However, because there is also growth on the associated NNW-trending splays, it is not possible to exclude the NNW-SSE compression model (Winefield et al., 1997; Fig. 1a), without proving that the syn-sedimentary displacement on the main E-W-trending structure did not involve a significant wrench component. This has not been possible due to poor outcrop in the fault zone, and the fact that the Tooganinie (?footwall) block immediately to the south is remarkably unaffected by minor structures. As a result, the BCDC depocentre in the SW Myrtle Basin could also be explained as a pull apart/releasing step over between NNW-trending strike-slip faults developed during regional NNW-SSE compression (Fig. 12b).

Conclusions

The Myrtle Basin is unique in that it is an area with locally continuous exposure where the BCDC is affected by E-W-trending folds and faults. Previous work had suggested that syn-BCDC structures that controlled basin formation should be of this orientation, associated with either broadly N-S extension (Etheridge and Wall, 1994; Neudert and McGeough, 1996) or broadly N-S compression

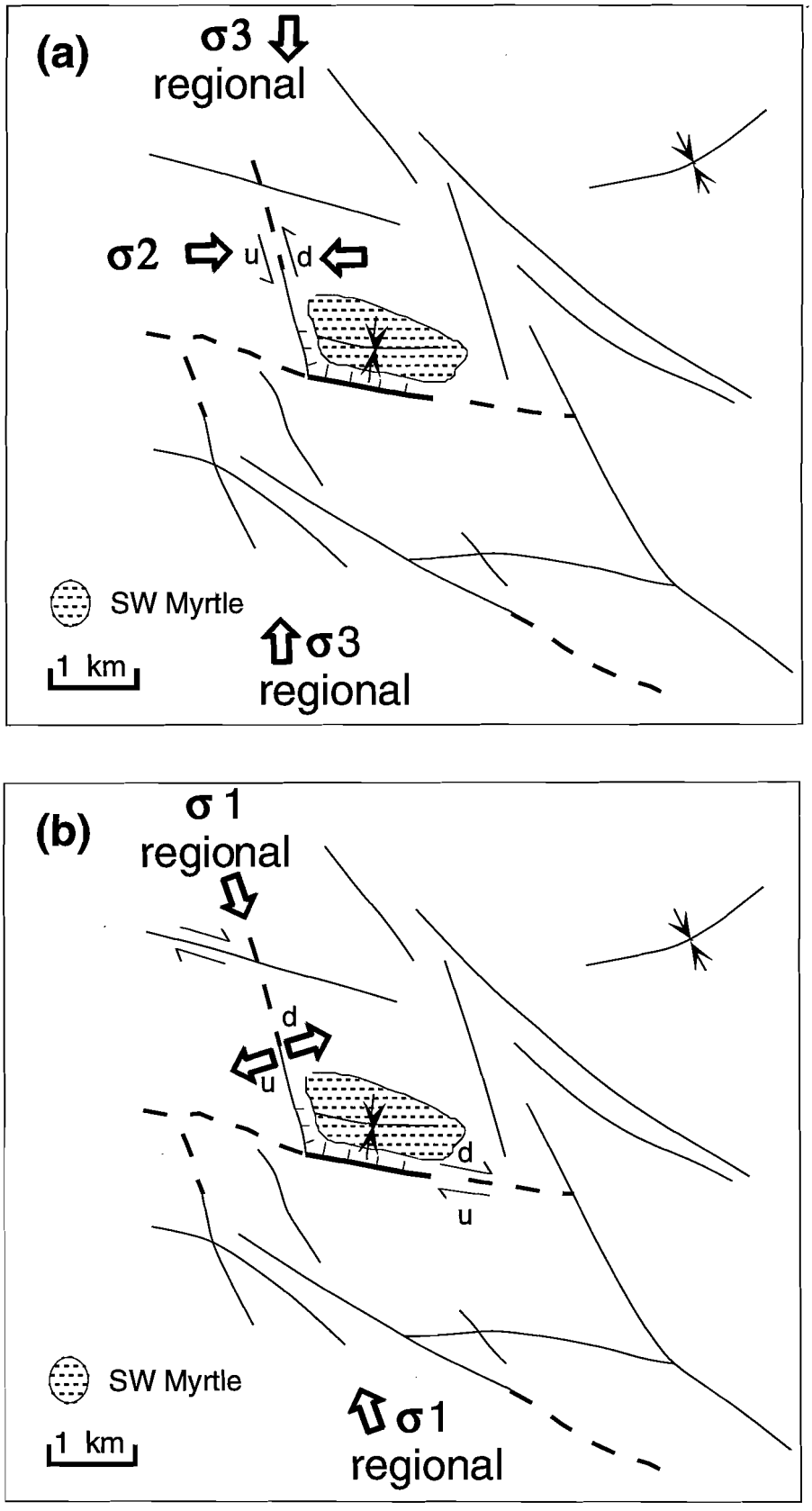

Figure 12. Schematic representation of the BCDC depocentre in the SW Myrtle Basin as: (a) A hanging wall syncline associated with a half graben developed adjacent to a N-dipping normal growth fault under conditions of ~N-S regional extension. (b) A pull apart/ releasing stepover, associated with strike-slip faulting on NNW-trending faults under conditions of regional NNW-SSE compression.

(Winefield et al., 1997). In addition, the Myrtle Basin is situated some distance from the major N-NNW-trending structures (eg. the Emu and Tawallah Faults), where the original basin geometries have been masked by major wrenching and associated transpressional folding during the Isan Orogeny, and possibly also at upper Barney Creek Formation time (Hinman, 1995). Integrated structural and sedimentological mapping and analysis of two sub-areas within the Myrtle Basin indicate the following:

1. Initial subsidence and basin formation was controlled by normal displacement on an E-W-trending growth fault and intersecting NNW-trending splay faults. This is the first example of a mapped syn-BCDC growth fault with an orientation consistent with a regional stress field comprising ~N-S extension as proposed by previous workers (Etheridge and Wall, 1994; Neudert and McGeough, 1996).

2. The earliest, and ultimately greatest normal displacement, occurred in the area where the E-W-trending growth fault intersected NNW-trending cross faults. This resulted in the generation of Basinal Facies "sumps" that were subsequently the sites of tight folding and basin inversion during the Isan Orogeny.

3. Later in the basin history, the same fault intersection was the source of talus blocks of underlying stratigraphy up to 7 m long indicating it was the site of maximum relief (~growth). Although the N-NNW-trending faults have been interpreted as transfers during McArthur Group deposition (Etheridge and Wall, 1994), they were clearly therefore also the sites of subsidiary syn-sedimentary growth in the Myrtle Basin area at least.

4. Subsequent more widespread Basinal Facies deposition was controlled mainly by the major E-W-trending growth fault. Slump folds at the base of this succession indicates the rapid development of a N-facing slope, now the southern limb of the open E-W-trending synclinal structure within which it occurs. This structure is interpreted to represent a syn-BCDC hanging wall syncline, subsequently tightened during the Isan Orogeny.

5. Overlying the basal Basinal Facies package (~Barney Creek Formation) is a complex dolomitic facies assemblage mapped as Reward Dolomite. It includes tabular bedded dolostone and dolomitic sandstone/gravel deposits (BCDC Deep Subtidal and Slope Facies respectively), plate breccias, microbially laminated and evaporitic units (BCDC Shallow Subtidal/ Peritidal Facies). Taken overall, this facies association represents a regression to above-wave base to intertidal conditions. A second cycle of flooding/transgression and subsequent regression generated the upper BCDC deposits consisting of an upper interval of sub-wave base Basinal Facies (~Caranbirini Member) overlain by another phase of Marginal/Platform sedimentation (~Hot Springs Member). The latter is considered to represent the infilling of the last of the tectonically formed accommodation space generated during the BCDC.

6. The geometry of the BCDC depocentre in the SW Myrtle area is consistent with either of the regional stress fields proposed (NNW-SSE compression or ~N-S extension), depending on the syn-sedimentary displacement on the main ~E-W-trending growth fault. This was unable to be determined in this study.

7. The BCDC stratigraphy in the Myrtle Basin area is host to considerable volumes of carbonate megabreccia. Similar units have previously been reported from the type section of the Caranbirini Member to the south of the Myrtle Basin (Jackson et al., 1987), however no analysis of these spectacular deposits was undertaken. Our study indicates that megabreccias occur over a considerably greater area, and affect a larger stratigraphic interval than was previously recognised.

8. The main level of brecciation begins above the basal Basinal Facies package (~Barney Creek Formation) in the lithologically diverse overlying package mapped as Reward Dolomite. However,

upward penetrating "dykes" of breccia locally subdivide the upper Basinal Facies package (~Caranbirini Member) into mega-clasts tens of metres long, and the overlying Shallow Subtidal/ Peritidal Facies (~Hot Springs Member) are also locally brecciated.

9. The carbonate megabreccias are interpreted to represent the sudden release of overpressured pore fluids in the Platform/Marginal and especially the porous Slope Facies deposits. The overpressure is thought to have developed because the overlying upper Basinal Facies siltstones (~Caranbirini Member), acted as an aquaclude during burial of the water-saturated sediment pile. As such, the megabreccias are clearly intraformational, with the clasts sourced from in-situ disaggregation and local transport of the various BCDC facies in which they occur.

10. Breccias similar to those from the Myrtle Basin occur in the Barney Creek Formation at HYC. Current models invoke intense syn-sedimentary deformation, accompanied by > 2 km of incision/ uplift to explain the wide variety of clast lithologies present in the breccias. Current exposure in the area of the HYC deposit is around the level of the upper Barney Creek Formation, and the upper BCDC units, if they were ever present, are not preserved. However, if the situation during BCDC-time was similar to that documented from the Myrtle Basin, these lithologically variable upper BCDC units would have provided an alternative source for the breccia clasts, making the dramatic syn-sedimentary tectonism currently proposed unnecessary.

References

Etheridge, M. and V. Wall. 1994. Tectonic and structural evolution of the Australian Proterozoic. Geol. Soc. of Aust. Abst. 37, 102-103.

Hinman, M. C. 1995. Base metal mineralisation at McArthur River: Structure and kinematics of the HYC-Cooley zone at McArthur River. AGSO Record 1995/5.

Jackson, M. D., M. M. D., et al. 1984. 1:100 000 scale Geology of the Abner Range region.

Jackson, M. J., M. D. Muir, et al. 1987. Geology of the southern McArthur Basin. B. M. R. Bull. 220, 173 pp.

Neudert, M. and M. McGeough. 1996. A new tectonostratigraphic framework for the deposition of the upper McArthur Group, N. T. New Developments in Metallogenic Research: The McArthur-Mount Isa-Cloncurry Minerals Province, MIC 96 Extended Abstracts. EGRU Contribution 55, 90-93.

Rogers, J. R. 1996. Geology and tectonic setting of the Tawallah Group, southern McArthur Basin, Northern Territory, University of Tasmania, 234pp.

Spence, G. H. and M. E. Tucker. 1997. Genesis of limestone megabreccias and their significance in carbonate sequence stratigraphic models: a review. Sed. Geol. 112, 163-193.

Winefield, P., D. Selley, et al. 1997. Day 6 and Day 7 - McArthur Basin. CODES: AMIRA/ARC Project P384A Report 4; Sponsors Field Meeting. , 53-85.

Walker, R. N., R. G. Logan, et al. 1977. Recent geological advances concerning the H.Y.C. and associated deposits, McArthur River, N.T. J. Geol. Soc. Aust. 24, 365-380.

BCDC basin evolution: implications of macroscopic compressional geometries

David Selley
North Limited

Introduction

Detailed analysis of BCDC facies architecture has revealed a complex sub-basin geometry controlled by the interplay of major NW- to NNE-striking fault zones and roughly E-W trending "hinge zones" or growth faults (Etheridge and Wall, 1994; Hinman; 1995; Neudert and McGeough, 1996; Winefield et al., 1997; Bull and Scott, this report). Unequivocal lateral facies variation (ie. deepening of BCDC depocentres) occurs in association with E-W structures west of HYC, at the Kilgour Gorge and at SW Myrtle Basin. However in terms of generating basin foundering maxima, these structures were sub-ordinate to major NW- to NNE striking fault zones. Within individual sub-basins, the greatest accumulation of lower BCDC strata at least, occur adjacent to fault segments which presently strike NW to N (eg. Emu Fault Zone, between HYC and Caranbirini; Tawallah Fault Zone at Top Crossing; Hot Springs Fault Zone at Leila Hill and sub-ordinate N-S structures at SW Myrtle Basin).

Various regional tectonic models which have been proposed to account for this basin architecture include: (1) regional strike-slip activation of major NNW- to NNE-striking fault zones and generation of proximal pull-apart sub-basins partly bounded by ENE-growth faults (Jackson et al. 1987; Davidson and Dashlooty, 1993). (2) regional N-S extension in which the major NNW- to NNE-striking fault zone acted as "passive" transfers to an E-W striking growth fault system (Etheridge and Wall, 1994). (3) regional NNW-SSE to NE-SW compression in which accommodation space was generated along NW- to NNW-striking transtensional segments of major N-S striking fault zones (?tear faults) and/or intersection of these segments with ENE-trending synclinal flexures (Winefield et al., 1997). Evidence for regional compression included thrust architecture at Kilgour Gorge and local uplift/ non-deposition along NNE striking segments of the Tawallah Fault Zone. Work carried out during this final field season, however, has indicated that at least some E-W structures are most likely to have undergone an extensional history during BCDC time (ie. SW Myrtle Basin) and that if NW-SE compression did occur, it was only local. This outcome is in accordance with Hinmans (1995) detailed analysis of the meso- and macroscopic structure around HYC, in which he postulated that localised transpression/transtension (accommodating local NW-SE shortening ~ NE-SW extension) occurred along the Emu Fault Zone during deposition of the BCDC. Critical to these latter two models, which invoke elements of shortening, is the recognition of macroscopic compressional geometries at BCDC basin margins and the interpretation that associated compressional structures were active and controlling sub-basin geometry during BCDC time.

The interpretation of macroscopic compressional syn-BCDC structural geometries is of fundamental importance to the tectonic development of the McArthur Basin, as a purely extensional regime becomes effectively impossible. The generation of large scale compressional structures which root into basement, even locally such as at HYC, demands at least some component of regional shortening. The remainder of this paper critically addresses the validity of the interpretation of compression during deposition of the BCDC.

Compression at BCDC time: did it exist?

Compressional structures including thrusts, high angle reverse faults, high amplitude close to isoclinal fold and locally developed cleavage are commonly developed in the vicinity of demonstrative BCDC sub-basin margins. In most cases, these structures can be attributed to phases of the Isan Orogeny (eg. Top Crossing: Fig. 2a. Bull and Scott, this report). However at three known localities, evidence (both circumstantial and direct) exists in support of syn-BCDC compression, although as discussed below, this evidence remains equivocal.

HYC

The most convincing example of syn-BCDC compression occurs at HYC and involves two lines of evidence. Firstly, clast-types (including altered dolerite clasts) within breccia units hosted by Barney Creek Shale have been interpreted to record progressive exhumation of levels of stratigraphy as low as the Tawallah Group (Walker and Logan, 1977; Hinman, 1995). This interpretation demands a significant component of shortening across the Emu Fault Zone and at least 2 km of tectonic uplift. The validity of this interpretation has, however, been questioned by Bull and Scott (this report), who document intrabasinally-derived breccia units containing a diversity of clast lithotypes within upper BCDC strata at the Myrtle Basin. They indicate that breccias at HYC may be of a similar origin, hence negating the requirement for significant uplift along the Emu Fault Zone. It is important to note however, that the presence of dolerite clasts remains a problem, and that the lack of evidence for mafic magmatism within BCDC strata or immediately underlying strata must be resolved if breccia units at HYC are considered to record either intrabasinal reworking or minor basement uplift.

The second and more rigorous line of evidence for compression at HYC, is the apparent upward decrease in strain within pre- and syn-BCDC strata, and most importantly the interpretation of an unconformable relationship between flat-lying Upper Barney Creek Shales and an inverted fault block comprising ?folded and brecciated Teena and Emmerugga dolomites (ie. Western Fault Block). This relationship is shown in Figure 1, with the interpretation outlined therein demonstrating onlap of upper BCDC strata on a reverse fault zone which thrusts "basement" over lower BCDC strata. This interpretation can only be discounted if: (i) evidence of strain can be demonstrated at the base of the Upper Barney Shales (ie. the "unconformity" is in fact a thrust), or (ii) the Mt Stubbs Fault Zone (ie. western margin of the inverted basement block) can be shown to have an extensional history during BCDC time and that the brecciation in the basement block is largely the result of growth faulting.

Although we have had no access to this data and hence can only speculate on the possible basin history in this region, we consider that as the critical relationships are unexposed and intersected only in a small number of diamond drill holes, potential exists for re-interpretation. Furthermore, our field mapping has indicated that similar geometries and apparent unconformable relationships are a characteristic result of Isan inversion and sinistral strike-slip reactivation of N-S striking BCDC basin margins. In examples of inverted growth faults at Top Crossing, Kilgour Gorge, the lower Kilgour River and SW Myrtle Basin, a marked vertical contrast in the level of strain was recognised. Figures 2 and 3 show that lower BCDC strata adjacent to inverted transfer zones (across which there has been growth) are tightly to isoclinally folded about sub-vertically to steeply inclined axial surfaces, whereas upper BCDC strata are relatively undeformed. In all cases, the upward decrease in strain is either progressive, or sharply bounded by sub-horizontal thrust surfaces. There is no direct evidence for unconformities between highly strained lower BCDC strata and overlying weakly deformed or flat-lying strata. Due to the rheological character of the thinly-bedded, relatively incompetent BCDC strata, thrusts rapidly shallow upward and outward from the inverted fault zone into bedding surfaces producing a positive flower geometry.

The kinematics of Isan inversion structures at the localities described above are also compatible with those recorded at HYC. Hinman (1995) interpreted two phases of syn-BCDC inversion: (i) an early NW-SE shortening phase, in which transport was directed NW, away from the Emu Fault Zone; and (ii) a second NE-SW shortening phase which resulted in SW-directed transport. Mescoscopic folds, which affect

stratigraphic levels at least as high as the lower Hot Springs Member at Kilgour Gorge, are also indicative of transport directions away from fault zones inverted during the Isan Orogeny. In Figure 2, the distribution of asymmetric folds record predominant NNW- to WNW- directed transport (F2A and F2B respectively) followed by SW-directed transport (F3) to the west of the inverted fault zone. To the east of the fault zone, F2 transport directions range NW to ESE and SE, whereas NE-transport occurred during D3. The transport directions recorded at both the Kilgour Gorge and lower Kilgour River locations are consistent with Isan D1 N-S compression and D2 E-W compression (O'Dea and Lister, 1997).

Kilgour Gorge

The fundamental basin architecture at Kilgour Gorge involved a N-dipping palaeoslope upon which BCDC Slope Facies strata accumulated (Winefield et al., 1997). A roughly E-W trending basin margin occurred in the southern part of the area, upon which BCDC Platform Facies was deposited. In the latter phase of BCDC deposition, this margin was inferred to have become emergent, with erosion of Teena and possibly older strata. Coincidence of major thrusts within pre-BCDC strata (Fig. 2) with this basin margin led Winefield (op cit.) to argue that the BCDC accommodation space was a small depression developed in front of a rising thrust culmination.

Evidence considered to support the above interpretation included the fact that major thrust surfaces do not penetrate or result in significant structural thickening of the BCDC stratigraphy. As shown in Figure 2 however, minor Isan thrust surfaces do penetrate lower levels of the BCDC stratigraphy and furthermore, major deep seated thrusts affecting lower levels of the stratigraphy could also be explained in terms of a flower geometry associated with Isan inversion. In order to demonstrate unequivocal syn-BCDC activation of deep-seated thrusts, it is necessary to document an unconformable relationship of BCDC strata above thrusted Teena and Emmerugga dolomites (c.f. HYC). Such a relationship is not known to exist.

Tawallah Fault Zone

The effects of local changes in geometry of major N-S striking fault systems on basin architecture was demonstrated along the Tawallah Fault Zone by Winefield et al. (1997). They documented systematic variance of BCDC facies with changes in the present day strike of the Tawallah Fault Zone from NNW to NE. Localised extension and growth during lower BCDC time was restricted to NNW-striking segments (ie. southern Top Crossing area), whereas sites of non-deposition or condensed BCDC stratigraphy coincided with NNE- to NE-striking fault segments (northern Top Crossing and Leila Creek). This relationship between facies architecture and fault geometry was considered to reflect interplay between local transtension (NNW- striking basin foundering domains) and local transpression (NE-striking basin highs) in response to sinistral activation of the Tawallah Fault Zone under regional NW-SE shortening. This model is in accordance with the local stress-field documented by Hinman (1995) at HYC, but does not invoke the same degree of syn-BCDC inversion as that interpreted along the Emu Fault Zone.

The main potential flaw in the model is that no direct evidence exists which proves that the present day trace of the Tawallah Fault Zone was the same as that during BCDC deposition. It can be shown however, that at Top Crossing at least, the marked swing of the Tawallah Fault from NNW to NE did exist during the earliest phase of the Isan Orogeny. Cross sections shown in Bull and Scott (this report) Figure 2a demonstrate a progressive increase in Isan strain from NNW- to N- to NE-striking segments of the Tawallah Fault (sections C-Cí; A-Aí; B-Bí respectively).

Discussion

The review of compressional structures presented above indicates that unequivocal evidence for syn-BCDC regional shortening has yet to be identified. In all cases, arguments can be mounted in which macroscopic compressional structures were generated largely during Isan orogenic episodes. We believe, however, that there is sufficient circumstantial evidence to militate against sub-basin geometry during BCDC time having formed under a regional N-S extensional stress field (eg. Etheridge and Wall, 1994). Firstly, the consistent occurrence of

basin foundering maxima adjacent to roughly N-S striking fault segments (regardless of whether or not they were major, deep seated pre-existing crustal-scale fractures), strongly implies that these were the dominant basin-controlling structures. E-W trending structures, whether growth faults or thrust culminations, were sub-ordinate and probably less continuous than N-S structures. Secondly, the association of BCDC basinal highs with NNE- to NE-striking fault segments is inconsistent with regional N-S extension. Under such a stress field, these structures would have been oriented within the extensional field of strain and would, therefore, be expected to have failed as growth faults. Finally, although we have expressed doubt concerning the degree of inversion interpreted along the Emu Fault Zone at HYC, it cannot be discounted without further review of data.

Considering all elements of basin architecture discussed in the preceding sections, the favoured model for the tectonic framework during BCDC time is local basin foundering in response to strike-slip activation of major N-S striking strike-slip fault zones (ie. Emu and Tawallah Fault Zones). The inferred regional stress field during this event involved a NW-SE directed maximum principal stress and a NE-SW directed minimum principal stress. This model has gross similarities to those of Jackson et al. (1987), Davidson and Dashlooty (1993) and Hinman (1995) in which accommodation space was generated within pull-apart sub-basins and/or fore-deeps associated with thrust culminations along trans-tensional NNW- and transpressional NE-striking fault segments respectively.

References

Davidson, G. J. and S. A. Dashlooty. 1993. The Glyde Sub-basin: a volcaniclastic-bearing pull-apart basin coeval with the McArthur River base-metal deposit, Northern Territory. A. J. E. S. 40, 527-543.

Etheridge, M. and V. Wall. 1994. Tectonic and structural evolution of the Australian Proterozoic. Geol. Soc. of Aust. Abst. 37, 102-103.

Hinman, M. C. 1995. Base metal mineralisation at McArthur River: Structure and kinematics of the HYC-Cooley zone at McArthur River. AGSO Record 1995/5.

Jackson, M. J., M. D. Muir, et al. 1987. Geology of the southern McArthur Basin. B. M. R. Bull. 220, 173 pp.

Neudert, M. and M. McGeough. 1996. A new tectonostratigraphic framework for the deposition of the upper McArthur Group, N. T. New Developments in Metallogenic Research: The McArthur-Mount Isa-Cloncurry Minerals Province, MIC 96 Extended Abstracts. EGRU Contribution 55, 90-93.

O'Dea, M. G., G. S. Lister, et al. 1997. Geodynamic evolution of the Proterozoic Mount Isa Terrain. Orogeny through time. J.-P. Burg and M. Ford, Geological Society Special Publication. 121, 99-102.

Rogers, J. R. 1996. Geology and tectonic setting of the Tawallah Group, southern McArthur Basin, Northern Territory, University of Tasmania, 234pp.

Spence, G. H. and M. E. Tucker. 1997. Genesis of limestone megabreccias and their significance in carbonate sequence stratigraphic models: a review. Sed. Geol. 112, 163-193.

Winefield, P., D. Selley, et al. 1997. Day 6 and Day 7 - McArthur Basin. CODES: AMIRA/ARC Project P384A Report 4; Sponsors Field Meeting. , 53-85.

Walker, R. N., R. G. Logan, et al. 1977. Recent geological advances concerning the H.Y.C. and associated deposits, McArthur River, N.T. J. Geol. Soc. Aust. 24, 365-380.

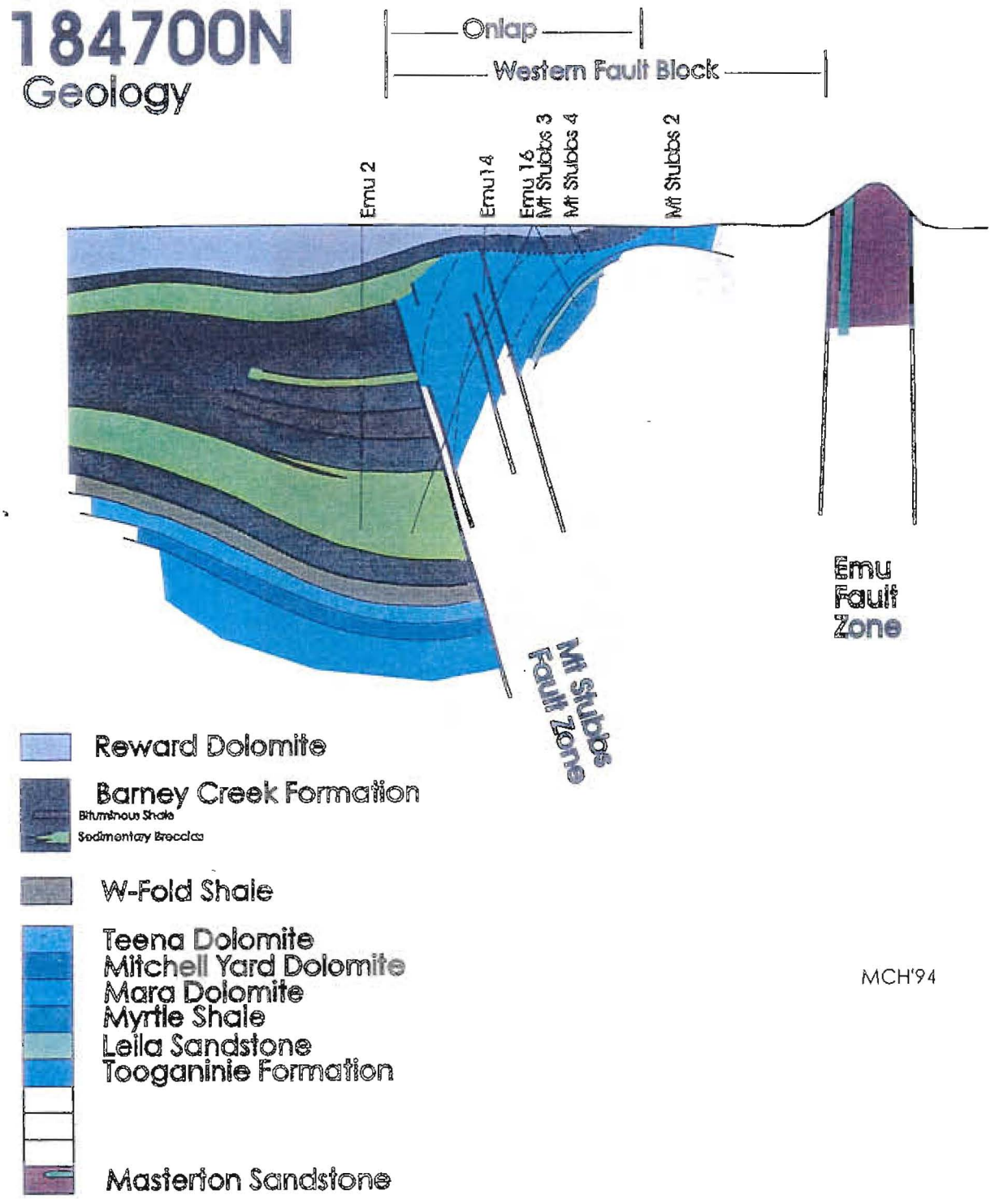

Figure 1. Section 184700N geology (after Hinman, 1995).

Kilgour Gorge Section

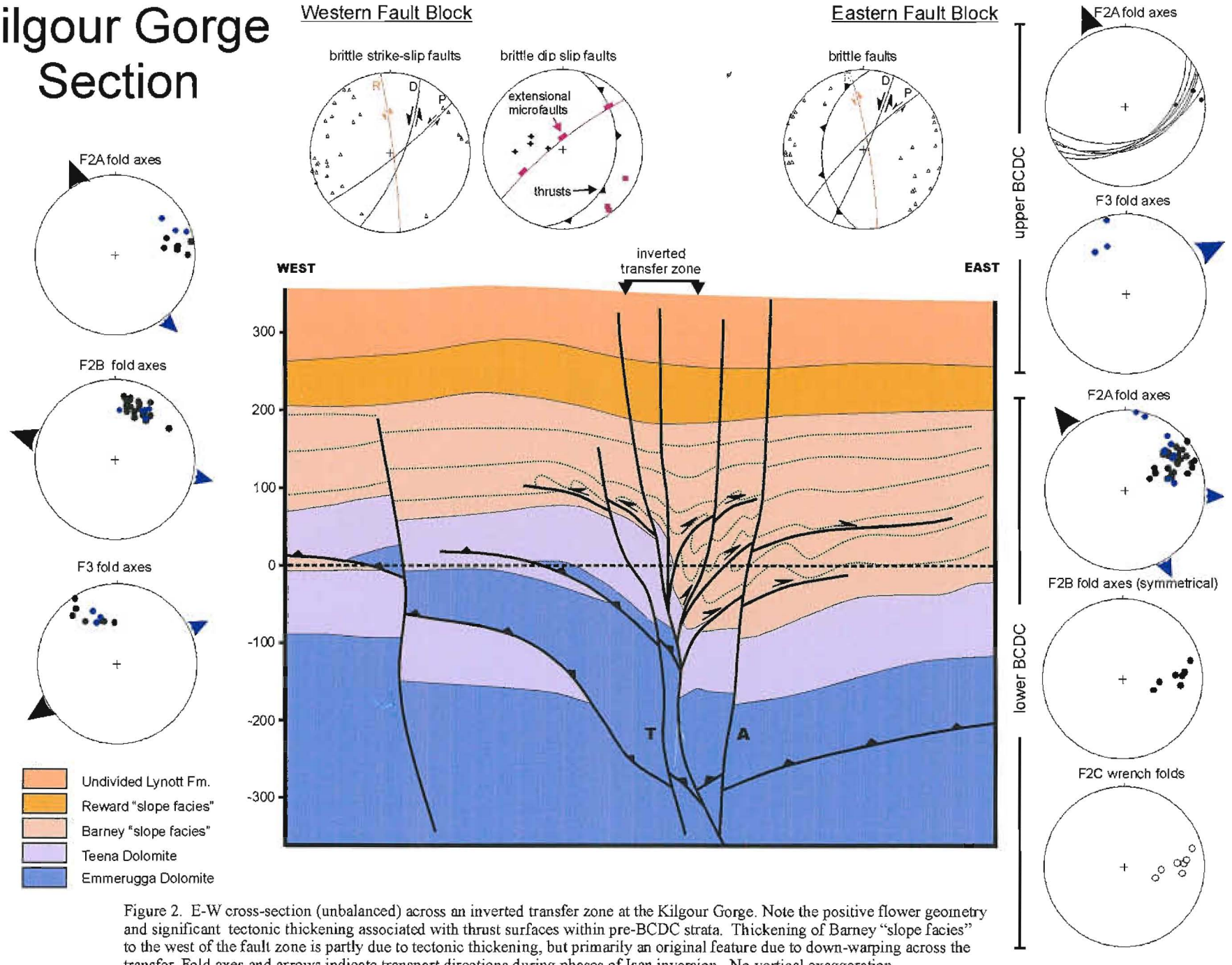

Figure 2. E-W cross-section (unbalanced) across an inverted transfer zone at the Kilgour Gorge. Note the positive flower geometry and significant tectonic thickening associated with thrust surfaces within pre-BCDC strata. Thickening of Barney "slope facies" to the west of the fault zone is partly due to tectonic thickening, but primarily an original feature due to down-warping across the transfer. Fold axes and arrows indicate transport directions during phases of Isan inversion. No vertical exaggeration.

Kilgour River Section

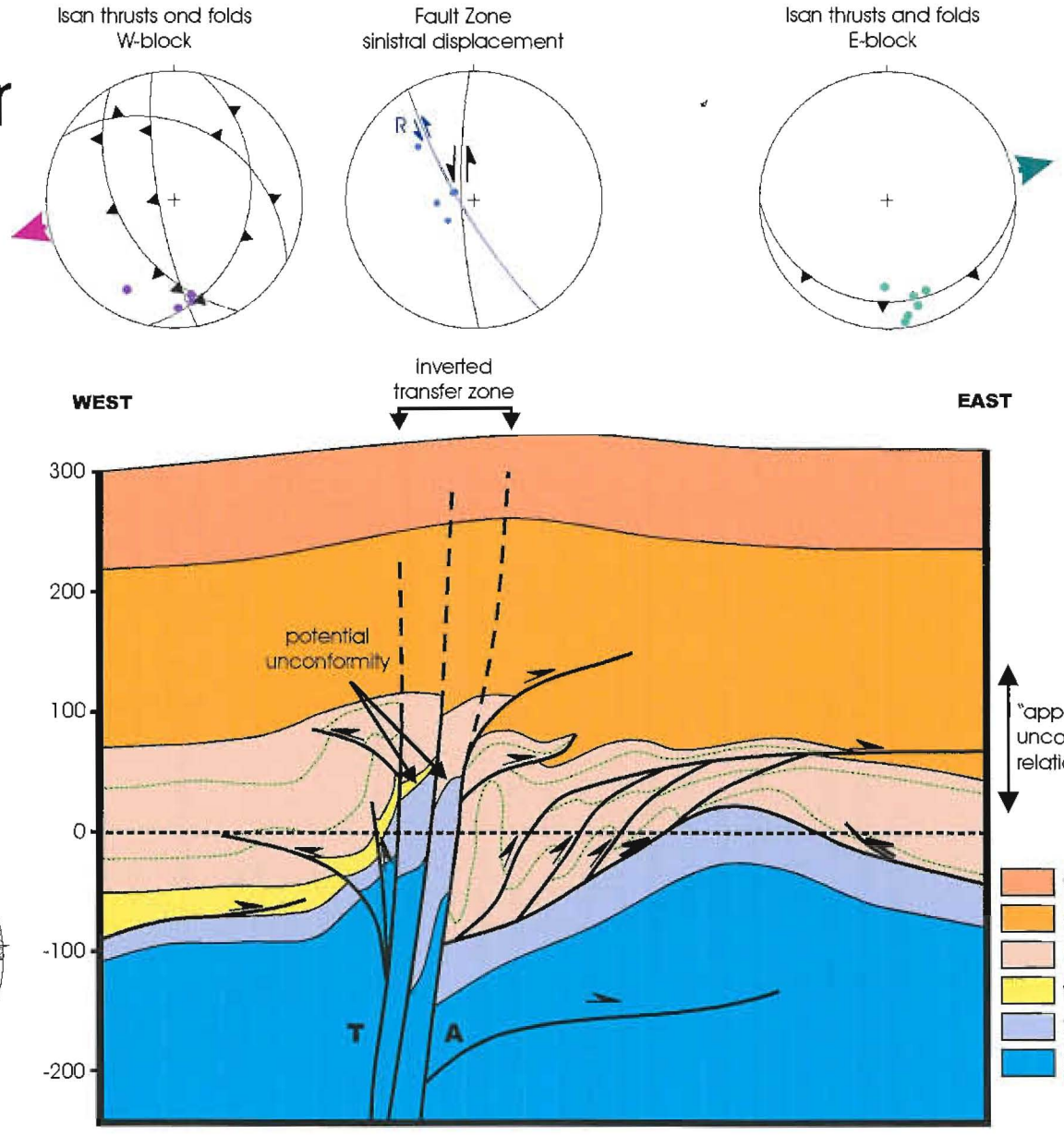

3. E-W cross section (unbalanced) through BCDC strata adjacent to the Kilgour River near 8160000N:6055000E. Growth on the fault zone at the centre of the section is indicated from restriction of "transitional facies" (W-fold Shale equivalent) to the western, down-thrown block. TFigure he orientation of syn-BCDC folds and neptunian dykes within Coxco Member indicate components of both N and ESE transport during sub-basin development. Isan inversion of the fault zone has resulted in high amplitude isoclinal folding of lower BCDC strata, whereas upper BCDC remain relatively undeformed. This vertical partitioning of strain gives the appearance of an unconformity near the base of Reward "slope facies". No vertical exaggeration.

Sedimentology of the Torpedo Creek Quartzite in the Lady Loretta area; implications for the tectono-sedimentary setting of northern Australian Proterozoic Zn-Pb-Ag deposits

Stuart W Bull
Centre for Ore Deposit Research

Introduction

The Lady Loretta Deposit is a relatively small but high grade sediment-hosted base metal deposit (8.3 Mt at 18.4% Zn, 8.5% Pb and 125 g/t Ag; Hancock and Purvis, 1990). The mineralization occurs within the Mount Isa Group equivalent McNamara Group, approximately 115 km NNW of Mount Isa Mine (Fig. 1).

Recent sedimentological work on the Lady Loretta Formation that hosts the mineralisation, concludes that the package in the mine area is indistinguishable, in terms of thickness and sedimentary facies, from the formation regionally (Dunster, 1996; Dunster and McConachie, 1998). This observation apparently invalidates prior models for the setting of the mineralisation, that have proposed a genetic link with the development of a local basinal feature, termed the "Paradise Creek Graben" (Dunnet, 1976), for which various orientations and scales have been proposed (eg. Large, D. E., 1980; Amade, 1986; Lemcke, 1986; Dunster and McConachie, 1998; Fig. 2). Structures interpreted as growth faults active during the basin-forming event (eg. the Carlton Fault; Large, D. E., 1980) were envisaged to have been the conduits for mineralising fluids.

Given the apparent absence of growth-faulting and graben formation, the Lady Loretta Formation appears to have accumulated during a period of relative tectonic quiescence. As a result, twin problems arise with regard to the base-metal mineralisation; what controlled the deposition of the host "trap" rocks?; and what were the conduit/s for the mineralising fluid?

In order to address this important question, this study was initiated to examine the setting of the Lady Loretta mineralisation in the broader context of its position within the lower McNamara Group stratigraphy. Previous studies have shown the potential of the basal sandstone units, for example the Masterton Sandstone at the base of the McArthur Group in the southern McArthur Basin, to record the initial tectonic regime of the basin phase in which they occur (Bull and Rogers, 1996). Specifically, facies and palaeocurrent patterns within these clastic units have proved critical in determining which faults were active during sedimentation, because these sedimentary features are preserved, even where the original structural and stratigraphic framework has

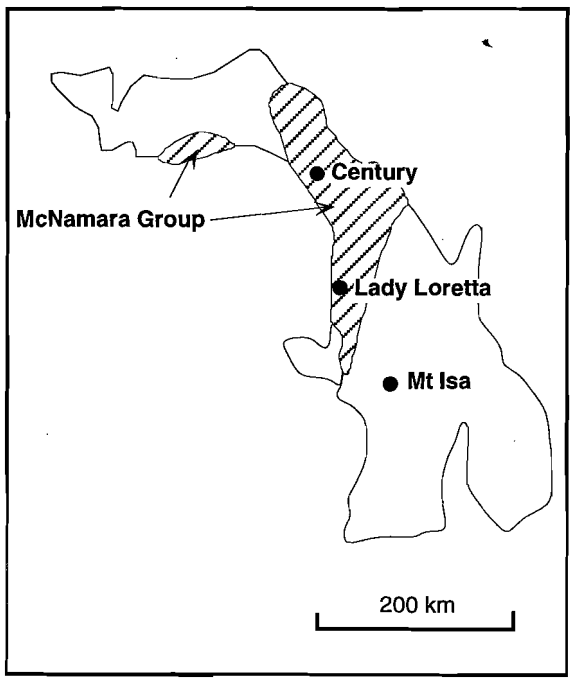

Figure 1. Location of the Lady Loretta, Mount Isa and Century deposits.

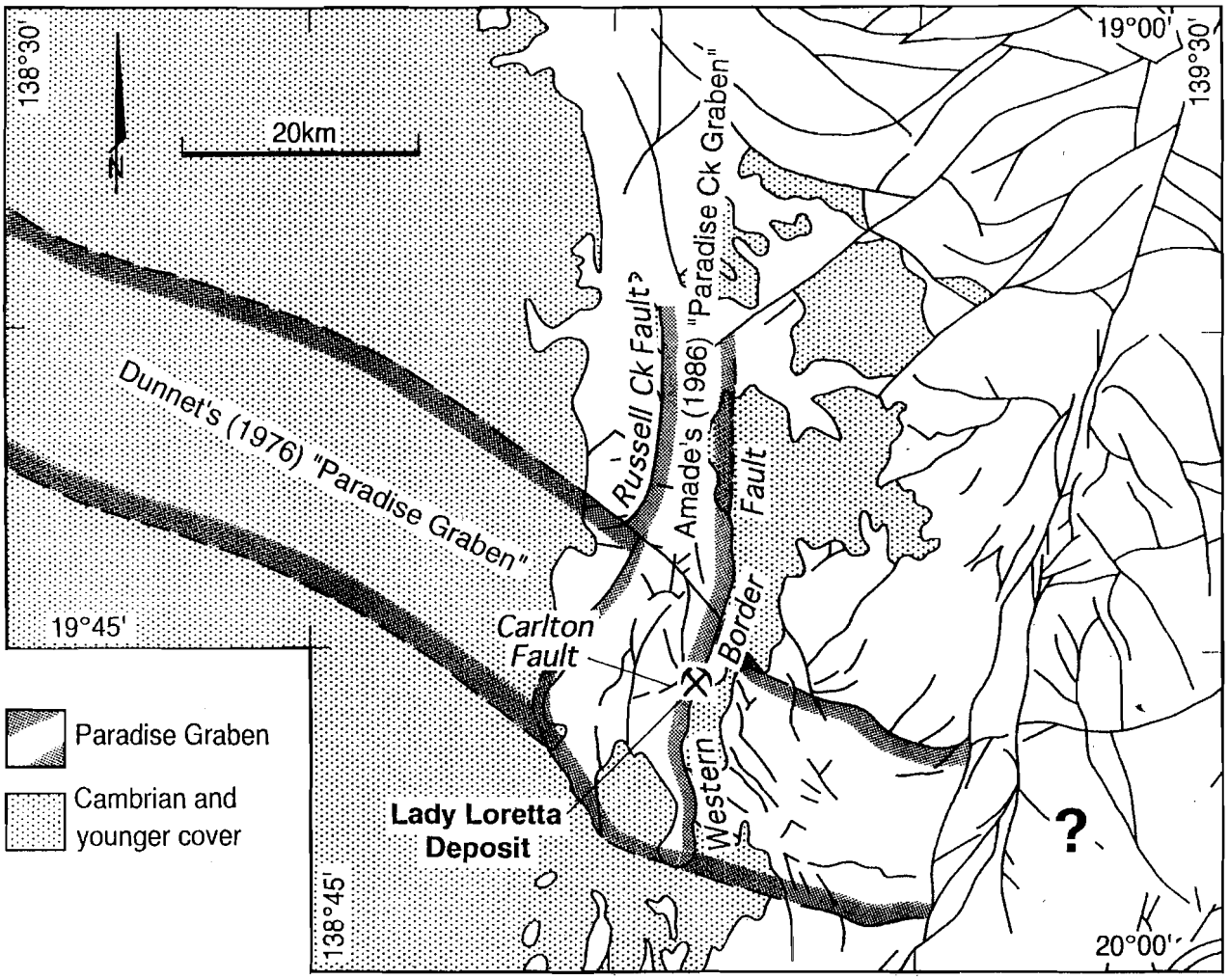

Figure 2. Schematic representation of the proposed locations/orientations for the Paradise Graben in the Lady Loretta area (after Dunster and McConachie, 1998).

been extensively modified by subsequent tectonic events. As a result, the basal unit of the McNamara Group, the Torpedo Creek Quartzite which outcrops to the north and east of the Lady Loretta deposit, was targeted for sedimentological examination.

Geological setting

The Mount Isa Inlier (Blake, 1987; also variously referred to as "Basin" and "Terrain") has been mapped in terms of a number of tectonic elements bounded by regional faults. The stratigraphy within these elements that post dates the ~1870 Ma Barramundi Orogeny has been subdivided into three tectono-stratigraphic packages, termed Cover Sequences 1, 2 and 3. The Lady Loretta deposit occurs towards the southeastern end of the westernmost tectonic element, the Lawn Hill Platform. Outcropping units in this area are restricted to Cover Sequence 3 of the Blake (1987) classification scheme (cf. Discussion section below).

The regional geological framework of the Lady Loretta area outlined below, is summarised after the Mammoth Mines 1:100,000 scale geological map and its accompanying explanatory notes (Hutton and Wilson, 1985). In general, the clastic units locally form resistant ridges, however, exposure of the fine-grained carbonate-dominated units is poor due to a deeply developed weathering profile. The oldest unit exposed, the Surprise Creek Formation, is a fine- to medium-grained quartzo-feldspathic sandstone. Its base is not exposed in the Lady Loretta area, but at other localities it unconformably overlies older Cover Sequence 3, and in some cases Cover Sequence 2 units. Conglomerate facies are present locally, and stromatolitic dolomitic siltstone interbeds in the upper part of the unit are interpreted to represent a transgression from fluvial to shallow marine conditions.

The Surprise Creek Formation is overlain, with mild angular unconformity, by the McNamara Group. The basal unit, the Torpedo Creek Quartzite, is a sequence of up to 420 m of coarse-grained clastics that forms the main focus of this study. Lithologies range from poorly-sorted pebble to boulder conglomerate to quartz sandstone, and regionally the unit is interpreted as the product of a range of environments from alluvial fan to shallow marine settings. In the Lady Loretta area, the Torpedo Creek Quartzite is conformably overlain by the Gunpowder Creek, Paradise Creek, Esperanza and Lady Loretta Formations. Overall, this interval is informally referred to as the lower McNamara Group.

The Gunpowder Creek Formation comprises shallow marine deposits that accumulated after a transgression that began in late Torpedo Creek Quartzite time. It has been subdivided into; a lower part consisting of up to 630 m of red and green micaceous siltstone and fine-grained micaceous sandstone; and an upper part consisting of 140 m of dolomite and variably carbonaceous dolomitic siltstone. The remaining three units of the lower McNamara Group, the Paradise Creek, Esperanza and Lady Loretta Formations, are comprised of different combinations of the same shallow marine to locally emergent facies. These include; sub-tidally deposited, variably dolomitic and carbonaceous siltstones; and inter- to locally supra-tidally deposited, variably stromatolitic and evaporitic dolomites, sandstones and siltstones.

Torpedo Creek Quartzite outcrops in two discrete areas were examined for the purpose of this study. In the immediate Lady Loretta region, the unit crops out at four localities to the north of the deposit (Hutton and Wilson, 1985; Fig. 3). In each case it occurs as a thin but laterally persistent selvedge adjacent to the northern and/or western edge of blocks of the underlying Surprise Creek Formation. These block lie within a 120 km long, 10-15 km wide, N-S trending zone of folding, shearing and faulting informally termed the Paradise Creek High Strain Zone (Keele et al., 1996). This zone, bound by the Russell Creek Fault to the west and by the Western Border Fault to the east (Fig. 3), has been the site of considerable E-W shortening (~25-30%) during the Isan Orogeny. As a result, the Surprise Creek Formation blocks form an en-echelon set of rigid NNW-trending anticlinal horsts. These have a shallow northward tilt and are flanked by synclines developed in the overlying McNamara Group (Fig. 3).

In order to study an area where similar geological relationships existed outside the Paradise Creek High Strain Zone, the Torpedo Creek Quartzite was also examined in the Redie Creek area, 20 km east of Lady Loretta (Fig. 3). As is the case in the area of the

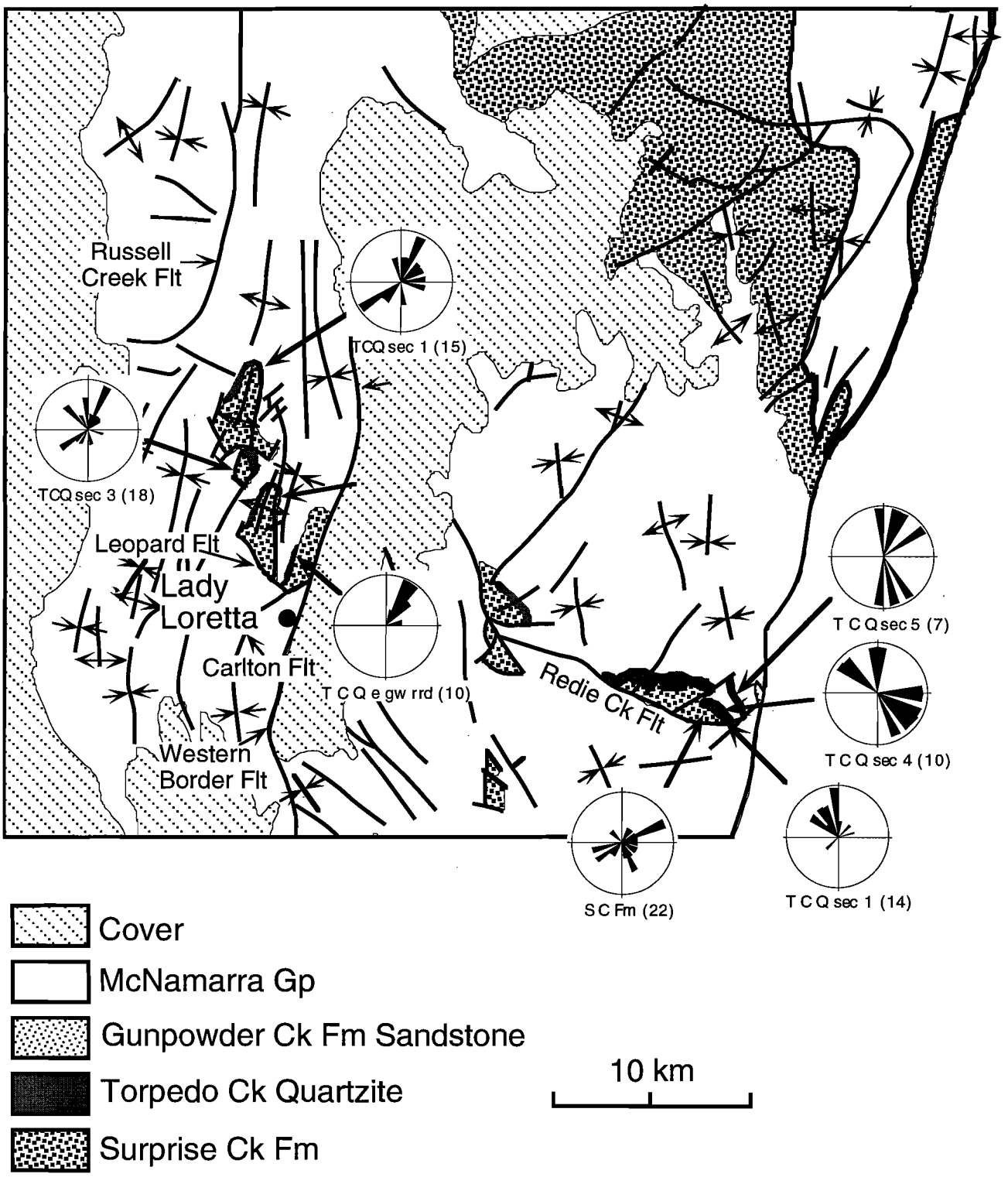

Figure 3. Outcrop geology and palaeocurrent data from the Surprise Creek Formation and Torpedo Creek Quartzite in the Lady Loretta and Redie Creek areas.

deposit, the unit occurs as a continuos selvedge at the northern edge of a block of the older Surprise Creek Formation. In this case however, although there are local offsets across faults, there are no tight folds, and the Surprise Creek Formation block comprises a coherent, 5 km long, dominantly ENE-trending body. It is bounded at its southern margin by the Redie Creek Fault (Fig. 3), and at its eastern margin by the Mount Gordon Fault Zone, a major NNE-trending structure that has been extensively mobilised in the Isan orogeny.

The Surprise Creek Formation that underlies the Torpedo Creek Quartzite at both localities studied, consists in each case of fine- to coarse-grained, moderately-sorted quartzo-feldspathic sandstone. Although the contact, where it is simplest in the Redie Creek area, is an unconformity, the change in dip of strata is relatively minor (ie. < 10°). In the field, the two units are therefore similar in appearance, and the Surprise Creek Formation is chiefly distinguished by; a pervasive pink colouration and higher proportion of feldspar grains relative to typical white Torpedo Creek Quartzite; and by the fact that it underlies the basal conglomerate facies of the latter where present. In order to check that the two units are mappable stratigraphic entities in the Lady Loretta-Redie Creek region, sedimentological data was collected from the Surprise Creek Formation for comparison with that from the overlying Torpedo Creek Quartzite that is the main focus of this study.

Sedimentology

Surprise Creek Formation

The base of the Surprise Creek Formation is not exposed in either the Lady Loretta or Redie Creek areas, however, at the latter locality the upper 300 m is exposed. In each case, the unit comprises medium- to thin-bedded, grey to pale pink coloured, fine- to coarse-grained, moderately- to well-sorted sandstone. The dominant sedimentary structures present are planar and cross-lamination (Fig. 4a), which ranges in scale from ripples to dunes with amplitudes of up to 40 cm. Palaeocurrrent data was collected from the dune bedforms in a section at the top of the unit in the Redie Creek area. It shows a well defined, ENE-WSW-trending, bimodal bipolar pattern (Fig. 3).

Petrology

Thin section examination of representative samples of the Surprise Creek Formation indicates that quartz is the dominant framework grain present (> 85%), occurring in a grain-supported fabric with a clear quartz cement (Fig. 5a). The main accessory grain present (~5%) is distinctive fresh microcline that is well-rounded and usually fine-grained. Other accessory grains (all < 5%) include partly serecitised euhedral feldspars (?plagioclase), strained poly-crystalline quartz aggregates (? metamorphic lithic fragments), chert fragments, white mica, tourmaline and zircon.

Interpretation

In terms of depositional environment, the lack of fines and abundant cross lamination indicate a predominance of tractional current activity. The bimodal bipolar palaeocurrent pattern is strongly suggestive of tidally influenced (ie. shallow marine) sedimentation (eg. Terwindt, 1988).

Torpedo Creek Quartzite

In the Lady Loretta area, the Torpedo Creek Quartzite varies in thickness from < 10 m to several tens of metres (Fig. 4b), and can be considered in terms of three constituent facies:

- A basal pebble-boulder conglomerate facies is not always present, but in places reaches a thickness of > 10 m. Clasts are sub- to well-rounded quartz sandstone (Fig 4c). They are variable in shape from spherical to tabular, however, the largest clasts, which have long axes of > 3 m, are all tabular in shape. In places the sandstone clasts are a distinctive pale pink colour (Fig. 4c). The matrix to the sandstone clasts is generally a clean, medium- to coarse-grained sandstone identical to that described below. However, at one locality there is a significant mud component present in the matrix of a massive boulder conglomerate.
- A well sorted clean, white, fine- to coarse-grained quartz sandstone facies forms the lower to middle part of the unit in all sections (Fig. 4b). It is medium- to thinly-bedded and up to 20 m thick. The predominant sedimentary structures present are planar lamination and small- to medium-scale cross bed sets with amplitudes between 10 and 40 cm (Fig. 4d&e).

- A thinly-bedded, poorly-sorted quartz sandstone facies forms the upper few metres of the Torpedo Creek Quartzite. It is grey brown in colour due to the presence of a significant mud component in the sandstone matrix. The sedimentary structures present are similar to those in the underlying well-sorted sandstone, but abundant symmetrical ripples/dunes in also present in some exposures.

Paleocurrent measurements were collected from cross-bed sets in Torpedo Creek Quartzite sandstone sections at three localities in the immediate Lady Loretta area. In each case, the unfolded data indicates a dominant NNE component of palaeoflow (Fig. 3). A subordinate SW component of palaeoflow, present at two of the localities, is due to data from the uppermost poorly-sorted quartz sandstone facies.

In the Redie Creek area, the Torpedo Creek Quartzite as mapped comprises 45 m of quartz sandstone. No basal conglomerate facies was observed, however, the other two facies described from the Lady Loretta area are present in the same stratigraphic arrangement. Palaeocurrent data from the sandstone section is effectively unimodal recording N-directed palaeflow (Fig. 3).

Petrology

Thin section examination was undertaken of representative samples of the dominant facies present in the Torpedo Creek Quartzite in both areas studied, the clean fine- to coarse-grained quartz sandstone facies. Quartz is the dominant framework grain present (> 90%), and is arranged in a fabric in which grain contacts are planar or sutured and there is effectively no preserved cement (Fig. 5b&c). Accessory grains (all < 5%) include heavily sericitised euhedral feldspars, strained poly crystalline quartz aggregates (? metamorphic lithic fragments), chert fragments, tourmaline and zircon.

The sandstone clasts in the basal conglomerate were also examined. They consist of medium- to coarse-grained quartz (> 90%) with a relatively high proportion (~ 5%) of rounded, serecitised, fine-grained feldspars (Fig. 5d). Accessory grains (all < 5%) include polycrystalline quartz aggregates, muscovite, zircon and tourmaline.

Interpretation-basal conglomerate

In terms of sedimentary environments, the coarse-grained nature of the initial Torpedo Creek Quartzite conglomerate deposits, indicates that the McNamara Group depositional cycle was initiated by a relief-forming tectonic event. These pebble-boulder conglomerate facies units are interpreted as debris flows and/or alluvial channel deposits, and their lateral restriction indicates that they accumulated either in erosive channels or as fans sourced from uplifted blocks of older material.

The distinctive pink colouration of many of the sandstone clasts is identical to that of the underlying Surprise Creek Formation, suggesting that the current stratigraphic configuration is depositional, and that the unit comprised local "basement" at lower McNamara time. This similarity is confirmed in thin section, in which the two lithologies are identical in every respect, except in that the rounded fine-grained feldspars that are clearly fresh microcline in Surprise Creek Formation samples, are intensely serecitised in the basal Torpedo Creek Quartzite conglomerate clasts. This is consistent with the latter having undergone alteration/weathering during post lithification uplift, erosion and re-deposition during the event that initiated the onset of McNamara Group sedimentation.

Interpretation well-sorted sandstone

The well-sorted, fines-free nature of the sandstones that are laterally equivalent to and overly the basal conglomerate facies, and the predominance of moderate- to high-energy tractional sedimentary structures with essentially unimodal palaeocurrents, indicates sedimentation controlled by strong, unidirectional tractional currents. A genetic relationship with the conglomerates is indicated by the close spatial association, and the fact that these sandstones are identical in petrology to the matrix of the coarser-grained units. They are interpreted to represent high-energy (ie. braided) alluvial/fluvial systems. Initially these deposits would have accumulated as lateral and distal equivalents to individual conglomeratic channels/fans. However, the occurrence of the clean, fine- to coarse-grained quartz sandstone facies though the bulk of the unit indicates that the initial relief of the uplifted Surprise Creek Formation blocks was rapidly subdued by

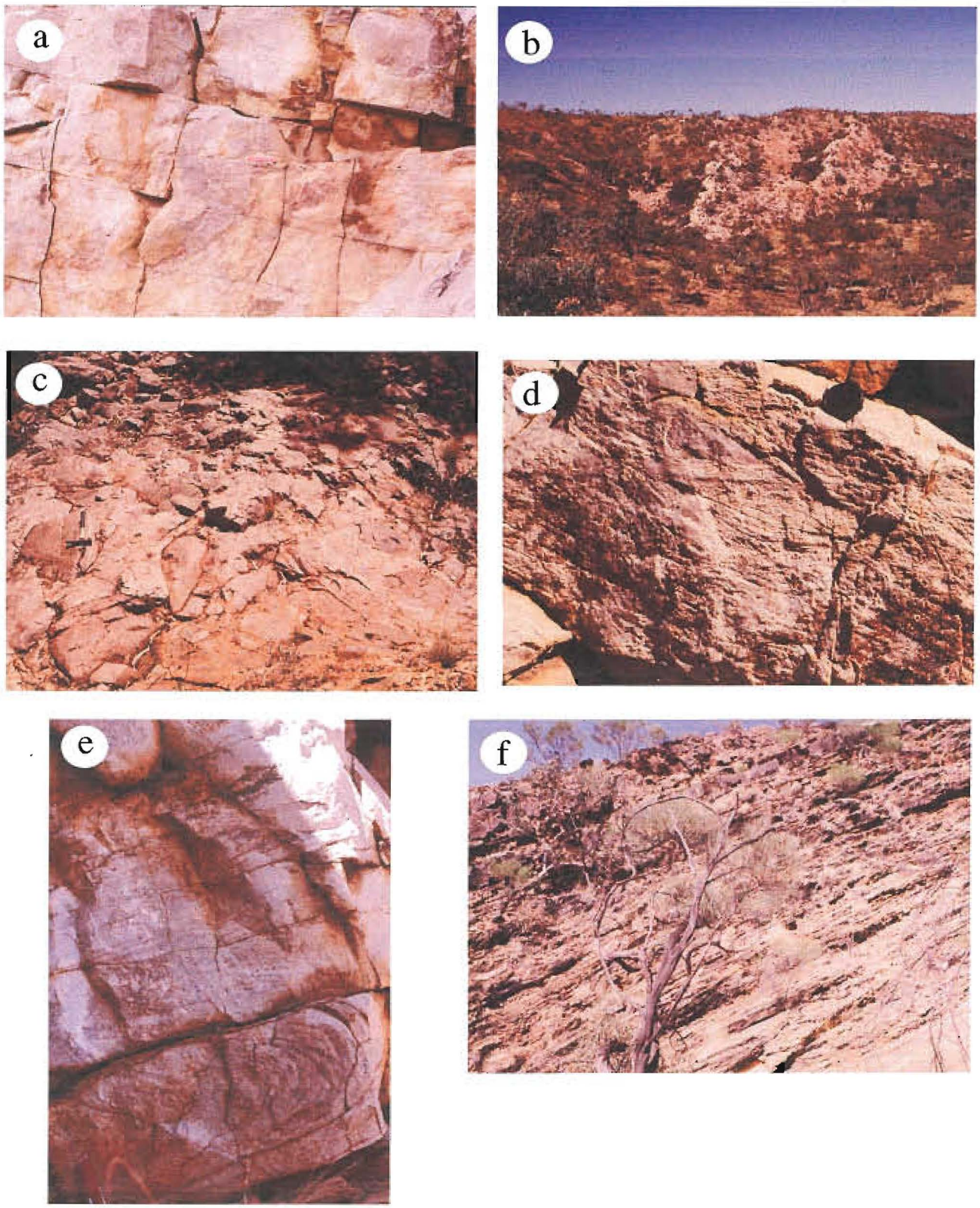

Figure 4. (a) Typical bedded pink Surprise Creek Formation sandstone; note tabular cross-bed set behind knife. (b) White Torpedo Creek Quartzite overlying pink Surprise Creek Formation sandstone (arrowed) north of Lady Loretta. (c) Torpedo Creek Quartzite basal boulder conglomerate; note pink colouration of sub-rounded sandstone clasts. (d) Trough cross-bed typical of those used to collect palaeocurrent data from the Torpedo Creek Quartzite well-sorted sandstone facies. (e) Overturned (fluvial) cross-bed in Torpedo Creek Quartzite well-sorted sandstone facies. (f) Typical Gunpowder Creek Formation outcrop at Redie Creek. Upward thickening and coarsening (~shallowing) cycle from thinly-bedded dolomitic siltstone to thickly bedded ferruginous sandstone on ridge line.

erosion/deposition, allowing the braided fluvial systems to became dominant.

Interpretation poorly-sorted sandstone

The uppermost poorly-sorted quartz sandstone facies contains symmetrical ripples/dunes generally taken as indicative of wave activity is shallow water conditions (eg. Walker, 1984). It also records a markedly different palaeoflow pattern to the underlying clean sandstones. This unit is interpreted to represent the onset of the transgression that marks the transition to the Gunpowder Creek Formation throughout the Lawn Hill Platform region (Hutton and Wilson, 1985).

Upper sandstone units at Redie Creek

Although the structure of the Redie Creek area is simple relative to the Lady Loretta area, it is more complex stratigraphically. In the Lady Loretta area, as in most areas of lower McNamara Group exposure (eg. Sweet and Hutton, 1982; Hutton and Wilson, 1984;Hutton and Wilson, 1985), the Torpedo Creek Quartzite occurs as a discrete body of clean quartz sandstone that has a gradational contact with the overlying finer-grained carbonaceous siltstones and carbonates of the GCF. However, in the Redie Creek area, two parallel striking sandstone units of similar thickness to the Torpedo Creek Quartzite occur stratigraphically above it (Fig. 3). Although they have been mapped as part of the overlying GCF (Hutton and Wilson, 1985), sandstone units of this thickness and lateral persistence are not present in this generally fine-grained unit regionally. In fact, the first of these sandstone bodies strongly resembles the Torpedo Creek Quartzite, which is a distinctive white colour on the 1:25,000 scale colour aerial photographs used for this study.

Sedimentological data was collected from these upper sandstone units for comparison with the Torpedo Creek Quartzite. The Gunpowder Creek Formation in this area consists of thinly-bedded/laminated dolomitic siltstone with interbedded ferruginous, poorly-sorted dolomitic sandstone intervals up to several metres thick (Fig. 4f). The first sandstone ridge occurs approximately 90 m above the base, and consists of 30 m of clean, fine- to coarse-grained quartz sandstone. This facies is indistinguishable from that which forms the bulk of the Torpedo Creek Quartzite as mapped. Thin section examination confirms that the two sandstones are petrologically identical (Fig. 5e). Palaeocurrent patterns are, however, distinct in that although the characteristic N-directed component of palaeoflow is present, it is minor compared to a SE-directed component not recorded from the Torpedo Creek Quartzite elsewhere in the region (Fig. 3).

The second sandstone ridge occurs approximately 250 m stratigraphically above the first (ie. approximately 370 m above the base of the Gunpowder Creek Formation; Fig. 3). It consists of crudely bedded, coarse-grained sandstone with abundant distinct pink and white feldspar grains. Scattered rounded quartzite pebbles are present locally. This unit does not resemble typical Torpedo Creek Quartzite, highlighted by the fact that the cross-bed sets suitable for palaeocurrent determination that are ubiquitous within the latter were not observed. Thin section examination confirms the difference, with the upper sandstone unit comprising poorly- to moderately-sorted quartz-dominated sandstone (Fig. 5f). Accessory grains (all < 5%) include serecitised fine-grained quartz lithic fragments (?altered volcanic lithics), strained and unstrained poly-crystalline quartz aggregates (metamorphic and sedimentary lithic fragments respectively), fresh microcline, heavily serecitised euhedral feldspars (?plagioclase) and tourmaline.

Interpretation

From the descriptions above, it is clear that the lower of the two sandstone ridges that occur within the Gunpowder Creek Formation in the Redie Creek area is a virtually identical to the underlying Torpedo Creek Quartzite. This means that either; the conditions for formation of the clean, fine- to coarse-grained quartz sandstone facies were repeated, in this area alone, after the onset of the regional transgression that initiated the deposition of the Gunpowder Creek Formation; or the Torpedo Creek Quartzite is repeated by thrusting in this area, probably during the Isan Orogeny. Although the base of the sandstone ridge where the thrust would occur is obscured by talus, the latter is the favoured explanation. This is because there is considerable field evidence in the section along Gunpowder Creek just to the east for thrust splays off the Mount Gordon

Fault Zone (eg. stratigraphic dismemberment along bedding parallel structures). One of these structures apparently hosts the Cu prospect shown on the 1:100,000 scale geological map (Hutton and Wilson, 1985).

The upper sandstone ridge within the Gunpowder Creek Formation in the Redie Creek area is markedly different from the Torpedo Creek Quartzite. It has a different provenance, including volcanic lithic fragments and the re-introduction of fresh microcline to the sedimentary system. This may indicate that it records significant tectonic uplift subsequent to that which controlled deposition of the Torpedo creek Quartzite.

Implications for the Lady Loretta mineralisation

Sedimentary setting

The sedimentological data presented above provides a valuable insight into the tectono-sedimentary setting of the Lady Loretta mineralisation on both a local, and a basinal scale. The abrupt change of environment between the Surprise Creek Formation and the Torpedo Creek Quartzite, from shallow marine tidally influenced to subaerial alluvial/fluvial sedimentation, is clear evidence of a significant uplift event in the Lady Loretta area at the onset of McNamara Group deposition. In addition, the presence of boulders of lithified Surprise Creek Formation in the basal Torpedo Creek Quartzite conglomerate facies, suggest that this uplift represents the culmination of a major burial/exhumation cycle. On a basin-wide scale this contact must, therefore, represent a significant time break between two major basin phases.

Given that the Surprise Creek Formation in the Lady Loretta area was lithified at the time of onset of McNamara Group deposition, then sedimentation patterns in the Torpedo Creek Quartzite will reflect the structural template/basin geometry for this widely mineralised basin phase. The relationship is most clearly illustrated in the Redie Creek area, where the Isan deformation is less intense. In this case, the palaeocurrent data from the Torpedo Creek Quartzite has a dominant northerly component. This indicates palaeoflow directed approximately normal to the WNW-trending axis of the Surprise Creek Formation block (Fig. 3), which has been implicated as a source for the clasts in the base of the TCQ. The latter was, therefore, an actively eroding ridge with a relatively steep N-NE-dipping slope at its northern margin at this time. This configuration suggests that, in this area at least, WNW-trending growth faults controlled the onset of McNamara Group sedimentation. No information is available for Torpedo Creek time from the southern margin of the ridge. It is defined by the Redie Creek Fault that separates Surprise Creek from the middle McNamara Lady Loretta Formation so the Torpedo Creek Quartzite, if present, is deep in the subsurface.

In the more deformed Lady Loretta area, palaeocurrent data from the Torpedo Creek Quartzite, when unfolded, has a dominant northerly component effectively identical to that from Redie Creek. This suggests that, prior to the en-echelon dismemberment and folding that occurred during the Isan Orogeny, the Surprise Creek Formation blocks in this area formed a semi-continuous, WNW-trending ridge similar to that currently exposed at Redie Creek. In this case, the basement ridge, and the associated syn-sedimentary faults, would have passed immediately to the north of the site that would ultimately host the Lady Loretta mineralisation (Fig. 6).

Syn-sedimentary faulting initiating/accompanying the onset of McNamara Group sedimentation has previously been proposed by the author, based on facies pattern and thickness changes in drill core intersections from the southern flanks of Kamarga Dome (Bull, 1996). In the Kamarga area, the resultant relief was suppressed fairly rapidly (ie. by middle Gunpowder Creek Formation times). Poor outcrop of the relevant McNamara Group units precludes an analysis of this kind in the Lady Loretta area. However, the recent proposal of Dunster and McConachie (1998), that there is no evidence of syn-sedimentary structural activity in the Lady Loretta Formation, suggests that any tectonically generated relief had been infilled by that time. In terms of the tectono-sedimentary setting of the Lady Loretta deposit, the implication is that although the mineralised site is proximal to a growth fault, the major activity on the structure occurred in early McNamara times, and had effectively ceased prior to the time of deposition of the host sediments. The

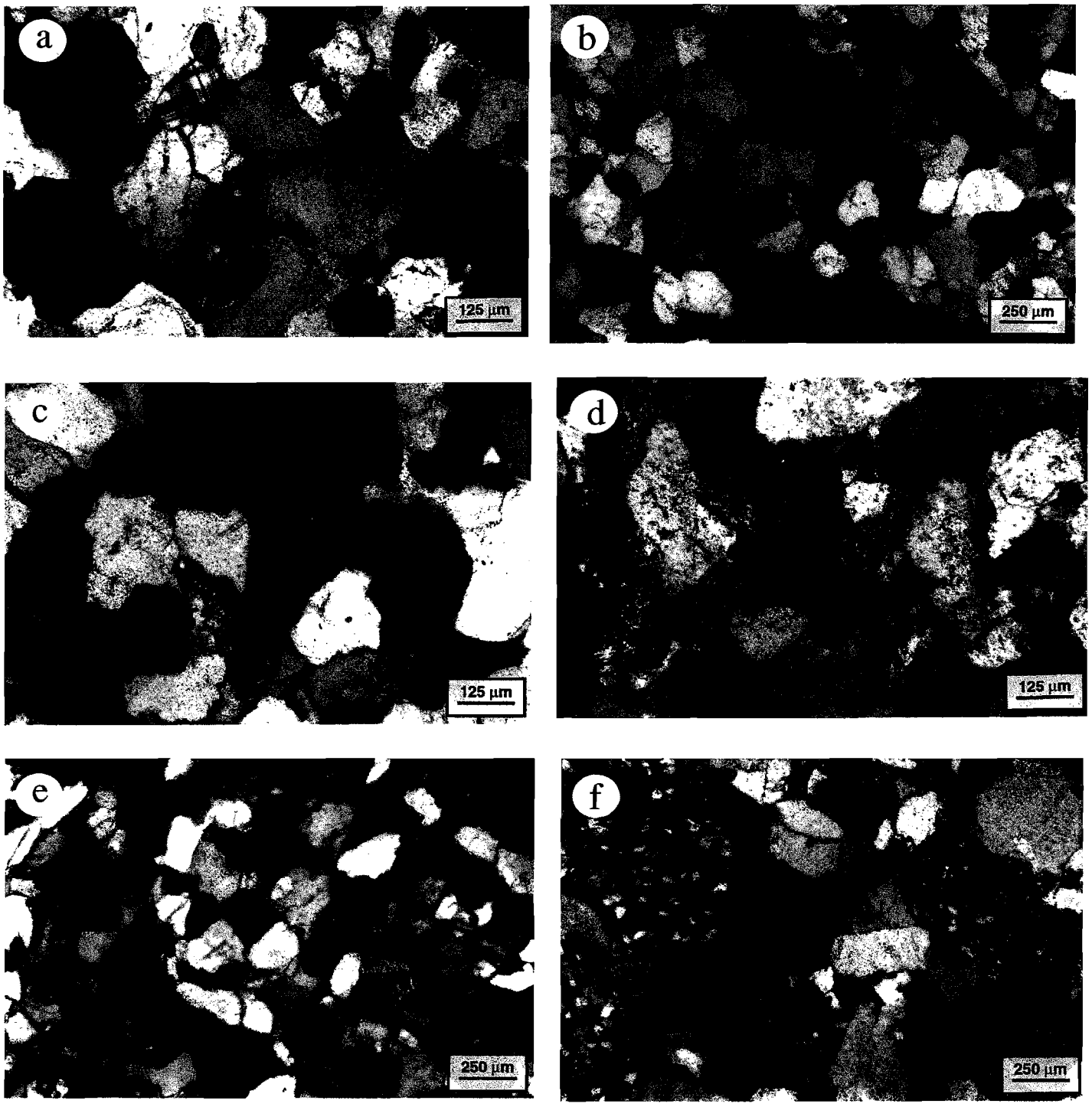

Figure 5. (a) Photomicrograph (x10) of Surprise Creek Formation sandstone; note fresh rounded microcline grain at upper left. (b) Photomicrograph (x5) of Torpedo Creek Quartzite well-sorted sandstone facies; note abundance of planar and sutured grain boundaries and scattered sericitized (?feldspar) grains. (c) Close up (x10) of 5c. (d) Photomicrograph (x10) of sandstone clast from basal Torpedo Creek Quartzite conglomerate; note extensively sericitized rounded feldspar grains. (e) Photomicrograph (x5) of lower sandstone ridge from within the Gunpowder Creek Formation at Redie creek; note similarity to typical Torpedo Creek Quartzite at same magnification in 4b. (f) Photomicrograph (x5) of upper sandstone ridge from within the Gunpowder Creek Formation at Redie creek; note abundant fine grained matrix (upper centre) and abundant sedimentary lithic fragments.

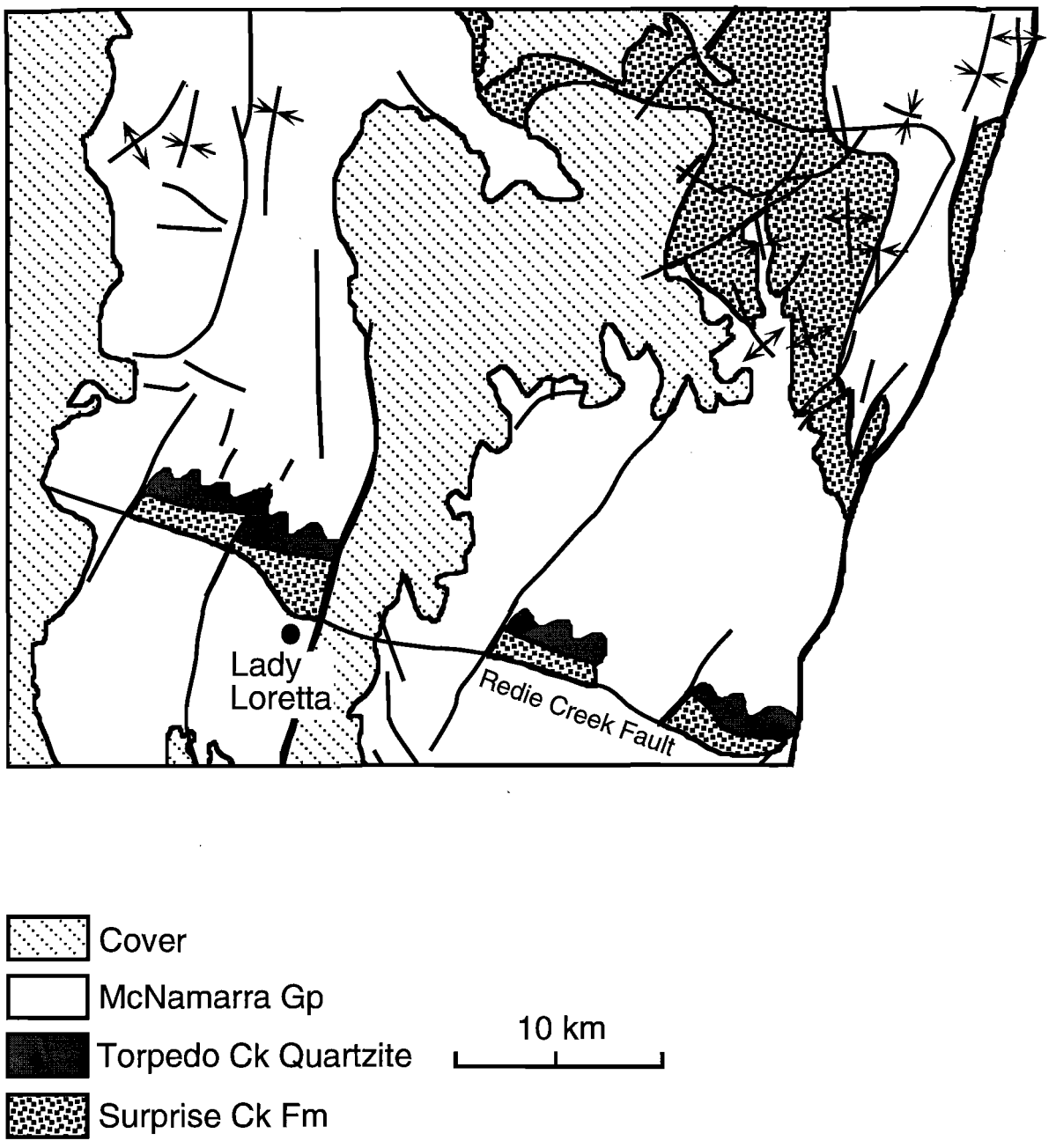

Figure 6. Schematic representation of proposed pre-Isan Orogeny configuration of the Lady Loretta-Redie Creek region.

significance of this setting, compared to traditional genetic models for sediment hosted Zn-Pb-Ag-mineralisation that invoke essentially synchronous syn-sedimentary faulting, sub-basin development and mineralisation, will be addressed in the discussion section below.

Controlling structures

It is not possible to present a constrained structural model that explains the early McNamara basin configuration presented above, without a detailed understanding of which faults were present at the time of sedimentation, and their attitudes and styles. This is beyond the scope of this sedimentologically-based study, due to the obvious extensive re-configuration during the Isan Orogeny. However, some comment can be made on possible structural scenarios, based on the crude reconstruction of the pre-Isan configuration of major faults indicated by the sedimentation patterns defined here (Fig. 6). Any early McNamara structural framework must explain a semi-continuous, WNW-trending ridge of actively eroding Surprise Creek Formation "basement", flanked by syn-sedimentary faults. This feature extended from the Redie Creek area passing just to the north of the site that would ultimately host the Lady Loretta mineralisation.

Further constraints are provided by; geophysical evidence that indicates the current bounding structures (eg. the Redie Creek Fault) are steeply-dipping (Duffett, 1997). If this attitude in any way reflects that which existed at early McNamara time, then it suggests that the structures were not detachment or thrust faults; and by the fact that the clastic Torpedo Creek Quartzite presages a period of regional subsidence that provided the accomodation space for the accumulation of the platform carbonate-dominated lower McNamara Group.

A structural model that could explain all of the above considerations is a regime of roughly N-S oriented regional extension, with resultant ~E-W growth faulting and half-graben formation. In this case the Surprise Creek Formation ridge in the Redie Creek-Lady Loretta area would represent a tilt block crest separating half-graben depocentres, and the bounding syn-sedimentary fault system a planar or listric normal growth fault. Studies of active extensional half-graben systems (eg. Lake Tanganyika; Tiercelin et al., 1992) indicate that clastic wedges analogous to the Torpedo Creek Quartzite accumulate, in this case as fan-deltas, in piedmont positions on the subsiding hanging wall block immediately adjacent to the border (ie. growth) fault scarp.

A potential problem with a tilt-block model is illustrated in a schematic cross-section from the Redie Creek area (Fig. 7a). Both the Surprise Creek Formation and the Torpedo Creek Quartzite dip to the NE, and there is unconformable relationship between the two units because dips in the latter are ~10° steeper. Although an unconformable relationship is predicted in a tilt-block model, the fill should dip more shallowly than the "basement" (Fig, 7b). In addition, in the current configuration the Torpedo Creek Quartzite is onlapping the Surprise Creek Formation "basement" to the NE. However, palaeoflow in the Torpedo Creek Quartzite sandstone apron is also directed to the north (Fig. 3; Fig. 7a), ie. toward the "basement" block, rather than away from it as would be expected in a tilt block model (Fig. 7b). These factors suggest, that although the overall geometry of an elongate ridge of Surprise Creek Formation "basement" flanked by Torpedo Creek Quartzite rift clastics is consistent with tilt-block formation, the current unconformable relationship between the Surprise Creek Formation and the Torpedo Creek Quartzite reflects subsequent deformation. This seems reasonable, given the likelihood of Isan thrusting associated with wrenching on the Mount Gordon Fault Zone, as proposed above to explain the stratigraphic repetition of the Torpedo Creek Quartzite facies in this area.

The other major fault set that exists in the Lady Loretta and Redie Creek areas are numerous N-NNE-trending structures. These dominate the current 1:100,000 scale geological map pattern, especially within the Paradise Creek High Strain Zone (eg. the Western Border and Russell Creek Faults and parallel unnamed structures in between; Fig. 3), where they have been active during Isan E-W shortening. Dips on these structures are interpreted to be steep based on geophysical evidence (Duffett, 1997). There is no sedimentological evidence that these N-NNE trending structures existed at McNamara Group times, or structural evidence that they were wrench faults early in their history. However, if this had

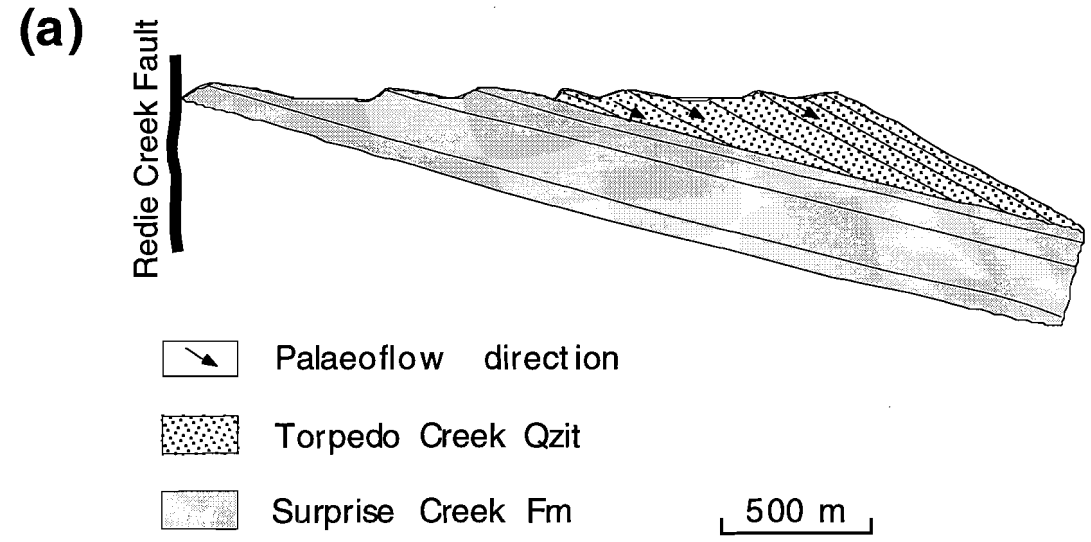

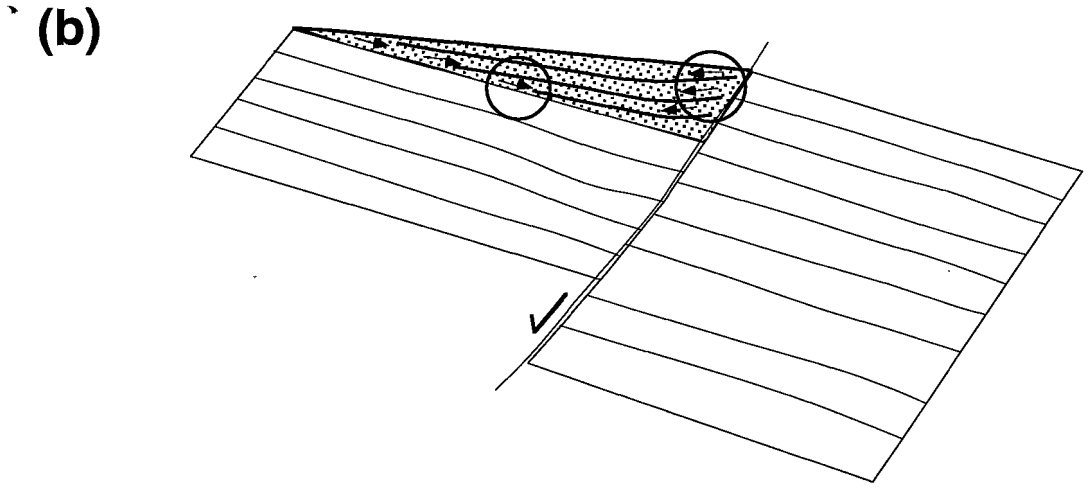

Figure 7. (a) Schematic cross-section showing relationship between Surprise Creek Formation and Torpedo Creek Quartzite from Redie Creek. (b) Predicted onlap/palaeoflow relationships between pre- and syn-rift sediments in a half-graben depocentre.

been the case, they would fit into a model involving regional N-S extension as transfers to the WNW-trending normal faults.

The proposal that the N-NNE-trending structures in the Redie Creek and Lady Loretta region represented transfer faults in early McNamara times is appealing for two reasons:

- Firstly, growth and transfer fault intersections are widely recognised as important sites of hydrothermal activity in modern extensional settings (eg. Lake Tanganyika; Tiercelin et al., 1992; Coussement et al., 1994). The occurrence of several closely spaced transfers cutting a growth fault in the Lady Loretta area could, therefore, be a factor in the formation of the mineralisation.
- Secondly, if N-NNE-trending structures were present in the area prior to the onset of the Isan Orogeny, they would have been in the right orientation to be extensively re-activated during E-W shortening. The occurrence of several closely spaced transfers in the Lady Loretta area could therefore explain the high degree of Isan deformation, both folding and faulting, that characterises the Paradise Creek High Strain Zone. This is sufficient to mask the WNW-oriented Redie Creek Fault trend in the Lady Loretta area on present day map patterns, even though it is clear in the Redie Creek area to the southeast where there are fewer and smaller scale N-NNE trending structures. A clear implication of this suggestion, is that other areas of comparable McNamara Group structural complexity in the region may have a similar structural framework, and hence have the capacity to host base metal mineralisation.

Discussion

Implications for cover sequence scheme

Successive phases of extensional tectonism, involving rifting and tilt block development accompanied by clastic sedimentation ± volcanism and subsequent thermal sag phase sedimentation, have been widely advocated to explain the complex stratigraphy of the Mount Isa Terrain. Blake (1987) subdivided the stratigraphic succession that accumulated after the ~1870 Barramundi Orogeny into three "cover sequences", interpreted as discrete rift/sag cycles separated by regional unconformities. More recently, it has been proposed that there are at least four cover sequences (O'Dea et al., 1997). These authors concur with Blakes' (1987) cover sequences 1 and 2, but have further subdivided cover sequence 3 into cover sequences 3 and 4. In addition, O'Dea et al. (1997) have used thickness variations of sedimentary packages to determine the regional stress regimes under which some of the extensional events occurred. The rifting associated with cover sequence 2 is interpreted to have occurred in response to initial E-W and subsequent N-S extension; and the rifting associated with cover sequences 3 and 4 in response to E-W to NW-SE extension.

The stratigraphic interval exposed in the Lady Loretta-Redie Creek area is all assigned to cover sequence 4 by O'Dea et al. (1997). In this model, the Surprise Creek Formation is interpreted as the clastic rift package that was deposited on the hanging walls of rotating tilt blocks. Regional thickness trends within the clastic package, which is described as thickening to the east and tapering to the west, suggest that rifting developed in response to regional E-W to NW-SE extension The O'Dea et al. (1997) interpretation of the regional stress field, implies that faults with the most potential to act as major normal growth faults during this period would have been oriented approximately N-S to NE-SW. No mention is made of the Torpedo Creek Quartzite in the O'Dea et al. (1997) study, in which the entire McNamara Group is interpreted to represent the thermal sag phase sedimentation of cover sequence 4.

Interpretation of the sedimentological data collected in the current study suggests the need for a further revision of the cover sequence scheme. The presence of boulders of Surprise Creek Formation sandstone in the basal conglomerate of the Torpedo Creek Quartzite, clearly indicates that the units are separated by a cycle of burial, lithification and inversion. The contact therefore represents a major basin phase (ie. cover sequence) boundary, within cover sequence 4 as currently defined (O'Dea et al., 1997). The structural model presented here, although relatively poorly constrained, suggests that the onset of McNamara Group sedimentation (?cover sequence 5) occurred in response to regional N-S extension. This has been previously proposed for the latter phase of rifting associated with cover sequence 2 (O'Dea et

al., 1997), and may have involved reactivation of some of the same structures.

Significance of thickness

Maximum thicknesses (Blake, 1987) for the rift phase subaerial and shallow marine clastics identified by O'Dea et al. (1997) in the Mount Isa system are generally well in excess of 1000 m (eg. the 6,200 m thick Mount Guide Quartzite at the base of cover sequence 2 and the 2000 m thick Surprise Creek Formation at the base of cover sequence 4). The exception is the 600 m thick Bigie Formation that forms the rift phase to cover sequence 3. The Torpedo Creek Quartzite has a maximum recorded thickness of 420 m (Hutton and Wilson, 1985). At face value, this suggests a relatively low degree of extension, tilt block rotation and subsidence associated with this rifting event. However, the lack of carbonate in the fine-grained, clastic marine package that comprises the base of the overlying Gunpowder Creek Formation (Hutton and Wilson, 1985), suggests that accomodation space was still being generated more rapidly than could be infilled by the microbial community. This package, which is up to 630 m thick, may therefore also be part of the actively subsiding rift phase. Accessory evidence in support of this proposal was encountered in this study, in the form of the provenance of the upper sandstone unit that occurs in the Gunpowder Creek Formation at Redie Creek. It contains abundant lithic fragments and fresh microcline not present in the underlying sandstones, and may represent structural exhumation of different source rocks.

A possible explanation for the transition from subaerial/shallow marine clastic sedimentation to fine-grained shelf deposits during active rifting, is that a higher base sea level existed by this relatively late stage of the basin history, presumably due to a lower regional thermal regime. This would facilitate the existence of marine conditions during rifting, and could have led to the generation of normal growth fault bound sub-basins filled with reduced shelf sediments. Areas of maximum subsidence within this basin configuration, often discussed in terms of "third order basins", are widely considered to have the potential to host base metal mineralisation.

The upper 140 m of the Gunpowder Creek Formation consist of stromatolitic and evaporitic platformal dolomite (Hutton and Wilson, 1985) similar to that which comprises the overlying lower McNamara Group units. This is interpreted to represent the onset of true thermal sag phase sedimentation, during which the microbial community was able to infill accomodation space essentially as it formed.

Implications for setting of mineralisation

Widely proposed models for sediment hosted base metal mineralisation, stress the importance of settings where fault bounded sub-basins are generated during the accumulation of the fine-grained, reduced host sediment package. Such a situation is proposed above for the basal part of the Gunpowder Creek Formation, although no deposit of this type is known to occur in the unit. It has also been proposed for the HYC deposit in the southern McArthur Basin (eg. Walker et al., 1977; Large et al., 1996). In this case, syn-sedimentary (growth) faulting and sub- basin formation were clearly associated with the mineralising event (Fig. 8a), as evidenced by the anomalous thickness of the host Barney Creek Formation siltstones in the immediate area of the deposit, and by the abundant inter-ore mass-flow breccias (eg. Walker et al., 1977).

A similar intra-graben setting was originally proposed for the Lady Loretta deposit (eg. Large, D. E., 1980). Although the proposed association between sub-basin formation and mineralisation has recently been refuted in this case (Dunster and McConachie, 1998; Fig. 8b), this poses additional question as to what controlled the deposit site. In the light of the interpretation presented in this study, two important points can now be made with regard to the revised tectono-stratigraphic setting of the Lady Loretta mineralisation:

1. It lies close to a pre-existing WNW-trending syn-sedimentary fault system, the main phase of growth of which occurred prior to the time of the deposition of the host sedimentary package.
2. It occurs in an area where the growth fault appears to have been cut by several relatively closely spaced N-NE-trending (?transfer) faults.

The relationship between growth and transfer fault intersections and hydrothermal activity has been widely recognised in modern rift settings (eg.

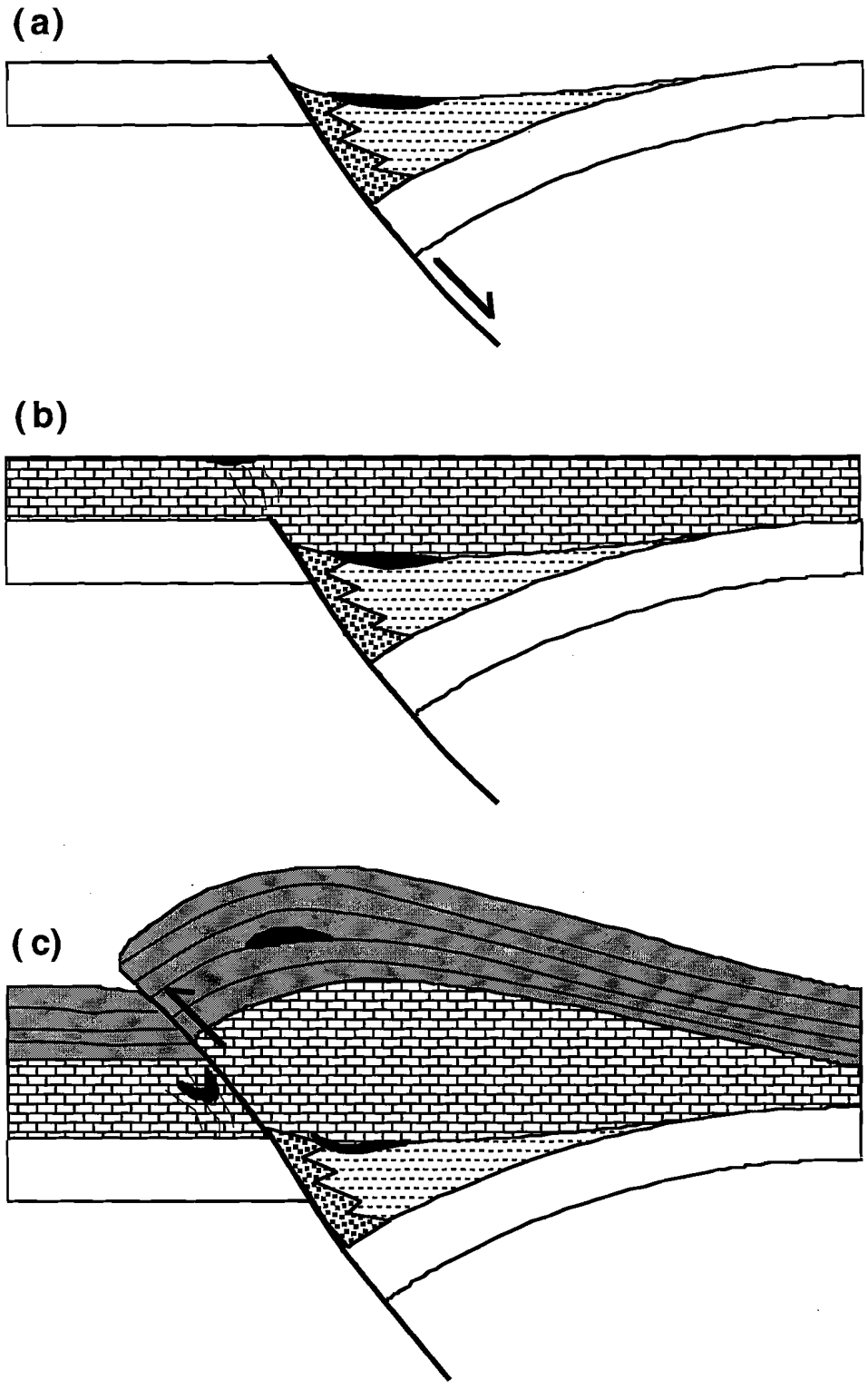

Figure 8. Schematic representation of the potential different settings/timing for base metal mineralisation in the Proterozoic of northern Australia (a) syngenetic exhalative during active subsidence (~HYC deposit) (b) syngenetic exhalative during passive subsidence (~Lady Loretta deposit) (c) epigenetic replacement during basin inversion (~Century deposit).

Tiercelin et al., 1992; Coussement et al., 1994). Fault intersections have also been proposed as a significant factor in the siting of ancient base metal deposits (eg. Höy, 1982; Large, D. E., 1983; Werner, 1990). This relationship has commonly been envisaged in terms of essentially synchronous syn-sedimentary faulting, sub-basin formation and mineralisation (eg. in the case of the world class Sullivan deposit in British Colombia; Höy, 1982). In this type of system, intersecting syn-sedimentary faults are implicated in both; the formation of a sub-basin depocentre which was the site of accumulation of suitable fine-grained, reduced "trap" lithologies for initiating precipitation of base metals; and in maintaining the conduit/s for ascension of metal-bearing brines. However, the setting proposed here for the Lady Loretta deposit suggests some revision is needed to this type of model. The implication is, that areas of growth/transfer fault intersections are potential sites for significant fluid flow even after active rifting and syn-sedimentary faulting have ceased. If this is the case, the potential for mineralisation in this structural setting is dependant on the existence of suitable "trap" lithologies (ie. reduced fine-grained sediments) accessed by fluid conduits in the thermal sag package (Fig. 8b).

In the absence of active growth faulting in this type of system, the specific nature of the conduit allowing ascension of mineralised brines is unclear. One possibility would be systems of minor faults and/or fractures developed in the sag package sediments above the subsurface growth and/or transfer faults in response to minor movement due to weak tectonic events or sediment loading (Fig. 8b). Such conduits could be quite subtle and difficult to recognise in ancient mineralised successions. However, evidence of this type of activity could include the presence fluid escape pipes or fluidisation breccias, both of which have been described from the Lady Loretta ore zone (McGoldrick, 1993).

Implications for timing/processes of mineralisation

The setting proposed here for the Lady Loretta deposit also has implications for the timing of sediment-hosted base metal mineralisation. This has been the subject of considerable debate, exemplified by the HYC deposit, for which both syngenetic exhalative and epi-genetic (syn-diagenetic) models have recently been proposed by Large et al. (1996) and (Hinman et al., 1994; Hinman, 1995) respectively. A syngenetic model predicts that base metal mineralisation should be located in the deepest portion of a rapidly subsiding basin. This is because in order to be effective agents of base metal mineralisation, a high-salinity (and high-density) exhalative system would require a topographic depression to allow fluid ponding and resultant generation of a constrained brine pool for mineral deposition. This site may occur at some distance from the syn-sedimentary (growth) faults normally thought to have acted as conduits for the mineralised fluids, particularly if there aprons of debris sourced from erosion of the growth fault scarp are present. This is effectively the situation at HYC which accords well with the Large et al (1996) syngenetic model for the mineralisation

However, no such constraints exist for base metal mineralisation that is epigenetic in origin. In this case, metal precipitation would occur wherever an ascending brine interacted with a suitable reduced "trap" lithology, and there is no requirement that this site was a depocentre when the host package was deposited. In the case of Lady Loretta, the host pyritic siltstones were deposited in a relatively small, shallow, lagoonal depocentre (Dunster, 1996; Dunster and McConachie, 1998; Fig. 8b), situated within the thermal sag package when generation of accomodation space was slow. Due to the considerable degree of deformation that the deposit has undergone, it is not an ideal case for studies of the timing of mineralisation. However, current genetic models using the best available evidence invoke syn-genetic exhalation (McGoldrick et al., 1995) similar to that proposed for the HYC deposit (Large et al., 1996). This is consistent with its location in a local depocentre, and if this interpretation is correct, then it has significant implications for the processes involved in exhalative mineralisation. For example given that there is no evidence of fluid boiling at Lady Loretta, the occurrence of this type of system in such a shallow water setting indicates, that in this case at least, the metal bearing brines were relatively low temperature.

Comparison between setting of Lady Loretta and Century

In some respects, the Lady Loretta tectono-stratigraphic setting resembles that of the Century deposit, a major mineralised system containing 118 Mt of 10% Zn, 1.5% Pb and 36g/t Ag (Broadbent et al., 1996). It is situated 125 km to the northwest (Fig. 1) and hosted in upper McNamara Group sediments immediately adjacent to a regional NW-trending structure, the Termite Range Fault (Fig. 9).

Thickness changes in members of the upper McNamara group stratigraphy indicate that the Termite Range Fault had a long and complex history of syn-sedimentary (growth) activity separated by periods of quiescence (Andrews, 1996; Fig. 10). This included; operating as a major growth fault with downthrow to the southwest during deposition of much of the Riversleigh Siltstone; having little effect on the overlying Termite Range Formation; becoming active again as a major growth fault with the opposite sense polarity (ie. downthrow to the northeast) during deposition of the basal (H1) member of the Lawn Hill Formation; having more subtle effects on the overlying members of the Lawn Hill Formation.

With regard to the host rocks to the Century deposit (ie. member H4s of the Lawn Hill Formation), on the scale of the Andrews (1996) cross-section, there is a subtle change in thickness across the Termite Range Fault (Fig. 10). This suggests that the Termite Range Fault was active as a growth fault at this time, but on a limited scale relative to periods of activity earlier in the deposition of the upper McNamara Group. The sedimentological similarity of the ore sequence to adjacent non-mineralised units (Broadbent et al., 1996), and the absence of mass flow breccias (eg. compared to HYC), supports a lack of aggressive sub-basin formation during deposition of the host rocks to the deposit.

The position of the Century deposit adjacent to a sub-surface growth fault that had limited effect on the host rocks is analogous to that proposed here for the Lady Loretta deposit. This similarity is strengthened by the published mapping, that clearly indicates several roughly orthogonal structures cutting the Termite Range Fault in the area of the Century mineralisation (Fig. 9).

The Century deposit lies immediately to the southwest of the current expression of the proposed growth structure, the Termite Range Fault. However, according to the Andrews (1996) cross-section, the sense of growth during accumulation of the host rocks is downthrow to the northeast (Fig. 10). If the current configuration has not been too affected by subsequent tectonism, this has implications with respect to the timing of the mineralisation. It would be difficult to reconcile this position with a syn-genetic exhalative model for the mineralisation, because the topographic depression required to trap exhaled ore fluids and form a brine pool would normally occur on the downthrown (ie. northeast) side of the fault. However, this limitation does not apply to the current model for the Century mineralisation (Broadbent et al., 1996), which advocates epigenetic mineralisation of a petroleum reservoir. In fact, the area above a growth fault in the subsurface is a recognised site for the development of fold structures in overlying sedimentary packages during basin inversion. In this situation, metal-bearing fluids mobilised during a basin inversion event could use the subsurface fault as conduit into any resultant anticlinal petroleum trap.

The exploration implications of the above discussion, are that syn-sedimentary (growth) faults, especially where cut by other orthogonal structures (?transfers), are likely to be important in focussing base-metal mineralisation regardless of whether it is syngenetic or epigenetic in origin. In summary:

1. Where a period of syn-sedimentary faulting associated with a particular basin phase was synchronous with accumulation of suitable reduced "trap" rocks (eg. at HYC), a syn-genetic model for mineralisation is likely to be appropriate. In this case, a topographic depression is required to facilitate ponding of exhaled metal-bearing brines. As a result, the long envisaged third order/sub-basin style targets likely to occur on the downthrown side of growth faults remain relevant.
2. Given the existence of suitable reduced "trap" lithologies, the sedimentary package is also prospective above the stratigraphic level/s at which active growth faulting occurred (ie. within the thermal sag package). An epigenetic model may be more appropriate in this situation, in which case the "trap" site for base metal mineralisation need not be associated with a

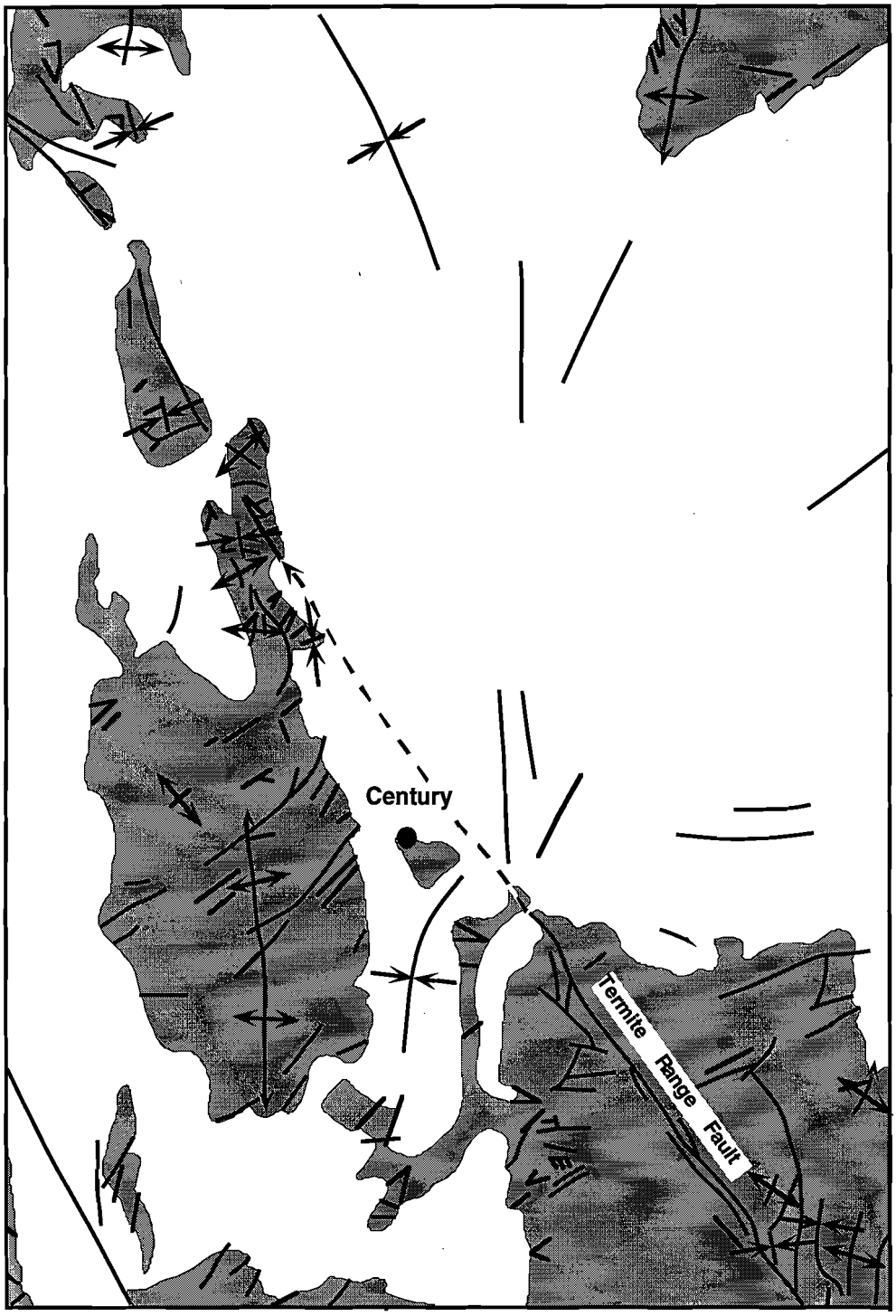

Figure 9. Location of the Century deposit adjacent to the Termite Range Fault; note the NE-trending faults that intersect the Termite Range Fault west of the deposit (geology modified after Sweet and Hutton, 1982).

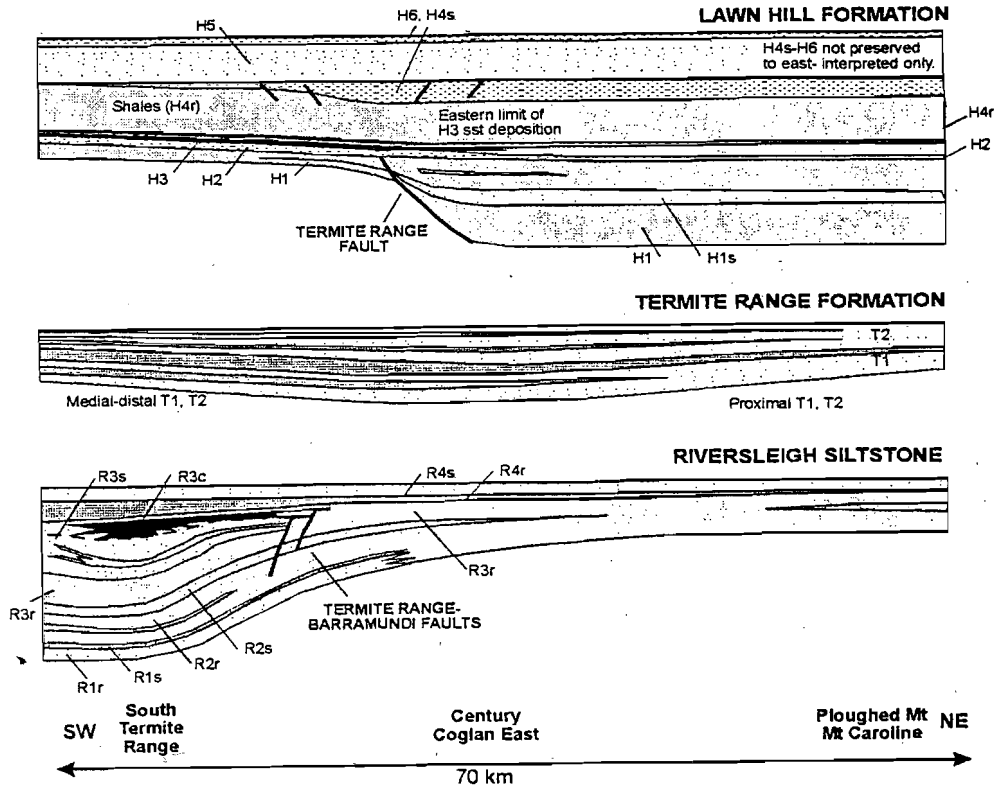

Figure 10. Cross-section of the Upper McNamara Group in the region of the Century deposit (modified after Andrews, 1996).

depocentre in the host sediments. However, fluid conduits that would facilitate this type of mineralisation are still likely to be situated near subsurface growth faults that were active earlier in the basin phase, in particular in areas where they were cut by orthogonal fault (?transfer) systems. Such areas may manifest as sites of anomalous degrees of strain during subsequent regional deformation.

Conclusions

This study illustrates the importance of understanding the rift architecture of mineralised basin settings, even where deposits occur in the tectonically quiescent sag package. Sedimentological analysis of the Torpedo Creek Quartzite in the Lady Loretta area indicates that:

1. Although there is no evidence of syn-sedimentary faulting in the Lady Loretta Formation itself, the mineralisation hosted in the unit sits adjacent to a growth fault in the subsurface.
2. This structure was a northwestern continuation of the Redie Creek Fault trend, which was active during the onset of McNamara Group deposition as growth fault.
3. This structure may have been cut/offset by a number of relatively closely spaced, roughly orthogonal faults (?transfers), subsequently re-activated during the Isan Orogeny to produce the present day structural complexity of the Lady Loretta area. If this was the case, other areas of equivalent structural complexity on the Lawn Hill Platform may be prospective for base metal mineralisation.

4. The setting of the Lady Loretta and Century Deposits indicates that, given the presence of appropriate reduced "trap" lithologies, the sedimentary packages adjacent to demonstrated syn-sedimentary (growth) faults are prospective within the overlying thermal sag package, well above the stratigraphic level/s at which the fault was active.

References

Amade, E. 1986. Le gisement eshalatif-sedimentaire de Zn-Pb-Ag de Lady Loretta (Queensland, Australie). Chronique de la Recherche Miniere. 54/483, 41-63.

Andrews, S. 1996. Stratigraphy and depositional setting of the Upper McNamara Group, Lawn Hill Region. New Developments in Metallogenic Research: The McArthur-Mount Isa-Cloncurry Minerals Province. EGRU Contribution 55, 5-9.

Broadbent, G. C., R. E. Myers, et al. 1996. Geology and origin of shale-hosted Zn-Pb-Ag mineralisation at the Century Mine, Northwest Queensland. New Developments in Metallogenic Research: The McArthur-Mount Isa-Cloncurry Minerals Province. EGRU Contribution 55, 24-27.

Bull, S. W. 1996. Progress Report: Sedimentology of the lower McNamarra Group, Riversleigh Fold Zone nortwestern Queensland. CODES: AMIRA/ARC Project P384A Report 1, 1-10.

Bull, S. W. and J. R. Rogers. 1996. Recognition and significance of an early compressional deformation event in the Tawallah Group, McArthur Basin, N. T. New Developments in Metallogenic Research: The McArthur-Mount Isa-Cloncurry Minerals Province. EGRU Contribution 55, 28-32.

Blake, D. H. 1987. Geology of the Mount Isa Inlier and environs, Queensland and the Northern Territory. B.M.R. Australia Bulletin. 225, 83 pp.

Coussement, C., P. Gentle, et al. 1994. The north Tanganyika hydrothermal fields, East African Rift System - Their tectonic control and relationships to volcanism and rift sedimentation. Tectonophysics. 237(3-3), 155-173.

Dunster, J. N. 1996. Sedimentology of the Lady Loretta Formation - a comparison of the regional setting to that of the Lady Loretta orebody. New Developments in Metallogenic Research: The McArthur-Mount Isa-Cloncurry Minerals Province. EGRU Contribution 55, 47-50.

Dunster, J. N. and B. A. McConachie. 1998. Tectono-sedimentary setting of the Lady Loretta Formation - synrift, sag or passive margin. Aust. J. E. Sci. 45(1), 89-92.

Dunnet, D. 1976. Some aspects of the Panantarctic cratonic margin in Australia. Phil. Trans. Roy. Soc. 280, 641-654.

Duffett, M. L. 1997. Gravity, magnetic and radiometric evidence for the geological setting of the Lady Loretta Pb-Zn-Ag deposit - a qualative appraisal. CODES: AMIRA/ARC Project P384A Report 4, 37-52.

Hoy, T. 1982. The Purcell Supergroup in southeastern British Columbia: sedimentation, tectonics and stratiform lead-zinc deposits. Geol. Assoc. Canada Spec. Pap. 25, 127-147.

Hinman, M. C. 1995. Base metal mineralisation at McArthur River: Structure and kinematics of the HYC-Cooley zone at McArthur River. AGSO Record 1995/5.

Hinman, M., V. Wall, et al. 1994. The interplays between sedimentation, deformation and hydrothermal activity at the the McArthur River Pb-Zn(Cu) Deposit. Geol. Soc. Aust. Abst. 37, 176-177.

Hancock, M. C. and A. H. Purvis. 1990. Lady Loretta silver-lead-zinc deposit. Geology of the Mineral Deposits of Australia and Papua New Guinea. F. E. Hughes. Melbourne, Aus. IMM, 943-948.

Hutton, L. and I. H. Wilson. 1985. Mammoth Mines Region, Queensland – 1:100,000 geological map commentary. BMR Australia.

Hutton, L. and I. H. Wilson. 1984. Mount Oxide Region, Queensland – 1:100,000 geological map commentary, BMR Australia.

Keele, R. A., S. W. Bull, et al. 1996. Possible rifting events in the Paradise Creek high strain zone, Lady Loretta region, Mount Isa. CODES: AMIRA/ARC Project P384 Report 2, 9-32.

Large, D. E. 1980. Geological parametres associated with sediment-hosted exhalative Pb-Zn deposits: an empirical model for mineral exploration. Geologisches Jahrbuch. 40, 59-129.

Large, D. E. 1983. Sediment-hosted massive sulfide lead-zinc deposits: an empirical model. Mineralogical association of Canada Short Course Handbook. 8, 1-30.

Large, R. R. L., S. W. Bull, et al. 1996. Review of genetic models from the HYC deposits: constraints from sedimentology, alteration halo and fluid chemical modelling. New Developments in Metallogenic Research: The McArthur-Mount Isa-Cloncurry Minerals Province, MIC 96 Extended Abstracts. EGRU Contribution 55, 72-74.

Lemcke, D. 1986. Pancontinental - Outokumpu Exploration JV, Lady Loretta area - the Big Syncline: a reappraisal. internal Company Report (unpublished).

McGoldrick, P. 1993. Geology of the Lady Loretta Deposit: review, new developments and implications for ore genesis. AMIRA/ARC Project P384 Report 3, 1-23.

McGoldrick, P., J. Dunster, et al. 1995. The Lady Loretta Zinc-Lead-Silver deposit: primary dispersion halos, sedimentology, ore textures, stable isotopes, and metal distributions - towards a genetic model. CODES: AMIRA/ARC Project P384 Final Report, 409-446.

O'Dea, M. G., G. S. Lister, et al. 1997. Geodynamic evolution of the Proterozoic Mount Isa Terrain. Orogeny through time. J.-P. Burg and M. Ford, Geological Society Special Publication. 121, 99-102.

Sweet, I. P. and L. J. Hutton. 1982. Lawn Hill Region, Queensland. BMR Australia 1:100,000 geological map commentary.

Terwindt, J. H. J. 1988. Palaeo-tidal reconstructions of inshore tidal depositional environments. Tide-influenced sedimentary environments and facies. P. L. De Boer, A. Van Gelder and S. D. Nio. Dodrecht/Boston/Lancaster/Tokyo, D. Reidel Publishing Co., 233-263.

Tiercelin, J.-J., M. Soreghan, et al. 1992. Sedimentation in large rift lakes: example from the Middle Pleistocene — modern deposits of the Tanganyika Trough, East African Rift System. Bull. Centre Rech. Explor. Prod. Elf Aquitaine. 6(1), 83-111.

Werner, W. 1990. Examples of structural control of hydrothermal mineralisation: Fault zones in epicontinental sedimentary basins - A review. Geol. Rundsch. 79(2), 279-290.

Walker, R. N., R. G. Logan, et al. 1977. Recent geological advances concerning the H.Y.C. and associated deposits, McArthur River, N.T. J. Geol. Soc. Aust. 24, 365-380.

Walker, R. J. 1984. Facies Models, Geoscience Canada.

Myrtle Basin – Lithogeochemistry and isotope chemostratigraphy

Ross Large and Stuart Bull
Centre for Ore Deposit Research

Summary

DDH Myrtle 5 (17 km south of HYC) shows strong Zn, alteration index and MnO_d anomalies in the base of the HYC Pyritic Shale Member. The other two holes, Myrtle 3 and Myrtle 4, show less well developed lithogeochemical indicators. Overall this outlines a northward vector towards mineralisation that appears unrelated to the bouger gravity anomaly developed south east of the Myrtle Basin. This is in the direction of HYC, and could indicate that its halo extends about 18 km south along the Emu Fault system. Alternatively it may reflect an intra-Myrtle Basin brine source associated with a growth-fault in the area of DDH Myrtle 5.

Introduction

A lithogeochemical study of three drill holes from the Myrtle Basin 15-20 km south of HYC (Fig. 1) was undertaken as part of our final six month research program in AMIRA Project P384A. The purpose of this study was three-fold:

1. To provide further information on the lithogeochemical halo to the HYC deposit. Our previous studies have relied on only the drill holes SW of HYC (Homestead 6, Barney 3 and BMR 2). The three Myrtle holes provided a further test of the halo model previously proposed (Large and Bull, 1996).
2. To test the significance of the gravity high south of HYC (Fig. 2) which may relate to the development of a thick sequence of pyritic black shales in the Myrtle Basin.
3. To relate lithogeochemistry to sedimentology structure and hydrothermal fluid flow regimes in the Myrtle Basin.

Sampling strategy

Samples were collected from each drill hole at 5-15 m spacings. A total of 48 samples were collected and analysed at the University of Tasmania for major and trace elements: 21 from DDH Myrtle 3, nine from DDH Myrtle 4 and 18 from DDH Myrtle 5. Insufficient time was available to undertake detailed sedimentological logs of each hole.

Myrtle Basin geology

The geology of the outcropping Myrtle Basin stratigraphy has been the focus of recent P384A fieldwork for the Basin Analysis Module (Bull and Scott, this volume). In summary, the area is a Barney Creek Depositional Cycle depocentre consisting of two transgressive/regressive cycles developed above the Coxco Dolomite. These have lower intervals of sub-wave base Basinal Facies sediments (mapped as Barney Creek Formation and Caranbirini Member) and upper intervals of deep sub-tidal to peritidal deposits (mapped as Reward Dolomite and Hot Springs Member). The cycles are thickest in two E-W-trending synclines, interpreted to be depositional features (hanging wall synclines), associated with E-W-trending growth faulting and tilt-block formation that controlled subsidence and sub-basin formation.

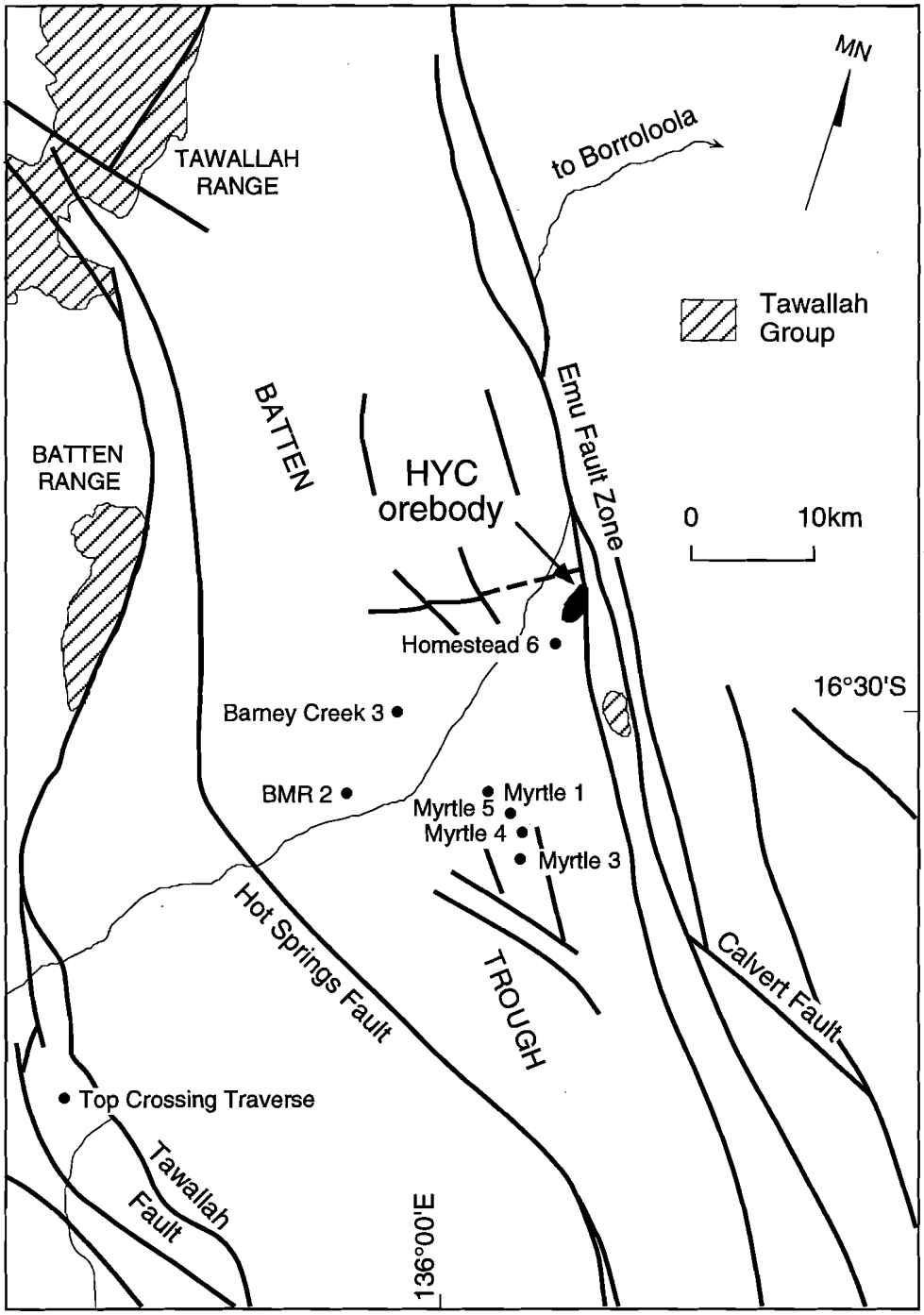

Figure 1. Location of drill holes in the Myrtle Basin in relation to HYC and other DDH sampled in this project.

McArthur Basin Gravity, Prospects & Drillholes

Grid cell size 200m

Bouguer gravity isogals at 1 mgal interval

Scale: 1:300,000

0 5 10 15 20

kilometres

Australian Map Grid, Zone 53

*Gravity station location

Stratiform Pb-Zn

Reducing units

CODES

Geology from NTGS Bauhinia Downs 1:250K, BMR McArthur Basin 1:1M, David Selley

December 1997

DDH Myrtle 3

This hole was collared 20.6 km south of HYC, and is the furthest south of the three Myrtle holes (Fig. 1). It was drilled to 273.4 m intersecting Reward Dolomite, Barney Creek Formation and Coxco Dolomite (Fig. 3).

Low levels of zinc (Zn <100 ppm) and alteration index (AI3 <30) indicate the hole is outside the ferroan dolomite halo to mineralisation (Figs 3 and 4). However Tl shows mild enrichment above 2 ppm in the base of the BCF that may relate to the HYC ore position.

DDH Myrtle 4

Collared 18 km south of HYC (Fig. 1) this hole intersects the same stratigraphy as DDH Myrtle 3. Is shows elevated Zn and Tl at the base of the BCF, however AI3 and MnO_d values are generally low. The Zn vs SEDEX AI plot shows a positive linear trend toward ore.

DDH Myrtle 5

This hole is yet closer to HYC (17 km distant) and intersects the same stratigraphy as DDH Myrtle 3 and 4. However, the succession at this locality is thicker, and there is a well-developed W-Fold Shale intersection at the base of the Barney Creek Formation that is not present in the other holes. DDH Myrtle 5 exhibits strong anomalies in AI Mark 3, Tl, Zn and MnO_d at the base of the HYC Pyrite Shale and top of the W-Fold Shale Member (Fig. 7). These patterns are very similar to those recorded in DDH Barney 3 and suggest that DDH Myrtle 5 is within the ferroan dolomite and manganese carbonate halos to mineralisation. In the priority discrimination plot (Fig. 8b), four samples (22%) are within priority 3, indicating the outer halo to SEDEX mineralisation.

K-feldspar:illite relationships

Downhole K_2O/Al_2O_3 plots for the three drill holes are shown in Figure 9. These plots show that sediments within DDH Myrtle 3 and Myrtle 4 have K_2O/Al_2O_3 ratios greater than 0.6 and therefore consistently contain K-feldspar > illite. This signature is typical of recharge (downflow) areas of hydrothermal fluid circulation (Large et al., this volume).

The K_2O/Al_2O_3 pattern in DDH Myrtle 5 is distinctly different to the other two holes (Figs 9 and 10). The Reward Dolomite and upper HYC Pyritic Shale (down to 230 m) exhibits $K_2O/Al_2O_3 > 0.6$ and a recharge signature, whereas the lower HYC Pyritic Shale and W-Fold Shale shows low K_2O/Al_2O_3 ratios suggesting illite >K-feldspar and a discharge signature.

This discharge zone in Myrtle 5 corresponds to the interval of elevated Zn, Tl and SEDEX AI. The mineral percentages of samples from DDH Myrtle 5, calculated using the MINSQ program (Fig. 10), indicate the interval of illite (phengite) dominance below 220 m, corresponding to the discharge zone.

Carbonate isotope chemostratigraphy

C/O isotope results from DDH Myrtle 3 and 5 are not yet to hand. They will be reported at the final meeting. The isotope results will provide a good test of the discharge/recharge model based on K_2O/Al_2O_3 and Oxygen isotope patterns proposed by Large et al., (this volume).

Discussion

The lithogeochemical results from the three Myrtle drill holes provide a vector northwards away from the centre of the Myrtle Basin gravity anomaly (Fig. 2). This suggests that the gravity anomaly may not be due to a thickened section of pyritic black shales within the BCF at this locality.

The gravity anomaly may be caused by:

(a) an abnormal thickness of dolomites within the section, repeated by faulting or folding (Mark Duffett, pers. comm.);

(b) pyritic black shales at a different stratigraphic level to the BCF.

The northward lithogeochemical vector in the Myrtle Basin is towards HYC some 17 km to the north, raising the possibility that it records the outer

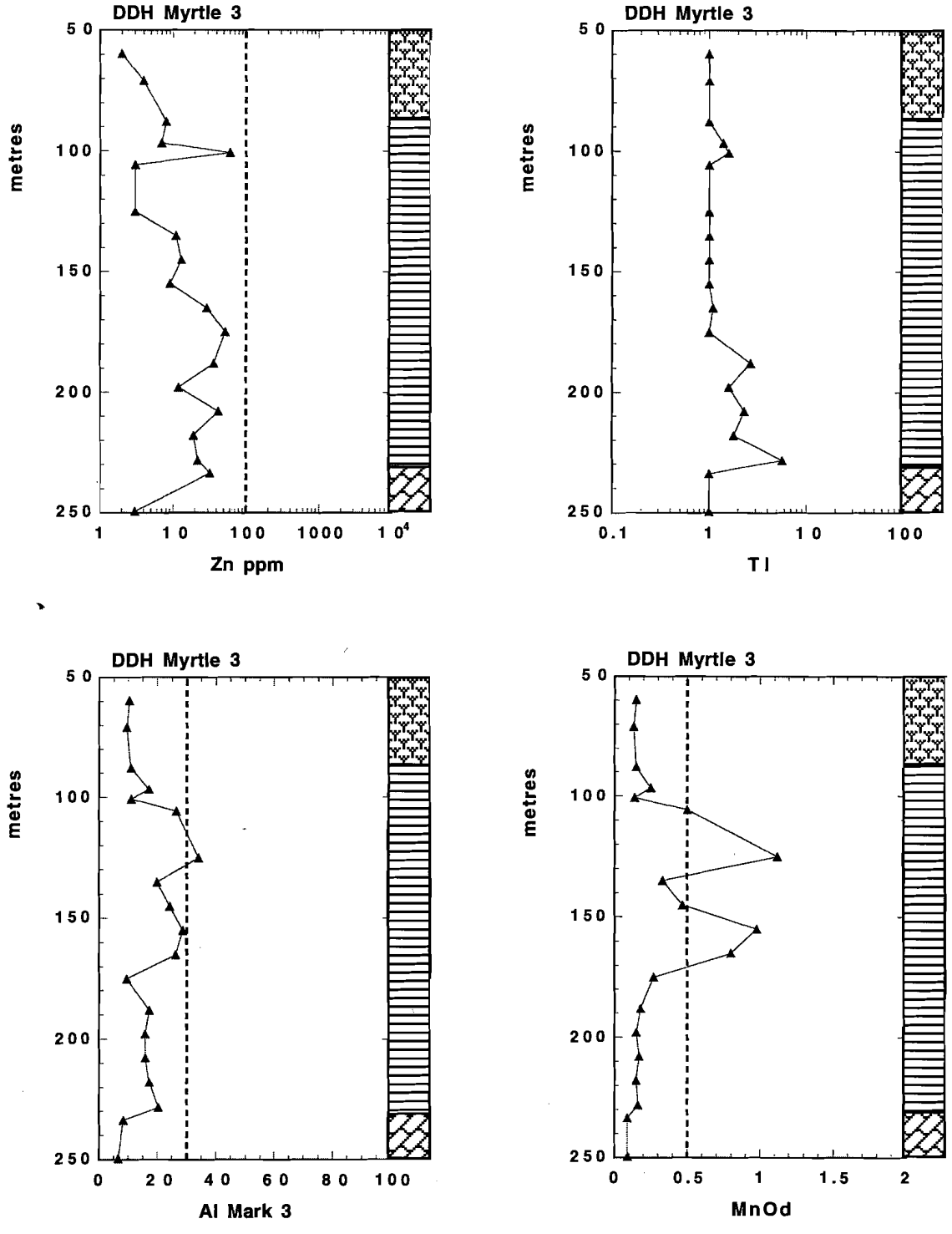

Figure 3. Downhole plots of Zn, Tl, Al_3 and MnO_d for DDH Myrtle 3.

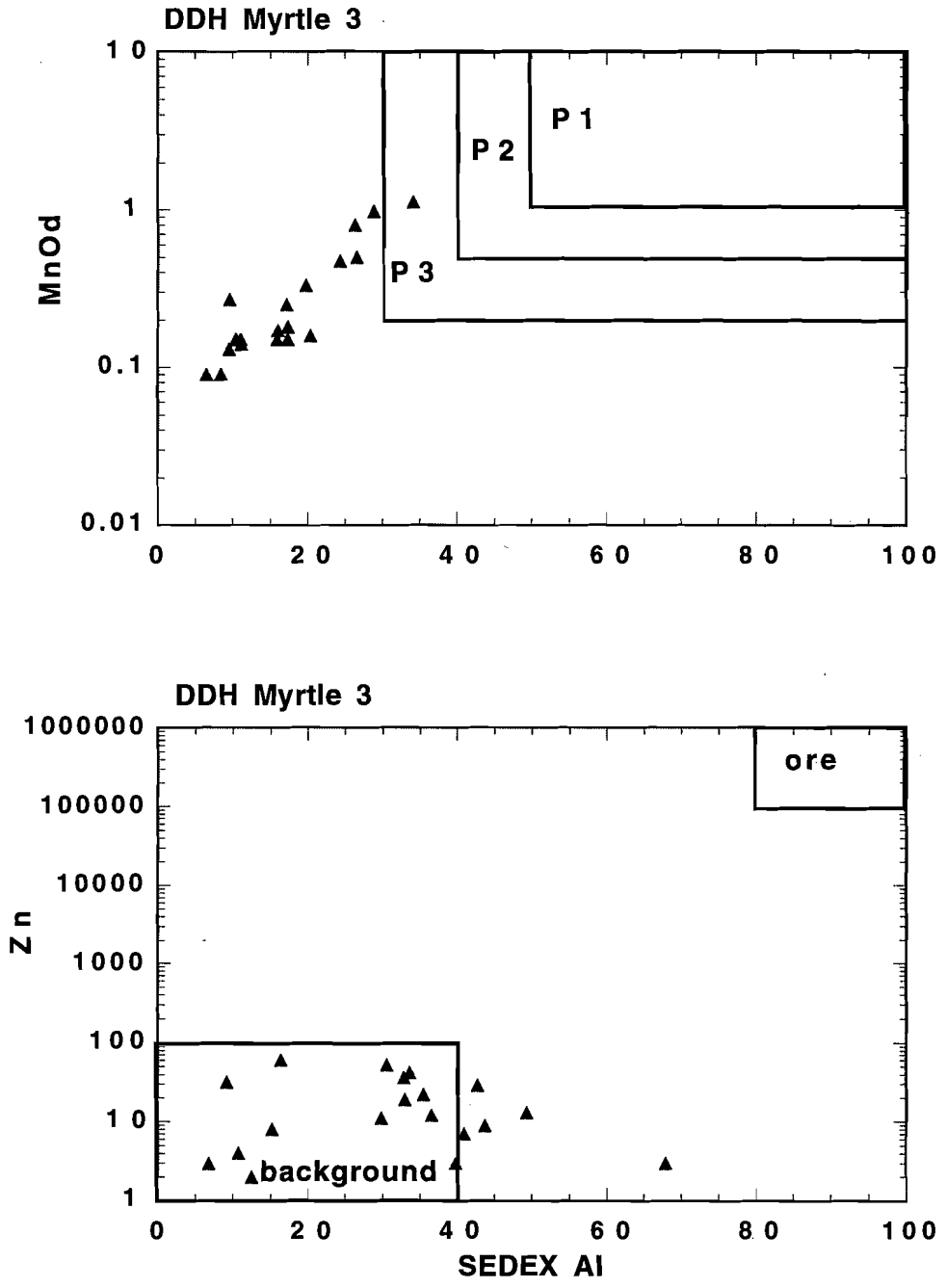

Figure 4. Zn vs SEDEX Al and MnO_d vs Al3 plots for DDH Myrtle 3, indicating low priority.

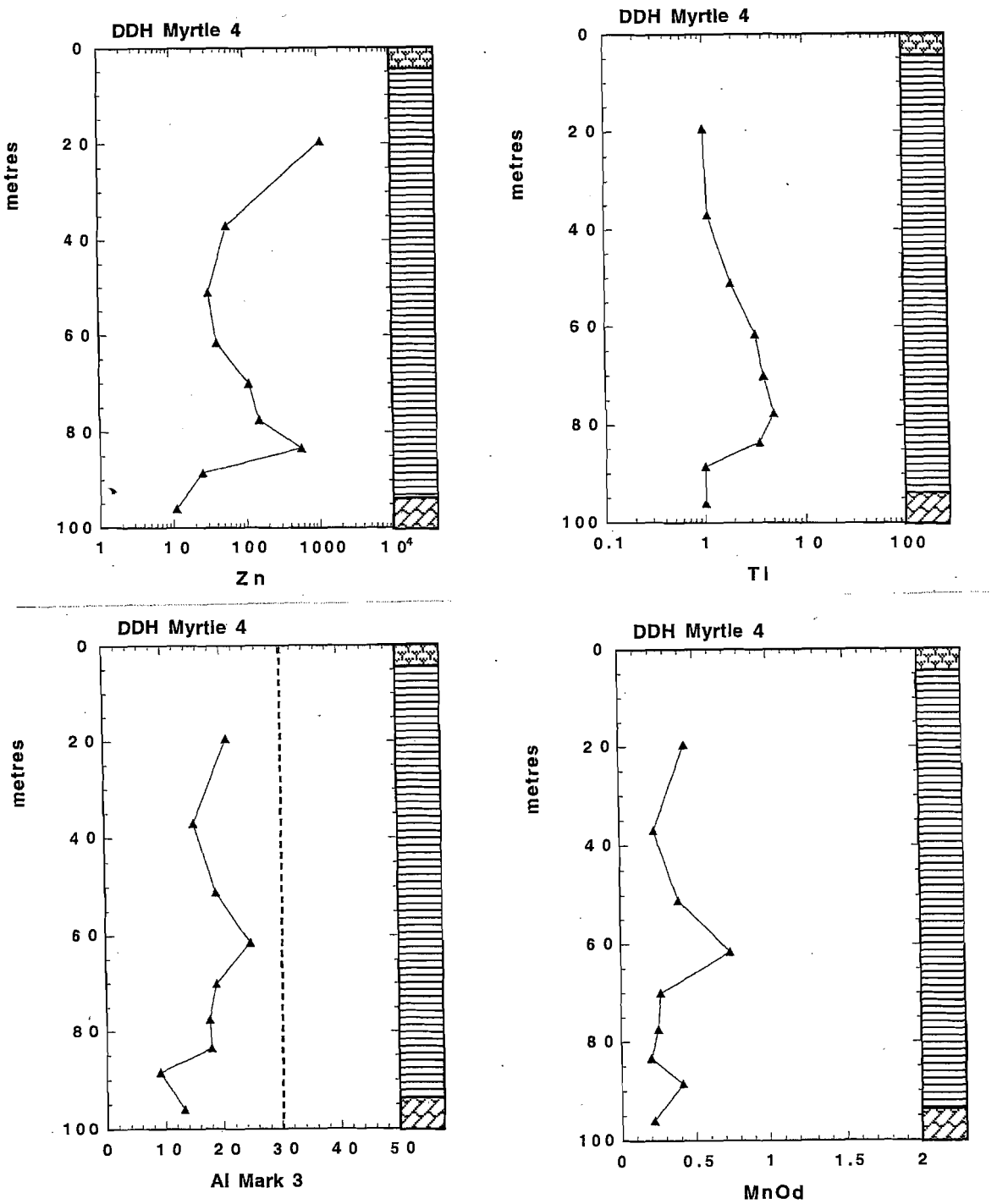

Figure 5. Downhole plots of Zn, Tl, Al3 and MnO_d for DDH Myrtle 4.

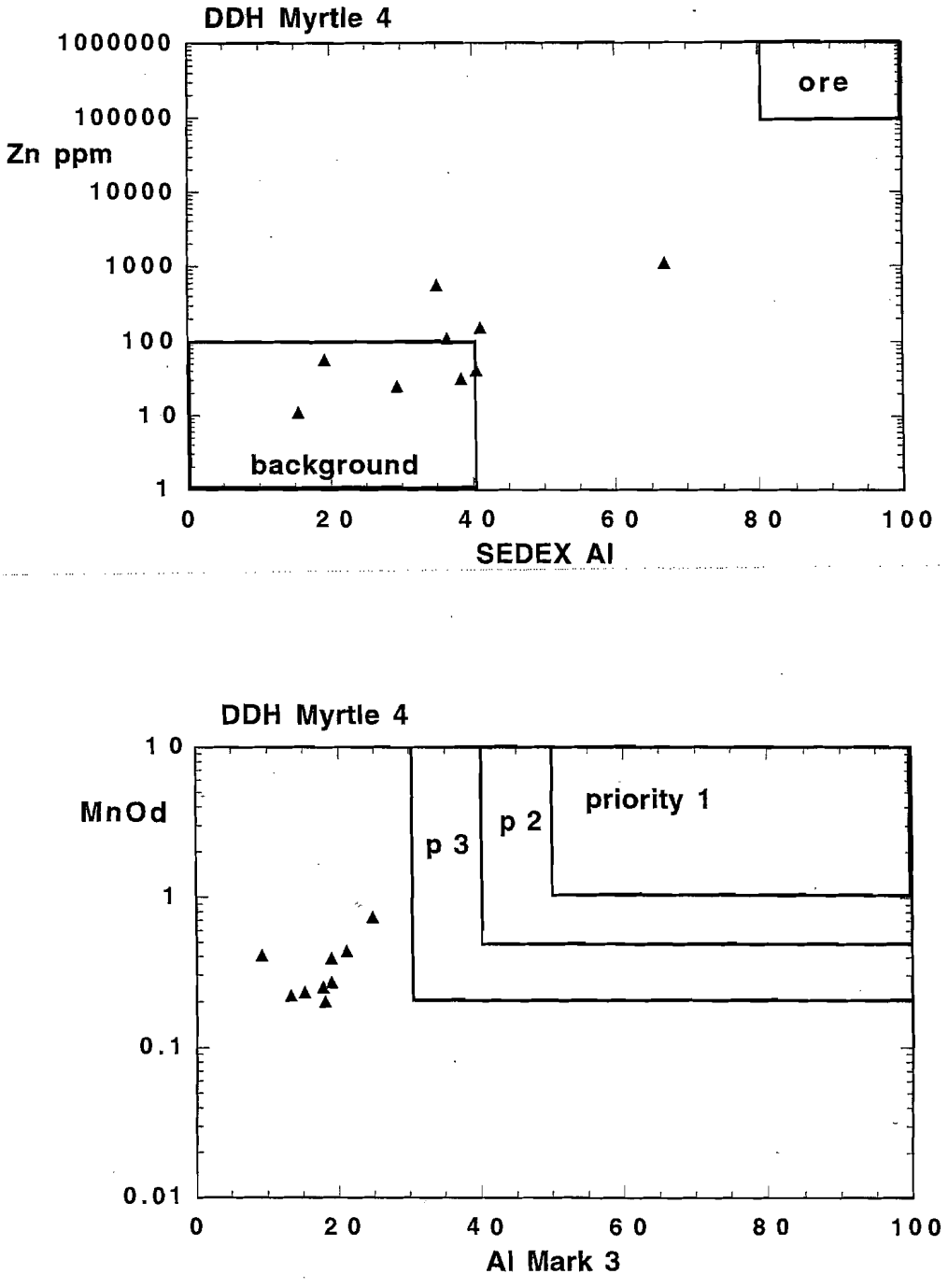

Figure 6. Zn vs SEDEX Al and MnO_d vs Al3 plots for DDH Myrtle 4. The upper plot shows a positive trend toward ore.

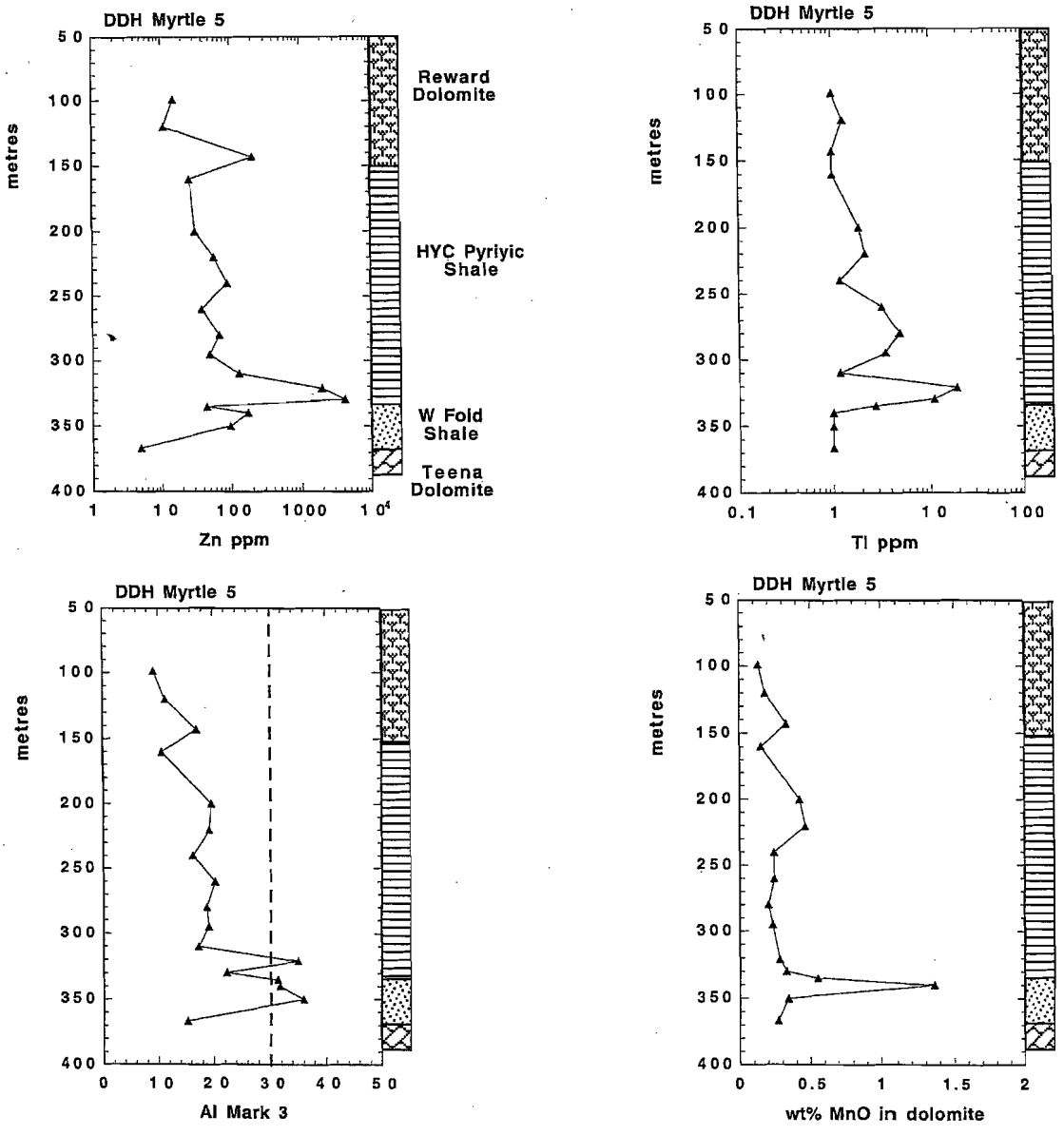

Figure 7. Downhole plots of Zn, Tl, Al3 and MnO_d for DDH Myrtle 5.

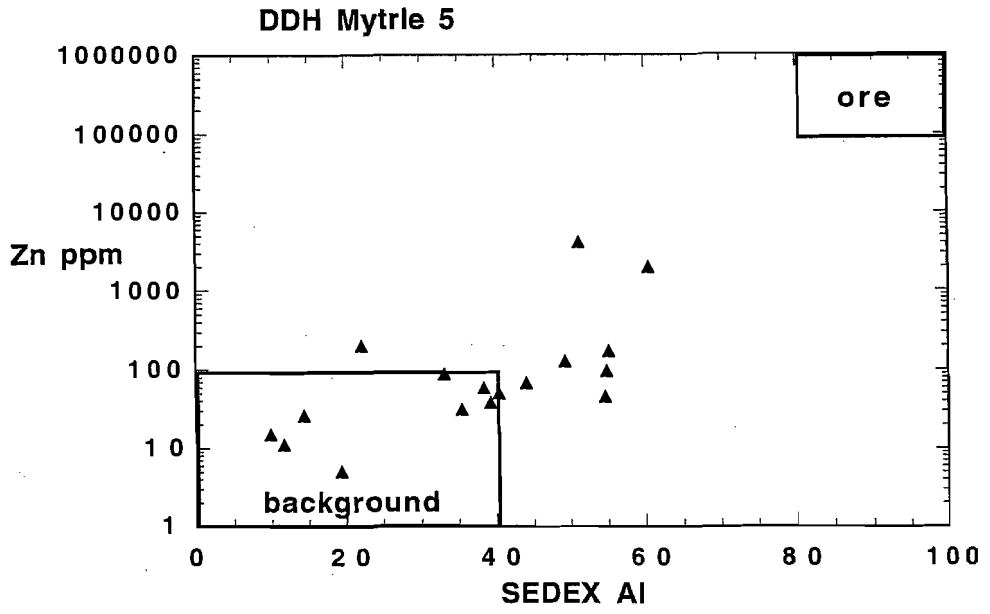

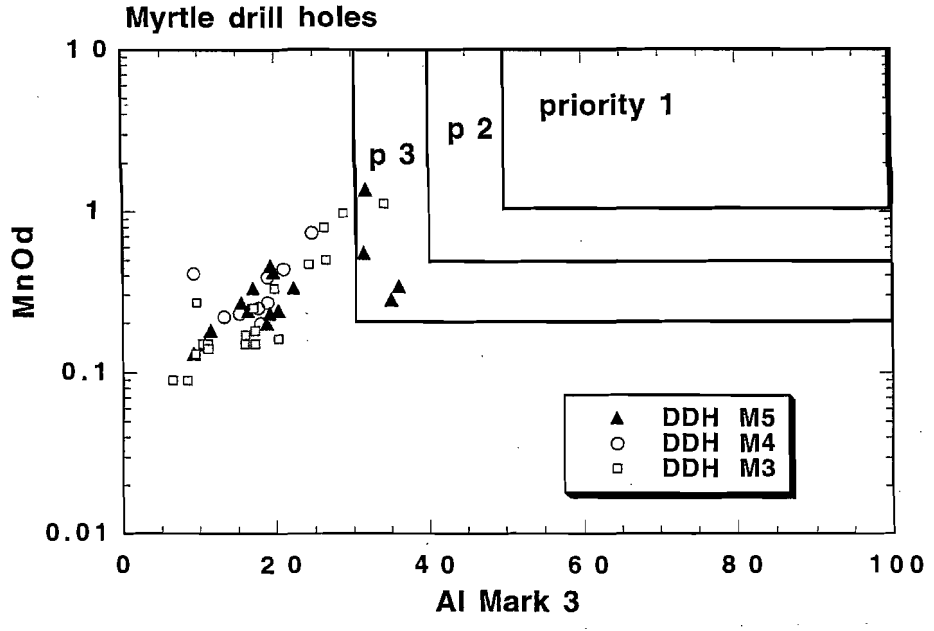

Figure 8 . Zn vs SEDEX Al and MnO_d vs Al3 plots for DDH Myrtle 5. Both plots indicate the classic pattern of the outermost halo to a SEDEX deposit.

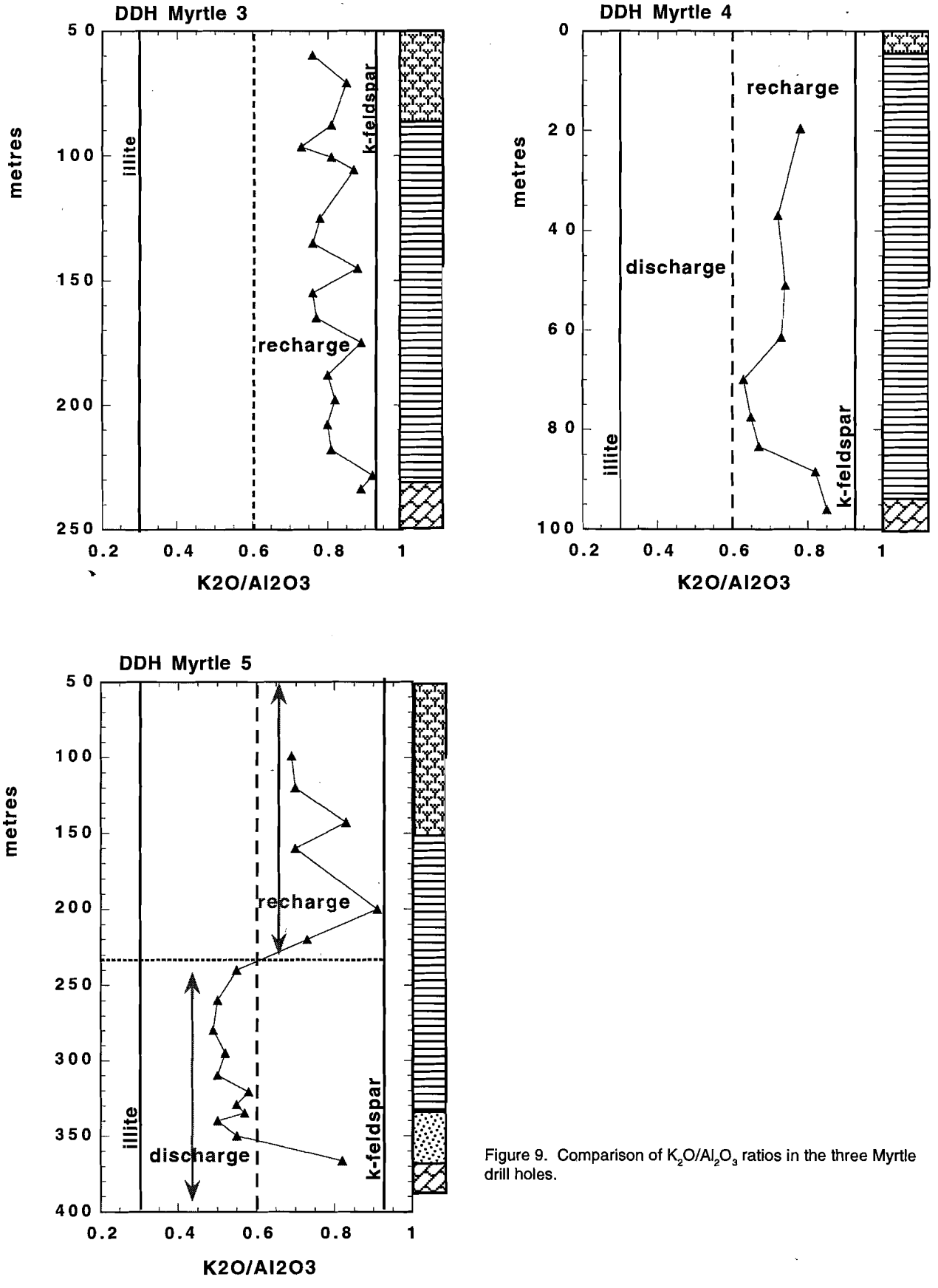

Figure 9. Comparison of K_2O/Al_2O_3 ratios in the three Myrtle drill holes.

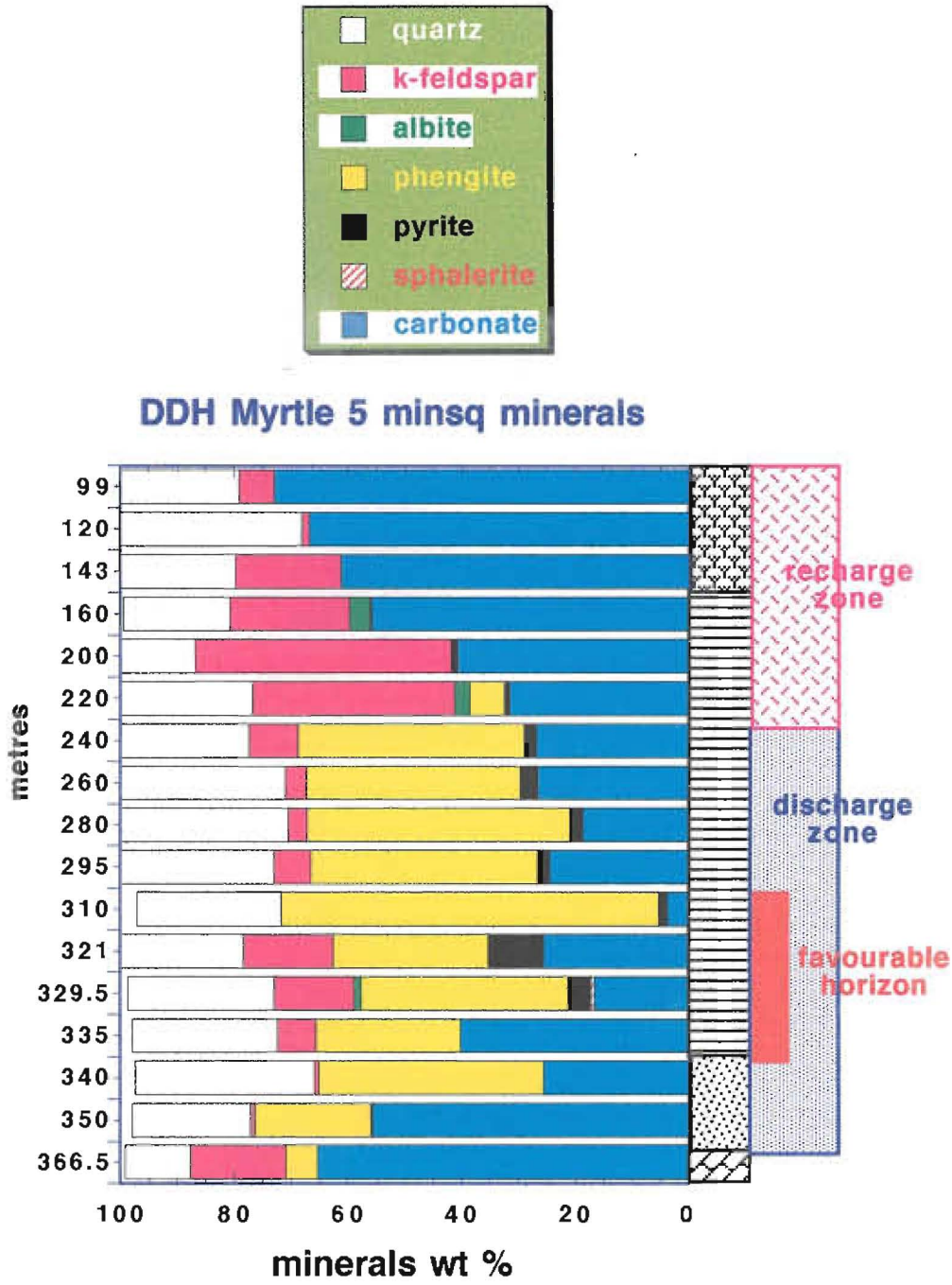

Figure 10. Mineral percentages of samples from DDH Myrtle 5, calculated using the MINSQ program.

edge of the Fe-Mn dolomite, Zn, Tl halo to the deposit. However, results of the Basin Analysis fieldwork in the Myrtle Basin (Bull and Scott, this volume) provide an alternative explanation. DDH Myrtle 5 was collared within one of the two structures interpreted as hanging wall syncline depocentres during sedimentation. This is consistent with the thicker intersection of Barney Creek Depositional Cycle deposits at this locality, and suggests proximity to a growth fault that controlled sub-basin formation. During the early phase of the Barney Creek Depositional Cycle, when the HYC deposit was forming to the north in a similar setting, this structure could have acted as a local source of metal-bearing brines that formed a lithogeochemical anomaly within the Myrtle Basin.

The latter interpretation is partly substantiated by lithogeochemical work carried out early in the project, that examined open file geochemistry from DDH Myrtle 1 (Large and McGoldrick, 1993), located 2.5 km northwest of DDH Myrtle 5 (Fig. 1). Although there was significant zinc anomalism, the intersection recorded generally lower values of alteration index and % MnO in dolomite at this locality closer to HYC than DDH Myrtle 5. This is consistent with the association of the lithogeochemical anomalism with a local source within the Myrtle Basin, centred on the hanging wall syncline depocentre that hosts DDH Myrtle 5. It is also consistent with the K_2O/Al_2O_3, pattern, which suggests hydrothermal discharge during accumulation the lower part of the BCF in DDH Myrtle 5, which would correspond to the period of maximum activity on the nearby growth fault.

Conclusions

1. Lithogeochemical data suggests that DDH Myrtle 5 may lie within the outer Fe-Mn dolomite, Zn, Tl halo to mineralisation.

2. DDH Myrtle 4 lies at the margin of the halo, while DDH Myrtle 3, 2 km to the south, is outside the halo extremity.

3. The lithogeochemical data appears to be unrelated to the gravity high south south east of the dill holes. It may record the outer edge of the halo to the HYC deposit. Alternatively, a more favoured explanation, is that it may reflect an intra-Myrtle Basin brine source associated with a growth-fault in the area of DDH Myrtle 5.

4. K_2O/Al_2O_3 relationships are consistent with this interpretation. They indicate that the lower BCF interval in Myrtle 5, which would have been deposited when activity on the nearby growth fault was at a maximum, is affected by hydrothermal discharge. In contrast, the patterns in Myrtle 3 and 4 are evidence of hydrothermal recharge zones.

References

Bull, S. W., and Scott, R., this volume. Geology of the BCDC in the Myrtle Basin area, southern McArthur Basin, Northern Territory., AMIRA P384A, Final Report, November 1998.

Large, R.R., Bull, S. and Garven, G., this volume, Criteria to determine recharge (downflow) and discharge (upflow) zones related to stratiform Zn-Pb-Ag deposits, McArthur Basin, N.T., AMIRA P384A, Final Report, November 1998.

Large, R.R. and Bull, S., 1996, Lithogeochemistry and isotope chemostratigraphy of the Barney Creek Formation, McArthur Basin, AMIRA P384A, Report 2, p. 41-86.

Large, R.R., and McGoldrick, 1993, Primary geochemical halos related to Proterozoic sediment hosted Pb-Zn deposits and applications to exploration. AMIRA P384, Report 3, October, 1993.

Geochemical data sets for northern Australian Proterozoic sedimentary rocks: background variations in lithogeochemical vectors to sedimentary Zn-Pb deposits

Peter McGoldrick
Centre for Ore Deposit Research

Summary

This report describes the various geochemical data generated during the course of AMIRA Project P384A. A table listing of individual samples sets and elements analysed is provided.

A PC format diskette containing Excel Workbooks and text files for all new data acquired in AMIRA P384 and P384A is appended to this volume.

A subset of 189 unmineralised, or very weakly mineralised, samples from the Lawn Hill Platform was chosen to generate 'average background' data for late Palaeoproterozoic fine grained sedimentary rocks. Summary diagrams and statistics are presented for these samples.

Introduction

Over 400 high quality multi-element analyses were carried out at the University of Tasmania as part of AMIRA Project P384. This work continued in P384A, and a further 446 samples were analysed. In all cases XRF was the method used to measure both major and trace elements.

New data for AMIRA P384A

As part of the continuing investigation of litho-geochemical halos to the northern Australian Sedex style Zn deposits an additional 446 high quality multi-element geochemical analyses of barren or very weakly mineralised sedimentary rocks were performed.

Approximately 150 samples were from unweathered surface outcrops and drill core from three areas in the southern McArthur Basin (see Table 1):

1. Drill core from the Berjaya prospect to the west of HYC (Cooke et al., this volume);
2. Drill core from the Myrtle sub-basin to the north of HYC (Large and Bull, this volume), and
3. Core and surface samples from the Gorge area south of the Abner Range (Winefield et al., this volume)

In addition, 20 samples from a drill hole 2 km S of HYC (DDH Homestead 6) were analysed to complete the halo studies of the HYC deposit (Large and Bull, 1996).

The remainder of samples were from the Western Succession of the Mount Isa Inlier (see Table 2). These included sample sets collected for halo studies at :

1. Mount Novit (McGoldrick, 1996)
2. Grevillea (McGoldrick, AMIRA P384A Final Report v. 2)

and, unmineralised (or weakly mineralised) drill core for background geochemical studies, from:

1. Lady Loretta Formation, 4 km NNE of Lady Loretta mine, and from the Carrier area E of Riversleigh station
2. Paradise Creek Formation and Gunpowder Creek Formation at Bloodwood Bore (Kamarga).

All these data are included on a PC format diskette as a series of Excel Workbooks and text files in a pocket at the back of this report.

Table 1. AMIRA P384A Geochemical data sets from the McArthur Basin

	#samples	*Elements*
Gorge Prospect drill-core	20	Majors+As,Ba,Cu,Pb,Rb,Sr,Tl & Zn
Gorge Prospect KP97-4 traverse	23	Majors+As,Ba,Cu,Pb,Rb,Sr,Tl & Zn
Berjaya drill core	21	Majors+As,Ba,Cu,Pb,Rb,Sr,Tl & Zn
Boko 5 drill-core	36	Majors+As,Ba,Cu,Pb,Rb,Sr,Tl & Zn
Myrtle Basin drill-core	45	Majors+As,Ba,Bi,Cu,Ni,Pb,Rb,Sr,Th,Tl, U,V,Y,Zn & Zr
Homestead 6 drill-core	20	Majors+As,Ba,Cu,Pb,Rb,Sr,Tl & Zn

Table 2. AMIRA P384A Geochemical data sets from the Mount Isa Basin

	#samples	*Elements*
Moondarra Siltstone (DDH SA10)	10	Majors+As,Ba,Cu,Pb,Rb,Sr,Tl & Zn
Moondarra Siltstone (Mt Novit drill core)	61	Majors+As,Cu,Pb,Rb,Sr,Tl & Zn
Bloodwood Bore drill core	45	Majors+As,Ba,Cu,Pb,Rb,Sr,Tl & Zn
Lady Loretta Formation (DDH CM40)	15	Majors+As,Ba,Cu,Pb,Rb,Sr,Tl & Zn
Lady Loretta Formation (DDH CM35)	22	Majors+As,Ba,Cu,Pb,Rb,Sr,Tl & Zn
Lady Loretta Formation (DDH LA64)	54	Majors+As,Ba,Cu,Pb,Rb,Sr,Tl & Zn
Lady Loretta Formation (DDH LA67)	9	Majors+As,Ba,Cu,Pb,Rb,Sr,Tl & Zn
Grevillea samples	55	Majors+As,Ba,Cu,Pb,Rb,Sr,Tl & Zn

Background variations in important chemical parameters

A subset of these samples, representative of unmineralised McNamara Group sediments, has been combined with background data from AMIRA P384 (McGoldrick, 1994) to produce a set of 189 analyses that can be used to gauge background variability in all the important fine grained rock types. The CaO analytical data was used to calculate 'normative dolomite' for each sample (calculated by assuming all CaO is contained in dolomite) has been used to subdivide the samples into four 'rock types': dolomite (>75% normative dolomite), shaley dolomite (50–75%), dolomitic shale (25–50%) and shale (<25%).

This classification generates subsets of 64 shales, 38 dolomitic shales, 59 shaley dolomites and 28 dolomites. Summary statistical data (median, interquartile range, mean and standard deviation) from each subset are presented on Table 3. A series of box-plots are presented in Figures 1,2,3 and 4 for important pathfinder elements and element ratios for each of these sample groups. Box-plots are a useful, non-parametric, graphical representation of the centre (uses the median) and spread (uses the interquartile range and 'whiskers' to the furthest data point within 1.5 times the interquartile range from the 'box') of a data set. Figure 5 displays standard cross-plots (Large and McGoldrick, 1998) for the stratiform sediment-hosted geochemical vectors: Sedex AI, AI3, Zn and MnO_d.

Zr, TiO_2 and Rb

These three elements are all good discriminants of rock type, with shales having highest and dolomites having lowest levels of each element. Zr and TiO_2 are probably hosted in detrital heavy minerals, which are likely to be more abundant in the fine grained clastic rocks than in 'cleaner' carbonates. Rb will be hosted in phyllosilicates and K-feldspar, and hence be more abundant in 'dirty' clastic rocks.

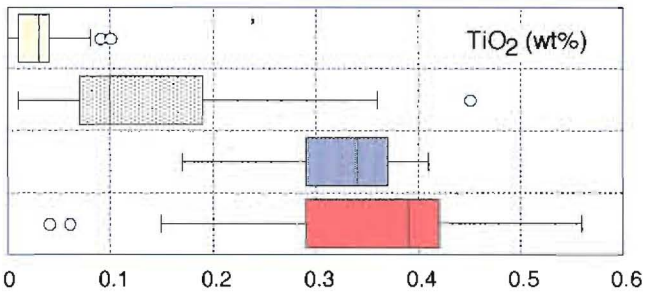

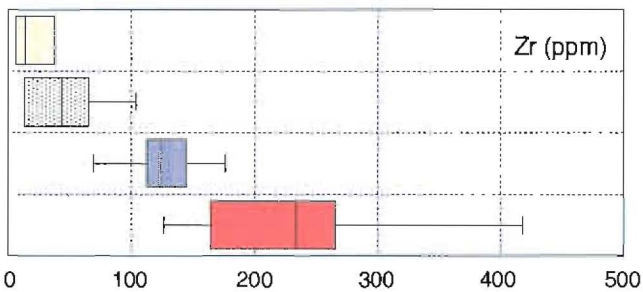

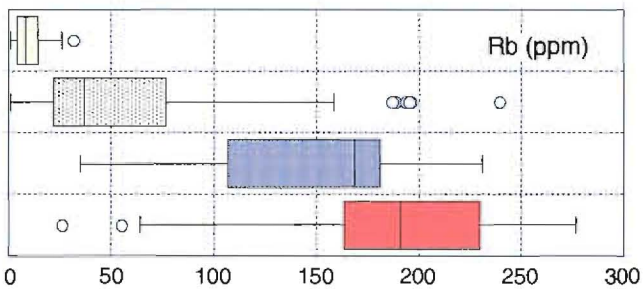

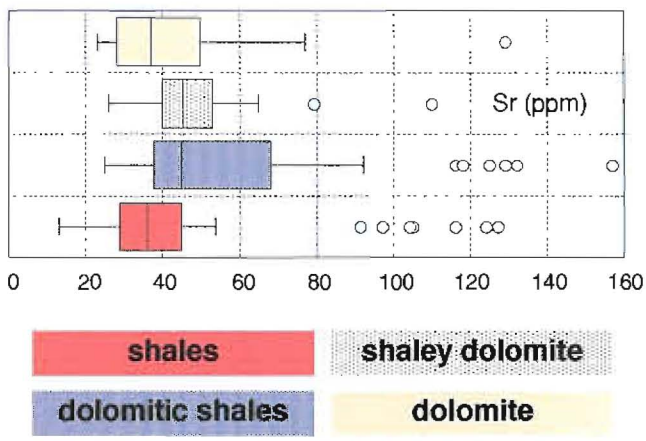

Figure 1. Boxplots for TiO_2, Zr, Rb, and Sr for 189 McNamara Group sediments; the 'box' spans the 25th to 75th percentile (the interquartile range), the 'bar' is the median value, 'whiskers' extend to the most extreme value within 1.5 x interquartile range from the upper and lower limit of the box.

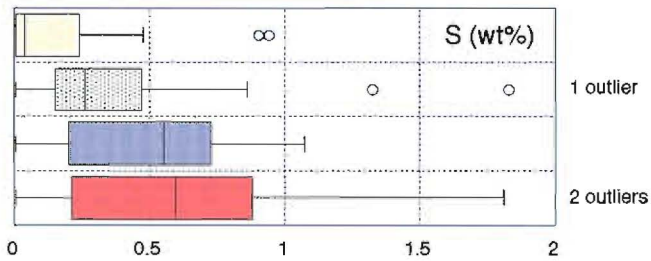

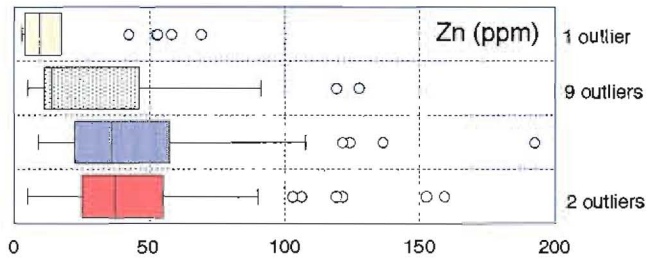

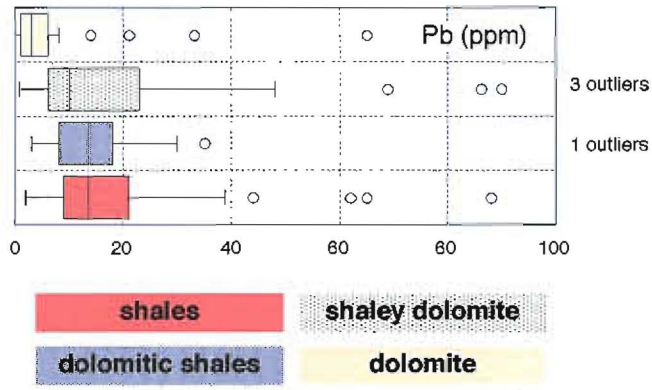

Figure 2. Boxplots for S, Zn, and Pb for 189 McNamara Group sediments.

Ba

Ba tends to be lowest in dolomites (median=40 ppm) and increases to a median of 422 ppm in the shales. The reason for this trend is not known.

S, Zn, Pb, Cu, As, and Tl

In general the chalcophile elements are a little higher in the shales than the more dolomitic lithologies, and Zn>Pb>Cu for a given rock type. Tl in most samples is below 2 ppm, and in the more dolomitic rock types often below 0.5 ppm, the limit of detection by XRF.

Sedex AI, AI 3, MnO_d and Metal Index

The 'shale effect' (Large, 1994) is evident in the higher Sedex AI values in the shales, but AI3 does not vary significantly with rock type, and a 'background' value of 30 or less (Large and McGoldrick, 1998) is confirmed by these data. MnO_d shows a wide range in the shales, and there is clearly a 'shale effect', even though low carbonate samples were not included in the statistical analysis. The variation in MnO_d for the other three rock types suggests that the cut-off for anomalous values is about 0.5 wt% MnO. The range shown by the Metal Index data indicate a level of 3000 (Large and McGoldrick, 1998) is a reasonable upper limit to background values.

Cross-plots

The Zn/SedexAI and Zn/AI3 plots show a scatter of data that are not anomalous, and with higher Zn samples having low AI values (cf. Kamarga case study data, McGoldrick (1995) and v. 1 of this report). By contrast, many of the shales and dolomitic shales plot in the 'Prospectivity 3' boxes of MnO_d/SedexAI and MnO_d/AI3 plots. This suggests that there is a 'shale effect' that is not accounted for in MnO_d calaculations, and that less emphasis should be placed on samples with weakly anomalous MnO_d values if they are shales or dolomitic shales.

Conclusions

Over 400 new high-quality whole rock analyses are appended to this report; the data are from halo case studies and background samples sets.

Data from 189 McNamara Group sedimentary rocks largely confirm the background values empirically derived from various halo case studies in AMIRA Projects P384 and P384A.

The 'shale effect' which causes high Sedex AI values in 'background' shaley rocks may also be biasing these lithologies to weakly anomalous MnO_d values (0.2 to 0.5wt%).

References

Large, R. R., and P. J. McGoldrick, 1994, Refinement of the Sedex Alteration Index and MnOD vectors: CODES AMIRA/ ARC Project P384 — Proterozoic sediment-hosted base metal deposits Report No. 5, p. 1-17.

Large, R. R., and S.W. Bull, 1996, Lithogeochemistry and isotope chemostratigraphy of the Barney Creek Formation CODES AMIRA/ARC Project P384A —Sediment-hosted base metal deposits Report No. 2, p. 41-88.

Large, R.R., and McGoldrick, P.J., 1998, Lithogeochemical halos and geochemical vectors to stratiform sediment-hosted Zn-Pb-Ag deposits. Part 1: Lady Loretta deposit, Queensland, Journal of Geochemical Exploration, 63, 37-56.

McGoldrick, P., 1994, The geochemistry of 'barren' late Palaeoproterozoic sediments from the McNamara Group: background values for the Sedex AI, AI Mk3 and MnOd, AMIRA P384 Report 7, 141-148.

McGoldrick, P., 1995, The alteration index and MnOd at Kamarga re-visited: new geochemicsl data, AMIRA P384 Final Report, pp 303–318

McGoldrick, 1996, Primary dispersion halos associated with the Mount Novit Zn-Pb-Ag mineralisation, AMIRA P384A Report 2, 135-156.

Table 3: Summary statistics for 189 McNamara Group fine grained sedimentary rocks

		Median	*IntQRange*	*Mean*	*StdDev*	*# samples*
SedexAI	shales	55	21	56	14	64
	dolomitic shales	40	15	37	10	38
	shaley dolomites	18	22	24	15	59
	dolomites	16	6	17	8	28
AI3	shales	20	7	22	8	64
	dolomitic shales	19	8	20	6	38
	shaley dolomites	15	11	18	9	59
	dolomites	16	5	16	7	28
MnOd	shales	0.49	0.47	0.62	0.43	47
(wt%)	dolomitic shales	0.28	0.27	0.35	0.19	38
	shaley dolomites	0.17	0.22	0.24	0.16	59
	dolomites	0.16	0.07	0.19	0.12	28
Metal Index	shales	1589	1126	1993	1591	64
	dolomitic shales	1714	986	3509	11747	38
	shaley dolomites	1256	2552	4265	12935	59
	dolomites	357	462	905	1429	28
TiO2	shales	0.39	0.36	0.13	0.11	64
(wt%)	dolomitic shales	0.34	0.32	0.08	0.07	38
	shales	0.10	0.14	0.12	0.10	59
	dolomites	0.03	0.03	0.03	0.03	28
Zr	shales	234	88	229	67	24
(ppm)	dolomitic shales	124	40	129	33	9
	shales	43	47	48	32	7
	dolomites	14	18	17	14	4
Rb	shales	191	66	187	58	64
(ppm)	dolomitic shales	169	74	153	47	38
	shales	37	53	61	59	59
	dolomites	8	10	10	8	28
Sr	shales	36	16	43	27	56
(ppm)	dolomitic shales	45	36	63	37	37
	shales	46	13	47	14	54
	dolomites	37	20	43	22	28
S	shales	0.60	0.65	0.70	0.71	64
(wt%)	dolomitic shales	0.55	0.53	0.50	0.32	38
	shales	0.26	0.32	0.39	0.54	59
	dolomites	0.04	0.22	0.16	0.25	28
Zn	shales	38	28	61	116	64
(ppm)	dolomitic shales	36	35	48	39	38
	shales	14	34	500	2330	59
	dolomites	10	12	106	471	28
Pb	shales	14	12	18	15	64
(ppm)	dolomitic shales	14	10	33	118	38
	shales	10	16	37	109	59
	dolomites	3	4	7	13	28
Ba	shales	422	145	453	193	56
(ppm)	dolomitic shales	362	160	487	725	37
	shales	264	476	588	916	54
	dolomites	39	214	337	738	28
Cu	shales	8	9	27	102	64
(ppm)	dolomitic shales	6	9	8	5	38
	shaley dolomites	6	10	9	10	59
	dolomites	8	38	4	3	28
As	shales	12	10	11	12	64
(ppm)	dolomitic shales	8	7	6	11	38
	shaley dolomites	6	10	9	10	59
	dolomites	2	1	4	3	28
Tl	shales	1.0	1.5	1.5	1.2	64
(ppm)	dolomitic shales	1.6	1.5	1.6	1.0	38
	shaley dolomites	0.5	1.1	1.1	1.0	59
	dolomites	0.5	0.0	0.7	0.7	28

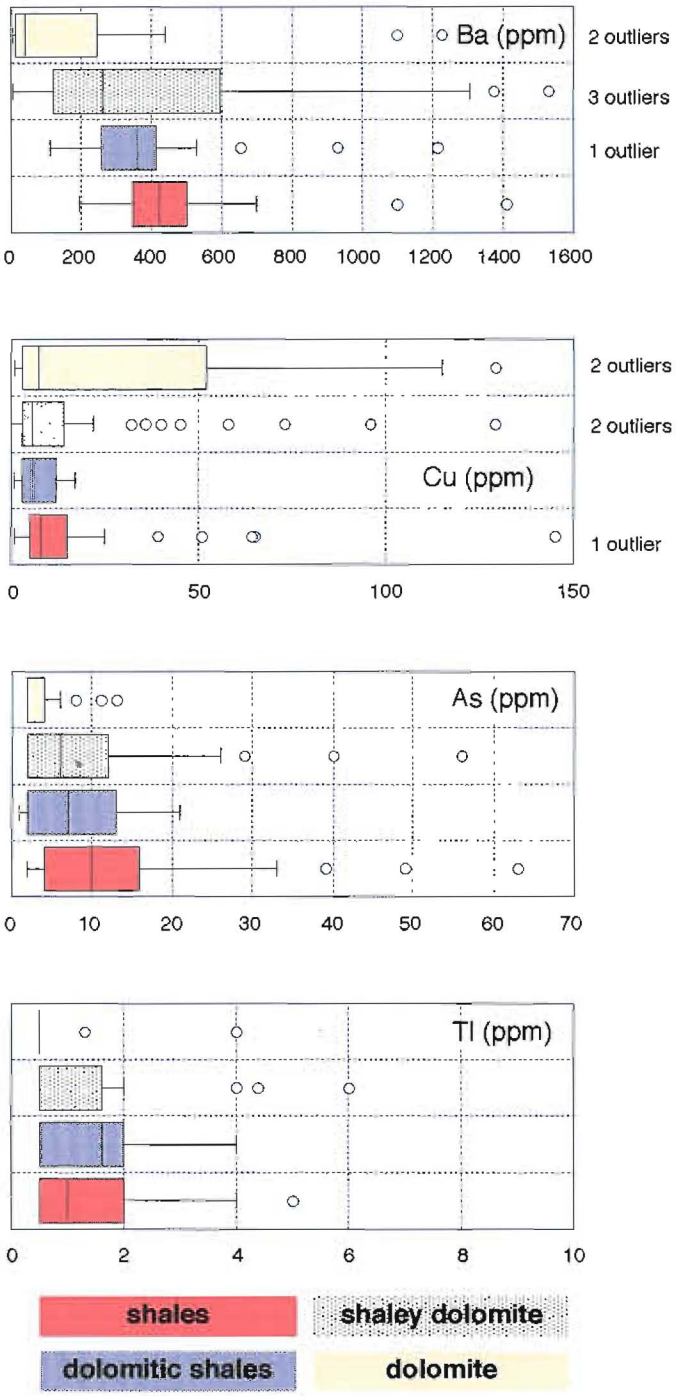

Figure 3. Boxplots for Ba, Cu, As and Tl for 189 McNamara Group sediments.

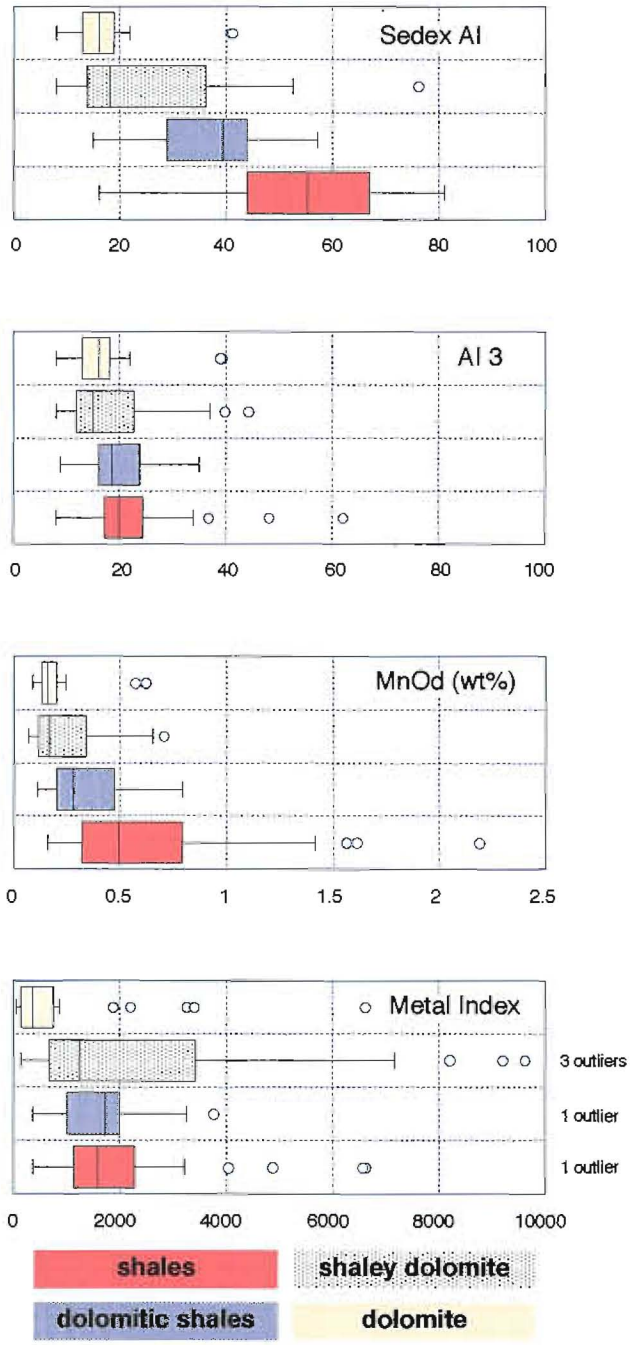

Figure 4. Boxplots for Sedex Al, Al3, MnO_d and Metal Index for 189 McNamara Group sediments.

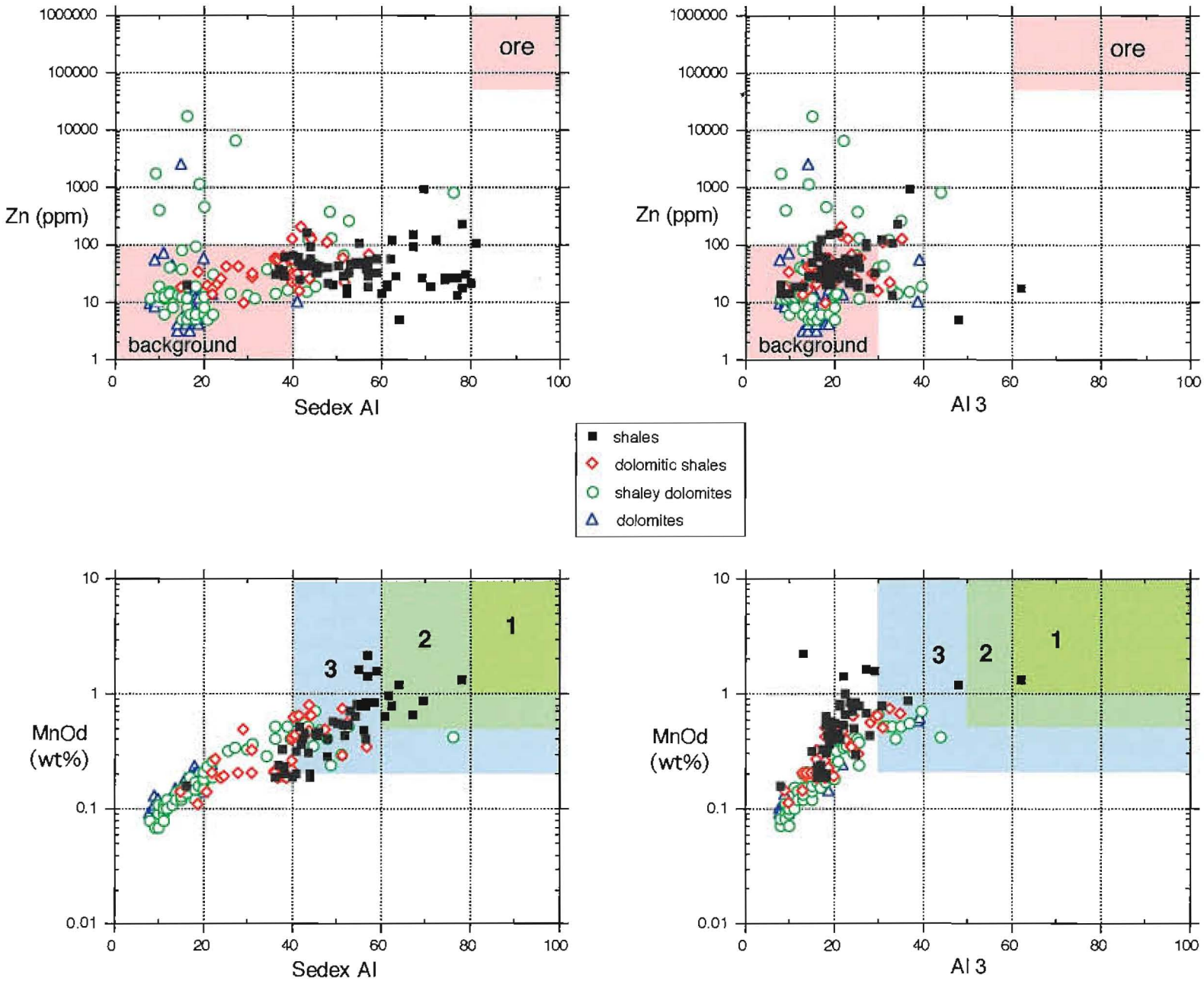

Figure 5. Cross-plots of Zn, Sedex Al, Al3 and MnO_d for 189 McNamara Group sediments.

Lithogeochemical, isotopic and petrographic studies of the Grevillea prospect, Riversleigh area, northwest Queensland

Peter McGoldrick
Centre for Ore Deposit Research

The Grevillea prospect is an important recent discovery in the Carpentaria Zinc Belt of northern Australia. Geologists working for Coolgardie Gold recognised the gossanaous outcrop of sedimentary sulfides during follow-up of a stream geochemical survey. Subsequent drilling in the vicinity of the gossan confirmed the presence of significant base metal sulfide in pyritic sediments (RVC001 intersected 25 m @ 4.68 wt% Zn, 0.98 wt% Pb and 29 g/t Ag. At the time of writing the prospect is a North Ltd/Coolgardie Gold joint venture.

In 1996 core and percussion pulps from the prospect were made available by Coolgardie Gold for lithogeochemical halo studies as part of AMIRA Project P384A. Preliminary results were presented at a P384A sponsors meeting in Hobart in April 1997. This report describes that work and subsequent stable isotopic investigations of sulfides and carbonates.

Geological setting

The Grevillea prospect is located 8 km S of Riversleigh Homestead, approximately 200 km NNE of Mount Isa (Fig. 1). Mineralisation occurs in pyritic and carbonaceous fine grained sedimentary rocks of the Riversleigh Siltstone of the McNamara Group. A simplified geological plan and cross-section from Coolgardie Gold data are presented in Figures 2 and 3. The Riversleigh Siltstone is over 3 km thick in the type section (Sweet and Hutton , 1982). At Grevillea there is less than 1000 m of Riversleigh Siltstone. This may represent a condensed section closer to the basin margin (see below).

The base metal mineralisation (Plates 1 and 2) is confined to a 120 m thick sequence of pyritic, carbonaceous shales and siltstones and is overlain by a sandstone dominated sequence and underlain by grey dolomitic siltstones. The sandstones are well bedded, with bed thicknesses of a few centimetres to a few decimetres. Symmetrical ('herring bone') cross bedding is common. Flute marks occur on some bedding surfaces.

The host shales and siltstones contain barite as well as sulfides. Some of this barite occurs as distinctive lath-shaped crystals resembling gypsum forms (e.g., Plate 3). There are also scattered carbonate grains with a gypsum morphology within some mudstone beds (Plate 3), and irregular, bedding parallel, carbonate veins with shapes resembling enterolithic anhydrite (Plate 5). Poorly preserved oolites, sometimes showing replacement by sulfides, (Plate 4) occur in the mineralised sequence. Patchy and pervasive brown discoloration of siltstone beds, identical to the siderite alteration in the Lady Loretta ore sequence, is a common feature of the mineralised zone at Grevillea. Microscopic examination (Plate 5) and lithogeochemistry (see below) confirm the presence of neomorphic siderite in these samples.

Discussion: the environment of deposition of the Grevillea prospect

Regionally, the Riversleigh Siltstone represents a deepening event with thick accumulations of carbonaceous fine grained sediments in the depocentre to the N of the Grevillea area (Sweet and Hutton, 1982). However, at Grevillea, the features described above are more consistent with a relatively shallow setting for the host sediments. Hence, the Riversleigh Siltstone at Grevillea may be a near shore transitional sequence from the underlying terrestrial and shallow marine Shady Bore Quartzite.

Ore textures

A small number of doubly polished thin sections of Grevillea sulfides and host sediments were examined as part of this study.

The sulfide mineralogy is very simple with pyrite, sphalerite and galena as the dominant sulfides. In core, pyritic beds are often poorly preserved (Plate 1a) and textures are difficult to discern. However, cutting and coarse grinding reveals much more detail (e.g., Plate 1 c&d). Much of the bedded pyrite has a 'crinkly' appearance and displays a fine, sub-millimetre lamination (Plate 1c). Base metal sulfides are recognisable as infillings and disseminations in this crinkly pyrite (Plate 1d).

Microscopically the crinkly pyrite comprises distinctive continuous and discontinuous, convex-up lamellae 50 to 100 microns thick. In massive pyrite beds these lamellae are close packed, but can be quite porous giving the pyrite layers a 'spongy' appearance. In base metal-rich samples the pyrite lamellae are separated by fine grained sphalerite (Plate 2), and not as closely packed; sphalerite also infills the pore spaces in the spongy pyrite.

Discussion

The crinkly, laminated pyrite texture at Grevillea is identical to microbial pyrite textures from Walford Creek prospect (Rohrlach et al., 1998). Much of the fine grained pyrite at Lady Loretta is also very similar to Grevillea pyrite, and was interpreted to have microbial origin by McGoldrick et al. (1996) and Dunster (1997). The crinkly lamination and porous character of the pyrite was thought to be inherited from the original microbial mat textures, with the mat being pyritised immediately on burial. The occurrence of Grevillea base metal sulfides as pore infillings, and separating pyrite lamellae, indicate base metal sulfides precipitated within these porous and permeable pyrite beds prior to significant compaction.

Sulfur isotopes

Sulfur isotope signatures of sulfide and sulfate minerals can yield insights into the source(s) of S in mineral deposits, and (when equilibrium has been attained between sulfide phases) about the physico-chemical conditons of sulfide precipitation.

At Grevillea S isotopes were measured in ten pyrite and two barite samples, using conventional techniques, and a further twenty pyrites were measured using laser ablation techniques. Eight sphalerites and three galenas from a single sample were measured by laser ablation. The S isotope data are presented on Table 1 and in Figure 4.

Pyrite $\delta^{34}S$ values are heavy and show a wide range (13 to 34 permil, mean: 26.3 permil), and approach (and in one case exceed) the sulfate S values recorded in the barite samples. There is no systematic within sample variation, nor does there appear to be a stratigraphic control on S isotope signature (cf Lady Loretta where pyrite S becomes heavier moving up sequence). These heavy S values are consistent with pyrite S deriving from a sedimentary and/or seawater S source. High degrees of closed and/or partly closed system biogenic sulfate reduction would have provided variably heavy S to form FeS precursors to the pyrite. Thermochemical sulfate reduction process cannot be excluded, but, the early timing of pyrite formation and microbial textures favour a biogenic mechanism.

Limited laser ablation data for sphalerite and galena indicates the base metal sulfides also contain heavy S, with eight sphalerites having a mean of 13 permil and three galenas having a mean of 16 permil. These data indicate that sphalerite and galena are not in equilibrium, nor are the base metal sulfides in isotopic equilibrium with the pyrites. More measurements of sphalerite and galena are required to confirm a common S source for pyrite and base metal sulfides.

Lithogeochemistry

Sampling

A suite of 55 samples from Grevillea were used to test the various geochemical indices developed for other Carpentaria Zinc Belt deposits. Samples comprised quarter core from cored holes beneath the gossan, and assay pulps from percussion holes to the north. The core samples were deliberately selected to avoid sulfide-rich material, and, although it was not possible to avoid sulfide in percussion pulps, most

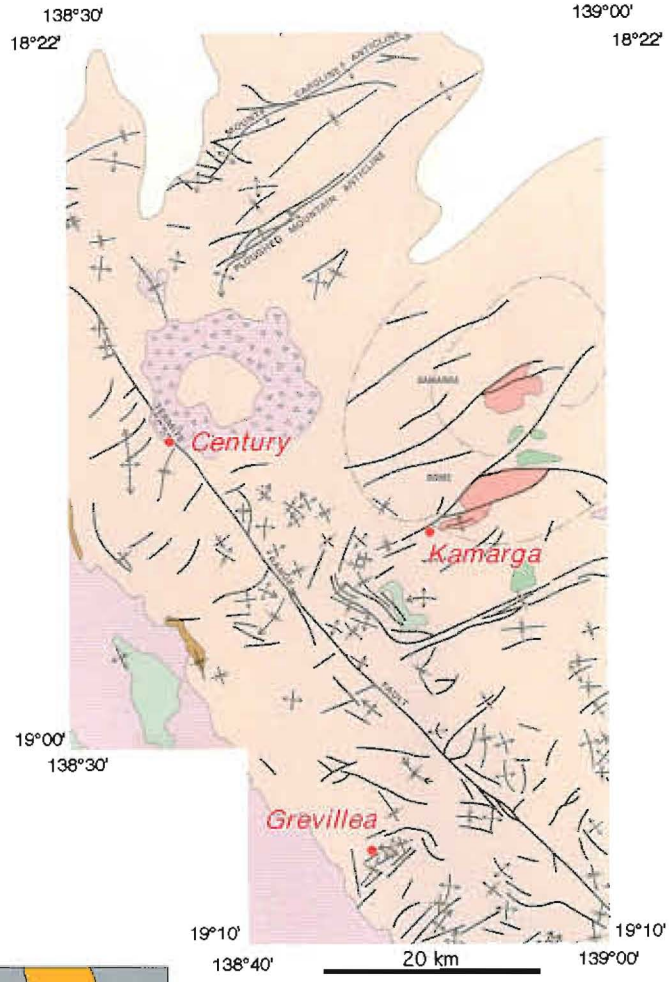

Figure 1. Structural sketch map from the Lawn Hill Region 1:100,000 geology map showing the location of Grevillea prospect.

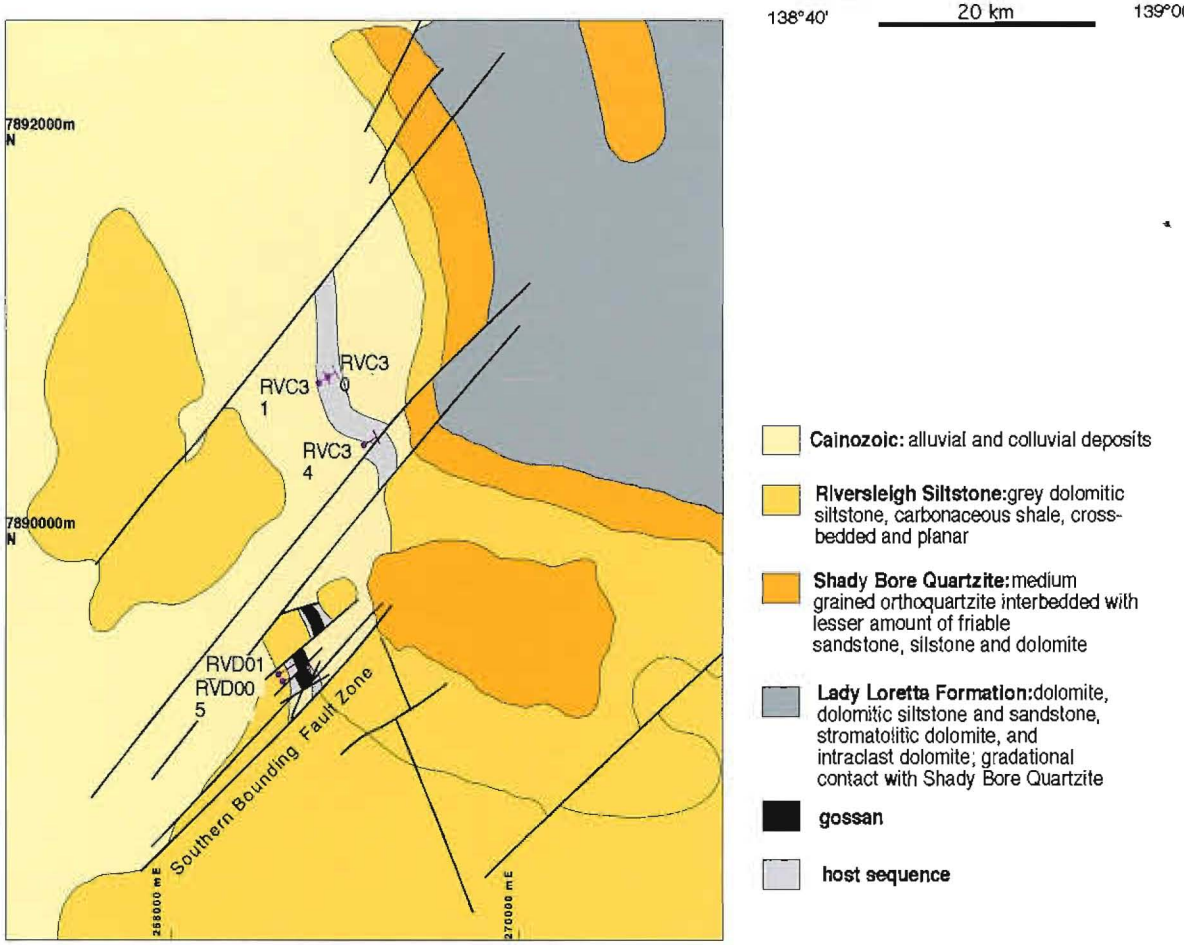

Figure 2. Geological map of the Grevillea prospect showing the location of diamond and percussion drill holes sampled for this study (modified from Coolgardie Gold unpublished data and Sweet and Hutton (1982).

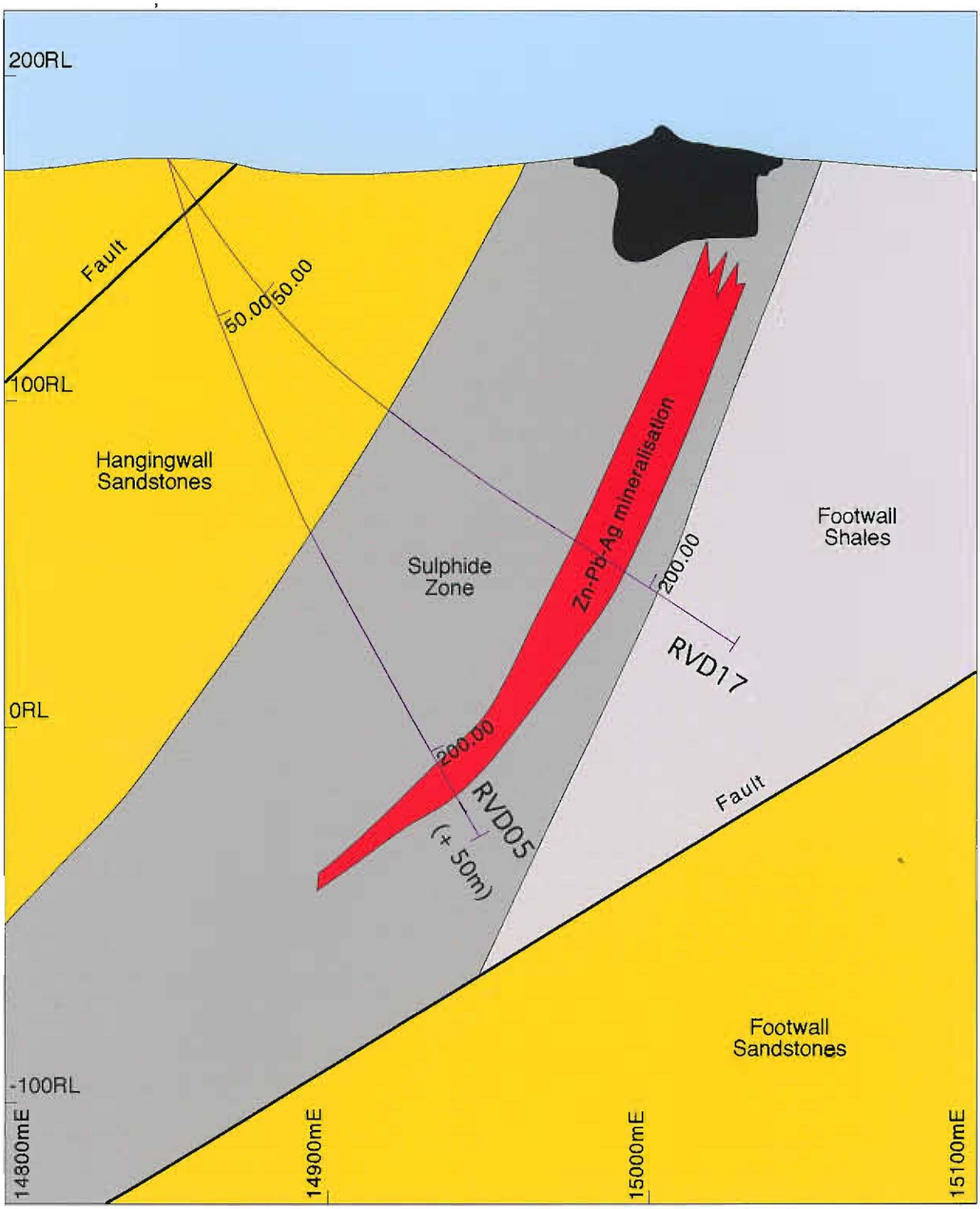

Cainozoic alluvial and colluvial deposits

Riversleigh Siltstone: grey dolomitic siltstone, carbonaceous shale, cross-bedded and planar laminated sandstone

Shady Bore Quartzite: medium grained orthoquartzite interbedded with lesser amount of friable sandstone, silstone and dolomite

Lady Loretta Formation: dolomite, dolomitic siltstone and sandstone, stromatolitic dolomite, and intraclast dolomite; gradational contact with Shady Bore Quartzite

gossan

host sequence

Figure 3. Cross-section of the gossan area at the Grevillea prospect showing the location of drill holes used for this study with respect the base metal mineralisation (Coolgardie Gold).

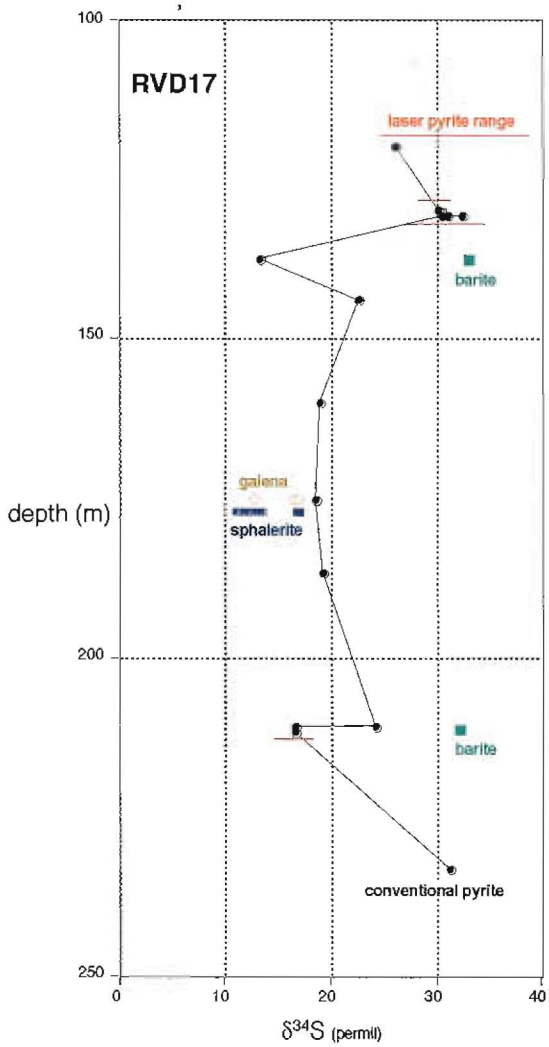

Figure 4. Down-hole S isotope variation for sulfides from DDH RVD17.

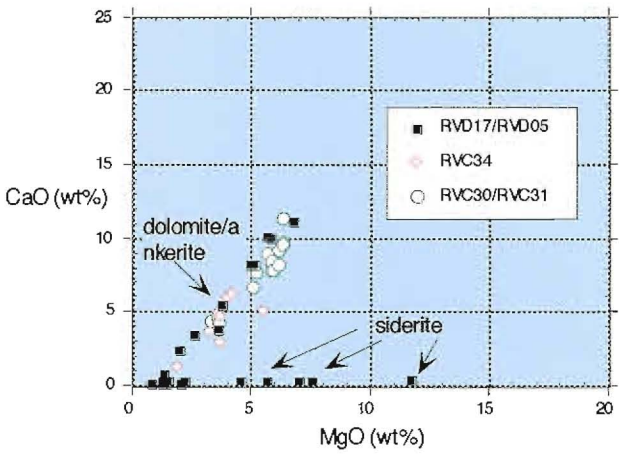

Figure 5. CaO and MgO relationship for 55 samples from Grevillea.

Table 1. Grevillea sulfur isotope data

Conventional			$\delta^{34}S$ permil	*Laser*			$\delta^{34}S$ permil
RVD17	125	pyrite	26.2	RVD17	130.8A	pyrite	31.1
RVD17	135.8	pyrite	30.5	RVD17	130	pyrite	29.9
RVD17	137.5	pyrite	13.2	RVD17	130	pyrite	30.5
RVD17	144.1	pyrite	22.7	RVD17	130	pyrite	31.3
RVD17	160.2	pyrite	19.0	RVD17	130	pyrite	28.9
RVD17	175.5	pyrite	18.5	RVD17	120	pyrite	31.5
RVD17	186.9	pyrite	19.3	RVD17	120	pyrite	28.7
RVD17	211.1	pyrite	24.3	RVD17	120	pyrite	28.9
RVD17	211.9	pyrite	16.6	RVD17	120	pyrite	25.2
RVD17	233.5	pyrite	31.2	RVD17	120	pyrite	38.4
				RVD17	130.8B	pyrite	27.5
RVD17	137.5	barite	33.1	RVD17	130.8B	pyrite	31.9
RVD17	211.1	barite	32.2	RVD17	130.8B	pyrite	33.5
				RVD17	130.8B	pyrite	34.4
				RVD17	130.8B	pyrite	33.2
				RVD17	130.8B	pyrite	34.3
				RVD17	211.1	pyrite	18.1
				RVD17	211.1	pyrite	17.0
				RVD17	211.1	pyrite	15.2
				RVD17	211.1	pyrite	16.6
				RVD17	175.5A	sphalerite	12.2
				RVD17	175.5A	sphalerite	11.8
				RVD17	175.5A	sphalerite	13.3
				RVD17	175.5A	sphalerite	17.1
				RVD17	175.5B	galena	16.8
				RVD17	175.5B	galena	17.2
				RVD17	175.5B	galena	13.0
				RVD17	175.5B	sphalerite	13.6
				RVD17	175.5B	sphalerite	11.2
				RVD17	175.5B	sphalerite	11.3
				RVD17	175.5B	sphalerite	13.6

Table 3: Carbon and oxygen isotope data from Grevillea

Sample i.d.	mineralogy	$\delta^{13}C$ (permil- PDB)	$\delta^{18}O$ (permil-SMOW)
RVD05-112	Ankerite	-1.49	20.22
RVD05-115.2	Ankerite	-2.90	18.45
RVD17-133	Siderite	-2.75	19.26
RVD17-144.1	Siderite	-3.13	19.66
RVD17-194	Ankerite	-2.67	19.78
RVD17-201.5	Ankerite	-2.71	19.62
RVD17-216.4	Dolomite	-3.02	18.02
RVC030-39	Ankerite	-2.72	18.90
RVC030-59	Dolomite	-2.08	19.65
RVC030-69	Dolomite	-1.89	19.79
RVC031-69	Dolomite	-1.93	19.49
RVC031-79	Ankerite	-2.51	19.46

Table 2. Major and trace element geochemical data for 55 samples from Grevillea

Sample ID	SiO2	TiO2	Al2O3	Fe2O3	FeO	MgO	CaO	MnO	Na2O	K2O	P2O5	loss	TOTAL	H2O	CO2	Tic	Toc	S	As	Ba	Cu	Pb	Rb	Sr	Tl	Zn
	wt%	wt%	wt%	wt%	wt%	wt%	wt%	wt%	wt%	wt%	wt%	wt%	wt%	wt%	wt%	wt%	wt%	wt%	ppm	ppm	ppm	ppm	ppm	ppm	ppm	ppm
RVD05-112	54.83	0.46	14.29	2.84	2.56	3.82	5.37	0.16	0.10	7.87	0.12	9.95	99.99	1.70	8.35	8.04	0.09	0.15	12	1600	7	15	257	56	6.0	18
RVD05-115.2	54.15	0.47	14.17	5.35	4.81	3.63	3.73	0.24	0.10	8.08	0.13	9.71	99.96	1.43	8.68	6.03	0.72	0.27	12	1800	8	28	253	46	6.4	20
RVD05-118	61.24	0.42	13.96	7.40	6.66	1.49	0.20	0.45	0.04	8.20	0.12	5.77	99.48	1.79	3.96	0.15	1.04	0.61	21	1700	17	46	237	24	6.3	252
RVD05-120	59.48	0.52	17.02	4.92	4.43	2.07	0.19	0.18	0.07	8.79	0.14	5.85	99.52	2.59	3.59	0.68	0.80	0.44	21	2600	12	31	290	23	8.5	77
RVD17-131	31.62	0.18	6.34	25.86	23.27	7.58	0.25	1.35	0.08	4.91	0.08	21.29	100.22	0.54	22.97	1.99	5.73	1.08	35	6100	10	34	87	23	14.6	30
RVD17-133	26.09	0.17	4.96	32.75	29.47	11.69	0.40	1.88	<0.05	3.79	0.08	17.25	99.57	0.27	28.51	13.22	4.17	0.22	4	4200	8	14	66	20	7.0	38
RVD17-138	40.37	0.33	9.60	18.41	16.57	5.64	0.27	0.95	0.11	7.30	0.13	15.66	99.93	0.54	16.67	1.85	4.04	0.82	32	10400	13	43	143	39	12.4	25
RVD17-143	60.77	0.61	15.02	4.82	4.34	1.46	0.08	0.18	0.08	10.22	0.13	5.08	99.51	1.34	3.70	0.45	0.89	1.14	26	9500	13	37	244	49	33.5	21
RVD17-144.1	35.72	0.29	8.32	21.73	19.55	7.03	0.29	1.11	0.07	5.97	0.10	18.72	99.93	0.54	20.34	9.81	2.87	0.69	10	5200	11	28	130	22	20.4	27
RVD17-147.7	59.94	0.51	14.97	6.13	5.52	1.27	0.18	0.32	0.09	9.70	0.14	5.58	99.28	1.61	3.70	0.08	0.99	1.90	26	4000	12	41	241	44	33.7	20
RVD17-149.4	64.73	0.44	13.43	4.96	4.46	0.81	0.13	0.20	0.07	9.54	0.13	5.04	99.81	1.43	3.19	0.15	0.83	1.81	25	3000	10	46	200	36	27.1	21
RVD17-161.9	54.18	0.46	15.22	8.90	8.01	1.36	0.81	0.13	0.08	10.05	0.16	7.36	99.71	1.52	4.51	0.42	1.12	3.89	75	9000	18	60	275	41	26.6	70
RVD17-168.2	46.75	0.44	12.97	14.22	12.80	2.23	0.27	0.28	0.08	8.75	0.17	10.02	99.59	0.71	5.83	0.58	1.43	7.05	165	30500	30	227	232	96	39.0	34
RVD17-184.5	22.73	0.17	6.82	35.54	31.98	4.55	0.21	0.77	<0.05	4.63	0.08	23.76	100.06	1.16	13.12	1.18	3.26	16.48	833	7300	21	843	121	19	62.2	75
RVD17-194	42.70	0.34	10.82	5.44	4.89	5.80	9.96	0.46	0.08	6.86	0.13	17.02	99.90	1.07	16.53	13.66	0.78	1.71	36	2600	11	35	180	87	12.0	20
RVD17-197.2	64.29	0.48	16.57	3.15	2.83	1.26	0.26	0.00	0.06	9.77	0.18	3.43	99.76	2.32	0.73	0.07	0.18	0.64	18	2800	16	25	252	37	14.6	29
RVD17-201.5	46.13	0.37	10.93	6.03	5.43	5.10	8.21	0.42	0.08	6.38	0.13	15.76	99.74	1.34	15.32	11.30	1.09	2.26	36	1800	13	36	185	80	11.1	20
RVD17-209.1	38.94	0.30	8.34	10.44	9.39	5.66	10.06	0.43	0.07	5.46	0.13	20.24	100.45	0.89	18.43	12.91	1.51	5.61	119	3400	17	97	140	103	13.2	19
RVD17-216.4	41.15	0.30	7.95	6.69	6.02	6.75	11.10	0.30	0.06	5.12	0.11	19.36	99.09	0.98	21.11	15.23	1.60	3.20	66	1800	14	48	132	102	8.7	16
RVD17-222.9	63.06	0.40	11.99	4.42	3.98	1.99	2.34	0.12	0.04	7.05	0.13	7.72	99.39	1.70	6.38	2.22	1.13	1.94	45	1200	14	38	185	22	6.8	18
RVD17-226.3	46.95	0.33	9.70	6.76	6.08	4.98	8.20	0.31	0.06	6.20	0.12	15.92	99.64	1.07	15.72	11.27	1.21	3.18	67	1000	21	60	160	50	6.2	16
RVD17-229.8	55.04	0.42	11.77	4.61	4.15	3.76	5.38	0.25	0.16	7.14	0.16	11.20	100.00	1.34	10.55	7.22	0.91	1.89	44	1000	18	70	207	38	6.2	21
RVD17-233.5	55.56	0.37	11.30	7.11	6.40	2.64	3.44	0.21	0.04	7.67	0.14	11.16	99.80	1.16	12.46	4.06	2.29	3.36	55	1400	24	56	191	34	7.4	16
RVC030-9	49.98	0.41	11.72	7.17	6.45	5.30	6.45	0.11	0.19	5.25	0.07	12.76	99.41	3.66	8.90			0.20	89	503	24	70	187	56	2.1	34
RVC03019	59.22	0.46	12.46	14.18	12.76	1.14	0.24	1.06	0.07	6.30	0.18	4.21	99.52	3.04	0.59			0.09	139	511	31	101	228	54	14.4	112
RVC030-29	44.52	0.31	9.26	6.83	6.15	6.27	9.69	0.41	0.06	4.64	0.15	17.94	100.08	1.43	16.82	12.74	1.11	3.00	40	419	16	39	177	40	3.7	29
RVC030-39	46.18	0.30	10.22	5.93	5.34	6.12	9.23	0.36	<0.05	4.68	0.13	16.83	99.99	1.61	15.21	12.58	0.72	2.10	35	282	17	28	190	41	3.8	19
RVC030-49	50.51	0.37	12.45	5.42	4.88	5.06	6.66	0.25	0.05	5.51	0.15	13.38	99.82	2.06	11.58	9.23	0.64	1.95	34	292	17	20	242	29	2.2	19
RVC030-59	49.75	0.37	11.11	4.06	3.65	6.16	8.20	0.18	<0.05	4.83	0.14	15.18	99.98	2.14	14.22	11.45	0.75	1.04	20	310	13	14	222	40	2.6	24
RVC030-69	46.58	0.30	9.20	7.38	6.64	5.86	8.49	0.32	0.05	4.51	0.14	17.13	99.96	1.43	16.01	11.13	1.33	3.86	64	327	22	57	178	37	8.7	28
RVC030-79	48.64	0.32	10.02	6.68	6.01	5.19	7.63	0.34	0.01	4.98	0.13	15.58	99.52	1.61	14.18	10.10	1.11	3.17	66	378	27	40	195	35	5.4	28
RVC030-89	34.40	0.24	7.00	14.30	12.87	6.27	11.33	0.69	0.09	3.97	0.14	19.57	98.00	0.98	17.55	13.76	1.04	8.35	84	371	42	116	142	33	31.9	65
RVC030-99	48.97	0.36	11.16	5.18	4.66	5.80	7.86	0.36	<0.05	5.34	0.15	14.72	99.90	1.70	13.70	10.92	0.76	1.69	29	426	24	63	212	39	3.3	23
RVC031-9	65.05	0.46	14.93	5.95	5.35	2.21	0.12	0.11	0.09	5.64	0.07	4.61	99.24	3.75	0.11			0.06	16	778	17	13	274	35	1.6	24
RVC031-19	65.24	0.44	14.75	4.89	4.40	2.49	0.77	0.13	0.06	6.24	0.13	4.54	99.68	3.22	1.36			0.01	21	497	17	16	277	35	2.1	28
RVC031-29	58.16	0.44	12.86	4.41	3.97	3.59	4.30	0.19	0.05	6.08	0.15	9.12	99.35	1.97	8.10	5.86	0.61	1.12	27	478	15	18	239	33	2.6	22
RVC031-39	55.25	0.44	11.35	7.29	6.56	3.33	4.38	0.22	<0.05	5.76	0.17	11.36	99.55	1.79	10.37	5.27	1.39	3.71	76	468	25	51	210	35	3.7	37
RVC031-49	53.66	0.46	11.47	7.08	6.37	3.54	4.67	0.25	0.07	5.96	0.20	12.21	99.57	1.88	12.86	5.84	1.92	3.60	96	433	36	51	210	36	2.7	63
RVC031-59	44.20	0.34	9.14	8.10	7.29	5.67	9.00	0.55	0.06	4.72	0.17	17.97	99.92	1.43	17.55	12.08	1.49	4.13	70	317	21	60	166	38	5.3	67
RVC031-69	45.30	0.31	9.22	6.81	6.13	6.27	9.52	0.34	0.06	4.43	0.15	17.84	100.25	1.43	16.53	13.29	0.88	3.20	46	431	19	42	175	40	4.3	25
RVC031-79	49.42	0.31	9.91	6.20	5.58	5.80	8.36	0.35	0.09	4.37	0.14	15.70	100.65	1.70	14.03	11.47	0.70	2.36	35	288	22	25	186	36	4.8	24
RVC031-89	50.58	0.37	12.56	5.49	4.94	5.03	6.64	0.22	0.09	5.32	0.13	13.37	99.80	2.14	11.65	9.03	0.72	1.92	36	287	18	21	240	33	3.4	23
RVC031-99	50.26	0.37	11.35	4.33	3.90	5.89	7.83	0.15	<0.05	4.78	0.14	14.71	99.82	2.06	14.11	11.16	0.80	1.20	20	295	13	13	223	47	3.2	31
RVC034-9	63.95	0.53	15.49	6.19	5.57	2.66	0.19	0.07	0.10	6.87	0.15	3.82	100.02	2.86	0.26			0.05	34	815	19	19	304	31	1.5	34
RVC034-19	66.98	0.48	14.63	5.20	4.68	2.19	0.21	0.01	0.08	7.22	0.14	2.90	100.04	2.59	0.11			0.08	9	955	11	10	290	35	2.3	32
RVC034-29	67.46	0.50	14.12	4.45	4.00	2.47	0.25	0.03	0.07	7.07	0.16	2.99	99.57	2.86	0.81			0.30	8	801	10	13	259	28	1.3	44
RVC034-39	52.45	0.44	11.69	6.62	5.96	3.59	4.94	0.25	0.07	7.06	0.17	12.45	99.72	1.61	12.38	6.44	1.62	3.85	77	722	75	52	229	31	4.3	31
RVC034-49	55.58	0.47	11.77	6.62	5.96	3.21	3.69	0.28	0.07	7.15	0.18	10.50	99.52	1.79	10.30	4.88	1.48	3.65	75	452	42	49	219	30	4.1	29
RVC034-59	52.77	0.38	10.91	7.88	7.09	3.67	4.68	0.36	<0.05	6.61	0.17	11.74	99.17	1.61	11.51	6.11	1.47	4.25	78	427	37	55	203	29	5.5	28
RVC034-69	48.65	0.33	10.08	9.32	8.39	4.19	6.12	0.48	0.17	6.05	0.17	14.27	99.83	1.61	13.26	8.02	1.43	4.83	69	618	38	54	184	29	6.5	30
RVC034-79	52.79	0.40	11.79	11.49	10.34	1.93	1.32	0.07	0.14	6.39	0.30	12.28	98.90	3.22	7.88	1.57	1.72	8.13	115	362	55	98	195	16	17.8	45
RVC034-89	54.19	0.31	9.72	6.29	5.66	3.99	5.99	0.44	0.10	6.16	0.13	12.33	99.64	1.34	12.82	9.01	1.04	2.66	51	348	19	49	173	28	7.6	27
RVC034-99	34.93	0.23	6.83	21.36	19.22	5.53	5.08	1.34	0.10	3.79	0.10	19.65	98.94	1.34	18.28	13.72	1.25	6.94	48	301	36	116	120	23	17.4	45
RVC034-109	34.27	0.27	8.39	25.98	23.37	3.72	2.86	0.22	0.07	3.60	0.11	20.50	100.00	5.00	6.96	3.04	1.07	15.75	74	257	113	182	94	11	47.4	57
RVC034-119	62.15	0.31	8.79	7.04	6.33	3.37	4.44	0.51	0.08	5.29	0.13	7.08	99.19	0.89	7.00			0.08	17	471	8	15	142	24	2.9	24

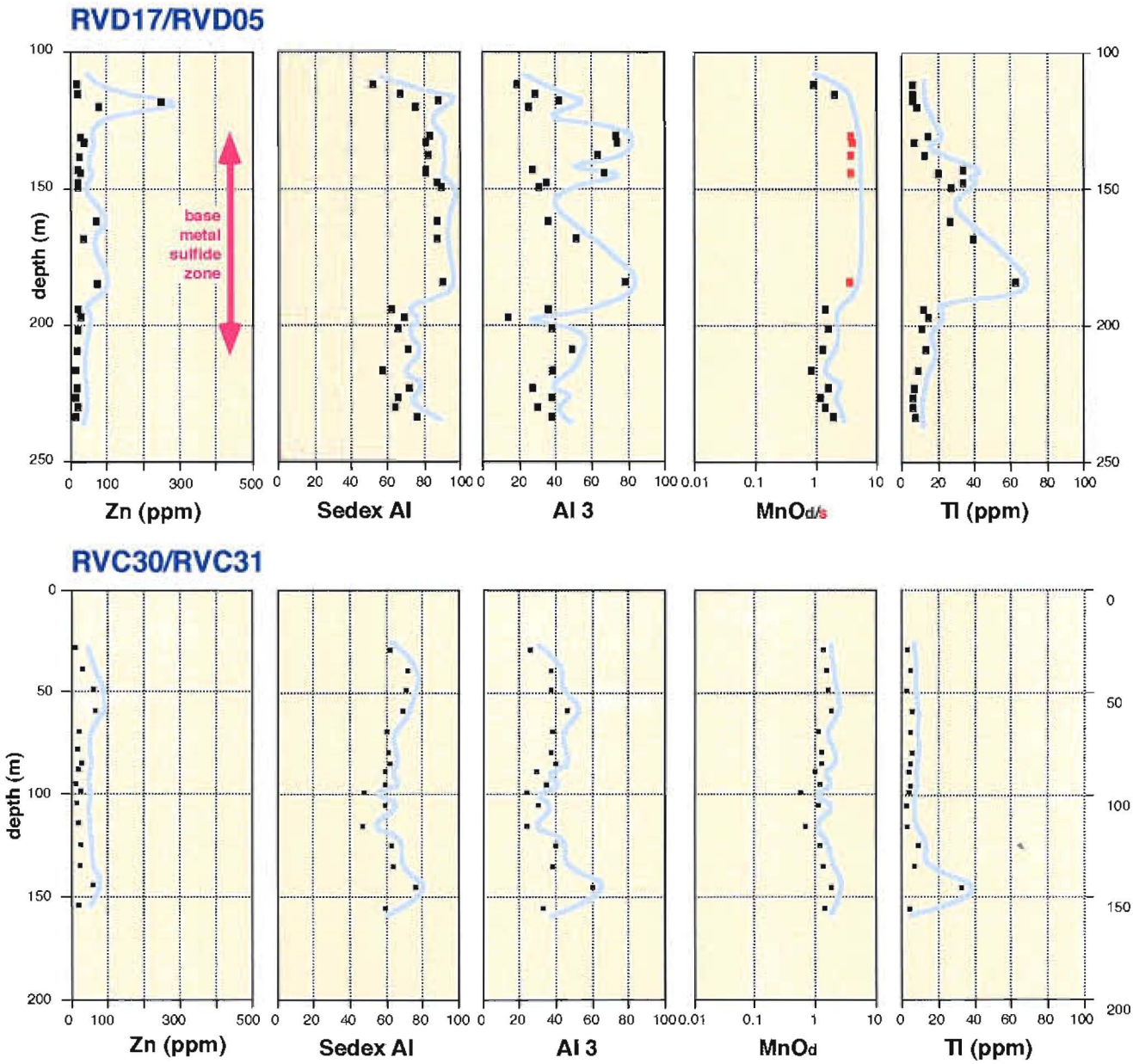

Figure 6. Downhole variation in Zn, Sedex Al, Al3, $MnO_{d/s}$ and Tl in proximal (RVD17/RVD05) and distal (RVC30/RVC31) samples from Grevillea.

analysed at less than four percent S. Diamond drill holes RVD05 and RVD17 provided samples through the mineralised pyritic sequence and for a few tens of metres into the hanging wall and footwall siltstones. Unmineralised 'distal' samples were obtained from two holes (RVC30 and RVC31) from a fence of percussion holes 450 m N of the gossan, that bracket the pyritic sequence. These samples contain base metals at background levels. An third percussion hole (RVC34), 250 m N along strike from the gossan, was also sampled. This hole cannot be directly correlated with the mineralised sequence, but is probably equivalent to the upper part of the pyritic unit.

The samples were analysed for a suite of major and trace elements by XRF at the University of Tasmania. All the geochemical data are presented on Table 2. A smaller number of samples were analysed for C and O isotopes and these results are presented on Table 3.

Host rock carbonates

Figure 5 displays the CaO and MgO data for all the samples. Most samples lie on a 'dolomite' (or ankerite) trend, but five low CaO, and high MgO samples from RVD17 are probably sideritic. Furthermore, recalculating the whole rock analyses, assuming all Fe is in pyrite and carbonate, indicates that most of the 'dolomite' samples are, by definition, ankerite (i.e, moles Fe+Mn:Mg > 0.25).

The sideritic samples correspond to the mineralised interval in RVD17. All samples from RVC34, and two thirds of samples from RVC30 and 31 are ankeritic.

Zinc dispersion

All but one of the samples analysed from Grevillea had less than 100 ppm Zn (Fig. 6), hence, there is no indication of enrichment in the host sediments nor does Zn form primary dispersion halo in the drill holes to the N. This is in marked contrast to Lady Loretta where Zn forms a broad primary dispersion, and zincian siderite is present in mine sequence rocks (Carr, 1981).

Manganese

Mn forms a broad primary dispersion at Grevillea. Most of samples contain anomalous Mn, and the MnO content of the carbonate (Fig. 6) ranges from about 1 wt% to 4 wt%. Sideritic samples from the mineralised interval of RVD17 are uniformly high in Mn (3 to 4 wt% MnOs).

Thallium

Down hole Tl distributions for RVD17/RVD05 and RVC330/RVC31 are presented in Figure 6. The entire sampled interval of RVD17 is strongly anomalous in Tl (6 to 60 ppm). All samples from RVC34, 250 m along strike, have more than 4 ppm Tl (up 47 ppm), and six (of sixteen) samples from RVC30/31, 450 m along strike, have more than 4 ppm. Clearly, Tl has a strong primary dispersion about the Grevillea mineralisation, that persists for at least 450 m along strike.

Alteration indices

Both Sedex AI and AI3 are anomalous in the mineralised interval of RVD17, with AI3 having a more 'spiky' pattern (Fig. 6). Anomalous values are still present in RVC30/RVC31, although absolute values are somewhat lower, and define a zone in the upper two thirds of the drill hole. On this basis this zone could be interpreted as the exact stratigraphic equivalent of the mineralised sequence in RVD17.

Sedex Metal Index

Sedex Metal Index (Zn + 100 Pb + 100 Tl) values are between 1000 and 10000 in most samples from Grevillea, similar to the range shown by host sediments to Lady Loretta (Large and McGoldrick, 1998). There is a systematic increase approaching the mineralised zone from the hangingwall in RVD17/RVD05, and high values in RVC30/RVC31 define the same interval as AI3 and Sedex AI in these holes.

Interelationships between Zn, Sedex AI, AI3 and MnOd/s

The Grevillea samples lie below the 'Lady Loretta trend' (Large and McGoldrick, 1998) on cross-plots of log Zn against Sedex AI and AI3 (Fig. 7), reflecting the overall low-Zn character of the host rocks. On plots of log MnO_d/s against the two alteration indices most samples lie in the prospective parts of the diagram (Fig. 7); all the siderite samples lie in the 'prospectivity 1' box.

Carbon and Oxygen Isotopes

Eleven carbonate-rich whole rock samples from Grevillea were analysed for C and O isotopes (Table 3). These data are insufficient to define spatial trends, but do suggest important similarities and differences between Grevillea and Lady Loretta (McGoldrick et al., 1998) with respect to O and C isotopes. In terms of O there is no overlap between the Grevillea data and the Lady Loretta data; the heavy O observed in Lady Loretta siderite is not evident at Grevillea. There is, however, an indication that, as at Lady Loretta, C in dolomites at Grevillea is lighter than C in ankerites and siderites.

Vectors to ore

The data reported here indicate that many of the vectors developed for the Lady Loretta deposit may be applicable to the Grevillea prospect.

These include:

1. Change in carbonate composition from dolomite to ankerite to siderite within the sediments. Ankerite is still present several hundred metres along strike from known mineralisation.
2. Systematic increase in MnO content of carbonate (MnOd and MnOs) toward mineralisation. More detailed sampling is required to confirm spatial changes in these parameters at Grevillea. The available data indicate that highest carbonate MnO occurs in the mineralised part of RVD17, and lower, but still anomalous, levels are present in the most distal samples.
3. The alteration indices (Sedex AI and AI3) are weakly anomalous 450 m along strike in the stratigraphic equivalent of the mineralised sequence, and show an increase toward mineralisation.
4. Anomalous Tl is present for at least 450 m along strike in the stratigraphic equivalent of the mineralised sequence, and increases toward mineralisation.
5. Sedex Metal Index (Zn + 100 Pb + 100 Tl) increases from around 1000 to over 10,000 towards ore both across strike and along strike.

Zinc by itself does not appear to be a useful vector to the Grevillea mineralisation. Further work is required to see if the trend to isotopically heavy O in carbonate approaching ore, observed at Lady Loretta (McGoldrick and Large, 1998) and HYC (Large et al., 1998), exists at Grevillea.

Size of the halos at Grevillea and implications for more mineralisation

The strong positive response from Grevillea for most of the 'basket of indices' developed for northern Australian Proterozoic stratiform deposits is a good indication that substantial (Lady Loretta size or bigger) base metal sulfide exists (or did exist) in the immediate vicinity. The intensity of the indices seems to drop away N along strike from the gossan, suggesting better mineralisation to the S. In the immediate area of the gossan faulting has removed the southern continuation of the host sequence, however, large areas of lower Riversleigh Siltstone crop out further to the S and E of the gossan and are highly prospective.

A genetic model for Grevillea mineralisation

Grevillea shares many features in common with the Lady Loretta deposit, and although it occurs at a higher stratigraphic level in the McNamara Group, it probably had a similar origin.

Many elements of the Lady Loretta model McGoldrick et al. (1996) can be invoked for Grevillea. The Grevillea system commenced with low temperature hydrothermal fluids (saline basinal brines) exhaling into a restricted water body thus providing nutrients and energy to support an abundant microbial biota. These fluids carried Fe, some Mn and Ba, but little Zn and Pb. Decomposition of microbial organic matter promoted extensive biogenic sulfate reduction and precipitation of diagenetic Fe sulfides. Local micro-environments with high effective pCO_2 and low sulfate favoured siderite precipitation and/or siderite replacement of existing carbonates. Manganese was fixed in these neomorphic carbonates. Barium accumulated in anoxic pore and basin waters and barite precipitated at the boundary between the anoxic fluid and oxidised parts of the basin. Reactions between the reduced, Ba-rich fluids, and evaporite sulfate minerals may also have precipitated barite. A change in hydrothermal fluid character, to being slightly more

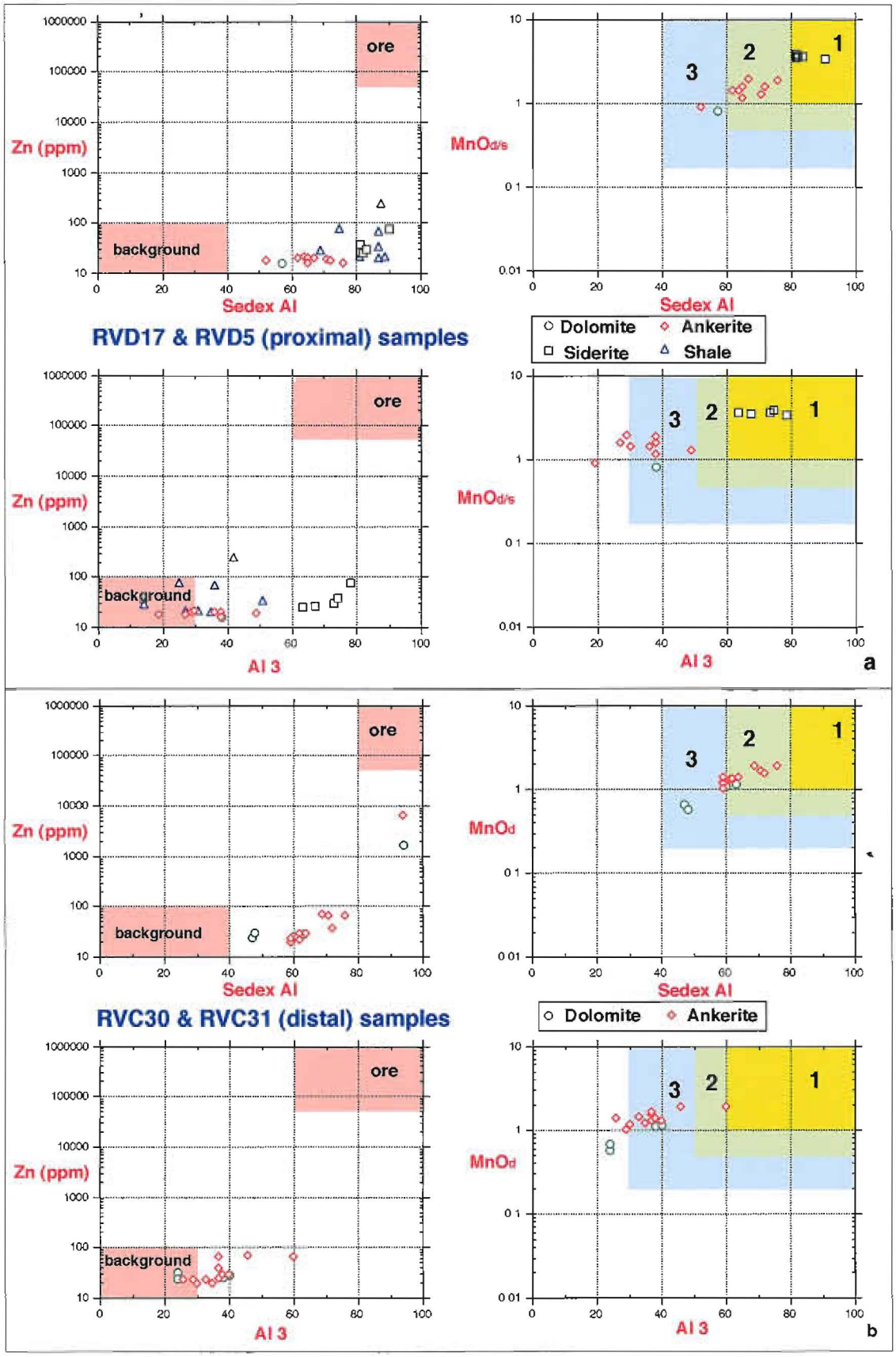

Figure 7. (a) Zinc, alteration indices and $MnO_{d/s}$ interrelationships for proximal samples from Grevillea (shales have not been used for $MnO_{d/s}$ calculations); (b) Zinc, alteration indices and $MnO_{d/s}$ interrelationships for distal samples from Grevillea.

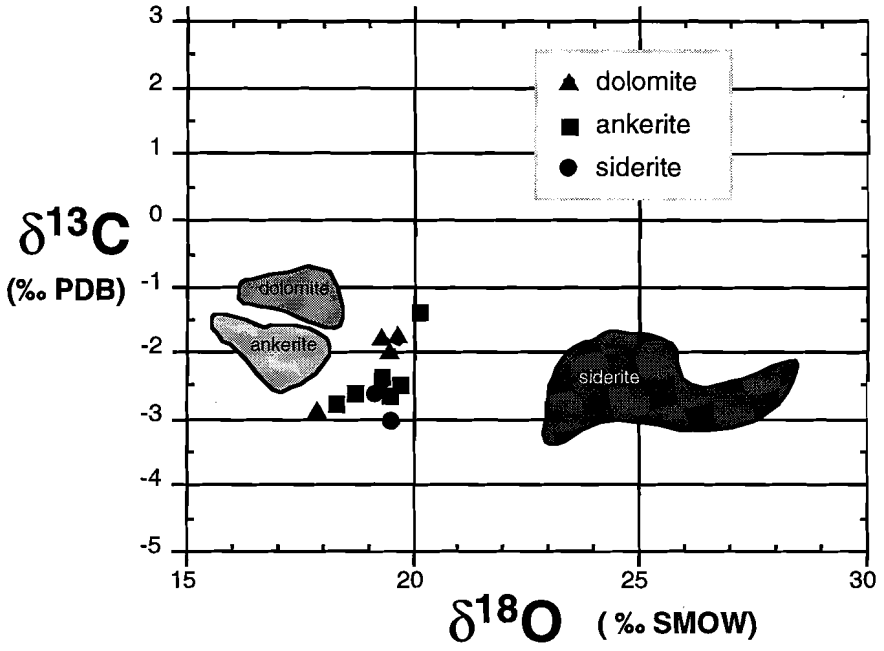

Figure 8. Cross plot of C and O isotope data for 12 samples from Grevillea; fields for 29 samples from Lady Loretta are plotted for comparison. Note: 'ankerite' samples are distinguished from dolomite samples by having moles (Fe+Mn)/Mg >0.25.

oxidised, allowed much larger amounts of Zn and Pb to be transported in solution. When these fluids encountered the anoxic, H_2S-rich, diagenetic environment of the carbonaceous and pyritic siltstones at Grevillea Zn and Pb sulfides were precipitated. At Grevillea much of this base metal sulfide precipitation took place in the pore spaces within pyritic sediments, prior to significant burial.

Acknowledgements

David Jenkins and Glen Feirclough from Terra Search are thanked for their assistance in carrying out the sampling of Grevillea core for this project.

References

Carr, G. R., 1981, The mineralogy, petrology and geochemistry of the zinc-lead-silver ores and host sedimentary rocks at Lady Loretta, northwest Queensland: Ph.D. thesis, The University of Wollongong.

Large, R.R., and McGoldrick, P.J., 1998, Lithogeochemical halos and geochemical vectors to stratiform sediment-hosted Zn-Pb-Ag deposits. Part 1: Lady Loretta deposit, Queensland, Journal of Geochemical Exploration, 63, 37-56.

Large, R.R., Bull, S. and McGoldrick, P., 1998, Halo model for the HYC deposit, Northern Territory. ARC/AMIRA P384A Final Report Volume 1

McGoldrick, P. 1998, Lithogeochemical, isotopic and petrographic studies of the Grevillea prospect, Riversleigh area, north west Queensland, ARC/AMIRA P384A Final Report Volume 2

P. McGoldrick, P. Kitto and R. Large, 1998, Variation of carbon and oxygen isotopes in the alteration halo to the Lady Loretta deposit: implications for exploration and ore genesis, in: Water-Rock Interaction, Proceedings of the 9th International Symposium on Water-Rock Interaction, G.B. Arehart and J.R. Hulston (eds), 561-564.

Sweet, I. P., and L. J. Hutton, 1982, Lawn Hill Region: 1:100,000 geological map commentary.

Plate 1.

(a) Core from the mineralised sequence at Grevillea (RVD17 ~190m down hole); grey siltstones and darker carbonaceous shales with beds of decomposed 'reactive' pyrite and associated brown (sideritic) beds.

(b) Core from the footwall of the mineralised sequence at Grevillea (RVD17 ~230m); grey and brown (sideritic) siltstones and dark grey carbonaceous siltstones and shales; nb, sedimentary breccia bed in second core run.

(c) Slabbed and polished core (RVD17 130.8m); massive pyrite with fine scale 'crinkly' laminations (e.g., see inset photo); nb, draping of silt layers over the 'spongy' pyrite bed at the top of the core.

(d) Slabbed and polished core (RVD17 175.5m); base metal sulfide mineralisation developed in pyritic beds; grey colour in the inset is sphalerite±galena; nb, 'crinkly' and porous appearance of much of the pyrite.

a

c

b

d

Plate 2.(a) Photomicrograph, reflected light (RVD17 175.5m). Detail of base metal sulfide mineralisation; convex-up light brown mineral is 'crinkly' pyrite which forms a framework to grey sphalerite; bedding parallels the base of the photograph (b) Photomicrograph, reflected light (RVD17 175.5). Detail of base metal sulfide mineralisation developed in 'microstromatolitic' crinkly pyrite; bedding parallels the base of the photograph.

Plate 3.

(a) Photomicrograph, transmitted and reflected light (RVD17 175.5m). Detail of the base of a siltstone bed overlying laminated pyrite (yellow). The transparent grains are carbonate pseudomorphs after (?) gypsum.

(b) Photomicrograph, transmitted light (RVD17 129.8m). Coarse barite laths intergrown with pyrite.

(c) Photomicrograph, reflected light (RVD17 129.8m). Coarse barite laths (pseudomorphous after ?gypsum) intergrown with sphalerite (brown).

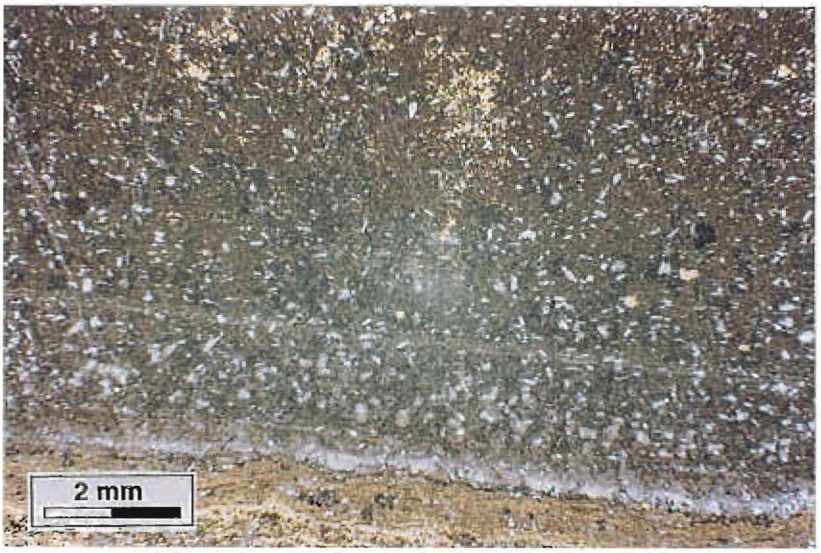

a

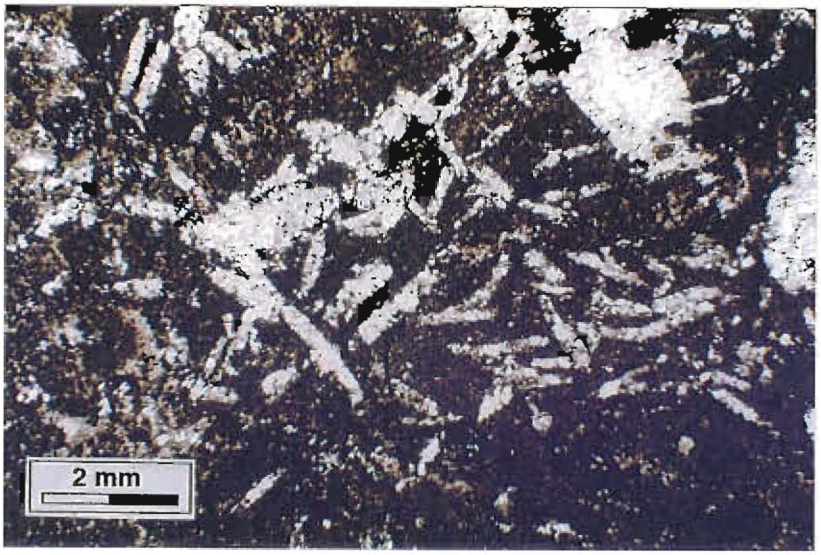

b

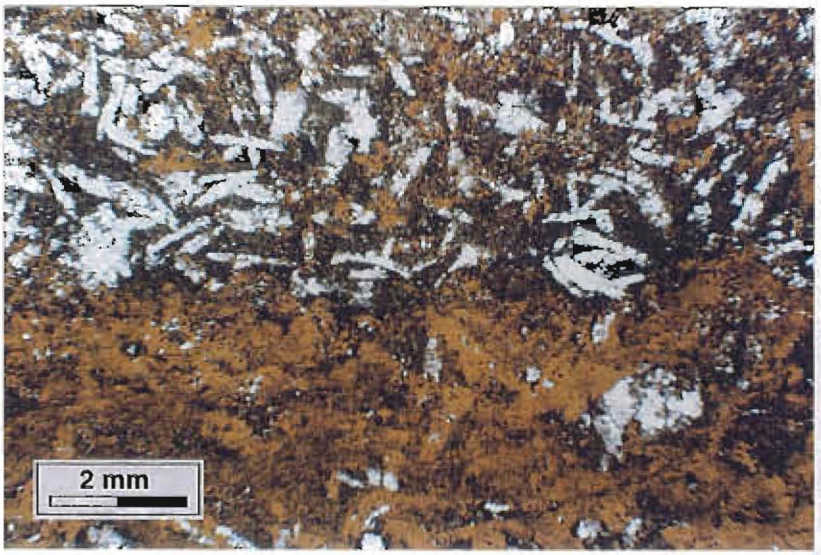

c

Plate 4.

(a) Photomicrograph, transmitted light (RVD17 129.8). Partly mineralised (mainly pyrite) sutured and corroded oolites; clear mineral is barite.

(b) Photomicrograph, transmitted light (RVD17 129.8). Barite (clear mineral) replacing pyritised and sutured oolites.

(c) Photomicrograph, transmitted light and reflected (RVD17 129.8). Recrystallised carbonate (?siderite) oolitic sandstone with minor pyrite.

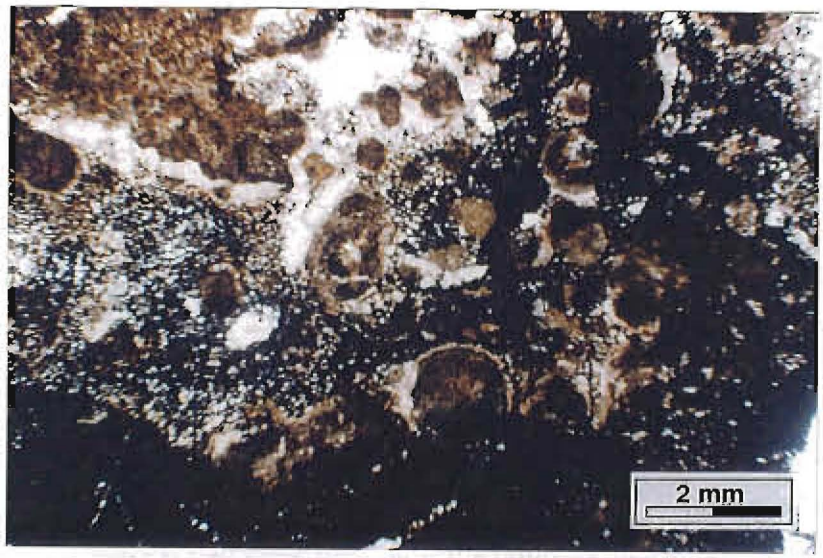

a

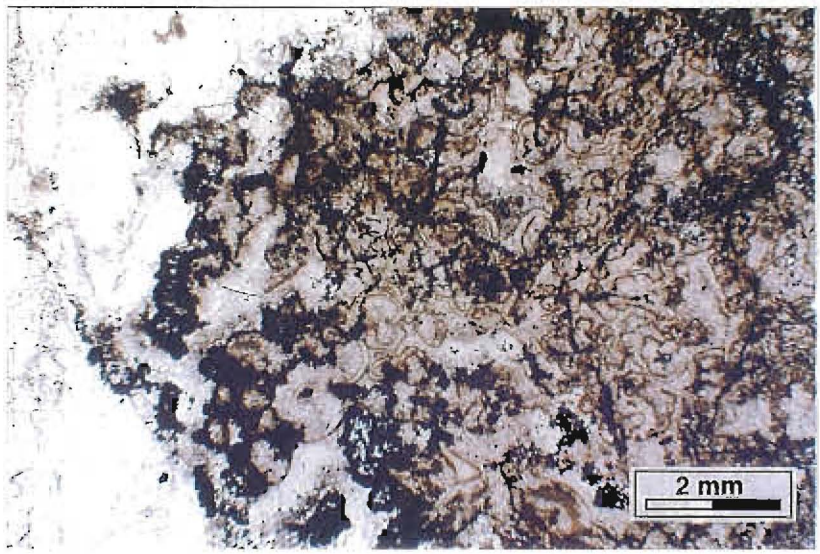

b

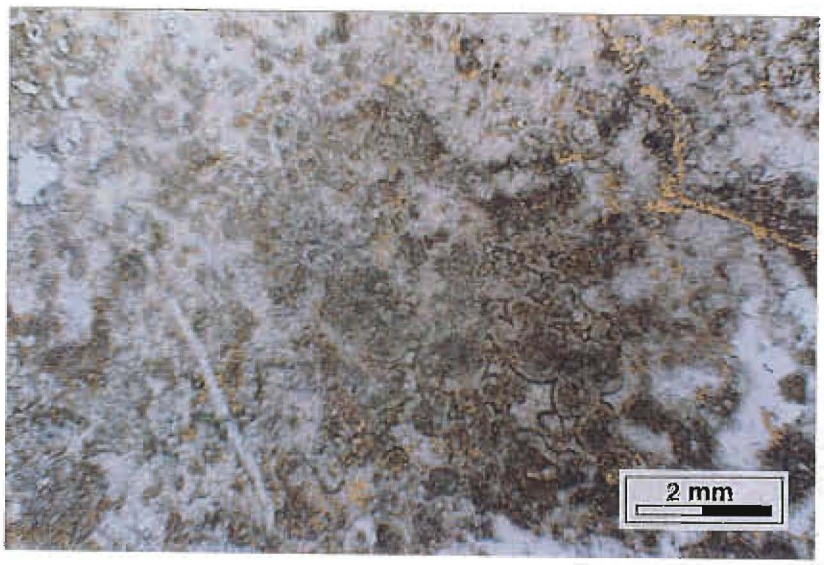

c

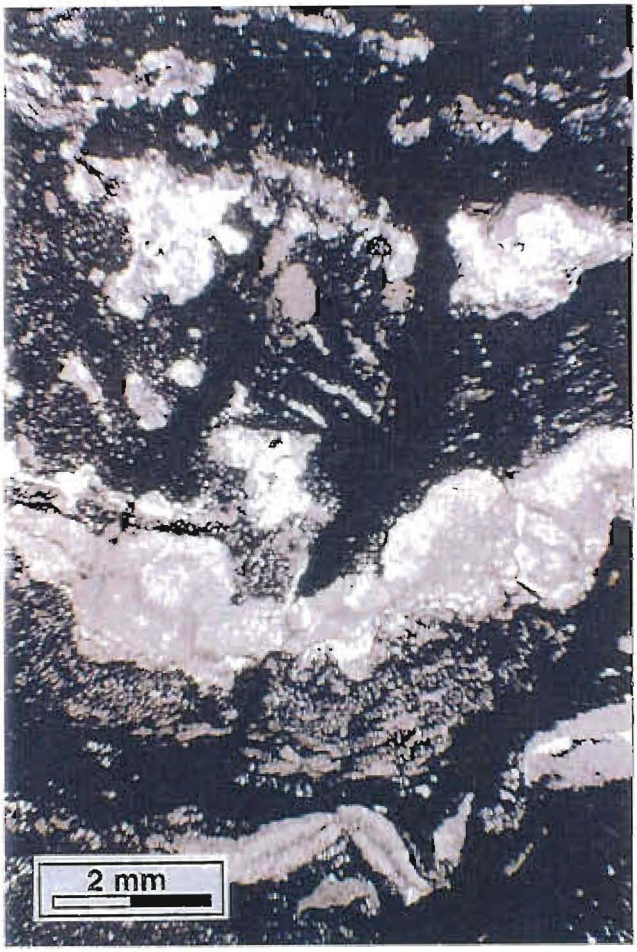

Plate 5. (a) Photomicrograph, transmitted light (RVD17 144.6m). Irregular shaped and disrupted carbonate bed in pyritic and carbonaceous shale; the morphology of the carbonate bed resembles enterolithic anhydrite
(b) Photomicrograph, transmitted light (RVD17 175.5m). Siltstone bed partly altered to siderite (lower two thirds of the bed); nb slightly coarser grain size of the siderite, bedding traces in the siderite, and irregular upper contact of the siderite alteration.

Testing lithogeochemical vectors for northern Australian Proterozoic Sedex Zn deposits at the Sullivan deposit, Canada

Peter McGoldrick
Centre for Ore Deposit Research

Introduction

Work in AMIRA Projects P384 and P384A has developed and refined a set of lithogeochemical indices for unweathered, low sulfide siltstones and shales that can be used as vectors to stratiform sediment-hosted (Sedex) style Zn-Pb-Ag mineralisation. All case studies to date have been from the northern Australian Proterozoic (Carpentaria) Zinc Belt, and, with the possible exception of Century (but see Large, 1998, AMIRA P384A Report 6), abundant carbonate is present in the rocks being tested for primary geochemical dispersions.

The Sullivan deposit was chosen to test the applicability of the lithogeochemical vectors developed for the Australian deposits to Sedex deposits hosted in carbonate-poor siliciclastic dominated sequences. Furthermore, differences in the nature of the Sullivan mineralisation and alteration (e.g., abundant pyrrhotite in the ores, intense tourmalinisation of the footwall rocks) to that seen in the northern Australian deposits suggests two fundamentally different fluids are involved in their formation (see Cooke et al., this volume). Hence, a secondary aim of a Sullivan study was to see what primary dispersions (if any) would be produced by a 'Sullivan-type' ore fluid.

The Sullivan deposit and its host sediments

The Sullivan deposit is a Mesoproterozoic Sedex Zn-Pb-Ag deposit hosted by biotite grade metasediments of the Aldridge Formation in SE British Columbia (Fig. 1). Hamilton et al., (1982) provide a detailed description of the deposit and a multidisciplinary report on the deposit and its geological setting is soon to be jointly published by the Geological Survey of Canada, the British Columbia Geological Survey and Cominco Ltd. The deposit contained 170 million tonnes of ore at an average grade of 5.5 wt% Zn, 5.8 wt% Pb and 59 g/t. The Aldridge Formation is a thick (>4.2 km) turbiditic sequence subdivided into a lower section of dominantly thin bedded, laminated fine grained quartz wacke and laminated pyrhotitic mudrocks ('argillites' and 'siltites'); the middle section is marked by the appearance of distinctive graded arenites which are volumetrically dominant over greywacke and mudrocks, and the upper section is dominated by thin-bedded carbonaceous mudstones. The Sullivan deposit occurs near the top of the Lower Aldridge Formation. Distinctive groups of dark laminated beds in the Lower Aldridge Formation and a carbonaceous wacke laminite at the Lower to Middle Aldridge transtion are used to bracket the 'favourable' stratigraphy regionally. Closer to the orebody (within a few kilometres) a pyrrhotite-rich laminite ('exhalite'), which crops out as the 'concentrator hill horizon' is interpreted to mark the equivalent of the ore sequence. Within a few hundred metres of ore, distinctive barren interore beds can be recognised and are used to define the 'Sullivan Sub-basin'.

Previous halo studies at Sullivan

There have been several efforts by Cominco over the years to define geochemical halos to the Sullivan deposit (D. Anderson, pers. comm.). These used multi-element and multivariate techniques and met

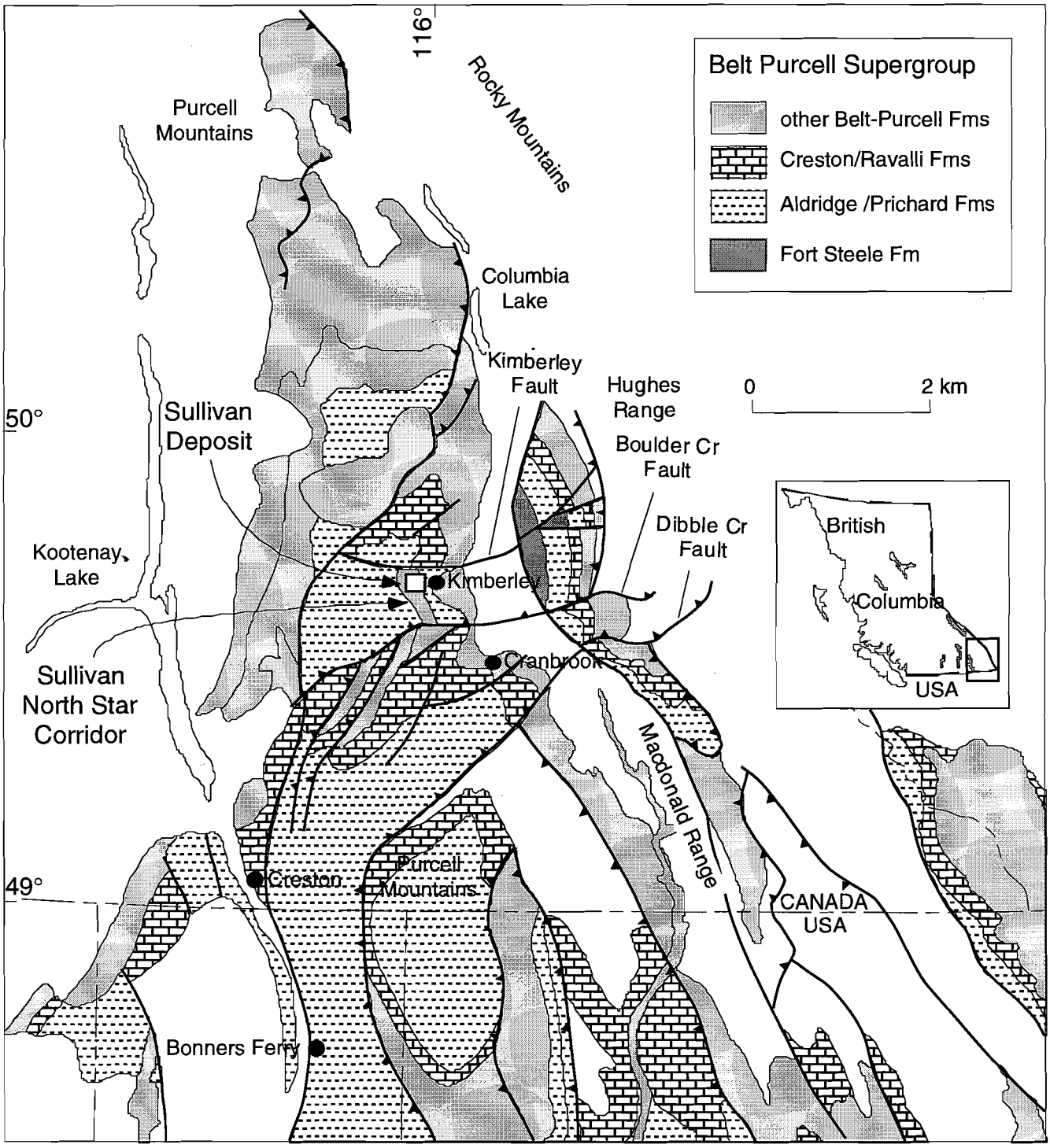

Figure 1. Geological setting of the Sullivan deposit (from Goodfellow, in press).

with limited success. A paper by Fedikow and Turek (1983) applied discriminant analysis to a small data set. More recently a major regional study has been carried out by Wayne Goodfellow of the Canadian Geological Survey (some of his data are used in this report – see below).

Sampling for this study

For this pilot study it was decided to restrict the lateral and vertical extent of sampling, and to use the same sample density as used for our northern Australian studies. Samples were collected approximately every 10 m for about 100 m either side of the Sullivan ore position and five drill holes were sampled (Fig. 2). DDH 478 is about 200 m from the eastern edge of the orebody. Two holes (DDH 6457 and DDH 2231) were needed to span the ore position at a distance of about 1500 m from the orebody. DDH 5452 was collared on concentrator hill about 4 km east of the orebody, and DDH 6466 was collared nearly 7 km east of the orebody. Individual samples comprise ten to thirty centimetre pieces of half and quarter core.

Data from three drill holes from Goodfellow's study have also been included for this analysis (Fig. 2).

A total of 82 low-sulfide, greywacke and argillite samples were analysed for major and trace elements by XRF at the University of Tasmania. The 68 samples from Goodfellow's collection were analysed by a combination of XRF and ICP techniques.

Results

Major and selected trace element analyses for the 82 samples analysed at the University of Tasmania are provided on Table 1.

Zn and the Metal Index

Downhole plots of Zn and Metal Index (Zn+ 100Pb+ 100Tl) for the drill hole nearest the orebody are depicted in Figure 3. The Sullivan Sub-basin is distinguished by Zn values of >100 ppm and Metal Index values of more than 2000. However, there are also high Metal Index values well below the Sullivan Sub-basin position. Figure 4 (DDHs 6457/2231 – 1500 m from ore) has a single sample with anomalous Zn and Metal Index).

Alteration indices and Mn

Figures 3 and 4 also depict Sedex AI, AI 3 and MnO_d data. None of these parameters can be used to define the Sullivan ore postion.

The poor response from the alteration indices and MnO_d for Sullivan host rocks is confirmed when the data for all samples are presented in 'standard' cross-plots used for northern Australian data sets (Fig. 5). Although the Sedex AI plots look encouraging, this is largely due to the 'shale effect', and AI 3 values (more appropriate for 'shaley' rocks) are virtually all below background. A few samples from DDH 6455 do plot in the anomalous areas of the diagrams, but these are high sulfide samples from a drill hole through the fringe of the Sullivan orebody!

Thallium

Figure 6a displays downhole plots of all the Tl data from the Sullivan samples. There is a weak response at the approximate postion of the Sullivan ore sequence in all holes (except DDH 6423).

Discussion: Interpretation of the Tl results is difficult because two different analytical techniques were used, and many samples were at or near the detection limit for XRF, however, the results are quite encouraging. Thallium is present in the Sullivan ores at levels of several tens of ppm and in sulfide rich samples near the orebody (e.g., Fig. 7a & 7b) is behaving as a chalcophile metal. However, there is evidence from the other samples (particularly from Goodfellow's ICP data) that Tl is correlated with K, not S, (e.g., Fig. 7c & 7d) and hence is behaving as a lithophile element away from the immediate vicinity of the Sullivan deposit.

If K minerals are hosting Tl, then normalising the Tl data using K may enhance the response of a primary Tl dispersion. Figure 6b shows downhole plots of 'normalised Tl' (i.e., $Tl/Tl+K_2O$ *100) and an arguably better response is obtained.

Carbonate content

An unexpected result from the study was the observation that many (about 20%) of the samples

contained significant carbonate (>2wt% CO_2). There is no consistent stratigraphic postion for these high CO_2 samples, nor is there any co-variance with Mn. Plots of CaO, MgO and CO_2 (Fig. 8) yield insights into the composition of this carbonate. Two samples are dolomitic and several others are calcitic or a mixture of dolomite and calcite.

Discussion: Previous workers had noted the presence of a few percent carbonate in the mineralised sequence at Sullivan. The relationship of these carbonates and to the carbonates recognised in this study warrants further study. If the ore carbonates have unique compositions it may permit the use of carbonate geochemistry from carbonate-bearing Aldridge Formation rocks to identify the Sullivan ore position.

Conclusions

- The indices developed for northern Australian 'Sedex' Zn deposits cannot be directly applied to the Sullivan deposit.
- Sedex AI, AI3 and MnO_d do not work.
- Zn and the Metal Index may be useful, but only very close to ore.
- There may be a laterally extensive weak Tl primary dispersion halo to the Sullivan deposit, but more work is required to confirm this.

Acknowledgements

I would like to thank Paul Ransom for his help in collecting samples for this work, and being a font of knowledge on all things Sullivan; and Wayne Goodfellow is thanked for making his unpublished Sullivan data set available to the author.

References

Fedikov, M.A.F. and Turek, A., 1983, The application of stepwise discriminant analysis to geochemical data from the host rocks of the Sullivan Pb-Zn-Ag deposit, Kimberley, B.C., Journal of Geochemical Exploration, 18, 231-244.

Hamilton, J. M., D. T. Bishop, H. C. Morris, O. E. Owens, R. W. Hutchinson, C. D. Spence, and J. M. Franklin, 1982, Geology of the Sullivan orebody Kimberely, B.C., Canada: Geol. Assoc. Canada Spec. Paper, v. 25, p. 597-665.

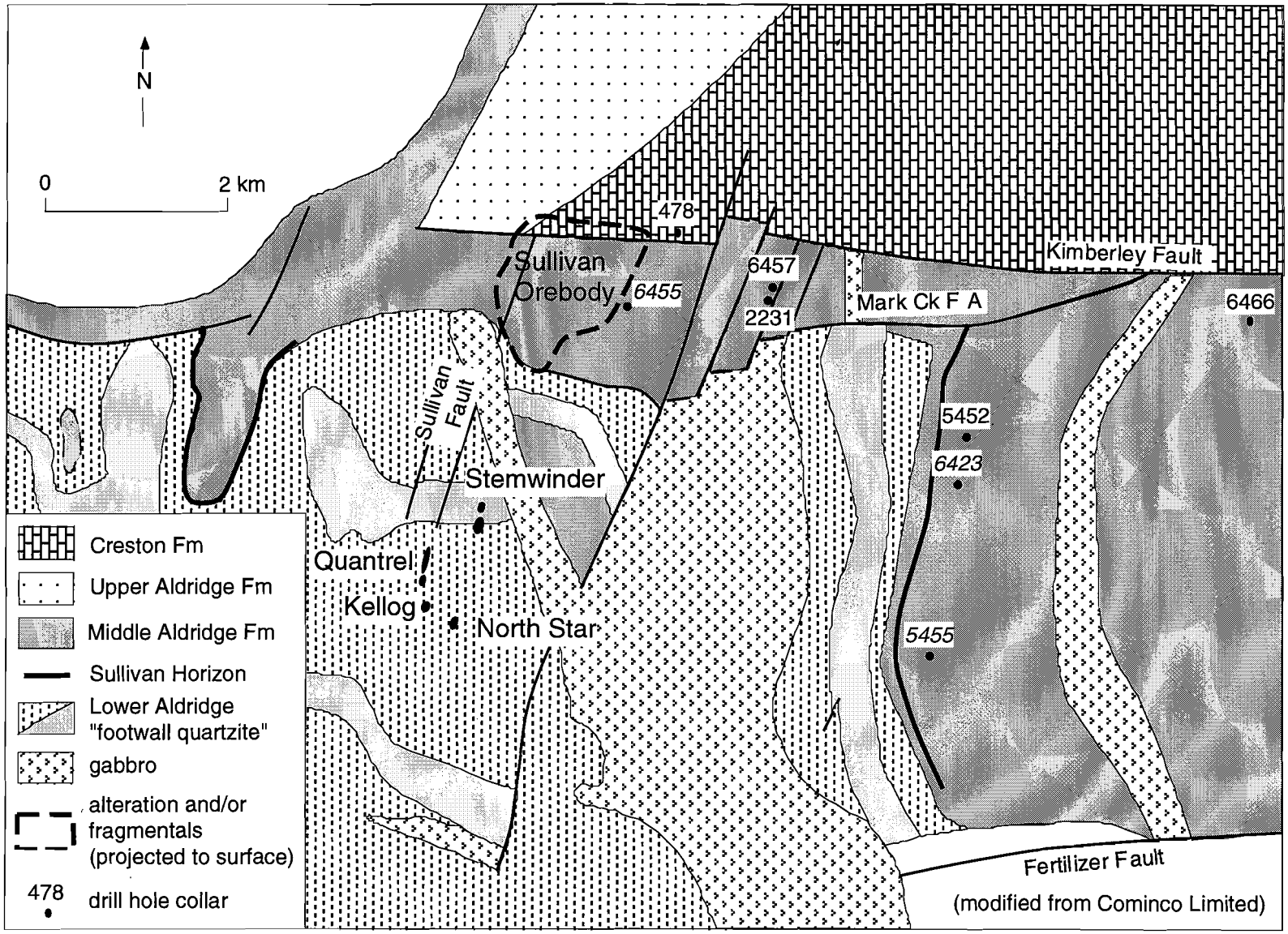

Figure 2. Geological plan of the area around the Sullivan deposit showing the location of drill holes referred to in this study (Goodfellow drill holes in italics)

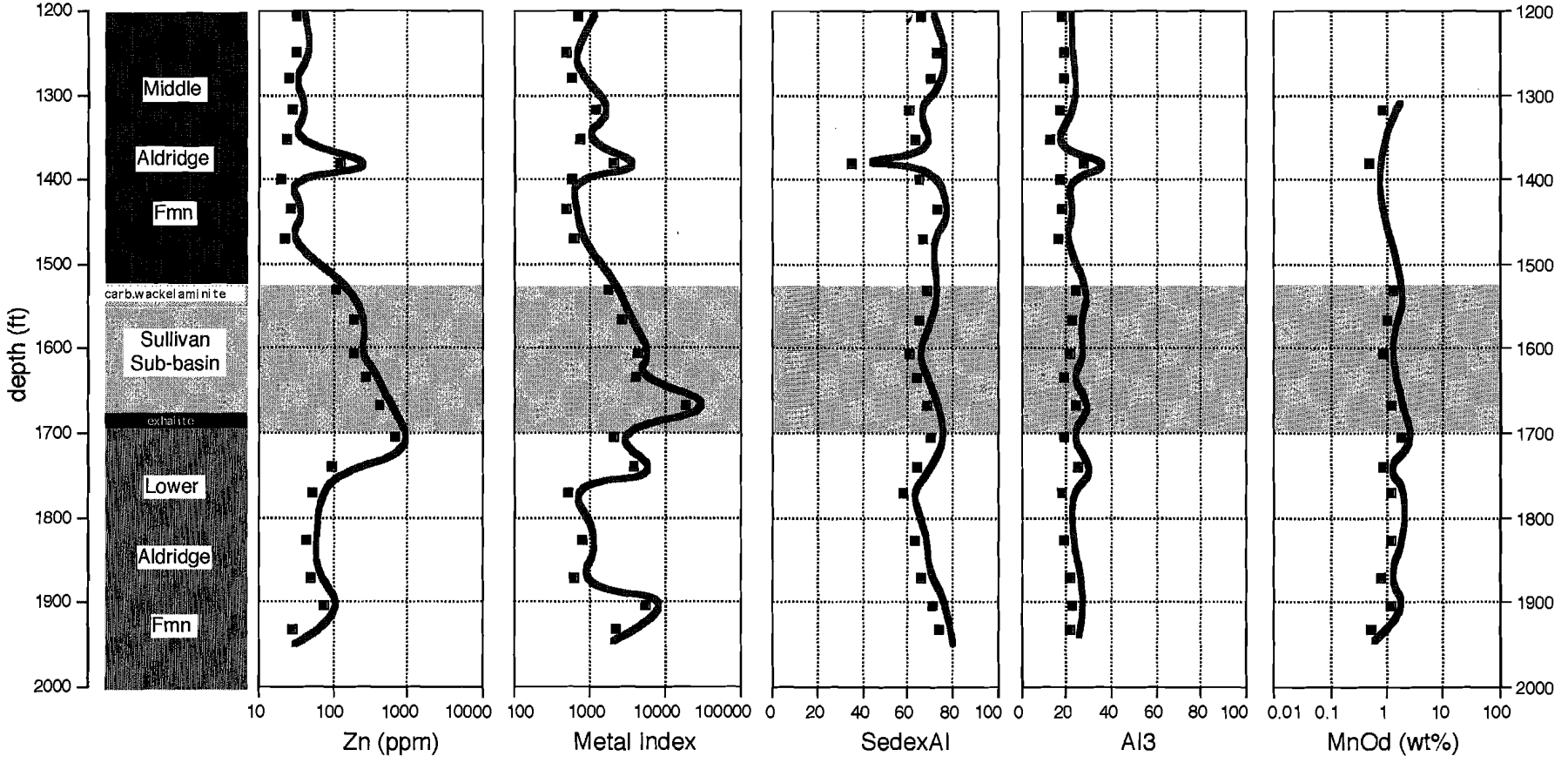

Figure 3. Downhole plots for DDH 478

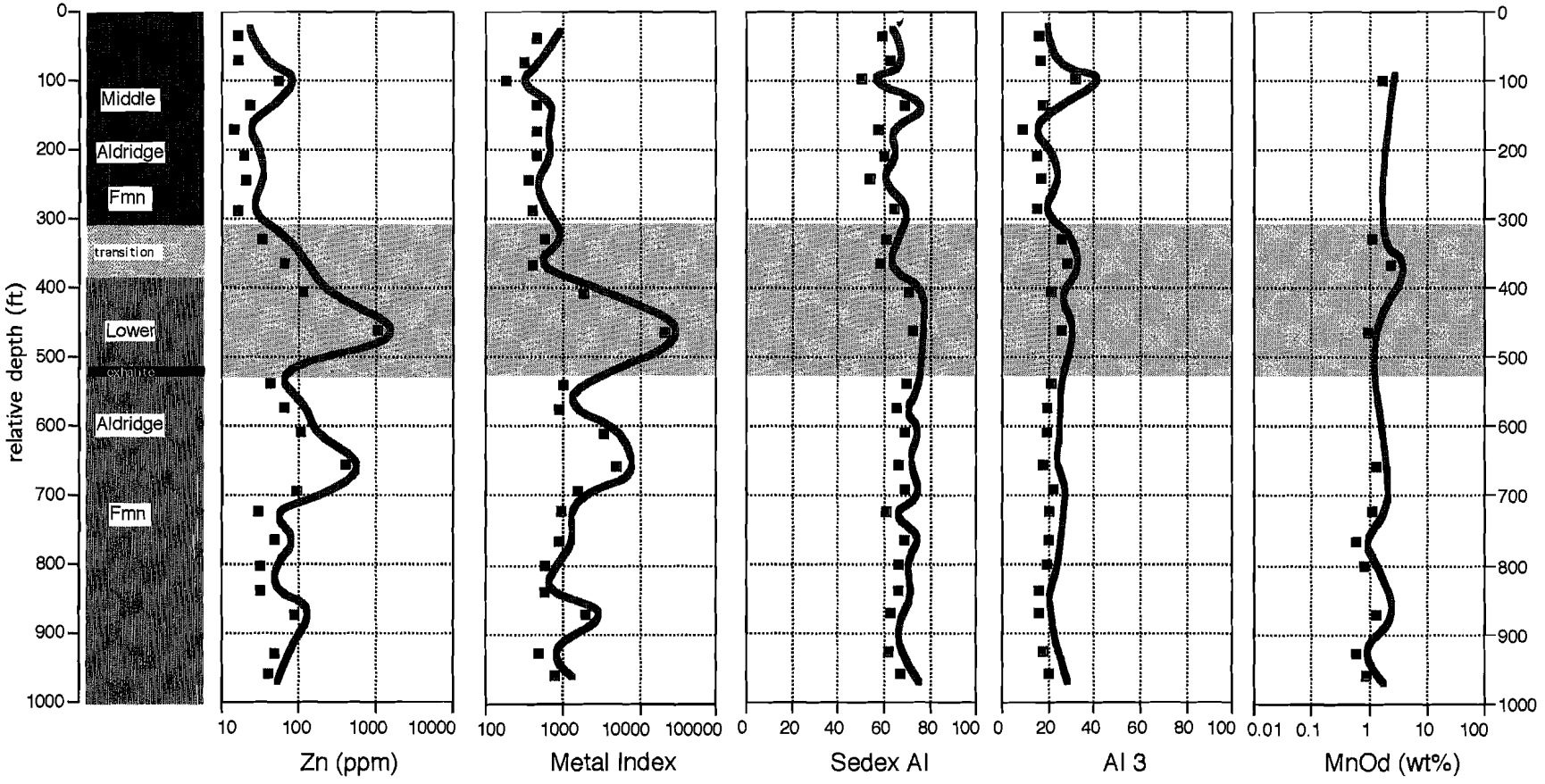

Figure 4. Downhole plots for DDHs 6547 & 2231

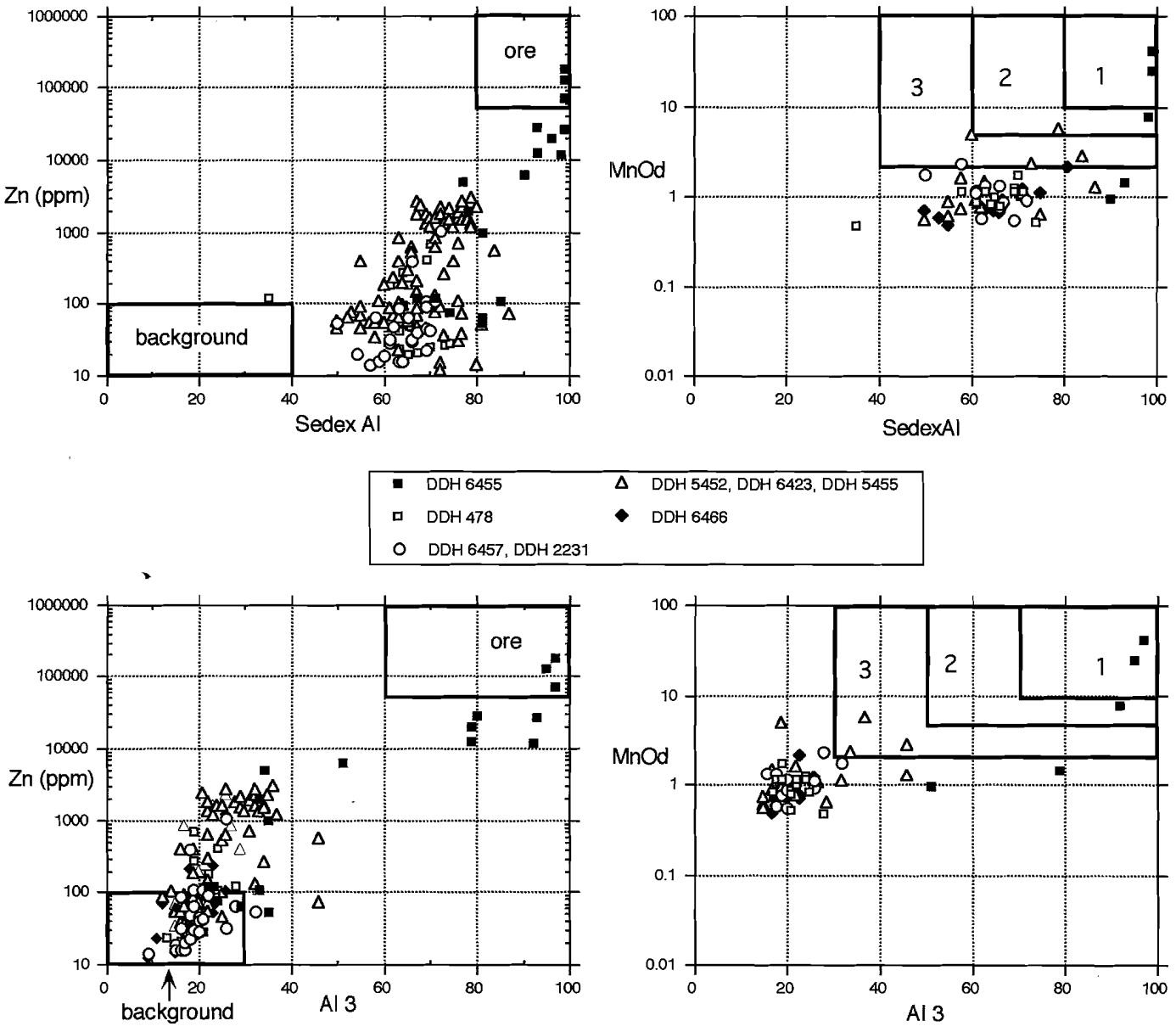

Figure 5. Zn/ Sedex Al / Al3 and MnO_d cross plots.

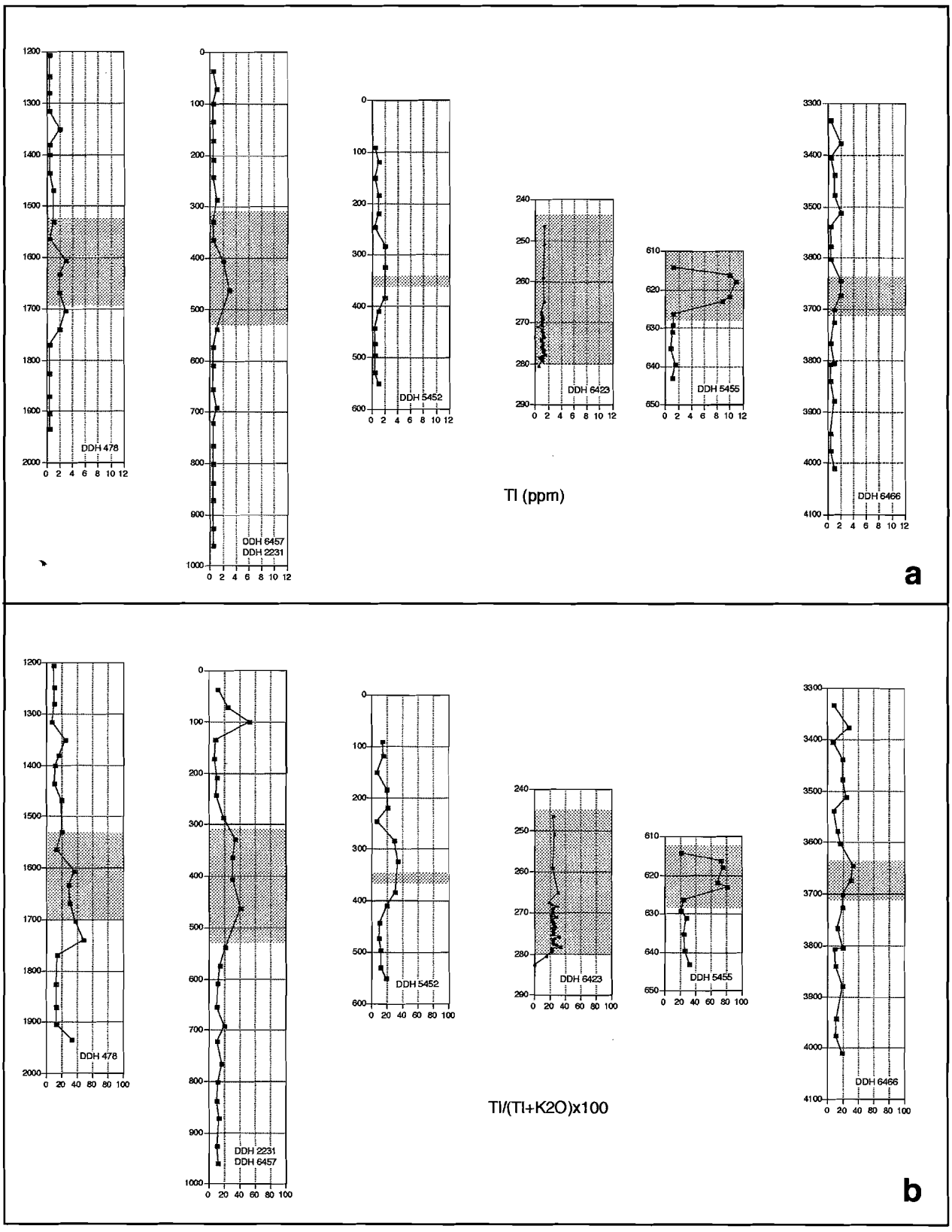

Figure 6. a) Downhole plots for Tl from all drill holes. b) Downhole plots for Tl/Tl+K_2O*100 from all holes.

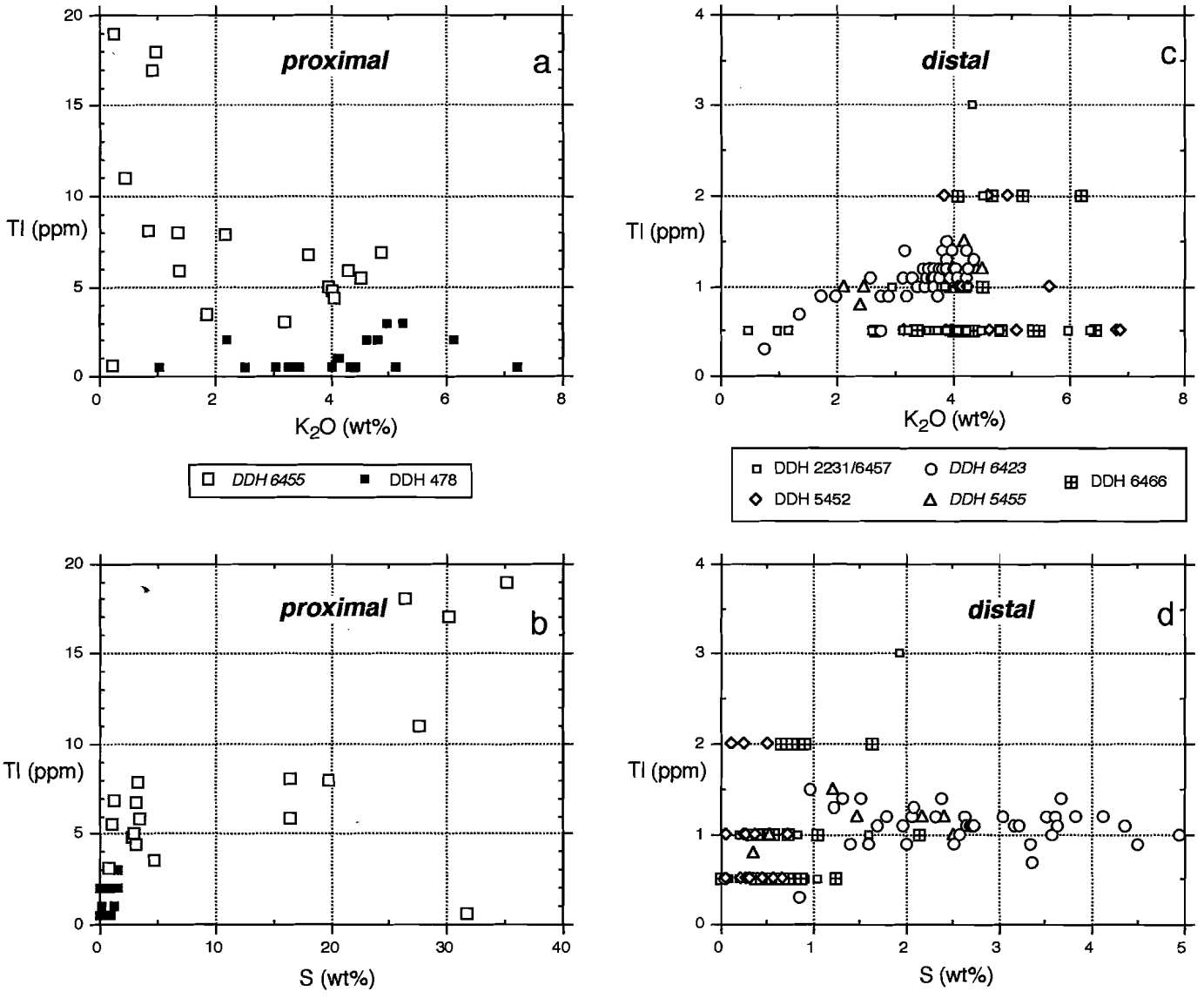

Figure 7. Tl / K_2O and Tl / S cross plots for all samples (proximal and distal); nb., samples from DDH 6455 are from a fringe ore position.

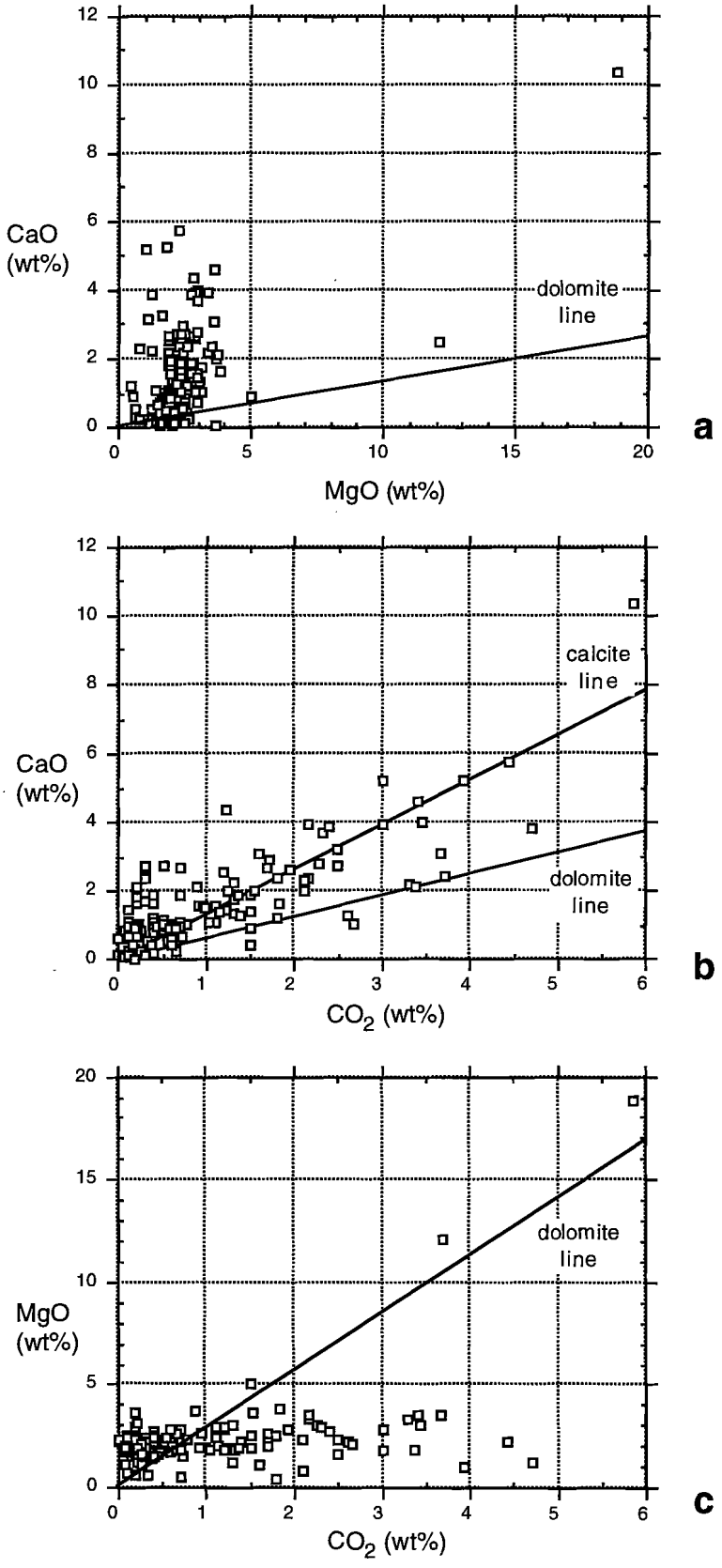

Figure 8. CaO / MgO / CO_2 cross plots for all samples.

Ident	Drill hole	from (ft)	SiO2	TiO2	AL2O3	Fe2O3	FeO	MgO	CaO	MnO	Na2O	K2O	P2O5	loss	Total	H2O	CO2	Total	S	As	Ba	Cr	Cu	Nb	Ni	Pb	Rb	Sr	Th	Tl	U	V	Y	Zn	Zr
other	other	other	wt%	wt%	wt%	wt%	wt%	wt%	wt%	wt%	wt%	wt%	wt%	wt%	wt%	wt%	wt%	wt%		ppm	ppm	ppm	ppm	ppm	ppm	ppm	ppm	ppm	ppm	ppm	ppm	ppm	ppm	ppm	ppm
478-1207	DDH 478	1207	62.28	0.71	19.44	5.04	4.54	2.47	0.14	0.02	1.00	5.11	0.10	3.55	99.36	3.31	0.40	0.28		<3	992	71	5	17	20	6	175	29	20	<1	5	97	49	32	230
478-1248	DDH 478	1248	63.63	0.71	18.85	5.36	4.82	1.89	0.16	0.02	1.78	4.43	0.10	2.88	99.27	2.95	0.22	0.16		<3	969	70	14	18	18	4	145	45	18	<1	3	93	44	32	233
478-1280	DDH 478	1280	64.79	0.67	17.89	4.92	4.43	1.94	0.13	0.02	1.50	4.42	0.09	3.02	98.90	2.95	0.07	0.50		9	856	63	17	16	19	5	151	39	18	<1	4	83	42	25	241
478-1316	DDH 478	1316	50.03	0.85	22.82	5.27	4.74	3.35	2.19	0.06	0.17	7.21	0.11	7.05	98.55	3.57	3.30	1.00		<3	1324	93	5	21	14	11	263	73	23	<1	7	128	49	29	279
478-1351	DDH 478	1351	61.24	0.82	21.20	3.73	3.36	2.06	0.12	0.02	1.21	6.12	0.10	3.19	99.44	3.04		0.02		<3	1229	72	3	21	16	5	209	48	18	2	4	94	48	24	344
478-1381	DDH 478	1381	37.02	0.88	7.33	9.37	8.43	18.84	10.35	0.16	0.31	2.52	2.55	9.81	98.20	4.83	5.86	0.07		<3	1984	1496	18	64	524	19	52	1393	20	<1	3	199	16	122	119
478-1400	DDH 478	1400	68.95	0.62	16.30	3.94	3.55	2.01	0.08	0.02	1.35	4.03	0.07	2.56	99.54	2.68	0.07	0.03		<3	824	54	3	15	13	5	129	43	15	<1	4	70	39	20	274
478-1435	DDH 478	1435	65.37	0.69	18.14	4.59	4.13	1.58	0.14	0.02	2.06	4.32	0.10	2.59	99.14	2.77	0.26	0.06		6	918	57	9	18	18	4	145	56	15	<1	4	74	42	27	276
478-1470	DDH 478	1470	66.20	0.65	17.71	3.97	3.57	1.86	0.14	0.02	1.85	4.10	0.08	2.84	99.02	2.77	0.07	0.15		<3	934	51	6	17	11	5	144	60	14	1	4	64	48	22	298
478-1531	DDH 478	1531	61.38	0.62	16.83	6.42	5.78	2.93	1.44	0.06	1.49	4.14	0.10	4.14	98.91	3.04	1.21	1.24		<3	968	64	37	14	22	15	169	51	13	1	5	87	38	112	213
478-1565	DDH 478	1565	66.17	0.58	14.31	4.47	4.02	2.56	2.39	0.08	1.75	3.27	0.11	3.72	98.96	2.50	1.80	0.71		<3	874	53	24	14	15	24	140	78	11	<1	5	75	37	189	253
478-1605.5	DDH 478	1606	60.12	0.68	16.82	5.41	4.87	3.53	2.39	0.07	0.98	5.24	0.13	4.30	99.13	2.86	2.16	0.92		<3	1179	65	27	15	21	37	225	63	13	3	5	96	40	185	227
478-1633.7	DDH 478	1634	66.16	0.63	16.05	4.33	3.90	2.38	0.56	0.04	1.02	4.80	0.12	3.46	99.12	2.59	0.55	1.28		<3	1011	59	21	14	14	37	197	39	13	2	5	83	39	278	245
478-1667	DDH 478	1668	63.07	0.64	16.01	5.84	5.25	2.67	1.59	0.06	1.09	4.62	0.12	3.70	98.82	2.68	0.95	1.58		<3	931	62	27	14	19	182	189	53	12	2	5	92	39	411	217
478-1703	DDH 478	1704	66.54	0.62	16.15	4.29	3.86	1.90	0.86	0.05	1.20	4.97	0.12	2.88	99.15	2.06	0.07	1.54		<3	923	59	25	15	17	11	202	63	13	3	5	78	41	688	239
478-1741	DDH 478	1741	65.59	0.49	12.86	4.85	4.36	2.97	3.68	0.10	3.35	2.21	0.12	3.35	99.08	1.43	2.31	0.71		4	461	48	20	14	13	35	111	180	11	2	3	50	38	95	290
478-1770	DDH 478	1770	67.24	0.57	15.15	3.86	3.47	2.83	1.06	0.04	2.70	3.03	0.13	3.01	99.23	2.14	0.59	0.87		4	900	55	26	15	14	4	98	71	12	<1	4	60	43	54	345
478-1827	DDH 478	1827	68.64	0.55	14.38	3.99	3.59	2.30	1.03	0.04	2.45	3.31	0.12	3.00	99.41	2.06	0.77	0.49		16	816	46	20	14	15	7	114	94	10	<1	4	58	33	43	243
478-1872	DDH 478	1872	64.43	0.60	15.00	4.30	3.87	2.32	2.71	0.07	2.36	3.32	0.17	4.37	99.22	2.32	2.49	0.52		9	821	47	18	13	14	5	103	123	10	<1	3	72	38	49	231
478-1903	DDH 478	1904	68.62	0.54	13.91	4.38	3.94	1.89	1.60	0.06	2.48	3.45	0.12	2.63	99.24	1.79	0.92	0.96		<3	741	44	26	12	13	55	126	129	9	<1	3	54	34	77	248
478-1934	DDH 478	1934	72.49	0.39	9.45	2.17	1.95	1.02	5.23	0.09	3.50	1.03	0.10	3.93	99.18	0.80	3.92	0.48		<3	318	38	13	10	7	21	27	210	8	<1	3	30	30	28	369
2231-7.0	DDH 2231	7	65.44	0.60	16.67	5.16	4.64	2.10	0.45	0.05	1.98	4.51	0.09	2.66	99.19	2.14	0.37	0.79		<3	867	53	21	15	20	16	194	98	12	2	4	72	36	112	207
2231-62.5	DDH 2231	63	65.71	0.55	14.09	5.85	5.26	2.19	1.30	0.04	1.63	4.31	0.12	3.35	98.55	1.79	1.39	1.93		<3	840	49	40	14	20	201	187	90	11	3	3	69	40	1038	228
2231-139.0	DDH 2231	139	69.80	0.51	13.62	4.26	3.83	1.84	0.95	0.04	2.19	3.78	0.11	2.55	99.22	1.52	0.18	1.59		<3	775	44	20	13	12	9	136	103	10	1	3	55	37	42	264
2231-174.0	DDH 2231	174	71.67	0.49	13.10	3.43	3.09	1.87	1.02	0.04	2.22	3.14	0.10	2.34	99.08	1.88	0.51	0.50		11	687	43	20	13	15	8	114	94	10	<1	4	51	37	63	293
2231-209	DDH 2231	209	72.18	0.50	13.16	3.52	3.17	1.64	1.01	0.04	2.32	3.57	0.11	1.83	99.53	1.43	0.44	0.56		7	719	43	18	14	13	32	129	117	11	<1	3	50	37	107	286
2231-256	DDH 2231	256	71.15	0.52	13.76	3.33	3.00	1.75	0.93	0.04	1.87	4.08	0.11	2.24	99.45	1.61	0.59	0.45		5	829	45	18	13	13	45	148	93	11	<1	4	54	39	397	295
2231-293.2	DDH 2231	293	68.90	0.55	14.25	4.69	4.22	2.15	0.83	0.05	1.93	3.86	0.12	2.38	99.24	1.79	0.40	0.83		<3	764	49	28	13	19	14	155	120	10	1	3	65	35	94	235
2231-323	DDH 2231	323	65.07	0.60	15.48	4.48	4.03	2.95	1.57	0.06	2.08	4.20	0.13	3.48	99.65	2.32	1.10	0.65		<3	618	44	15	12	10	9	91	123	9	<1	3	46	36	29	300
2231-366	DDH 2231	366	69.03	0.48	12.61	3.28	2.95	1.59	3.24	0.06	2.98	2.59	0.13	3.83	99.49	1.43	2.49	0.51		9	788	52	18	14	18	8	139	115	10	<1	3	63	40	47	255
2231-401.8	DDH 2231	402	68.31	0.57	14.59	3.86	3.47	1.96	1.55	0.04	2.20	3.73	0.12	2.95	99.49	1.88	0.99	0.63		<3	853	41	16	14	11	5	155	70	9	<1	3	55	34	31	253
2231-438.5	DDH 2231	439	69.37	0.58	15.52	3.32	2.99	1.73	0.46	0.04	1.52	4.47	0.10	2.57	99.32	2.14	0.15	0.64		<3	725	43	12	14	13	5	113	96	10	<1	4	50	36	32	247
2231-472	DDH 2231	472	70.99	0.52	14.41	2.98	2.68	1.84	0.92	0.04	2.44	3.23	0.10	2.39	99.56	1.79	0.66	0.32		4	926	59	21	16	17	19	163	136	11	<1	4	76	42	88	257
2231-528	DDH 2231	528	60.87	0.60	15.12	2.95	2.65	2.27	5.74	0.11	1.69	4.21	0.09	6.38	99.73	1.97	4.43	0.25		<3	912	65	10	17	8	4	158	100	13	<1	4	74	42	48	304
2231-560	DDH 2231	560	67.48	0.52	14.23	4.14	3.73	2.00	1.39	0.04	2.08	3.89	0.11	3.61	99.08	1.97	1.14	0.91		<3	831	32	30	13	15	7	137	104	10	<1	4	44	38	40	270
6457-636.5	DDH 6457	637	70.97	0.47	14.57	3.32	2.99	2.24	0.12	0.02	1.81	3.66	0.09	2.83	99.77	2.59	0.29	1.05		5	580	64	28	16	20	4	103	44	16	<1	4	87	41	16	221
6457-670.5	DDH 6457	671	64.67	0.66	17.55	4.27	3.84	2.34	0.13	0.02	3.95	2.95	0.07	2.83	99.01	2.23	0.11	0.56		4	774	37	10	15	13	2	132	22	12	1	4	49	43	16	246
6457-698.5	DDH 6457	699	49.05	0.61	13.13	11.80	10.62	12.11	2.46	0.14	0.95	0.45	0.05	8.69	98.26	6.34	3.70	0.01		<3	54	242	6	4	49	<1.5	15	21	2	<1	2	291	11	55	66
6457-735.3	DDH 6457	735	59.00	0.83	20.99	5.25	4.72	2.19	0.13	0.02	1.33	5.99	0.10	3.82	99.12	3.57	0.29	0.71		14	1124	77	15	21	22	4	194	38	21	<1	7	105	56	23	274
6457-772	DDH 6457	772	64.41	0.76	20.44	2.18	1.96	1.55	0.09	0.01	1.21	6.34	0.08	3.02	99.87	2.95	0.04	0.08		<3	1136	63	5	19	13	4	206	39	16	<1	5	86	46	14	335
6457-808.5	DDH 6457	809	68.54	0.62	16.23	3.44	3.10	2.18	0.11	0.02	2.06	4.03	0.08	2.58	99.55	2.50		0.06		<3	673	54	5	17	8	4	134	43	16	<1	5	74	41	19	339
6457-843	DDH 6457	843	64.92	0.68	16.87	4.59	4.13	3.63	0.04	0.02	0.39	4.80	0.07	3.53	99.08	3.31	0.18	0.20		<3	650	57	3	18	19	3	157	15	15	<1	4	95	71	20	268
6457-887	DDH 6457	887	67.46	0.66	17.57	3.54	3.19	1.87	0.10	0.02	2.23	4.26	0.07	2.65	100.08	2.68	0.07	0.20		<3	764	57	8	17	13	3	134	29	16	1	5	79	43	16	286
6457-929	DDH 6457	929	64.28	0.56	13.76	6.03	5.43	3.83	1.63	0.06	4.12	0.97	0.12	4.33	99.09	2.77	1.83	0.77		<3	191	52	23	13	21	5	34	49	12	<1	5	71	41	33	251
6457-965	DDH 6457	965	65.11	0.50	12.68	6.90	6.21	5.02	0.91	0.07	2.75	1.14	0.12	4.62	99.13	3.13	1.50	0.74		4	177	48	9	13	19	3	39	25	12	<1	3	62	39	64	238
5452-90.5	DDH 5452	91	73.43	0.61	13.89	3.21	2.89	1.12	0.14	0.02	2.53	3.16	0.07	1.75	99.61	1.70	0.07	0.07		3	679	49	9	16	16	10	117	73	17	<1	4	51	39	36	527
5452-119.0	DDH 5452	119	61.96	0.75	19.79	5.42	4.88	1.55	0.19	0.04	1.83	5.67	0.10	2.46	99.22	2.59	0.40	0.28		<3	977	72	14	18	11	10	211	65	18	1	4	94	40	73	235
5452-151.0	DDH 5452	151	60.33	0.80	21.76	3.44	3.10	1.65	0.16	0.02	0.96	6.89	0.09	3.44	99.20	2.77	0.22	0.67		<3	1495	83	31	19	24	6	236	58	19	<1	5	113	49	87	246
5452-184.5	DDH 5452	185	68.33	0.53	14.74	3.41	3.07	3.12	1.05	0.03	1.67	4.10	0.12	2.35	99.11	1.97	0.22	0.73		<3	813	47	25	14	16	15	171	149	12	1	4	58	43	65	262
5452-219	DDH 5452	219	63.15	0.54	15.87	3.02	2.72	3.37	3.92	0.07	2.18	3.89	0.11	3.35	99.17	1.70	2.16	0.37		<3	872	49	18	15	9	20	161	238	11	1	4	61	38	58	253
5452-245.5	DDH 5452	246	58.13	0.87	22.75	4.51	4.06	1.37	0.16	0.05	1.56	6.84	0.10	2.97	98.86	2.95	0.37	0.22		<3	1281	81	12	22	16	6	227	73	22	<1	6	109	60	39	282
5452-283	DDH 5452	283	65.32	0.52	15.00	3.20	2.88	2.98	2.81	0.08	0.69	4.94	0.10	3.55	98.87	2.41	2.27	0.12		<3	952	47	10	15	12	12	209	92	12	2	4	64	38	94	238
5452-323	DDH 5452	323	70.51	0.54	13.76	3.85	3.46	2.61	0.25	0.04	1.52	3.84	0.13	2.67	99.33	2.32	0.66	0.26		<3	685	50	15	14	16	9	138	41	9	2	4	64	35	179	274
5452-382.5	DDH 5452	383	68.26	0.55	15.31	3.26	2.93	2.55	1.20	0.05	1.42	4.60	0.14	2.20	99.21	1.97	0.40	0.51		<3	856	49	10	16	9	11	170	110	11	2	5	56	46	55	299
5452-410	DDH 5452	410	67.26	0.52	14.28	3.58	3.22	2.62	2.66	0.08	1.64	4.17	0.13	2.25	98.83	1.70	1.69	0.26		<3	771	49	9	14	8	20	155	139	10	1	3	51	36	84	297
5452-443.5	DDH 5452	444	68.11	0.58	16.27	3.17	2.85	2.10	0.85	0.03	2.02	4.62	0.13	2.04	99.60	1.97	0.26	0.31		<3	1004	46	11	16	11	7	152	130	10	<1	4	61	42	55	284
5452-473.3	DDH 5452	473	66.29	0.59	15.59	3.33	3.00	2.10	1.02	0.05	1.20	5.10	0.12	4.43	99.49	1.88	2.67	0.46		5	1079	53	13	16	11	9	168	103	11	<1	4	66	46	64	316
5452-497	DDH 5452	497	68.09	0.61	15.16	4.21	3.79	2.26	1.01	0.05	2.34	3.98	0.13	2.04	99.46	1.52	0.51	0.58		6	893	53	18	15	13	10	144	148	10	<1	4	69	40	58	252
5452-550.8	DDH 5452	551	68.30	0.57	16.31	3.08	2.77	1.82	0.49	0.03	2.80	4.25	0.14	1.75	99.23	1.79	0.22	0.07		4	846	50	13	12	16	31	144	154	11	1	4	60	33	102	239
5452-530	DDH 5452	530	66.13	0.52	14.04	4.46	4.01	3.73	2.12	0.11	2.49	3.88	0.13	1.98	99.14	1.52	0.88	0.28		<3	1018	47	6	15	8	4	140	109	8	<1	3	63	39	54	279
6466-3333	DDH 6466	3333	68.43	0.60	17.00	3.55	3.19	1.25	0.22	0.01	0.41	5.49	0.13	3.16	99.89	2.41	0.22	1.24		6	981	45	27	16	13	15	193	39	11	<1	4	59	45	15	286
6466-3377	DDH 6466	3377	66.67	0.60	17.62	4.82	4.34	1.50	0.19	0.03	1.15	5.18	0.09	2.74	100.11	2.41	0.18	0.91		<3	823	56	32	16	15	6	198	51	18	2	4	75	41	31	202
6466-3406	DDH 6466	3406	61.99	0.79	21.65	3.16	2.84	1.76	0.14	0.01	1.36	6.45	0.09	3.22	100.30	2.86	0.04	0.72		<3	995	81	18	20	14	4	234	73	18	<1	6	111	48	23	242
6466-3438	DDH 6466	3438	67.40	0.50	13.87	3.34	3.01	2.83	2.59	0.04	1.38	3.93	0.11	4.01	99.67	2.06	1.94	0.54		<3	601	46	15	14	9	6	165	109	10	1	4	59	39	45	248

Ident	Drill hole	from (ft)	SiO2	TiO2	AL2O3	Fe2O3	FeO	MgO	CaO	MnO	Na2O	K2O	P2O5	loss	Total	H2O	CO2	Total	S	As	Ba	Cr	Cu	Nb	Ni	Pb	Rb	Sr	Th	Tl	U	V	Y	Zn	Zr
other	other	other	wt%	wt%	wt%	wt%	wt%	wt%	wt%	wt%	wt%	wt%	wt%	wt%	wt%	wt%	wt%	wt%		ppm	ppm	ppm	ppm	ppm	ppm	ppm	ppm	ppm	Ppm	ppm	ppm	ppm	ppm	ppm	ppm
6466-3478	DDH 6466	3478	66.34	0.51	12.85	3.18	2.86	3.54	3.08	0.07	0.53	4.05	0.13	5.91	99.87	2.32	3.66	0.40		<3	589	36	14	13	10	7	160	61	9	1	3	51	37	46	275
6466-3513	DDH 6466	3513	58.04	0.79	20.90	6.91	6.22	1.53	0.70	0.05	0.90	6.20	0.11	4.02	99.46	2.86	0.73	1.63		<3	1015	81	44	18	20	14	228	70	20	2	6	110	53	52	241
6466-3539.2	DDH 6466	3539	50.32	0.90	21.64	9.02	8.12	3.68	2.00	0.08	1.73	5.38	0.06	5.40	99.31	4.02	1.54	0.87		4	926	492	58	10	35	9	215	134	2	<1	2	439	24	105	94
6466-3578	DDH 6466	3578	73.85	0.59	15.46	1.49	1.34	0.59	0.31	0.02	2.92	3.35	0.07	1.77	100.27	1.52	0.18	<0.01		<3	587	48	2	15	2	3	111	80	14	<1	4	61	41	12	279
6466-3603	DDH 6466	3603	76.98	0.49	12.06	2.21	1.99	0.56	0.57	0.02	2.31	2.64	0.05	1.26	98.93	1.25	0.33	0.37		<3	507	39	5	13	22	6	91	91	14	<1	3	46	33	14	349
6466-3644.5	DDH 6466	3645	64.43	0.54	13.20	4.39	3.95	2.98	3.98	0.10	1.05	4.07	0.12	4.87	99.29	1.97	3.44	0.65		<3	597	50	21	13	15	55	173	115	12	2	3	72	39	230	249
6466-3673	DDH 6466	3673	66.57	0.64	16.68	4.07	3.66	1.91	1.02	0.03	1.60	4.66	0.09	2.86	99.72	2.23	0.48	0.76		<3	754	54	24	16	14	10	183	132	13	2	4	73	39	43	255
6466-3702	DDH 6466	3702	66.70	0.53	14.24	5.75	5.17	1.81	1.12	0.04	0.66	4.18	0.10	4.38	98.93	2.41	1.03	2.14		<3	671	51	35	12	12	130	155	40	11	1	5	74	36	1180	230
6466-3727	DDH 6466	3727	66.87	0.57	14.76	4.71	4.24	1.92	1.92	0.06	1.77	4.18	0.12	2.90	99.31	1.70	1.50	1.05		6	675	48	28	14	18	9	165	112	10	1	3	63	40	89	264
6466-3767	DDH 6466	3767	70.23	0.46	12.66	3.47	3.12	2.03	2.66	0.06	1.96	3.37	0.12	2.48	99.15	1.34	1.69	0.53		<3	568	39	14	13	9	11	122	123	9	<1	3	45	36	55	256
6466-3805.5	DDH 6466	3806	68.09	0.59	14.78	3.50	3.15	1.86	1.79	0.04	1.87	4.16	0.14	3.10	99.57	1.79	1.32	0.57		5	728	48	21	15	12	14	149	127	10	1	3	65	39	50	264
6466-3807.2	DDH 6466	3841	63.41	0.53	13.66	4.22	3.80	2.78	4.38	0.10	1.27	4.36	0.11	4.99	99.39	1.61	1.21	0.56		<3	681	51	19	13	11	8	166	131	11	<1	4	63	33	66	257
6466-3841	DDH 6466	3879	67.73	0.64	14.95	3.68	3.31	1.88	1.89	0.05	1.80	4.12	0.12	2.68	99.17	1.79	1.36	0.72		<3	716	50	20	14	10	11	146	113	10	1	4	83	41	208	251
6466-3878.6	DDH 6466	3807	64.14	0.66	16.94	4.18	3.76	1.84	2.15	0.08	1.97	4.82	0.11	3.13	99.60	2.06	3.37	0.59		6	842	63	20	16	15	8	164	121	12	<1	4	85	39	76	246
6466-3943	DDH 6466	3943	69.66	0.55	13.97	3.57	3.21	1.89	2.00	0.06	1.75	3.99	0.12	2.51	99.71	1.43	1.25	0.65		5	652	45	20	13	10	8	144	105	10	<1	3	58	35	48	233
6466-3977	DDH 6466	3977	72.58	0.44	14.77	2.31	2.08	1.08	0.24	0.01	1.97	4.12	0.08	2.12	99.49	1.70	0.26	0.51		<3	876	33	15	13	8	4	129	62	15	<1	4	45	30	70	225
6466-4010.9	DDH 6466	4011	62.23	0.55	14.39	3.48	3.13	3.58	4.61	0.09	1.55	4.50	0.11	4.84	99.58	2.06	3.41	0.33		<3	996	48	12	15	11	16	155	187	9	1	4	61	36	75	252

Element associations and depositional processes for McArthur-Type and Selwyn-type sediment-hosted Pb-Zn deposits

David R Cooke, Stephen B. Bodon and Stuart W. Bull
Centre for Ore Deposit Research

Summary

Calculations presented in this report illustrate that iron and manganese are soluble in acidic hydrothermal solutions, and are insoluble in neutral to alkaline solutions. Both can be enriched in McArthur- and Selwyn-type brines. Europium has no potential for discriminating McArthur and Selwyn-type brines, but can be used to identify areas of hydrothermal discharge. Whereas copper has potential to be transported in elevated concentrations in McArthur-type brines, there is less potential for copper transport in Selwyn-type brines. High grade copper mineralisation could therefore be genetically related to Pb-Zn mineralisation in the Northern Australian zinc belt. Numerical simulations highlight that fluid mixing is the most effective depositional process for Pb-Zn mineralisation from McArthur-type brines. Mixing can involve anoxic seawater (syngenetic environment) or sour gas (epigenetic environment). Wallrock interaction also produces sulfide mineralisation, but should also produce wallrock alteration assemblages.

Introduction

Based on geological relationships and the results of chemical modelling, Cooke et al. (1998) proposed that two brine types can form stratiform sediment-hosted ("SEDEX") Pb-Zn deposits. *McArthur-type* SEDEX deposits form from oxidised brines, whereas *Selwyn-type* form from reduced, acid brines. The details of this model, and the predicted associations of barite, siderite, gold and tin to the two types of SEDEX deposit are discussed in Cooke et al., 1998. In the first section of this report, we extend our modelling results to consider several additional important elements that may be enriched in SEDEX systems, and/or have potential as pathfinder elements (Mn, Fe, Cu, Eu). The second section of this report presents the results of numerical simulations, whereby we test the effects of various possible depositional processes on a McArthur-type brine that carries high concentrations of Zn, Pb, Cu and Fe. The thermodynamic data used in this study has been taken from the SOLTHERM and SUPCRT92 databases (Spycher and Reed, 1990; Johnson et al., 1992).

Predicted element associations in McArthur & Selwyn-type SEDEX deposits

Manganese

Manganese is enriched in sedimentary lithologies that underlie HYC and other Australian Proterozoic SEDEX deposits, and is inferred to be (at least in part) a product of hydrothermal activity (ie. an alteration halo; Large et al., 1998). Manganese enrichment can also occur in sedimentary lithologies by 'normal' sedimentary and diagenetic processes.

Manganese in black shales

Redox processes are important for Mn transport and deposition in surface waters and low-T groundwaters. Manganese is generally enriched in black shales, and this has been attributed to chemical precipitation of manganese oxides or carbonates

under highly oxidised or reducing conditions respectively. Calvert and Pedersen (1996) summarised the hypothesised mechanisms for manganese carbonate deposition in black shales as follows:

i deposition in anoxic or oxygen-deficient bottom waters

ii deposition in mixing zones between shallow oxygenated and deeper anoxic or dysaerobic waters

iii deposition in 'anoxic' sediments

For point (iii), it is worth noting that black shales can form at any water depth, in oxygenated to anoxic conditions, and in fresh to estuarine to marine waters (Quinby-Hunt and Wilde, 1996). Black shale formation relates to the surface productivity of organic material (e.g., plankton), with high settling rates favouring black shale formation, as oxygen is consumed by organic decay in the sediment pile (Calvert and Pedersen, 1996). Figure 1 illustrates some of the redox transitions associated with progressive oxygen consumption by decay of organic matter within a porous sediment (from Drever, 1982).

Quinby-Hunt and Wilde (1993) summarised redox zonation within black shales based on the Eh-pH conditions of sediment deposition (Fig. 2). Manganese and iron vary as follows:

I Mn, Fe insoluble (high concentrations of Fe and Mn as oxides in black shales)

IIa Mn soluble, Fe insoluble (high concentrations of Fe as oxides, low concentrations of Mn as carbonates in black shales)

IIb Mn and Fe soluble (low concentrations of Fe and Mn in black shales); sulfides absent due to relatively oxidised Eh conditions

III Mn soluble, Fe insoluble (high concentrations of Fe as sulfides, low concentrations of Mn as carbonates in black shales)

IV Mn and Fe soluble (low concentrations of Fe and Mn in black shales); sulfides present due to reduced Eh conditions

Based on these relationships, Quinby-Hunt and Wilde (1996) proposed that the Mn and Fe chemistry and mineralogy of black shales can be used as indicators of depositional environments.

Manganese in hydrothermal solutions

Mn occurs naturally in a variety of oxidation states (Mn^{II}, Mn^{III}, Mn^{IV}, Mn^{VI}, Mn^{VII}). High temperature

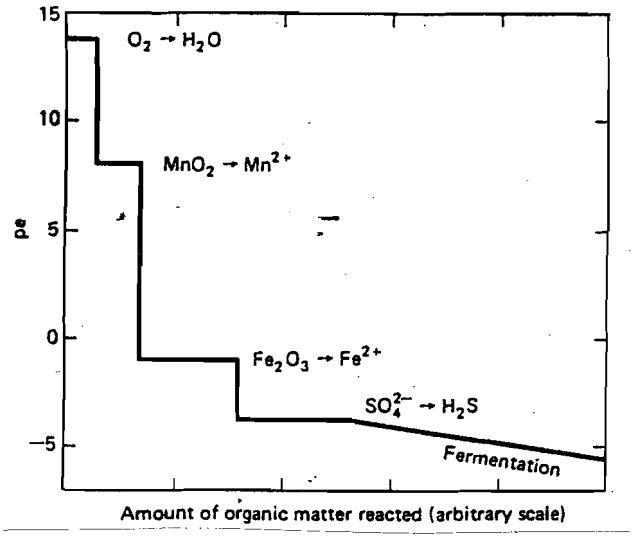

Figure 1. Change in pe of fresh water in contact with sediment as a function of the amount of organic matter decomposed. The lengths of the various horizontal segments are arbitrary, depending on the amounts of specific solid phases available for reaction. pH is assumed constant at 7.0. Reproduced from Drever (1982).

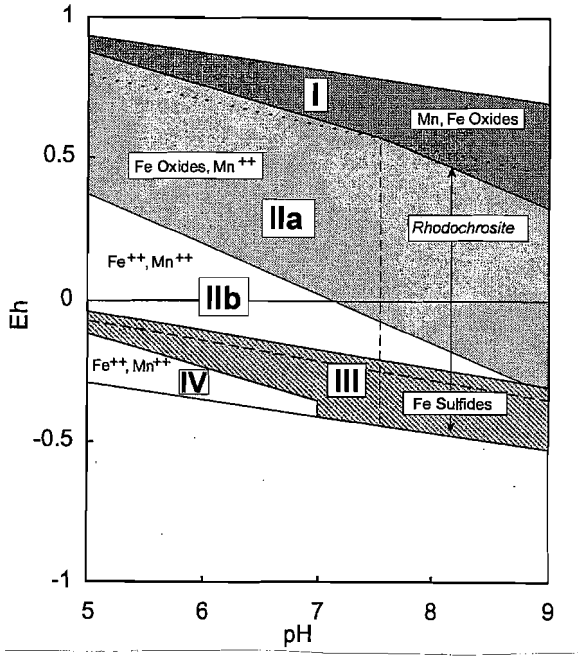

Figure 2. Combination pH-Eh diagram showing redox zonation of black shales based on mineral dissolution (from Quinby-Hunt and Wilde, 1993). Boundaries are based on dissolution of minerals from concentrations observed in oxygenated seawater. Reduction of NO_3^- to N_2 (indicated by the short dash line) is usually considered the boundary between oxic and anoxic conditions. Reduction of SO_4^{2-} to H_2S and HS- (long dashes) roughly corresponds to the boundary between oxic and sulfidic species. Note that the correspondence is not exact; pyrite can occur within the sulfate field.

thermodynamic data is available for the following Mn-bearing aqueous species:

Manganous Species (Mn^{II}: +2 valence state)
- Manganous ion: Mn^{+2}
- Chloride: $MnCl^{+}$, $MnCl_{2\ (aq)}$, $MnCl_3^-$
- Hydroxide: $MnOH^{+}$, $Mn(OH)_{2\ (aq)}$, $Mn(OH)_3^-$, $Mn(OH)_4^{-2}$
- Carbonate: $MnCO_{3\ (aq)}$, $MnHCO_3^-$
- Sulfate: $MnSO_{4\ (aq)}$

Manganate Species (Mn^{VI}: +6 valence state)
- Manganate ion: MnO_4^{-2}

Permanganate Species (Mn^{VII}: +7 valence state)
- Permanganate ion: MnO_4^-

For 10 eq. wt % NaCl brines that contain 1 wt % $CO_{2\ (aq)}$ and $\Sigma S = 0.001$ molal, distribution of species calculations have shown that $MnCl_3^-$ and $Mn(OH)_4^{-2}$ are the predominant aqueous manganese species at 150° and 250°C (Fig. 3). Furthermore, $Mn(OH)_4^{-2}$ is only predominant under extremely alkaline conditions (pH > 10), so $MnCl_3^-$ will be the dominant Mn species in saline brines at these temperatures and compositions. Increasing the salinity to 25 eq. wt. % NaCl at 150°C has no effect on the predicted predominant Mn-bearing species.

Manganese-bearing minerals

As for the aqueous Mn-bearing species, manganese can occur in a variety of oxidation states within common rock-forming minerals. Examples include:

Mn^{II} (+2 valence state)
- Rhodochrosite: $MnCO_3$
- Rhodonite: $MnSiO_3$
- Alabandite: MnS
- Manganosite: MnO

Mn^{III} (+3 valence state)
- Manganite: MnO(OH)

Mn^{VI} (+4 valence state)
- Pyrolusite: MnO_2

High temperature thermodynamic data is only available for the manganous (+2 valence state) minerals. Figure 2 shows that pyrolusite (the most common Mn-bearing mineral that contains Mn in the +4 valence state) only precipitates from highly oxygenated surface waters. Oxygen contents of sediments removed from contact with the atmosphere are too low for pyrolusite to be stable. Consequently, Mn is present as Mn^{II} in minerals formed within the hydrothermal environment.

Figure 4 illustrates how rhodochrosite ± rhodonite can be precipitated from alkaline to neutral pH brines at 150° and 250°C. Rhodochrosite is stable at lower pH values than rhodonite, resulting in it being more common in hydrothermal environments (eg. abundant rhodochrosite in some low sulfidation epithermal deposits, which form from near-neutral pH fluids). At low $a_{(CO2)}$, rhodonite is stabilised in preference to rhodochrosite. Alabandite (MnS) is unlikely to form in hydrothermal environments, requiring high ΣS concentrations and/or extremely alkaline (pH > 12) reduced fluids.

At HYC, Mn occurs within dolomite, rather than as a discrete Mn-mineral. Mn substitution into other carbonates can occur at lower pH values than illustrated on Figure 4. For $a(MnCO_3) = 0.1$, the $MnCO_3$-$MnCl_3^-$ solubility contours shift by 0.5 pH units to the left on Figures 4a and b. The low Mn contents of hydrothermal carbonates at HYC are consistent with deposition from near-neutral, rather than alkaline fluids.

Based on the relationships illustrated in Figure 4, temperature, pH and salinity control rhodochrosite and rhodonite solubilities in hydrothermal solutions, and redox is unimportant:

$$MnCl_3^- + H_2CO_{3\ (aq)} <=> MnCO_{3\ (s)} + 2\ H^+ + 3\ Cl^-$$

$$MnCl_3^- + H_2O + SiO_{2\ (s,\ aq)} <=> MnSiO_{3\ (s)} + 2\ H^+ + 3\ Cl^-$$

Rhodochrosite and rhodonite will precipitate via pH increase and/or dilution. If alabandite ever saturated in sedimentary brines (only possible at high ΣS concentrations), precipitation would occur via pH increase, sulfur loss and/or dilution from highly reduced and alkaline fluids:

$$MnCl_3^- + HS^- <=> MnS_{(s)} + H^+ + 3\ Cl^-$$

Implications for sediment-hosted Pb-Zn mineralisation

Figure 5 illustrates rhodochrosite, rhodonite, galena and sphalerite solubility contours, together with the

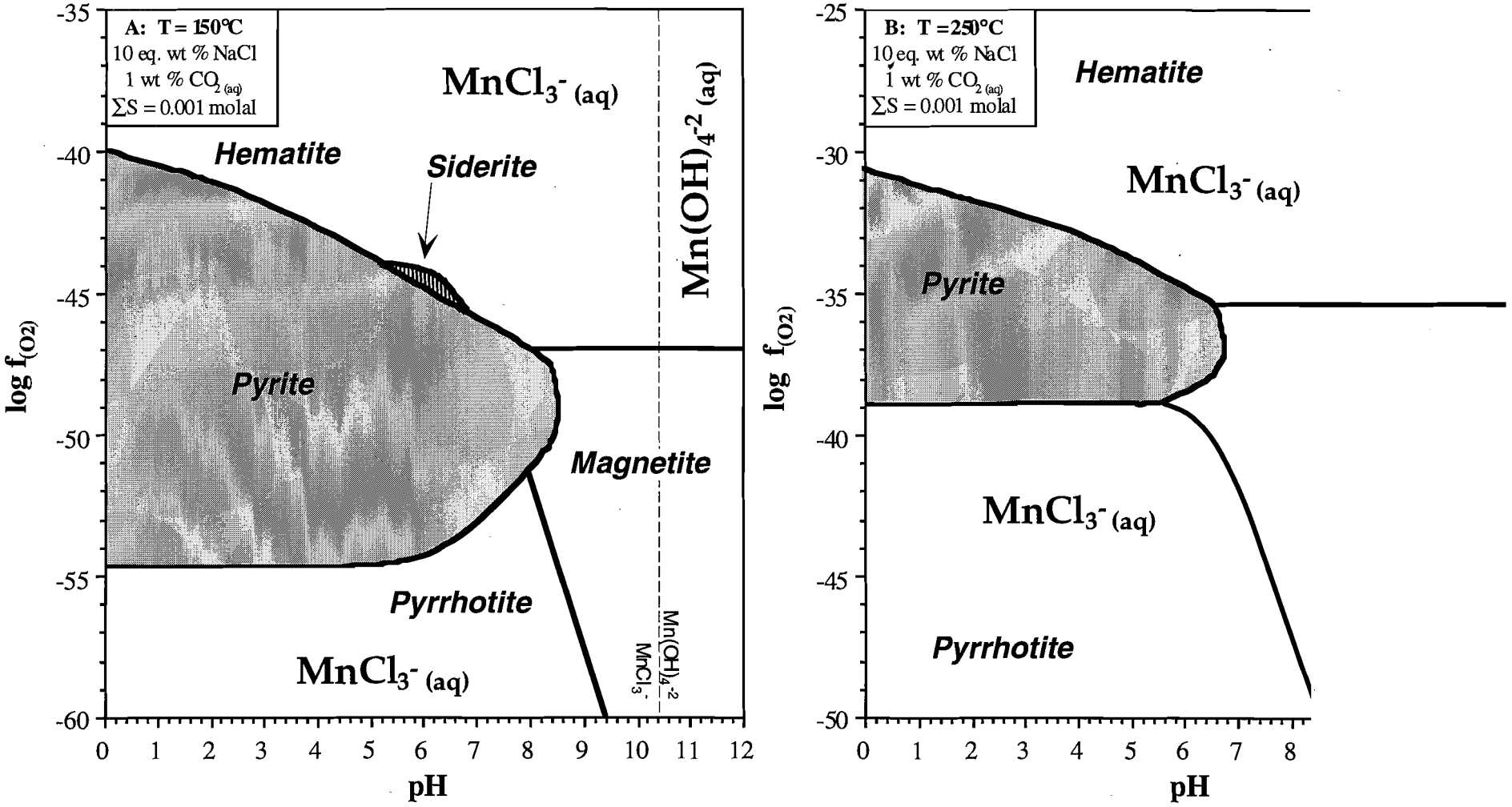

Figure 3: Log f_{O2}-pH diagrams showing the stability fields of the common Fe-O-S minerals (hematite, magnetite, pyrite, pyrrhotite) and siderite, and the predominance field boundaries for aqueous manganese species. (a) 150C. (b) 250°C. These diagrams have been constructed for 10 eq. wt. % NaCl brines that contain 0.001 molal ?S and 0.256 molal ?C (i.e. ~ 1 wt. % $CO_{2\,(aq)}$).

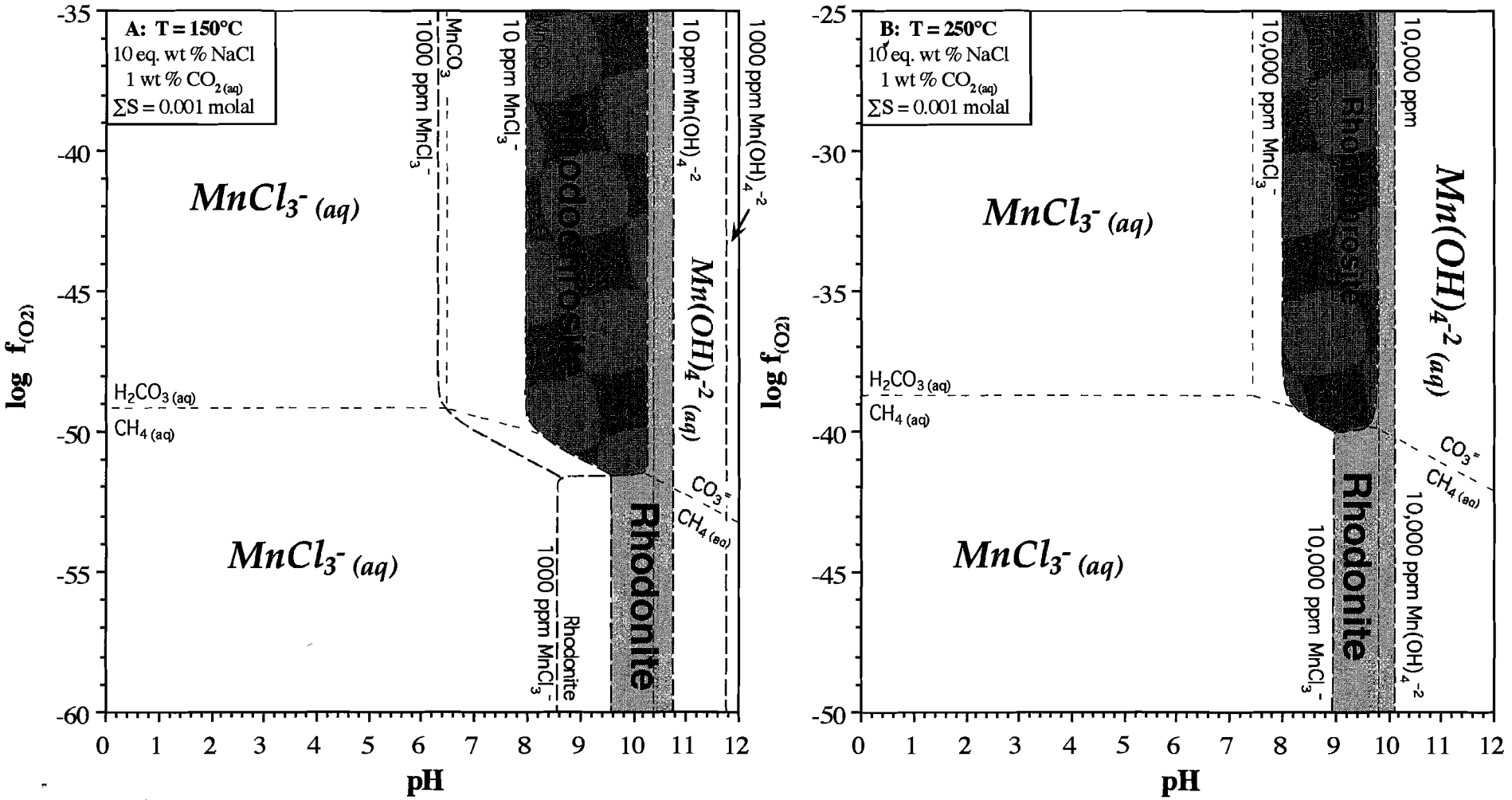

Figure 4: Log f_{O2}-pH diagrams showing the predominance field boundaries for aqueous carbon and manganese species, and the stability fields and solubility contours for manganese minerals. (a) 150C. (b) 250°C. These diagrams have been constructed for 10 eq. wt. % NaCl brines that contain 0.001 molal ΣS and 0.256 molal ΣC (i.e. ~ 1 wt. % $CO_{2\,(aq)}$).

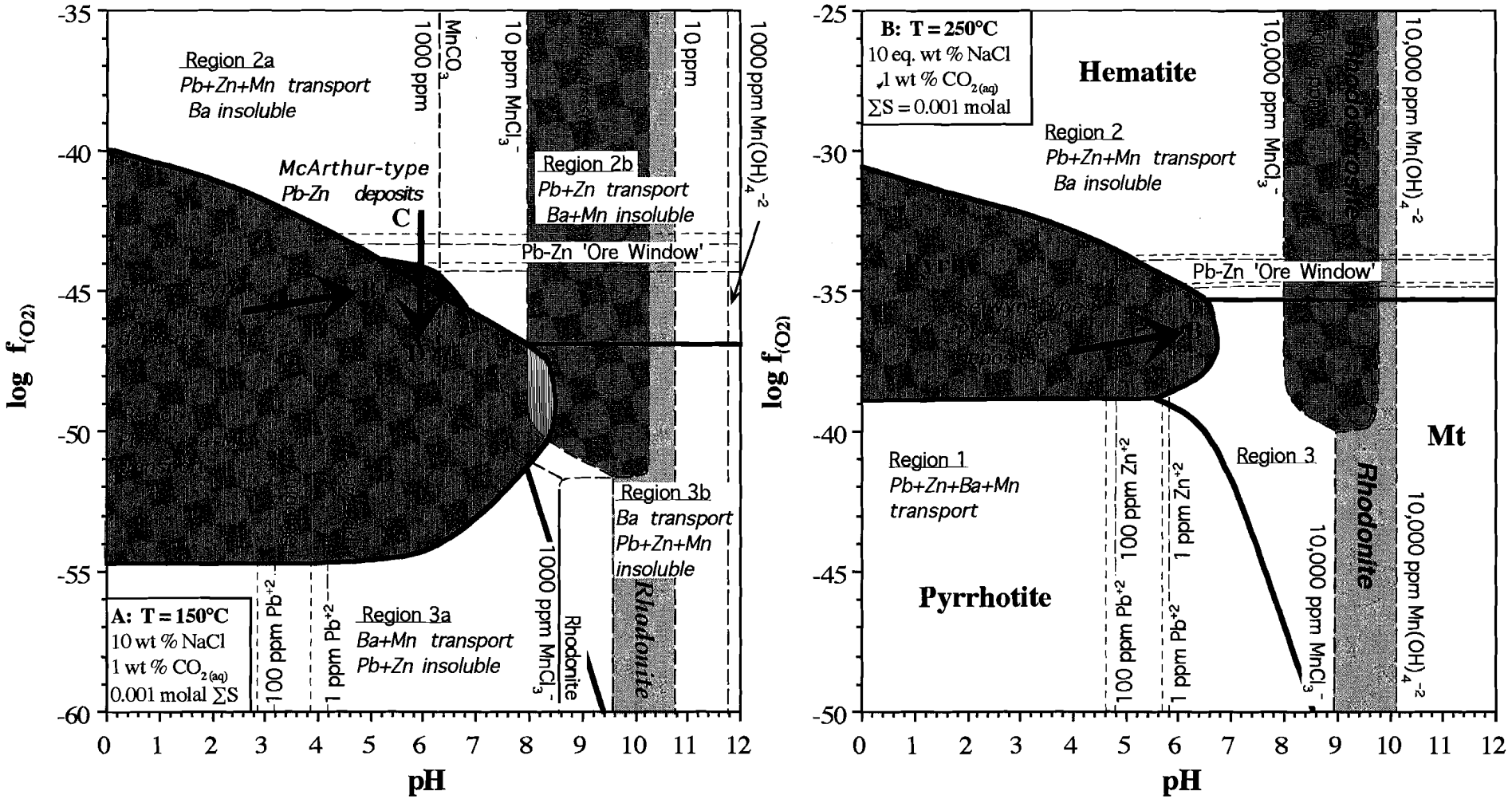

Figure 5: Log f_{O2}-pH diagrams showing the stability fields of the common Fe-O-S minerals, manganese minerals and solubility contours for Pb and Zn. (a) 150C. (b) 250°C. Both McArthur-type and Selwyn-type brines can carry Mn in solution, provided that pH remains in the acid to neutral range. These diagrams have been constructed for 10 eq. wt. % NaCl brines that contain 0.001 molal ΣS and 0.256 molal ΣC (i.e. ~ 1 wt. % $CO_{2\,(aq)}$).

stability fields for the common iron oxides and sulfides at 150° and 250°C. Figure 5b illustrates how at 250°C, Mn can be transported in large quantities (> 1000 ppm) by reduced and oxidised brines over a pH range of 0 to 8. Consequently, Mn is highly soluble in acid fluids, and is difficult to precipitate at 250°C

At 150°C, Mn can be transported together with Pb and Zn by reduced, acid brines (Region 1; Figure 5a), or oxidised, acid to neutral brines (Region 2a). Although Pb and Zn are soluble in region 2b, Mn solubilities are low (oxidised, neutral to alkaline brines), with the exact amount of Mn able to be transported in solution depending on the amount of dissolved CO_2 in solution, and on the amount of Mn substitution into carbonate minerals.

Despite its theoretically high solubility, manganese may precipitate from acidic hydrothermal solutions via coprecipitation reactions. This variety of sorption reaction can occur when a dissolved species is incorporated as a trace element into a mineral structure during precipitation. The solubility of any element is greatly decreased when it becomes a minor constituent of a solid solution phase (Stumm and Morgan, 1996). Coprecipitation reactions are therefore crucial for the deposition of elements that are otherwise strongly undersaturated in hydrothermal fluids (e.g. - silver in galena, manganese in carbonate, etc.):

$$CaCO_3 + x\ Mn^{2+} \leftrightarrow Ca_{(1-x)}Mn_xCO_3 + x\ Ca^{2+}$$

Region 1 corresponds to Selwyn-type brines, and region 2a to McArthur-type brines. Based on the calculations presented here, Mn could be enriched in the ore position sediments of both types of SEDEX deposit, if the mineralising solutions are acidic, and pH increase occurs during ore deposition. For example, exhalation of Mn-rich mineralising brines into seawater (pH = 8.0) will cause enrichment of Mn in seawater, and will possibly result in Mn deposition in the sediments (this also depends on the Eh of the marine waters; with high Eh (oxygenated) near-surface waters likely to precipitate manganese oxides).

Depositional processes

Given the complexities associated with its precipitation, manganese is not a diagnostic element in terms of fingerprinting the composition of mineralising brines. If Mn is enriched in the ore environment, it *may* indicate that the brines were acidic, and that pH and/or Eh increase were occurring in the trap environment. However, the possibility remains that Mn enrichment occurred in the host sediments as a consequence of normal marine processes. The added complication of coprecipitation reactions affecting Mn solubilities in the mineralising solutions makes it difficult to be predictive about Mn behaviour in SEDEX systems.

Assuming equilibrium conditions and a hydrothermal source of Mn, based on the change in rhodochrosite stability from 250° to 150°C (compare Figures 5b and 5a), rhodochrosite is predicted to be less soluble in lower temperature hydrothermal fluids (at constant $a_{(CO2)}$). Mn is insoluble in oxygenated surface waters, where it occurs in the +4 valence state. Pyrolusite (rather than rhodochrosite) will be stable at these conditions. Consequently, Mn can be precipitated from hydrothermal solutions as rhodochrosite or manganiferous carbonates at 150°C by pH increase and/or mixing with cold, oxygenated groundwaters, and also possibly by dilution or cooling.

Mixing of hydrothermal fluids with seawater can cause pH increase, dilution, cooling, and oxygenation, all of which would favour Mn deposition from a sedimentary brine, and may have been important for Mn enrichment around Selwyn and McArthur-type deposits. Sub-surface carbonate replacement should also cause pH increase and cooling, favouring Mn deposition (important for Mn halos around McArthur-type deposits?). The relative efficiency of these two processes for hydrothermal Mn precipitation needs to be assessed further, as do controls on Mn substitution in dolomite.

Iron

Although not mined for their Fe content, Paleoproterozoic and Paleozoic SEDEX-style Zn-Pb-Ag deposits are also major accumulations of iron, both as iron sulfides (many millions of tonnes) and Fe-bearing carbonates. At the HYC deposit, two generations of pyrite have been recognised. They have distinct sulfur isotope characteristics and

textural characteristic that have been interpreted to indicate that pyrite deposition pre-dated galena and sphalerite, a key observation that lead to the diagenetic replacement models for Pb-Zn deposition (e.g. Eldridge et al., 1993; Hinman et al, 1994). Large et al (1998) provided an alternative interpretation, whereby Pb and Zn were products of pulses of hot, dense, metalliferous brines into an euxinic basin, with Fe and Mn added by expulsion of low-temperature, reduced Fe- and Mn-bearing waters prior to mineralised brine expulsion. McGoldrick et al. (1995) proposed a similar model for Lady Loretta, although they proposed that the low temperature Fe-Mn-bearing fluid was relatively oxidised (pyrite-stable, but near the hematite-pyrite boundary)

Because Fe deposition appears to be de-coupled from Pb and Zn in Paleoproterozoic SEDEX deposits, the mobilisation and deposition of Fe warrants consideration, because it could provide important insights into the variations in fluid compositions and depositional processes that lead to metal deposition. It is well documented that redox processes are important for Fe transport and deposition in low temperature groundwaters and surface waters (e.g. Drever, 1982). The following sections discuss the geochemistry of iron in 150°C, 25 eq. wt. % NaCl hydrothermal brines, and comments on the implications for SEDEX genesis.

Iron transport in hydrothermal solutions

Fe commonly occurs in one of two oxidation states in hydrothermal environments (Fe^{II}, Fe^{III}). Iron is most soluble in the ferrous form (Fe^{+2}), and in saline brines, will typically be transported as chloride complexes ($FeCl^+$ and $FeCl_{2\,(aq)}$). Iron can be precipitated as ferrous iron (e.g., pyrite, pyrrhotite, siderite), ferric iron (Fe^{+3}; e.g., hematite), or as a combination of ferrous and ferric iron (magnetite). Iron solubilities are low in oxygenated surface waters, where iron occurs in the ferric state (Drever, 1982).

Figure 6 shows the stability fields for the Fe-O-S minerals and siderite, the predominance fields for the important aqueous sulfur species, and Fe solubility contours for 25 eq. wt % NaCl brines that contain 1 wt % $CO_{2\,(aq)}$ and a total sulfur concentration of 0.001 molal. From this diagram, it can be seen that large quantities of Fe can be transported in *acid fluids*, whereas Fe is insoluble in neutral to alkaline brines. Redox changes may only have a minimal effect on Fe solubilities in hydrothermal environments. For the common range of pH values in hydrothermal systems (≈ 3-7), the minimum solubility of Fe occurs in the pyrite field, at the SO_4^{-2} / H_2S predominance field boundary (Figure 6).

Pyrrhotite solubility

With regards to specific iron-bearing minerals, Fe has vertical solubility contours in the pyrrhotite field of Figure 6. This is because temperature, pH, ΣS concentrations and salinity control pyrrhotite solubility:

$$FeCl_{2\,(aq)} + H_2S_{\,(aq)} \Leftrightarrow FeS_{\,(s)} + 2\,H^+ + 2\,Cl^-$$

Iron deposition as pyrrhotite is therefore favoured by increasing pH and /or dissolved H_2S concentrations, and/or by decreasing salinity and/or temperature.

Pyrite solubility

For pyrite, Fe solubility contours have a negative slope in the H_2S predominance field (Fig. 6), because *increasing* pH and redox cause Fe deposition:

$$FeCl_{2\,(aq)} + 2\,H_2S_{\,(aq)} + 0.5\,O_{2\,(g)} \Leftrightarrow FeS_{2\,(s)} + 2\,H^+ + 2\,Cl^- + H_2O$$

Fe deposition also occurs via temperature decrease, dilution and/or increased H_2S concentrations for pyrite-stable H_2S-bearing fluids. A key point to note is that at constant pH for reduced, H_2S-rich fluids, decreasing redox can cause pyrite *dissolution* (Fig. 6), in contrast to the widespread dogma about the importance of reduction for pyrite deposition from reduced hydrothermal solutions.

When fluids are pyrite-stable and sulfates (SO_4^{-2} or HSO_4^-) are the predominant sulfur-bearing aqueous species, Fe solubility behaviour reverses with respect to redox and pH (Fig. 6). Consequently, *decreasing* pH and f_{O2} cause pyrite deposition from sulfate-stable brines via reactions such as:

$$FeCl_{2\,(aq)} + 2\,SO_4^{-2} + 2\,H^+ \Leftrightarrow FeS_{2\,(s)} + 2\,Cl^- + 3.5\,O_{2\,(g)} + H_2O$$

In other words, the Fe solubility minimum occurs

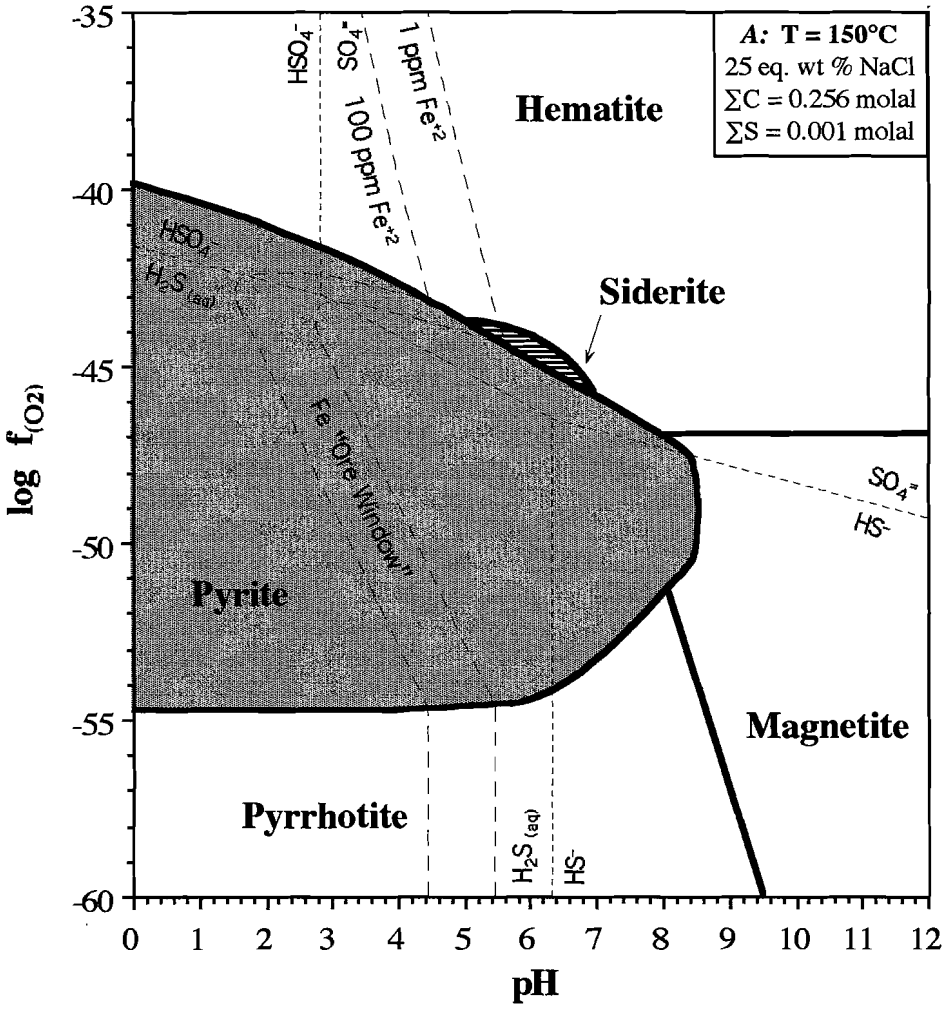

Figure 6: Log f_{O2}-pH diagram showing the stability fields of the common Fe-O-S minerals (hematite, magnetite, pyrite, pyrrhotite) and siderite, the predominance boundaries between oxidised and reduced sulfur species, and Fe solubility contours (as ΣFe = m(Fe^{2+}) + m($FeCl^{+}$) + m($FeCl_2$)) at (a) 150°C, 10 eq. wt% NaCl; and (b) 250°C, 25 eq. wt. % NaCl. If a hydrothermal fluid evolved along the trajectory indicated by the bold arrow (reduction without pH change) pyrite would dissolve, liberating Fe into the hydrothermal fluid. This diagram has been constructed for a 10 eq. wt. % NaCl solution that contains 0.001 molal ΣS and 0.256 molal ΣC (~ 1 wt. % $CO_{2\,(aq)}$).

in the pyrite field at the SO_4^{-2} / H_2S predominance field boundary, and Fe deposition as pyrite can occur via opposing processes above and below this boundary. However, pyrite deposition also occurs via temperature decrease, dilution and/or increased aqueous sulfate concentrations for pyrite-stable SO_4^{-2}-bearing fluids.

Siderite solubility

As for pyrrhotite, Fe has vertical solubility contours in the siderite field, although this is difficult to see from Figure 6. Decreasing temperature and salinity, or increasing pH and/or ΣC concentrations can cause siderite deposition:

$$FeCl_{2\,(aq)} + H_2CO_{3\,(aq)} \Leftrightarrow FeCO_{3\,(s)} + 2\,H^+ + 2\,Cl^-$$

Hematite solubility

For hematite, Fe solubility contours have a negative slope (Fig. 6). Increasing pH and f_{O2}, and decreasing salinity and/or temperature cause Fe deposition:

$$FeCl_{2\,(aq)} + H_2O + 0.25\,O_{2\,(g)} \Leftrightarrow 0.5\,Fe_2O_{3\,(s)} + 2\,H^+ + 2\,Cl^-$$

ΣC and ΣS concentrations are unimportant for Fe solubilities in the hematite field, unless they increase to the point where siderite or pyrite is stabilised respectively.

Implications for lead-zinc mineralisation

Iron can be transported with lead and zinc in McArthur and Selwyn-type brines, provided that they are acidic. Lead and zinc transport will be decoupled from iron in neutral to alkaline McArthur-type brines. In Selwyn-type brines, iron transport will be impeded if the brines are only weakly reduced (H_2S predominant, but close to the H_2S/SO_4^{2-} redox buffer; Fig. 6).

Copper

Copper sulfide minerals typically occur in subeconomic concentrations in SEDEX deposits. For example, most Selwyn-type deposits contain < 0.3% Cu based on the grade and tonnage data from Goodfellow et al., (1993).

This section examines the chemical relationships between Cu and Pb-Zn in sedimentary brines, and evaluates whether there is any potential for high grade copper mineralisation to be genetically associated with McArthur- or Selwyn-type SEDEX mineralisation.

Cu-sulfide stablities

Copper can have a complicated mineral paragenesis in hydrothermal ore deposits. It is possible to precipitate copper as Cu-Fe-sulfides ($CuFeS_2$ – chalcopyrite; Cu_5FeS_4 – bornite; $CuFe_2S_3$ – cubanite), Cu-sulfides (Cu_2S – chalcocite; CuS – covellite), Cu-bearing sulfosalts (Cu_3AsS_4 – enargite/luzonite; $Cu_{12}As_4S_{13}$ - tennantite), Cu-oxides (CuO – tenorite; Cu_2O – cuprite), Cu-carbonates ($Cu_2CO_3(OH)_2$ – malachite; $Cu_3(CO_3)_2(OH)_2$ – azurite), as the native metal (Cu), and as several other minerals. The Cu-oxides, carbonates and native copper will only form under extremely oxidised, near-surface weathering (supergene) conditions. Chalcopyrite, bornite and chalcocite can all form under hypogene conditions, and are the most common copper sulfides in sediment-hosted copper deposits. The following discussion is therefore restricted to these three copper sulfide minerals, for the sake of simplicity.

Compared to the Fe-O-S minerals (Fig. 3), the Cu-Fe-sulfides have a complicated distribution in log f_{O2}-pH space (Figs 7 and 8). Bornite and chalcocite can form under oxidised (hematite-stable) and extremely reduced (pyrrhotite-stable) conditions. Chalcopyrite is the stable Cu-bearing mineral over most of the pyrite field, although Figure 7 illustrates that chalcocite and bornite are stable in equilibrium with pyrite at low pH values and oxidised conditions. Although not illustrated on Figure 2, increasing the ΣS concentration would increase the size of the stability field for chalcopyrite-pyrite, with the bornite-pyrite and chalcocite-pyrite fields contracting to higher f_{O2} and (consequently) lower pH values:

$$5\ CuFeS_{2\ (s)} + 2\ H_2S_{(aq)} + O_{2\ (g)} <=> Cu_5FeS_{4\ (s)} + 4\ FeS_{2\ (s)} + 2\ H_2O$$

$$2\ Cu_5FeS_{4\ (s)} + H_2S_{(aq)} + 0.5\ O_{2\ (g)} <=> 5\ Cu_2S_{(s)} + 2\ FeS_{2\ (s)} + H_2O$$

To illustrate the complicated Cu-mineral paragenesis that could occur in a sedimentary basin, it is worth considering the sequence of mineral precipitation from a 150°C brine evolving along trajectory A-B (Fig. 9a). Such a fluid would potentially precipitate ore-grade galena and sphalerite, because it crosses the Pb-Zn 'ore-forming window'. In conjunction with this, the sequence of Fe-Cu sulfide deposition (from A to B) would be as follows:

- Hematite + chalcocite ***(A)***
- Hematite + bornite
- Siderite + bornite
- Siderite + chalcopyrite
- Pyrite + chalcopyrite
- Pyrite + bornite
- Pyrite + chalcopyrite ***(B)***

Even more complicated parageneses can be hypothesised for acidic fluids (eg. pH < 3), where chalcocite-pyrite becomes a stable mineral assemblage.

It is important to remember that the sequence of deposition for Cu-sulfides, and the relative positions of their stability fields on Figure 9a is strongly dependent on the assumed temperature, ΣS and (in the case of siderite) ΣC concentrations. To plot any natural system on such a diagram, it is important to try and constrain these variables as tightly as possible, to ensure that the Cu-sulfide stability fields are accurately plotted, and the diagram is relevant to that natural system.

Chalcopyrite, bornite and chalcocite have simpler

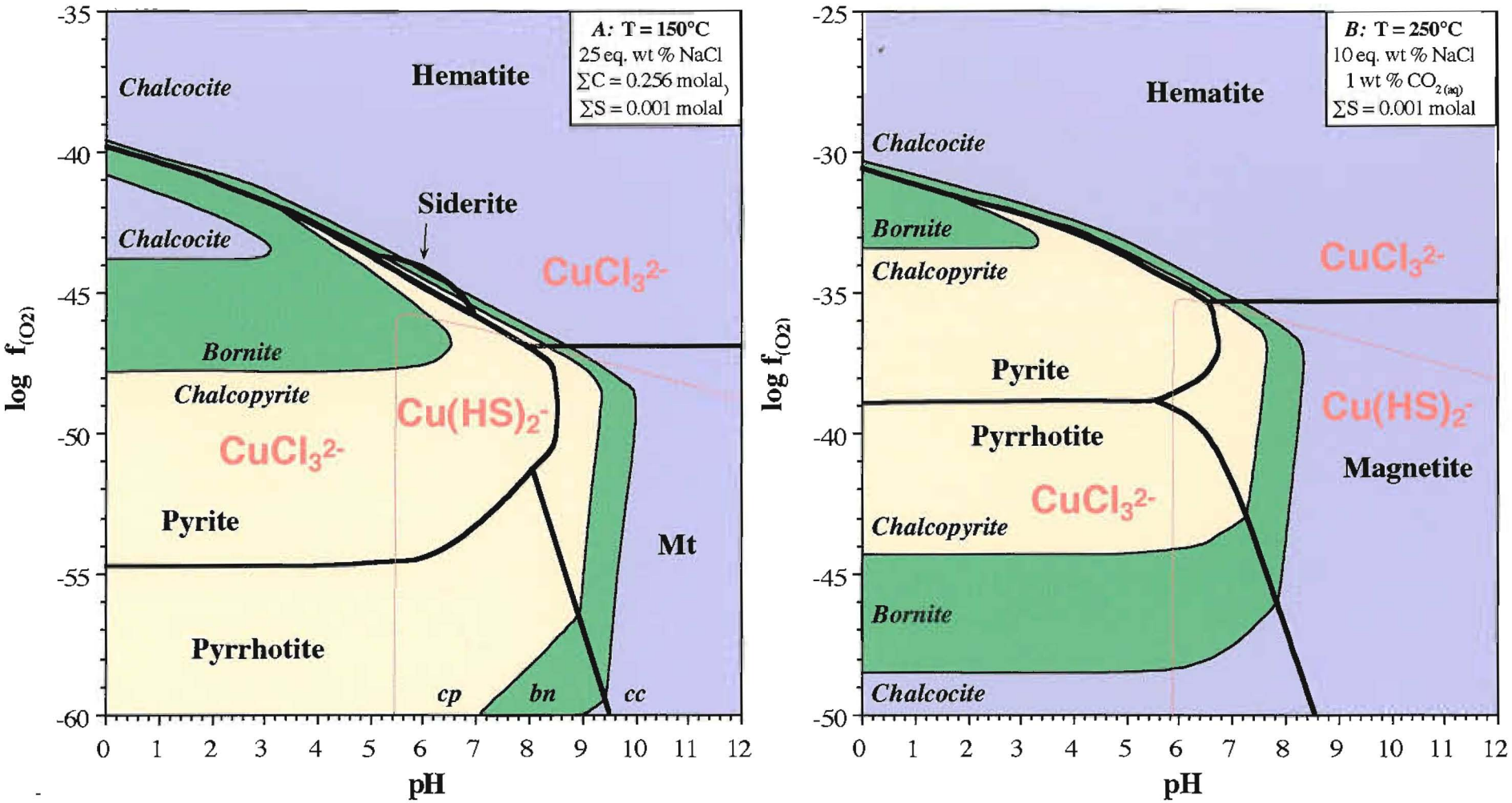

Figure 7: Log f_{O2}-pH diagrams showing the stability fields for the Fe-O-S-C minerals (pyrite, pyrhhotite, magnetite, hematite, siderite - bold lines), Cu-Fe-S minerals (chalcopyrite, bornite, chalcocite), and the predominance fields for $CuCl_3^{2-}$ and $Cu(HS)_2^-$. (a) 150C, 25 eq. wt. % NaCl. (b) 250°C, 10 eq. wt. % NaCl. These diagrams have been constructed for brines that contain 0.001 molal ΣS and 0.256 molal ΣC (i.e. ~ 1 wt. % $CO_{2\,(aq)}$).

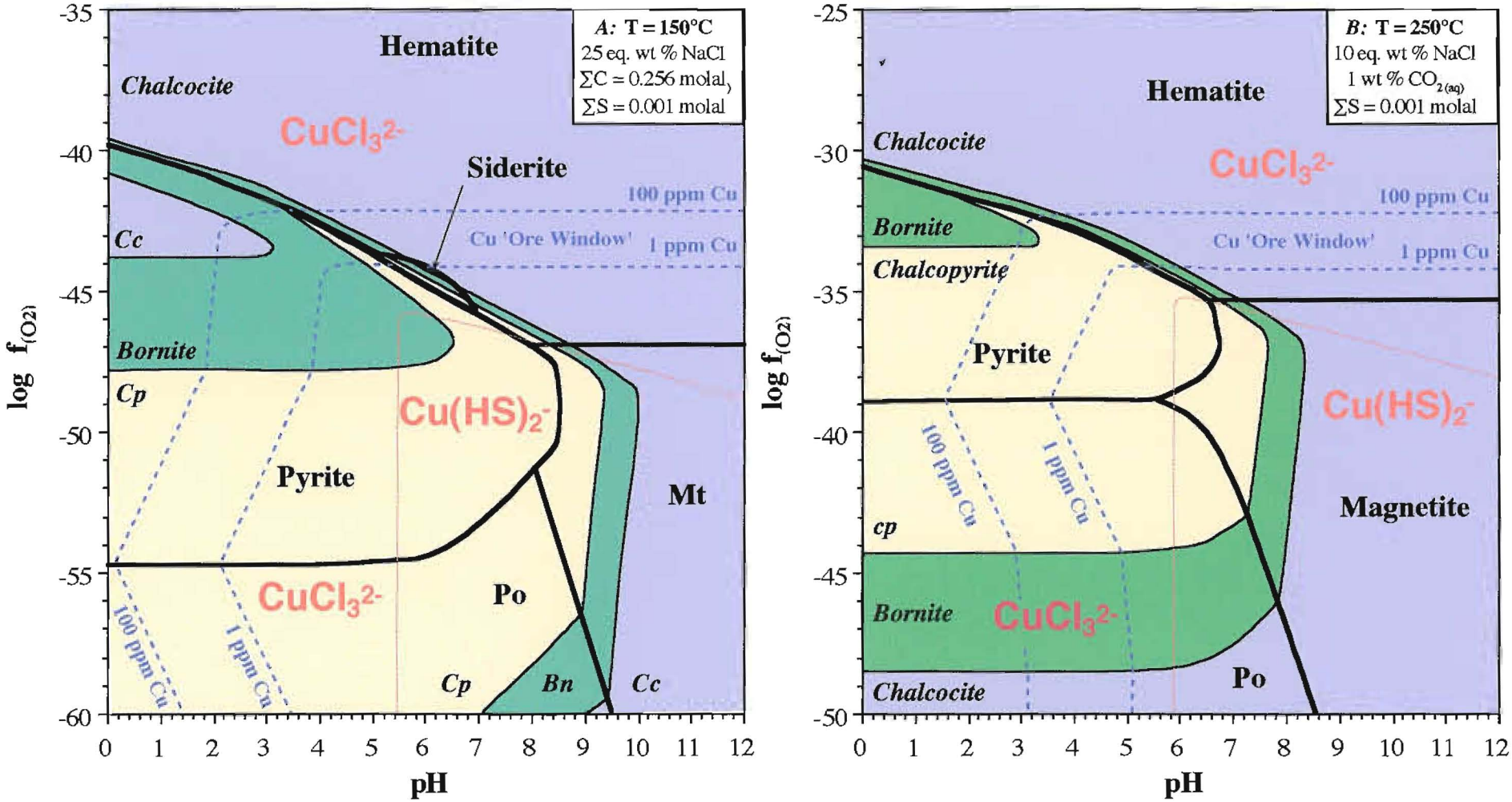

Figure 8: Log f_{O2}-pH diagrams showing the stability fields for the Fe-O-S-C minerals (pyrite, pyrhhotite, magnetite, hematite, siderite) and Cu-Fe-S minerals (chalcopyrite, bornite, chalcocite), and the solubility contours for Cu (1 and 100 ppm), and the predominance fields for $CuCl_3^{2-}$ and $Cu(HS)_2^-$. (a) 150C, 25 eq. wt. % NaCl. (b) 250°C, 10 eq. wt. % NaCl. These diagrams have been constructed for brines that contain 0.001 molal ΣS and 0.256 molal ΣC (i.e. ~ 1 wt. % $CO_{2(aq)}$).

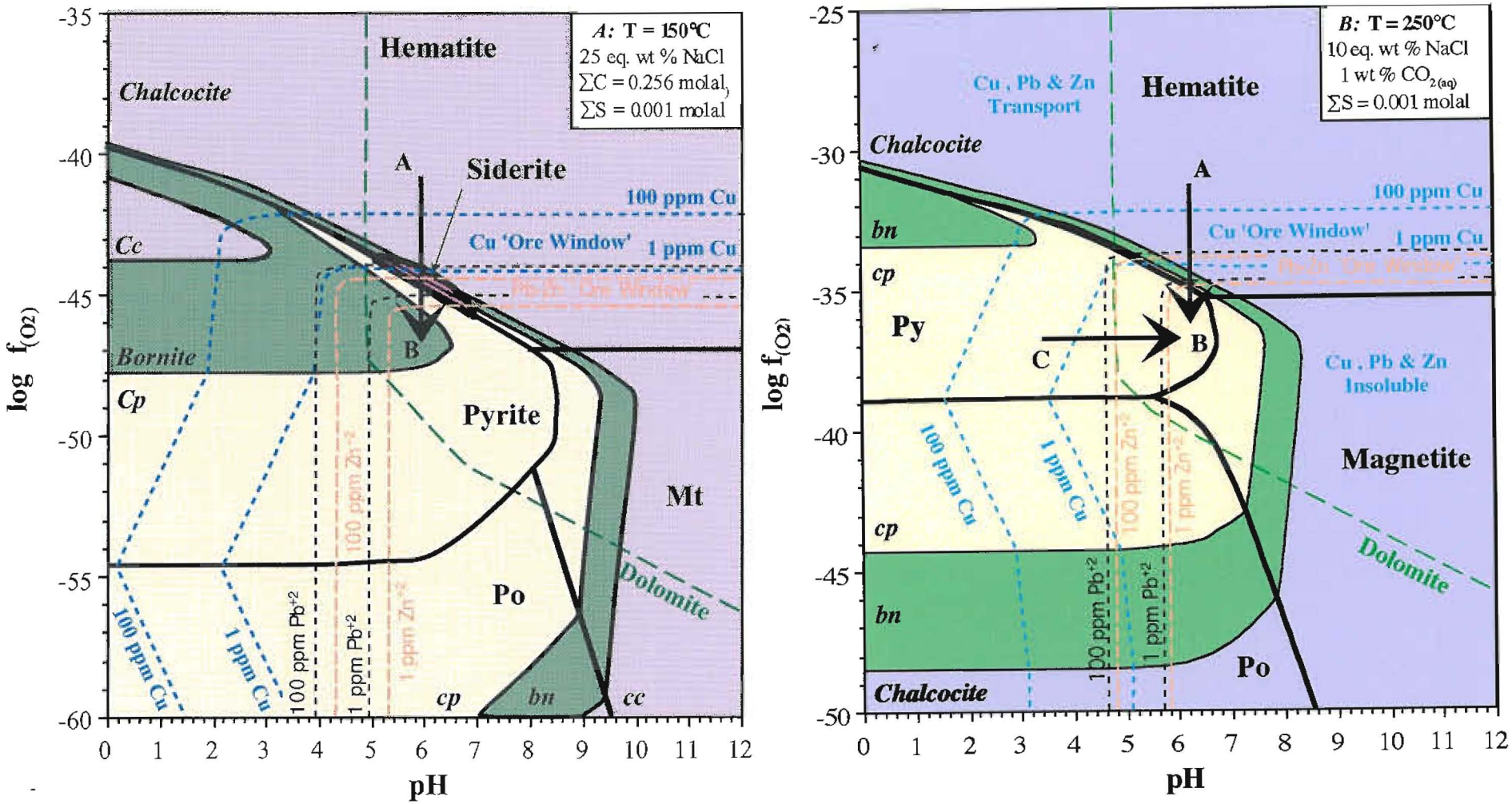

Figure 9: Log f_{O2}-pH diagrams showing the stability fields for dolomite, the Fe-O-S-C minerals (pyrite, pyrhhotite, magnetite, hematite, siderite), Cu-Fe-S minerals (chalcopyrite, bornite, chalcocite), and the solubility contours for Cu, Pb and Zn (1 and 100 ppm), and the predominance fields for $CuCl_3^{2-}$ and $Cu(HS)_2^-$. (a) 150C, 25 eq. wt. % NaCl. (b) 250°C, 10 eq. wt. % NaCl. These diagrams have been constructed for brines that contain 0.001 molal ΣS and 0.256 molal ΣC (i.e. ~ 1 wt. % $CO_{2(aq)}$).

paragenetic relationships at 250°C (Fig. 9b) compared to the 150°C case (Fig. 9a). The sequence of mineral precipitation from 250°C brine evolving along trajectory A-B (Fig. 9b) is as follows:

- Hematite + chalcocite *(A)*
- Hematite + bornite
- Hematite + chalcopyrite
- Pyrite + chalcopyrite *(B)*

This is a simpler paragenesis than for the equivalent reduction process at 150°C, because (1) siderite is not stable for the conditions portrayed at 250°C; and (2) chalcopyrite is stable over a larger proportion of the pyrite field than for the 150°C scenario.

Copper speciation

Distribution of species calculations have been completed for various aqueous Cu-bearing species over the pH and log f_{O2} ranges illustrated on Figures 7 and 8. A total of 11 species have been considered:

- Cu^{+}
- $CuCl_{(aq)}$
- $CuCl_2^-$
- $CuCl_3^{2-}$
- $Cu(HS)_2^-$
- $CuSO_{4\ (aq)}$
- $CuOH^+$
- Cu^{2+}
- $CuCl^+$
- $CuCl_{2\ (aq)}$
- $CuCl_3^-$

Copper commonly occurs in one of two oxidation states in aqueous solutions (Cu^I, Cu^{II}). Copper is most soluble in the cuprous form (Cu^+), and in saline brines, will typically be transported as cuprous chloride complexes ($CuCl_{(aq)}$, $CuCl_2^-$, and $CuCl_3^{2-}$). Bisulfide transport of Cu (eg. $Cu(HS)_2^-$) may be important in H_2S-rich fluids and/or high temperature magmatic volatiles, but is unlikely to be relevant for sedimentary brines.

Figure 7 illustrates the results of the distribution of species calculations for the 150°C and 250°C brines. Only two Cu-species are predicted to be predominant over the illustrated pH and log f_{O2} conditions. $CuCl_3^{2-}$ is predicted to be the predominant Cu-species over much of Figures 7a and b, although $CuCl_2^-$ and $CuCl_{(aq)}$ are also present in significant (but subordinate) quantities over the same range of conditions. In reduced, alkaline fluids, bisulfide transport becomes important, with $Cu(HS)_2^-$ predicted to be the predominant Cu-bearing species (Fig. 7).

Quality of thermodynamic data for copper species

The diagrams presented in this report have been constructed using thermodynamic data from the SUPCRT92 (Johnson et al., 1992) and SOLTHERM (Spycher and Reed, 1990) databases. The mineral data and some aqueous species data have been taken from SUPCRT92. Data for the aqueous metal-bearing species were generally taken from SOLTHERM. Note that thermodynamic data for the aqueous Cu-bearing species are more poorly constrained than for the equivalent Pb and Zn-bearing species. The exact position of the Cu-solubility contours in log f_{O2} space as discussed below and illustrated on Figures 8 and 9 are therefore likely to have larger error bars that the equivalent Pb and Zn solubility contours. The exact magnitude of the errors associated with these calculations is currently unquantifiable, but is probably less than one log unit.

Copper solubilities

Figures 8a and b illustrate the 100 ppm and 1 ppm copper solubility contours for 150°C, 25 eq. wt. % NaCl and 250°C, 10 eq. wt. % NaCl brines. In reduced (H_2S or HS- predominant) fluid, copper is only soluble when the pH is low. Copper cannot be transported in ore-forming (ppm) quantities by brines in equilibrium with magnetite at low temperatures, and only acidic (pH < 3) brines can transport large quantities of Cu when they are in equilibrium with pyrite or pyrrhotite. Given the high salinities of the brine modelled in this study, it is extremely unlikely that reduced (H_2S-bearing) brines can precipitate economic Cu mineralisation in association with Pb-Zn mineralisation at 150°C. Furthermore, only highly reduced (pyrrhotite-stable), moderately acidic H_2S-rich brines can transport Cu, Pb and Zn at 250°C (Fig. 8b).

Copper can be transported in ore-forming (1-100 ppm) quantities in oxidised (sulfate-dominated and hematite-stable) brines (Figure 8). Transport will be pH-independent, and can occur under neutral to alkaline (dolomite-stable) conditions (Figure 9). Reduction, mixing with H_2S-rich fluids and/or fluid-rock interaction with a large accumulation of pre-existing pyrite are the most likely Cu depositional mechanisms for oxidised 150°C or 250°C brines.

From Figure 9, it is apparent that ore-forming quantities of Cu, Pb and Zn can be transported together in oxidised brines, but that under equilibrium conditions, Cu deposition from oxidised brines should not occur in the same locality as Pb and Zn. Furthermore, Cu should be precipitated as chalcocite, with hematite the Fe-bearing gangue mineral. In summary, Cu, Pb and Zn may all be transported in the same brine, but Cu should be precipitated more proximal to source, whereas Pb and Zn will occupy a distal position.

At temperatures of 150°C and lower, there are problems with achieving sulfate-sulfide equilibrium due to chemical reaction rates. Direct deposition of Cu-sulfides from hematite-stable brines requires a sulfate reduction mechanism, because essentially the entire sulfur dissolved in solution is present as sulfate. Reaction rates for sulfate reduction are notoriously slow at low temperatures (around 10,000 years for a 150°C brine with ΣS = 0.001 molal; Ohmoto and Lasaga, 1982; Ohmoto et al., 1983). Bacterial sulfate reduction can speed up reaction rates, but temperatures above 80°C are unfavourable for the activity of sulfate-reducing bacteria. It is therefore possible that disequilibrium will play an important role in Cu deposition from oxidised sedimentary brines. Supersaturated Cu-bearing oxidised brines may not precipitate their metal load until a large sulfide-rich body (eg. pyrite or H_2S-bearing pore water) is encountered, resulting in copper deposition (as chalcopyrite?). If this occurs, then Cu may occur in close proximity to Pb and Zn.

The sequence of mineral precipitation from a 150°C brine evolving along trajectory A-B (Fig. 9) is as follows:

- Hematite + chalcocite ore *(A)*
- Siderite + minor chalcocite
- Siderite + galena + sphalerite ore + trace bornite/chalcopyrite
- Pyrite, galena and sphalerite with trace chalcopyrite/bornite *(B)*

Such a sequence of mineral precipitation seems unlikely, given the lack of documentation of Cu or Pb-Zn ore deposits with this mineral paragenesis.

A more likely scenario may be illustrated by trajectory D-E on Figure 10. In this scenario, the ore-forming brine would begin its life in an oxidised, clay-bearing aquifer (eg., the basal hematitic Westmoreland Conglomerate/Yiyintyi Sandstone package in the McArthur Basin). Leaching of metals from this aquifer and the underlying volcano-plutonic basement complex (eg., Murphy Inlier) could potentially produce an oxidised, acid brine that contained Cu, Pb, Zn, Ag, Au and U. By evolving this "super-brine" sub-parallel to the hematite-pyrite buffer (reduction + pH increase), the following sequence of precipitation could be produced:

- Hematite + minor chalcocite (+ U? + Au?) *(D)*
- Hematite + minor bornite
- Hematite + minor chalcopyrite
- Pyrite + chalcopyrite ore
- Pyrite, siderite & dolomite + sphalerite-galena ore + minor chalcopyrite
- Pyrite + dolomite + minor galena + sphalerite + trace chalcopyrite *(E)*

In such a scenario, Cu, Pb and Zn may all be initially transported in the same brine, but Cu will be precipitated proximal to source, and Pb and Zn will occupy a distal position. Note that 'proximal' and 'distal' potentially refer to the scale of the basin, not the deposit. The same evolving 'super-brine' may produce two or more distinct ore deposit types. These deposits may be separated vertically by kilometres (stratigraphically) and laterally by kilometres to tens of kilometres, or they may occur in close proximity, depending on the steepness of the chemical gradients the brine evolves through on its reaction path.. It seems likely that this is the most favourable reaction path for McArthur-type brines, as it allows elevated Fe concentrations together with Pb and Zn, and has the added bonus of the potential for elevated Cu. The redox state of the brine could therefore be buffered externally by pyrite-hematite-(siderite), or internally by sulfate-sulfide equilibria along its reaction path.

Europium

The application of rare earth-element systematics as geochemical indicators to solve petrogenetic problems in igneous petrology and sedimentology is well documented (e.g. Haskin, 1984; McKay, 1989; McDaniel et al., 1994). However, the application of rare earth elements to ore genesis studies is becoming increasingly popular as more is learnt about their

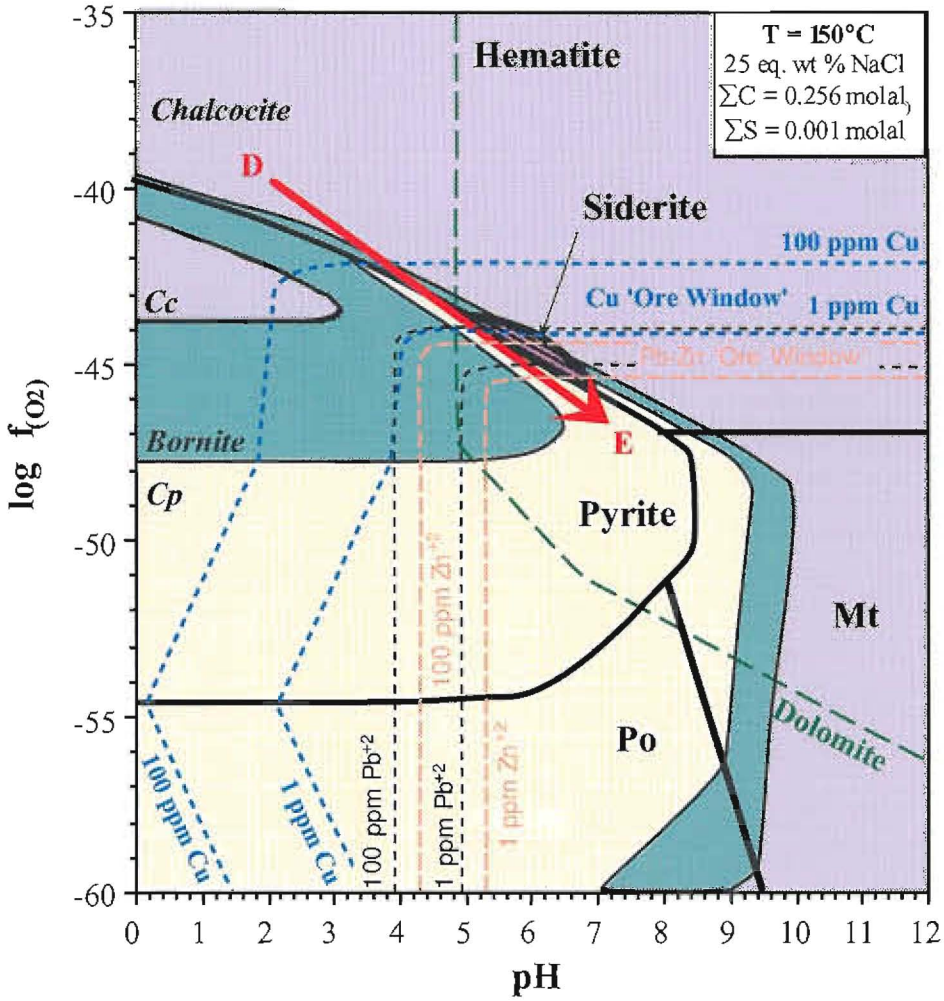

Figure 10: Log f_{O2}-pH diagram showing the stability fields for dolomite, the Fe-O-S-C minerals (pyrite, pyrhhotite, magnetite, hematite, siderite), Cu-Fe-S minerals (chalcopyrite, bornite, chalcocite), and the solubility contours for Cu, Pb and Zn (1 and 100 ppm), and the predominance fields for $CuCl_3^{2-}$ and $Cu(HS)_2^-$ at 150C. The red arrow (D-E) illustrates the predicted reaction path for acidic, oxidised McArthur-type brines derived from the Tawallah Group that migrates up into the McArthur Group. This diagram has been constructed for a 25 eq. wt. % NaCl brine that contain 0.001 molal ΣS and 0.256 molal ΣC (i.e. ~ 1 wt. % $CO_{2\,(aq)}$).

relative mobility in hydrothermal fluids. The results of such research have provided the foundation for constraining the sources and compositions of hydrothermal fluids, and some physicochemical conditions of ore formation when used in conjunction with isotopic data, fluid inclusions, mineral stabilities, etc. (e.g. Baker and Hellingwerf, 1988; Lottermoser, 1989 and 1992; Schandl and Gorton, 1991; Vander Auwera and André, 1991; Parr, 1992; Lapointe and Chown, 1993; McDaniel et al., 1994; Bierlein, 1995). However, interpretations are by no means simple, as the relative mobility of REE in a hydrothermal fluid is influenced by water/rock interaction, physicochemical properties of the fluid, temperature and pressure (Bau, 1991; Lottermoser, 1992). In addition, the influence of post-depositional processes such as diagenesis, metamorphism and hydrothermal alteration on REE mobility is debatable (MacLean, 1988; Whitford et al., 1988; Schandl and Gorton, 1991; McLennan and Taylor, 1991).

A feature of the mineralisation in Broken Hill-type and volcanic associated massive sulphide deposits is the existence of positive europium anomalies () on chondrite-normalised REE plots. These are produced by fractionation of Eu^{+2} over Eu^{+3} in the source reservoir of the hydrothermal fluid due to water/rock interaction, and are controlled by the fluid composition and physicochemical conditions. Sverjensky (1984) demonstrated that this fractionation is strongly temperature dependent and, to a lesser degree, fO_2 and pH dependent. Aqueous Eu^{+2} is claimed to be more stable in reduced hydrothermal fluids at temperatures >250°C, whereas Eu^{+3} requires more oxidised conditions and temperatures <250°C (Sverjensky, 1984). This behaviour enables prediction of temperature, fO_2 and pH conditions at the site of deposition and leads to the generalised interpretation that positive Eu anomalies (Eu^{+2}) may provide a "fingerprinting" tool for the characterisation of potential ore-bearing hydrothermal fluids. The aim of this report is to calculate the aqueous speciation of Eu for a generalised high salinity brine indicative of sediment hosted Pb-Zn deposits, and assess the plausibility that positive Eu anomalies at the sites of ore deposition reflect a "reduced" brine composition.

Previous work

Studies have shown that primary REE signatures of rocks remain unchanged during post-depositional metamorphism and hydrothermal alteration unless water/rock ratios are extremely high, e.g. $>10^6$ (Lesher et al., 1986; Michard and Albarède, 1986; Michard, 1989; Bau, 1991; Parr, 1992; Bierlein, 1995). Such a finding is particularly attractive when working in metamorphic terrains, as it leaves scope for the preservation of primary REE signatures in the rocks even if they have been metasomatised. Other studies, however, indicate compositional evidence for REE mobility during metamorphism and hydrothermal alteration from a variety of geological settings and rock types (Campbell et al., 1984; Lottermoser, 1990; McLennan and Taylor, 1991; Wood and Williams-Jones, 1994; Banks et al., 1994; Klinkhammer et al., 1994; Bingen et al., 1996; Lewis et al., 1997). From experimental measurements of the complexation constants of REE with inorganic ligands at 25°C and 1 bar, there is a strong tendency for the REE to form aqueous complexes at room temperature (Cantrell and Byrne, 1987; Lee and Byrne, 1992, 1993). Lottermoser (1992) suggests that REE mobility is favoured by large fluid residence times during fluid/rock interaction and abundance of REE complexing ligands in the hydrothermal solutions.

Given the potential for REE mobility during hydrothermal alteration, a distinction must be drawn between the source site of the REE and the depositional site. Firstly, the hydrothermal fluid must liberate the REE from a source reservoir, and secondly the REE complexes must be destabilised in the depositional site by a sharp change in pH, temperature, or fO_2 (more likely combinations of these). Eu^{+2} is preferentially partitioned into plagioclase (especially albite). Breakdown of plagioclase by the hydrothermal fluid (e.g. leaching of feldspathic volcaniclastic rocks) liberates Eu^{+2} which is incorporated into the hydrothermal fluid and transported to the ore-forming environment (Michard and Albarède, 1986; Klinkhammer et al., 1994; Blundy and Wood, 1991). The REE signature of the fluid would therefore be proportional to the amount of Eu^{+2} (i.e. plagioclase) in the source rock, as well as being a function of the degree of alteration. The physicochemical characteristics of the scavenging

fluid, abundance of plagioclase and degree of hydrothermal alteration (i.e. degree of plagioclase breakdown) are therefore, major controls on REE systematics in the hydrothermal fluid at the source region. In addition, variations in Eu signatures between different fluids may result from compositional differences in the plagioclase undergoing alteration (Klinkhammer et al., 1994).

The ability for the hydrothermal precipitates to reflect the REE composition of the fluid is questionable. Research suggests that the REE pattern of a precipitated mineral will be a function of the crystallographic ability of the particular mineral to accommodate the REE (Morgan and Wandless, 1980; Alderton et al., 1980). Nonetheless, while this is true for igneous processes and some simple hydrothermal phases regardless of fluid composition, other studies indicate a clear independence of mineralogy (Baker and Hellingwerf, 1988; Lottermoser, 1989; Parr, 1992; Bierlein, 1995). Adsorption of REE onto the surfaces of clays and/or Fe-hydroxides is another mechanism in which REE maybe deposited (c.f. Klinkhammer et al., 1994).

Europium in hydrothermal solutions

Eu occurs naturally in two oxidation states (divalent - Eu^{+2} and trivalent - Eu^{+3}). Thermodynamic data at elevated pressures and temperatures is available for the following Eu^{+2}- and Eu^{+3}-bearing aqueous species (Haas et al., 1995):

Eu^{+3}

- Europium ion: Eu^{+3}
- Chloride: $EuCl^{+2}$, $EuCl_2^{+}$, $EuCl_{3(aq)}$, $EuCl_4^{-}$
- Fluoride: EuF^{+2}, EuF_2^{+}, $EuF_{3(aq)}$, EuF_4^{-}
- Hydroxide: $EuOH^{+2}$, $EuO_2H_{(aq)}$
- Oxalate: EuO^{+}, EuO_2^{-}
- Nitrate: $EuNO_3^{+2}$
- Carbonate: $EuHCO_3^{+2}$, $EuCO_3^{+}$
- Phosphate: $EuH_2PO_4^{+2}$
- Sulphate: $EuSO_4^{+}$

Eu^{+2}

- Europium ion: Eu^{+2}
- Chloride: $EuCl^{+}$, $EuCl_{2(aq)}$, $EuCl_3^{-}$, $EuCl_4^{-2}$
- Fluoride: EuF^{+}, $EuF_{2(aq)}$, EuF_3^{-}, EuF_4^{-2}

In this study, Eu speciation calculations have excluded the fluoride, nitrate and phosphate complexes to simplify the system. These complexes (especially fluoride and phosphate) probably play a significant role in Eu speciation in BHT systems due to the relative abundance of fluorite and fluor-apatite associated with sulphides (e.g. Cannington). The importance of lanthanum and lutetium fluoride complexes in simplified geothermal fluids at various pressures and temperatures is well illustrated in the speciation calculations of Haas et al. (1995).

For 25 eq. wt% NaCl brines that contain ΣC=0.256 molal and ΣS=0.001 molal, distribution of Eu species calculations have shown that $EuCl^{2+}$, $EuCl_4^{2-}$ and EuO_2^{-} predominate at 150°C (Fig. 10a). $EuCl^{+2}$ predominates under extremely acidic conditions (pH<2), whereas EuO_2^{-} predominates under more alkaline conditions (pH>8). Therefore, trivalent Eu complexes only predominate at either extremely acidic conditions ($EuCl^{+2}$), or alkaline conditions (EuO_2^{-}). By far the most important complex for Eu transport at the calculated conditions is $EuCl_4^{-2}$ (Eu^{+2} species) which spans the majority of the Pb-Zn "ore window" (both the reduced acid Selwyn-type and the oxidised McArthur-type fields), as well as the siderite, kaolinite, muscovite, K-feldspar stability fields in Figure 10. A similar scenario is predicted for 250°C, 10 eq. wt. % NaCl brines, with the exception that $EuCl^{2+}$ is not predicted to be predominant over the portrayed conditions.

Implications for sediment-hosted Pb-Zn mineralisation

Based on our calculations, the predominant Eu aqueous species in SEDEX and Broken Hill-type fluids (given the conditions in Fig. 10) should be divalent Eu. Precipitates from this fluid should yield positive Eu anomalies assuming that they preserve the REE signature of the hydrothermal fluid. While we are unaware of the REE signatures of SEDEX deposits, positive Eu anomalies characterise mineralisation at Broken Hill and the Pinnacles (Lottermoser, 1989; Parr, 1992). From Figure 10, in hydrothermal environments, pH clearly controls the predominance of Eu^{+2} and Eu^{+3} rather than oxygen fugacity (fO_2).

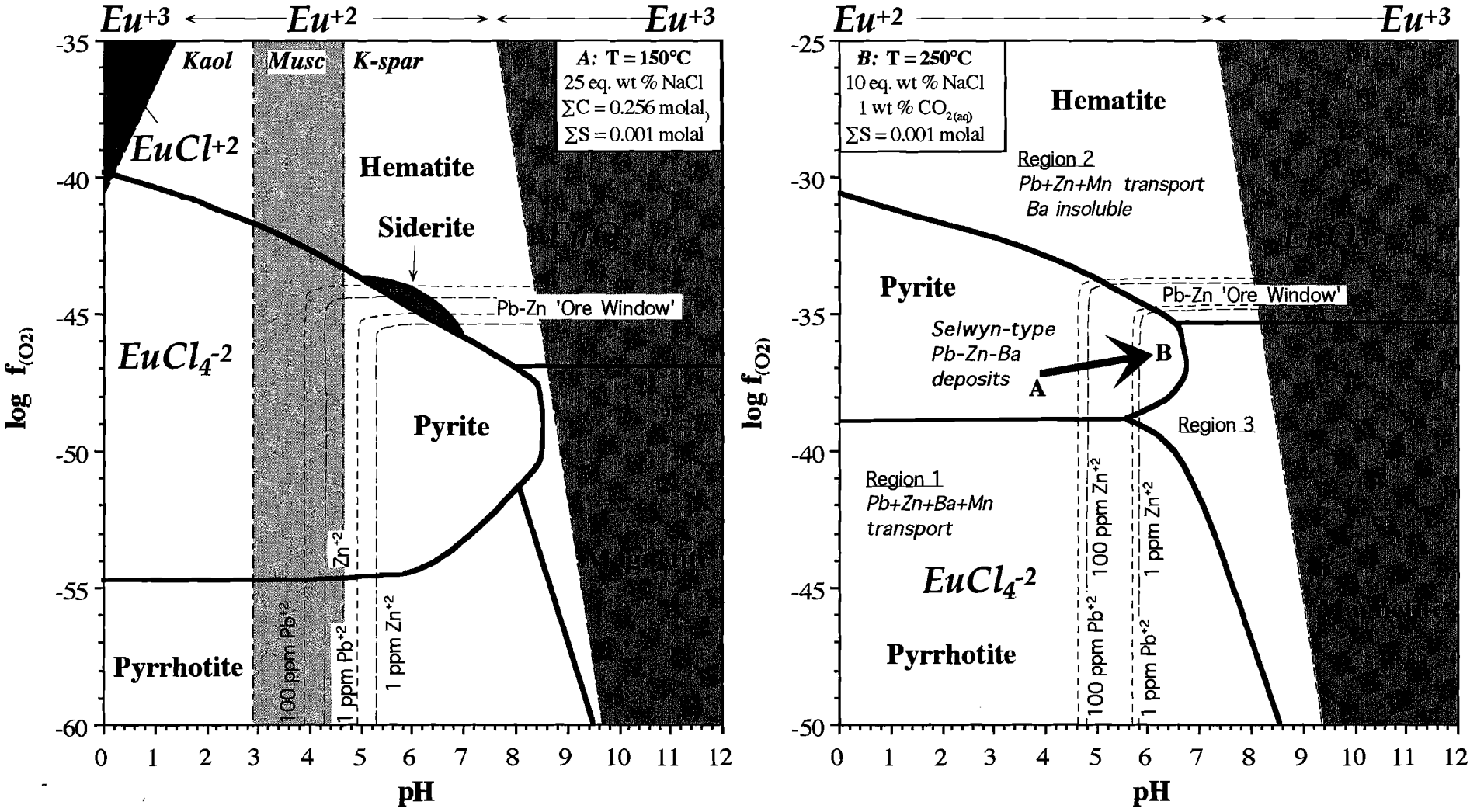

Figure 11: Log f_{O2}-pH diagrams showing the predominance fields for aqueous Eu species, together with the stability fields for pyrite, pyrhhotite, magnetite, hematite, siderite, kaolinite, muscovite and K-feldspar, and solubility contours for Pb and Zn. (a) 150°C, 25 eq. wt. % NaCl. (b) 250°C, 10 eq. wt. % NaCl. These diagrams have been constructed for brines that contain 0.001 molal ΣS and 0.256 molal ΣC (i.e. ~ 1 wt. % $CO_{2(aq)}$).

$EuCl^{+2} + 3Cl^- + {}^1/_2H_2O <=> EuCl_4^{-2} + H^+ + {}^1/_4O_{2(g)}$

$EuCl_4^{-2} + {}^3/_2H_2O + {}^1/_4O_{2(g)} <=> EuO_2^- + 4Cl^- + 3H^+$

These relationships suggest that a positive Eu anomaly relates to the pH of the hydrothermal fluid and not the oxidation state. Hence, the assumption that a positive Eu anomaly reflects reducing conditions in the ore-forming environment is incorrect. At 150°C and 25 eq. wt% NaCl, if the pH of the hydrothermal fluid is somewhere between 0 and 8 in the source reservoir and the transporting fluid, then a positive Eu anomaly is predicted in the hydrothermal precipitates in the ore-forming environment (based on the pretext that the precipitates reflect the REE signature of the hydrothermal fluid). Therefore, a whole-rock REE analysis of a single mineralised sample will yield more information about the processes involved in the source region of the hydrothermal fluid rather than the actual ore-forming environment. Measurement of physicochemical changes in the ore-forming environment using whole-rock REE systematics, requires recognition of paragenetically controlled REE zonation patterns. Further work is required to understand how changes in ΣS, ΣC, salinity and temperature influences Eu speciation in hydrothermal fluids in the ore environment.

Numerical simulations of ore deposition from McArthur-Type brines

Introduction

We have undertaken a series of numerical simulations using reaction path modelling software (CHILLER) to test our hypotheses about likely chemical traps for McArthur-type brines. The brine composition used in these simulations has been calculated by making initial assumptions about the fundamental intrinsic parameters of the fluid (T = 150°C; salinity = 25 eq. wt. % NaCl; ΣS = 0.001 molal; pH = 4.5; $\log f_{O2}$ = -43 = sulfate-predominant = oxidised; and ΣC = 0.256 molal). Forced mineral equilibration calculations were undertaken using CHILLPLUS (Turner and Cooke, 1998) and SOLVEQ (Reed, 1982; Spycher and Reed, 1990) to add additional chemical components to the brine. The components included in all calculations are:

- H^{2+} H_2O Cl^-
- HCO_3^- SO_4^{2-} $SiO_{2\,(aq)}$
- Al^{2+} Ca^{2+} Mg^{2+}
- Fe^{2+} Na^+ K^+
- Zn^{2+} Cu^+ Pb^{2+}
- Ag^+ $AuCl_2^-$ Ba^{2+}
- HS^- Sr^{2+} F^-
- $Sb(OH)_3$

The McArthur-type brine used in these calculations contains high concentrations of Zn (212 ppm), Pb (199 ppm) and Ag (72 ppb), even though it is undersaturated by up to two orders of magnitude with respect to these components (Table 1). The brine also contains elevated copper (1.5 ppm), antimony (0.4 ppm) and barium (9.7 ppm), and low gold (0.0008 ppb). Numerical simulations of depositional processes (cooling, water-rock interaction, mixing with seawater and interaction with a gas reservoir) were undertaken using the CHILLER software package (Spycher and Reed, 1990).

Results

Conductive cooling

The results of this simulation are illustrated in Figure 12a, in terms of the predicted mineral paragenesis. Conductive cooling of a highly mineralised McArthur-type brine from 150°C to 50°C in 5°C increments is predicted to result in the deposition of a quartz vein, with traces of copper mineralisation (as chalcocite and bornite) and very minor gold. Minor siderite and dolomite precipitate during the first increments of cooling. Note that the brine is predicted to still carry 200 ppm Pb and Zn at 50°C, demonstrating that conductive cooling in a fluid-buffered environment is ineffective at forcing base metal deposition from McArthur-type brines. Conductive cooling may have occurred in the quartz-armoured fracture arrays in the hematitic quartz sandstones of the Tawallah Group.

Mixing with reduced seawater

The anoxic seawater composition used in this simulation is the same as that used by Cooke (1993). The predicted mineral paragenesis is illustrated in Figure 12b. Mixing of the McArthur-type brine with H_2S-bearing 5°C seawater is predicted to result in the deposition of a zoned massive sulfide body, of which more than 75% of the total precipitate is sphalerite + galena. The predicted zonation is a core of siderite, quartz, pyrite and chalcopyrite; an intermediate zone of galena, quartz, bornite and native silver, and a distal zone of sphalerite and galena. Galena is predicted to precipitate earlier than sphalerite because the chosen undersaturation value for galena in the starting fluid (0.05) is less than that chosen for sphalerite (0.01; Table 1). The sequence of precipitation and the relative proportions of each sulfide can be changed by modifying the degree of undersaturation in the starting brine. Overall, this is an excellent depositional mechanism for Pb, Zn and Ag. It is also good for Cu, but is not particularly effective for Fe.

Water-rock interaction

Several hypotheses have been tested for possible water-rock interaction simulations. Firstly, the McArthur-type brine has been interacted with a "typical" unaltered siltstone of the Barney Creek Formation. The assumed mineralogy of the Barney Creek Formation was as follows: 23% quartz; 36% K-feldspar; 2.7% albite; 6.1% muscovite; 30.7% dolomite and 0.9% pyrite. Water-rock interaction was predicted to precipitate a proximal chalcopyrite-rich silica-dolomite zone (quartz-dolomite-muscovite-chalcopyrite), an intermediate barren pyrite-siderite zone (+ quartz, muscovite and dolomite) and a distal Pb-Zn zone associated with a complicated gangue assemblage (galena, sphalerite, chlorite, hematite, dolomite, quartz, muscovite, albite, K-feldspar; Fig. 12c).

A second simulation was undertaken using an almost identical rock composition, with the exception of adding 0.5% graphite (an analogue for organic matter) at the expense of 0.5% of the dolomite. The results, shown in Figure 12d, are similar to those predicted from the first WRI simulation. However, the presence of graphite as a reductant has forced sulfides to saturate earlier in the paragenetic sequence. The proximal chalcopyrite-rich silica-dolomite is predicted to also contain pyrite (quartz-dolomite-muscovite-chalcopyrite-pyrite. The intermediate pyrite-siderite zone (+ quartz, muscovite and dolomite) now also contains high grade galena plus graphite. The distal Zn-rich zone contains less galena, but base metals are still predicted to be associated with a complicated gangue assemblage (sphalerite, chlorite, galena, graphite, dolomite, quartz, muscovite, K-feldspar)

Whereas both water-rock interaction (WRI) simulations have predicted zoned sulfide deposition,

Table 1: Composition of the McArthur-type brine used in numerical simulations of ore deposition.

Trace element	ppm	% Saturation	Mineral
pH	4.5		
Salinity	25.0 wt %		
?S	0.001		
log $f_{(O2)}$	-43.0		
H^+	183.7		
H_2O	1 kg		
Cl^-	152009.1		
SO_4^{2-}	70.66		
HCO_3^-	11493.2		
HS^-	0.000119		
$SiO_{2\,(aq)}$	85.27	100	Quartz
Al^{3+}	0.00167	100	Muscovite
Ca^{2+}	9051.1		
Mg^{2+}	3709.7	100	Dolomite
Fe^{2+}	1467.5	100	Siderite
K^+	13138.9		
Na^+	71919.2		*<charge balance>*
Mn^{2+}	302.1	10	Rhodochrosite
Zn^{2+}	212..2	1	Sphalerite
Cu^+	1.48	10	Chalcocite
Pb^{2+}	198.7	5	Galena
Ag^+	0.072	1	Acanthite
$AuCl_2^-$	0.0000008	90	Gold
Sr^{2+}	75.78	10	Strontiatite
Ba^{2+}	9.678	10	Barite
F^-	0.106	1	Fluorite
$Sb(OH)_3$	0.369	1	Polybasite

the problem encountered when simulating WRI using CHILLER is that complicated mineralogies are typically predicted, which is not consistent with the observed mineralogies. Consequently, it was decided to undertake four additional WRI simulations, targeting the most likely reactive components of the Barney Creek Formation: pyrite, carbonaceous matter (graphite) and dolomite. These results are illustrated in Figure 13. Surprisingly, interaction with mono-minerallic assemblages, or with simple mixtures of pyrite, graphite and dolomite, is not particularly effective at forcing base metal precipitation from the McArthur-type brine. Minor chalcopyrite and galena are predicted to be deposited via these scenarios, although in each case the water rapidly equilibrates with the "rock", and no further mineralogical changes are predicted. Sphalerite was not predicted to be deposited in any of the four cases illustrated in Figure 13. There is a narrow zone predicted to consist of greater than 50% galena in Figures 13c and d. Overall, these simulations are not consistent with the process of selective replacement of one or more solid phases in the BCF being effective at forcing ore deposition

Interaction with a gas reservoir

Given the problems with obtaining reasonable mineral parageneses from water-rock interaction simulations, a series of simulations have been undertaken to test the potential of gas reservoirs as trap sites for McArthur-type brines (Fig. 14). These simulations are intended to illustrate the reactive capacity of water-rock-gas interaction as a viable depositional process in subsurface diagenetic/epigenetic environments.

The results of reacting the McArthur-type brine with H_2S gas are illustrated in Figure 14a. H_2S gas is potentially a highly reactive trap for base metals transported in oxidised brines, and could be the most important reactive component of a gas reservoir from a mineralisation perspective. However, the results illustrated in Figure 14a show that while massive pyrite (+ minor chalcopyrite, covellite and stibnite) are predicted to precipitate during brine-gas interaction, sphalerite and galena failed to precipitate. This is because the condensation of gases into an aqueous phase can lead to extreme acidification of the water (note the pH decrease from 4.5 to 1.7; Fig. 14a). Consequently, the effect of increasing $H_2S_{(aq)}$ concentrations, which promotes galena and sphalerite deposition, is outstripped by acidification, which promotes base metal dissolution. It is interesting to note that with continued reaction progress, native sulfur eventually saturates via brine-gas interaction (this is true for most of the simulations illustrated in Fig. 14). Native sulfur has been reported from the ore horizons at HYC (Hinman, 1998).

Given the problems associated with acidification, a second scenario was developed whereby in addition to H_2S gas, a pH buffer (dolomite) was reacted with the McArthur-type brine to stabilise the pH of the solution. These simulations could be conceived as interaction of brine with gas in a porous, reactive (dolomite-bearing) media. Two simulations were attempted, a 90/10 H_2S gas/dolomite mixture (Fig. 14b) and a 50/50 H_2S gas/dolomite mixture (Fig. 14c). In the first case, the preponderance of gas over dolomite causes an initial pH decrease from 4.5 to 2.6. This is accompanied by the deposition of massive pyrite, plus chalcopyrite, galena and graphite (Fig. 14b). The pH of the solution then increases back to 4.8, and as dolomite saturation is approached, essentially all of the sphalerite in solution is predicted to precipitate over a narrow titration increment, together with galena and bournonite. Continued water-rock-gas interaction eventually leads to the deposition of native sulfur and alabandite. Given the narrow windows of metal deposition, this is predicted to be an excellent depositional mechanism for a zoned pyritic orebody that contains proximal pyrite-chalcopyrite and distal pyrite-sphalerite-galena-graphite. For the case of reaction of the McArthur-type brine with a 50/50 mixture of $H_2S_{(g)}$ and dolomite, similar mineralogies are predicted (Figure 14c). However, the initial pH decrease does not occur, and pH values remain between 4.5 and 4.8 throughout the simulation.

Given that by itself, H_2S gas is a poor analogue for natural gas, additional simulations have been attempted using other reactive components that may be present in a gas reservoir. Figure 14d illustrates the reaction path for interaction of the McArthur-type brine with equal proportions of $H_2S_{(g)}$, $CH_{4\,(g)}$ and dolomite. Similar results are predicted as for the simulations in Figures 14b and c, although graphite is a more significant component of the precipitated

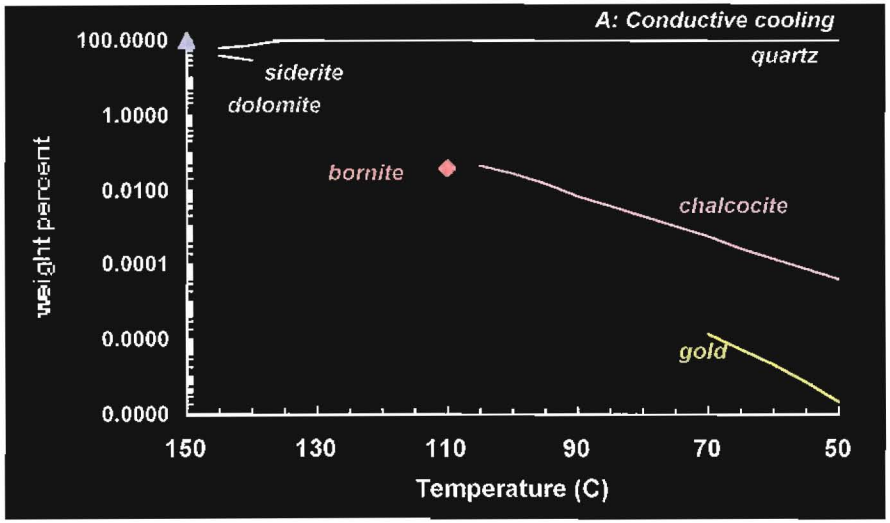

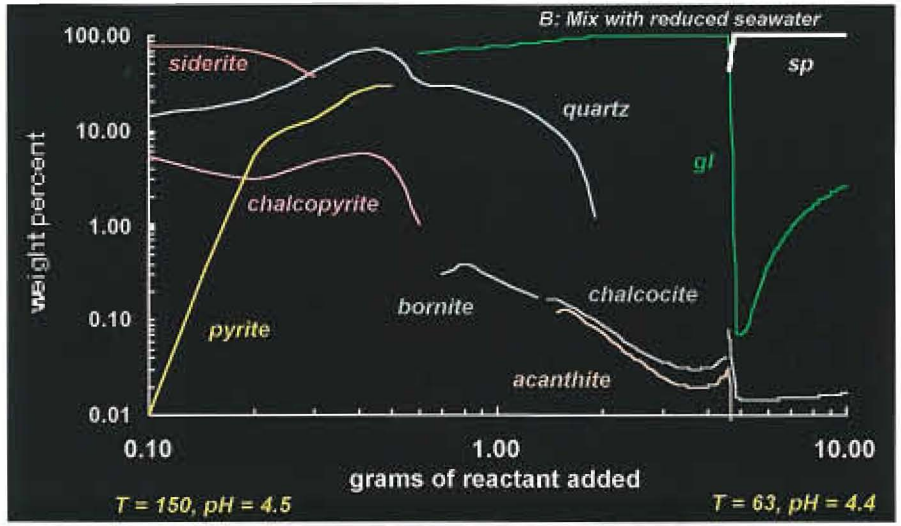

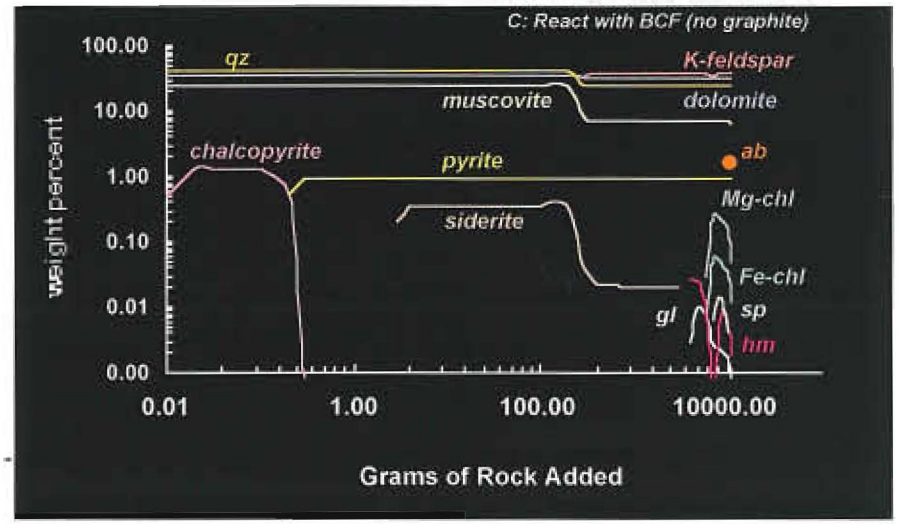

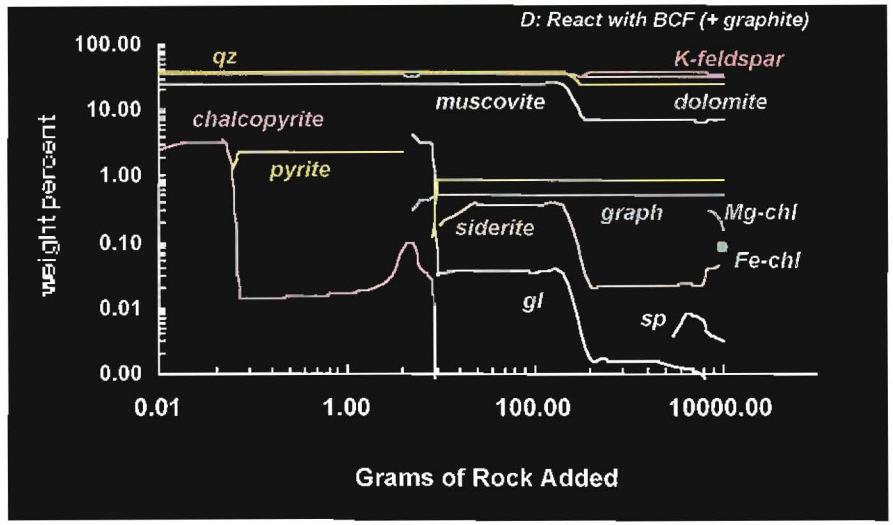

Figure 12: Predicted sequence of mineral deposition for numerical simulations involving the McArthur-type brine listed in Table 1. Acronyms: sp – sphalerite; gl – galena; qz – quartz; ab – albite; Mg-chl – Mg-chlorite; Fe-chl – Fe-chlorite; hm – hematite. (a) Conductive cooling from 150°C to 50°C in 5°C increments. (b) Mixing with H2S-bearing reduced seawater. (c) Interaction with 'unaltered', non-carbonaceous Barney Creek Formation: 23% quartz; 36% K-feldspar; 2.7% albite; 6.1% muscovite; 30.7% dolomite and 0.9% pyrite. (d) Interaction with 'unaltered', carbonaceous Barney Creek Formation: 23% quartz; 36% K-feldspar; 2.7% albite; 6.1% muscovite; 30.2% dolomite, 0.5% graphite and 0.9% pyrite.

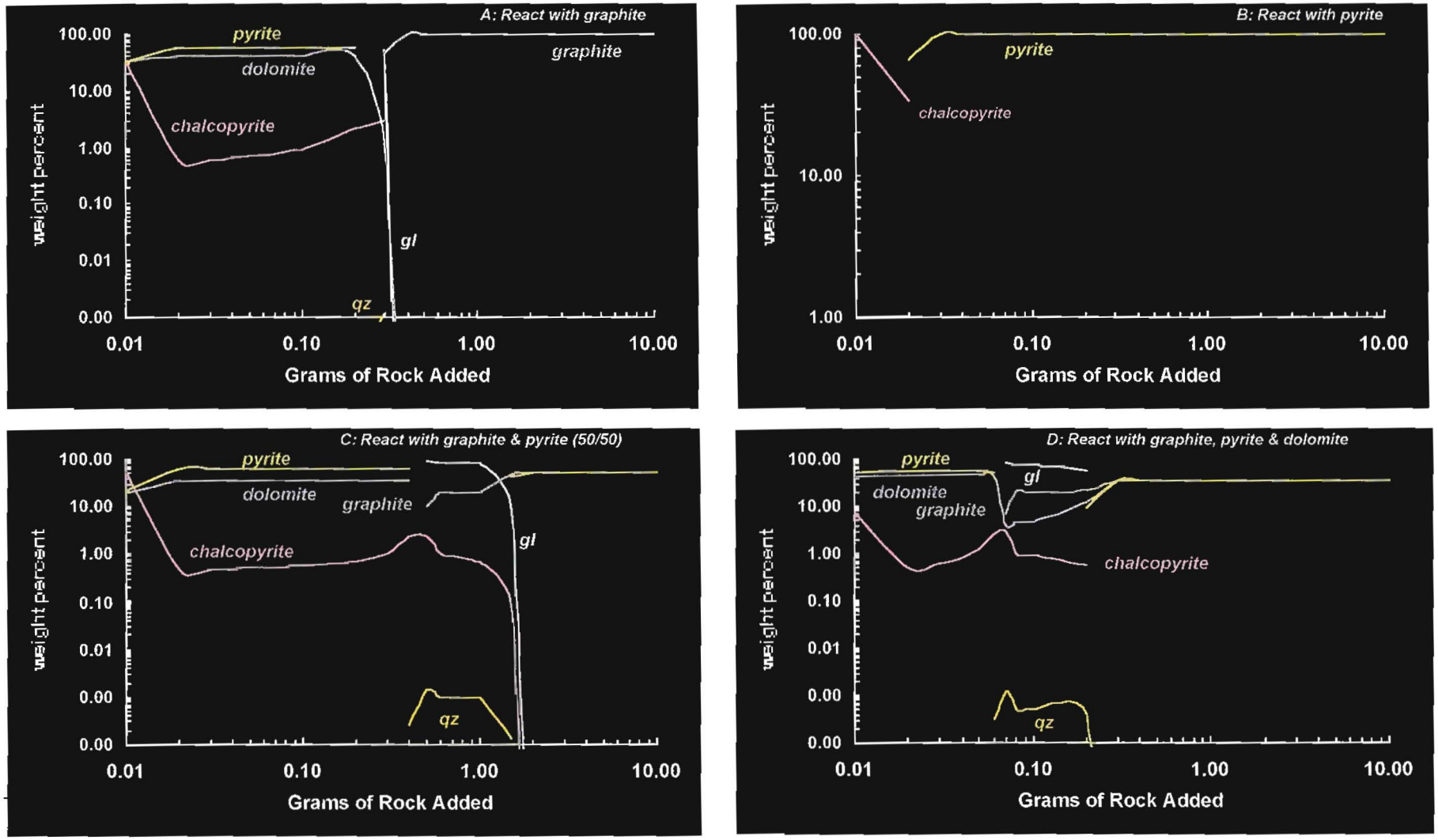

Figure 13: Predicted sequence of mineral deposition for numerical simulations involving the McArthur-type brine listed in Table 1. Acronyms: gl – galena; qz – quartz. (a) Interaction with graphite. (b) Interaction with pyrite. (c) Interaction with 50% graphite and 50% pyrite. (d) Interaction with 33% graphite, 33% dolomite and 33% pyrite.

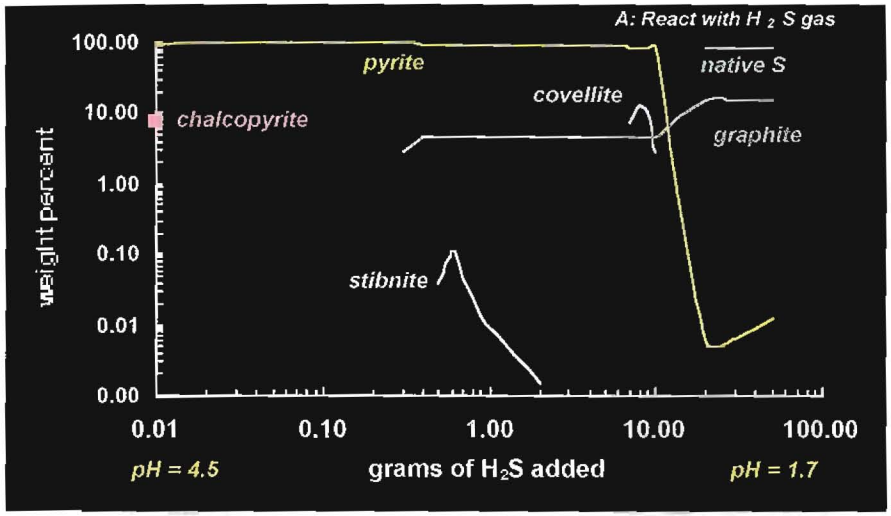

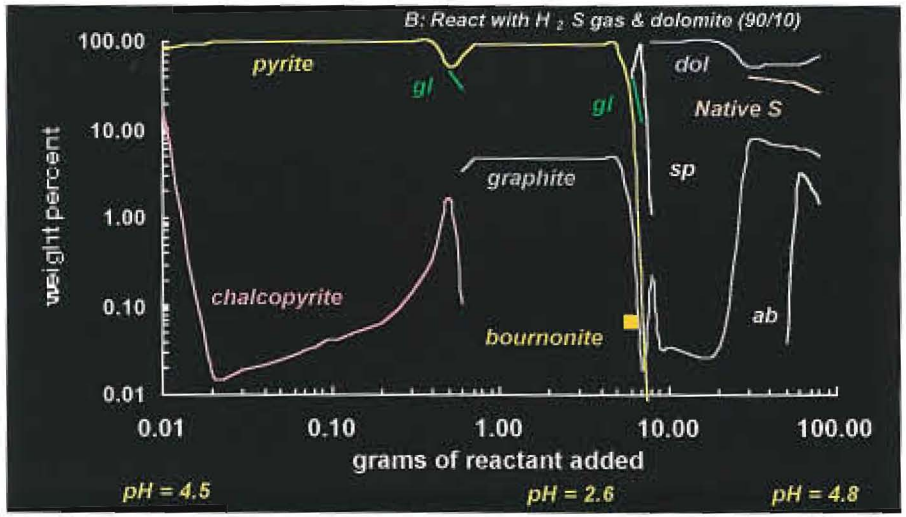

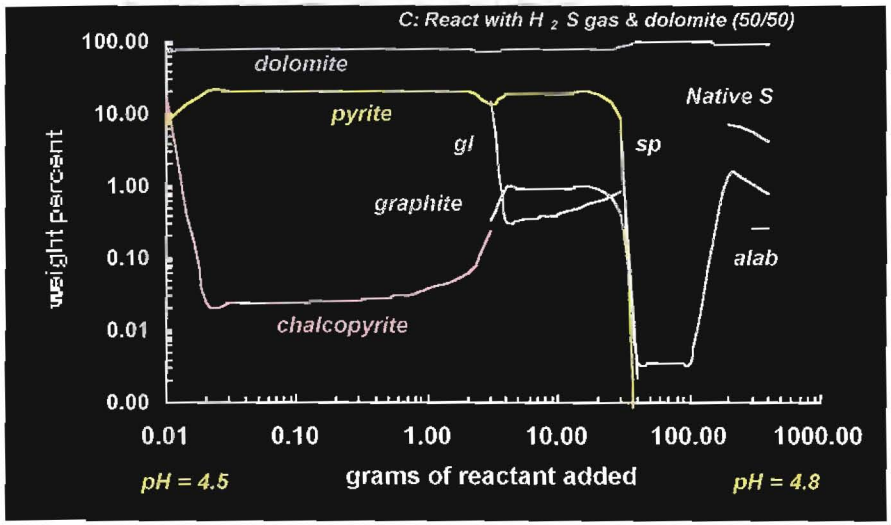

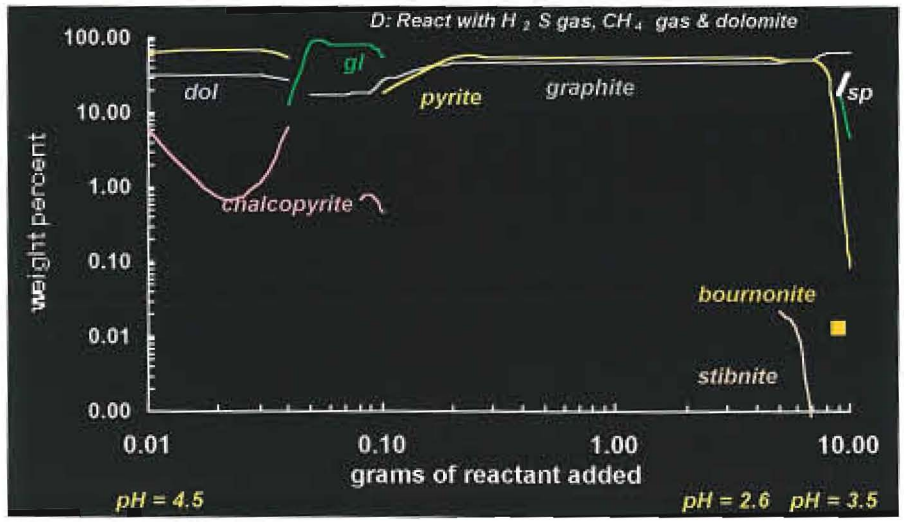

Figure 14: Predicted sequence of mineral deposition for numerical simulations involving the McArthur-type brine listed in Table 1. Acronyms: native S – native sulfur; dol – dolomite; alab – alabandite; sp – sphalerite; gl – galena. (a) react with H_2S gas. (b) react with 90% H_2S gas and 10% dolomite. (c) react with 50% H_2S gas and 50% dolomite. (d) react with 33% H_2S gas, 33% CH_4 gas and 33% dolomite.

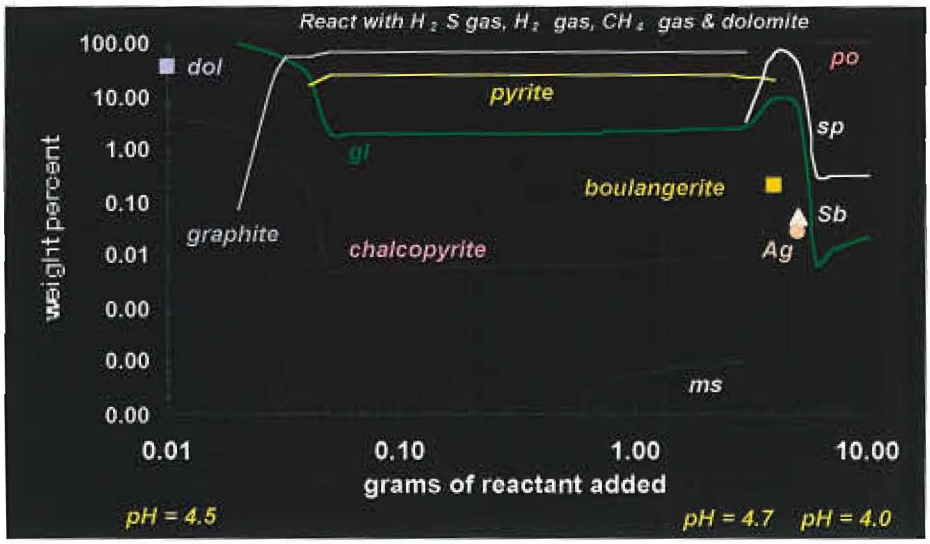

Figure 15: Predicted sequence of mineral deposition for a numerical simulation of interaction of the McArthur-type brine listed in Table 1 with 25% H_2S gas, 25% H_2 gas, 25% CH_4 gas and 25% dolomite. Acronyms: po – pyrrhotite; sp – sphalerite; gl – galena; Sb – antimony; Ag – silver ; ms – muscovite; dol - dolomite.

material, as it is acting as a sink for methane. Figure 15 illustrates how interaction of the brine with equal proportions of $H_2S_{(g)}$, $H_{2\,(g)}$, $CH_{4\,(g)}$ and dolomite still results in effective base metal deposition, although galena now precipitates with chalcopyrite, and graphite is predicted to be precipitated as the most abundant phase through much of the simulation. Pyrrhotite is predicted to precipitate in the later stages of the simulation, due to the incorporation of the highly effective reductant, $H_{2\,(g)}$. Interestingly, pH initially increases in this simulation, and then decreases, in contrast to the previous simulations of water-rock-gas interaction.

Overall, simulations of brine-dolomite-gas interaction show that this process could be highly effective at producing ore grade sulfide mineralisation, provided that pH buffering occurs (possibly via dolomite dissolution). These results indicate that brine migration to the base of a gas reservoir could result in the deposition of ore grade sulfide mineralisation at the gas/brine interface. The mineralisation would either occlude porosity, or there could be scope for replacement of reactive porous media by sulfide mineralisation. Such processes should produce discordant or stratabound Pb-Zn mineralisation.

Conclusions

The results of our chemical modelling have extended the results of Cooke et al. (1998). Economic copper mineralisation is predicted to be more likely to occur in association with McArthur-type sediment hosted Pb-Zn deposits. Iron solubilities are marginally affected by the redox state of the mineralising brines, and strongly affected by acidity. Consequently, Selwyn-type and acidic McArthur-type brines can carry Fe together with Pb-Zn in solution. However, if McArthur-type brines have near-neutral to alkaline pH values, then Pb-Zn may be transported in high concentrations, whereas Fe is insoluble and will not be readily mobilised. To accommodate coupled Pb-Zn, Fe and possibly Cu transport, McArthur type brines need to have acidic, oxidised compositions near the pyrite-hematite redox buffer (Fig. 10).

Positive europium anomalies have been considered by previous workers to be a fingerprint of reduced hydrothermal processes, and have been touted for their potential as an exploration vector. Our modelling has shown that europium is transported in the +2 valence state in both Selwyn- and McArthur-type brines, and as such has no potential to discriminate between the two brine types. Positive europium anomalies are not a good indicator of oxidation state in the hydrothermal environment, but may still discriminate hydrothermal activity from sedimentary and diagenetic processes. Elevated manganese may indicate the passage of acidic mineralising brines, or it may be a product of background sedimentary processes. It is not a discriminator for McArthur and Selwyn-type brines.

With regards to depositional processes, temperature decrease and dilution (fluid mixing), addition of H_2S and pH increase can all be important for deposition of Zn and Pb from reduced (Selwyn-type) brines. In contrast, reduction and/or addition of H_2S (via fluid mixing, sour gas or possibly via interaction with earlier-formed pyrite) will be the important processes for sphalerite and galena deposition from oxidised (McArthur-type) brines. Numerical simulations have demonstrated the effectiveness of mixing with reduced seawater (eg. Fig. 3) and interaction with gas reservoirs for extracting Pb-Zn massive sulfide mineralisation from McArthur-type brines. Simulations of interaction of a McArthur-type brine with the Barney Creek Formation produces more complicated gangue assemblages than observed in ore horizons at HYC, suggesting that wallrock replacement is not the principal depositional mechanism for Pb-Zn mineralisation. Cooling of McArthur-type brines produces barren quartz veins, which may be the typical mineral assemblage expected in faults that have acted as conduits for McArthur-type brines.

From an exploration perspective, oxidised sedimentary brines are likely to produce large tonnage Zn-Pb-Ag deposits that have siderite or ankerite alteration halos and commonly lack barite lenses and vent complexes. They may also have anomalous or ore-grade copper nearby. In contrast, Selwyn-type deposits form in reduced siliciclastic and shale-dominated basins are more likely to be lower tonnage, and to contain barite, vent complexes and minor gold or tin credits. Ore-grade copper is unlikely to be associated with Selwyn-type deposits.

Consideration should be given to exploring for (1) Selwyn-type Pb-Zn deposits in reduced sedimentary basins such as within the Lachlan Fold Belt, and (2) sediment-hosted copper in the northern Australian zinc belt.

The spectrum of s ediment-hosted Pb-Zn deposits

From a chemical perspective, it is feasible that a continuum of sediment-hosted Pb-Zn and Cu deposit styles can occur in sedimentary basins. Brines may either be oxidised (McArthur-type) or reduced (Selwyn-type). Their compositions will ultimately depend on the nature of the basinal fill, the role of volcanism/plutonism, and (in some cases) a contribution of basement-derived waters. Salinities may be near-seawater or hypersaline, depending on the presence or absence of evaporites. Temperatures of ore-forming brines are likely to be inversely related to salinities, with elevated temperatures required to accommodate base metal transport in lower salinity waters.

The so-called typical "style" of Pb-Zn mineralisation that occurs in a given sedimentary basin is ultimately the result of a conjunction of several factors. This may include tectonism, volcanism, style of basin fill (e.g., porosity and/or composition), the local marine/lacustrine environment (open vs closed basin), heat flow and biological activity. It is difficult to be predictive about whether 'SEDEX', MVT or Irish-type Pb-Zn mineralisation will occur in a given basin. Consequently the only real guide the explorationist has as to which is likely to be prevalent in a given basin is the presence of other known deposits. This may, of course, lead to erroneous conclusions as to the true economic potential of that basin.

The chemical composition and intensive parameters of brines that "Sedex", Irish-type and MVT deposits are sufficiently similar to allow all of these styles of mineralisation to occur in a given basin. The types of basin fill controls the redox state of the brine (McArthur-type vs Selwyn-type). The style of mineral occurrence will be controlled by the physical and chemical nature of the trap. A truly pro-active exploration program should allow for the possibility that all of these conventional "styles" may occur (even if only one of them is likely to be an economic proposition). Furthermore, from a chemical perspective, there is potential for McArthur-type brines to form Cu-rich MVT, Irish-type and/or SEDEX-style mineralisation, even though these are yet to be identified in the geologic record.

Figure 10 schematically illustrates a potential evolutionary trajectory (D-E) of a McArthur-type brine derived from hematitic, clay-bearing sandstones in the lower Tawallah Group, and one potential evolutionary trajectory for this brine as it migrates upwards through the basin. It is eventually reduced by interaction with pyritic and carbonaceous sediments, and neutralised by interaction with carbonates and feldspars. The "superbrine" represented by point D has the potential to carry economic Cu, Pb, Zn, Ag, and possibly Au and/or U. As it evolves along the illustrated reaction path towards point E, it would first precipitate U, then Au, Cu and finally Pb-Zn-Ag mineralisation, possibly over a lateral flow path of 10's to 100's of kilometres. Although there is no proof that these varied styles of mineralisation in the McArthur basin are genetically related, a link is feasible from a chemical point of view. Note, however, that the point here is not to try to genetically link all mineralisation styles to a common (superbrine) origin. It is to highlight that there is potential for two apparently quite different mineralisation styles (eg. sediment-hosted Cu and Pb-Zn deposits) to be related, and potentially to occur in the same general area or basin. A Pb-Zn mineralising brine may have also been a Cu-mineralising brine further back along its reaction path..

Conventional wisdom may be holding back the full exploration potential of the northern Australian zinc belt. A less conservative view of the mineralising capacity of sedimentary brines, coupled with a careful sedimentological and structural analysis of the basinal environment, and consideration of any related geochemical anomalism, could lead to the discovery of new or unconventional "styles" of Pb-Zn and/or Cu mineralisation.

References

Alderton, D. H. M., Pearce, J. A., and Potts, P. J., 1980, Rare earth element mobility during granite alteration: evidence from southeast England: Earth and Planetary Science Letters, v. 49, p. 149-165.

Baker, J. H., and Hellingwerf, R. H., 1988, Rare earth element geochemistry of W-Mo-(Au) skarns and granites from western Berslagen, central Sweden: Mineralogy and Petrology, v. 39, p. 231-244.

Banks, D. A., Yardley, B. W. D., Campbell, A. R., and Jarvis, K. E., 1994, REE composition of an aqueous magmatic fluid: A fluid inclusion study from the Capitan pluton, New Mexico: Chemical Geology, v. 113, p. 259-272.

Bau, M., 1991, Rare-earth element mobility during hydrothermal and metamorphic fluid-rock interaction and the significance of the oxidation state of europium: Chemical Geology, v. 93, p. 219-230.

Bierlein, F. P., 1995, Rare-earth element geochemistry of clastic and chemical metasedimentary rocks associated with hydrothermal sulphide mineralisation in the Olary Block, South Australia: Chemical Geology, v. 122, p. 77-98.

Bingen, B., Demaiffe, D., and Hertogen, J., 1996, Redistribution of rare earth elements, thorium, uranium over accessory minerals in the course of amphibolite to granulite facies metamorphism: The role of apatite and monazite in orthogneisses from southwestern Norway: Geochimica et Cosmochimica Acta, v. 60, p. 1341-1354.

Blundy, J. D., and Wood, B. J., 1991, Crystal-chemical controls on the partitioning of Sr and Ba between plagioclase feldspar, silicate melts, and hydrothermal solutions: Geochimica et Cosmochimica Acta, v. 55, p. 193-209.

Calvert, S.E., and Pedersen, T.F., 1996. Sedimentary geochemistry of manganese: implications for the environment of formation of manganiferous black shales. Economic Geology, 91, 36-47.

Campbell, I. H., Lesher, C. M., Coad, P., Franklin, J. M., Gorton, M. P., and Thurston, P. C., 1984, Rare-earth element mobility in alteration pipes below massive Cu-Zn-sulfide deposits: Chemical Geology, v. 45, p. 181-202.

Cantrell, K. J., and Byrne, R. H., 1987, Rare earth complexation by carbonate and oxalate ions: Geochimica et Cosmochimica Acta, v. 51, p. 597-605.

Cooke, D.R., 1993. Transport and deposition of base metals from high temperature (250°C) sedimentary brines. AMIRA/ ARC Project P.384, Report No. 4, 111-129.

Cooke, D.R., Bull, S.W., Large, R.R., and McGoldrick, P.J.1998. The importance of oxidised brines for the formation of Australian Proterozoic Stratiform Sediment Hosted Pb - Zn (SEDEX) deposits. Economic Geology (submitted).

Drever, J.I., 1982. The geochemistry of natural waters. Prentice-Hall, N.J.,p. 234.

Eldridge et al., 1993. Sulphur isotope variability in sediment-hosted massive sulphide deposits as determined using the ion microprobe SHRIMP II: a study of the HYC deposit at McArthur River, NT., Australia. Econ. Geol., 88: 1-26.

Goodfellow, W.D., Lydon, J.W., and Turner, R.J.W., 1993. Geology and genesis of stratiform sediment-hosted (SEDEX) Zn-Pb-Ag sulphide deposits. *in* R.V. Kirkham, W.D. Sinclair, R.I. Thorpe and J.M. Duke. Mineral Deposit Modelling. Geol. Soc. Can., Spec. Pub. 40., 201-252.

Haas, J. R., Shock, E. L., and Sassani, D. C., 1995, Rare earth elements in hydrothermal systems: Estimates of standard partial molal thermodynamic properties of aqueous complexes of the rare earth elements at high pressures and temperatures: Geochimica et Cosmochimica Acta, v. 59, p. 4329-4350.

Haskin, L. A., 1984, Petrogenetic Modelling - Use of rare earth elements: in P. Henderson (ed.), Rare Earth Element Geochemistry. Developments in Geochemistry: Elsevier, Amsterdam, v. 2, p. 115-152.

Hinman, M, 1998. Speculations on syn-diagenetic processes of sulphate reduction at the HYC Pb-Zn deposit, NT. Geol. Soc. Aust. Abst. 49, pp. 212.

Hinman, M, Wall., V., and Heinrich, C., 1994. The interplay between sedimentation, deformation and hydrothermal activity at the McArthur Pb-Zn(-Cu) deposit. Geol. Soc. Aust. Abst. 37, pp. 176-177.

Johnson, J.W., Oelkers, E.H. and Helgeson, H.C., 1991. SUPCRT92: A software package for calculating the standard molal thermodynamic properties of minerals, gases, aqueous species and reactions from 1 to 5000 bars and 0° to 1000°C. 50 p. Computers & Geoscience.

Klinkhammer, G. P., Elderfield, H., Edmond, J. M., and Mitra, A., 1994, Geochemical implications of rare earth element patterns in hydrothermal fluids from mid-ocean ridges: Geochimica et Cosmochimica Acta, v. 58, p. 5105-5113.

Lapointe, B., and Chown, E. H., 1993, Gold-bearing iron-formation in a granulite terrane of the Canadian Shield: a possible deep-level expression of an Archean gold-mineralizing system: Mineralium Deposita, v. 28, p. 191-197.

Large, R.R., Bull, S.W., Cooke, D.R., and McGoldrick, P.J., 1998. Review of genetic models at HYC: constraints from new sedimentology, alteration halo studies and fluid chemical modelling. Economic Geology, v93, no8 (in press).

Lee, J. H., and Byrne, R. H., 1992, Examination of comparative rare earth element complexation behavior using linear free-energy relationships: Geochimica et Cosmochimica Acta, v. 56, p. 1127-1137.

Lee, J. H., and Byrne, R. H., 1993, Complexation of trivalent rare earth elements (Ce, Eu, Gd, Tb, Yb) by carbonate ions: Geochimica et Cosmochimica Acta, v. 57, p. 295-302.

Lesher, C. M., Gibson, H. L., and Campbell, I. H., 1986, Composition-volume changes during hydrothermal alteration of andesite at Buttercup Hill, Noranda District, Quebec: Geochimica et Cosmochimica Acta, v. 50, p. 2693-2705.

Lewis, A. J., Palmer, M. R., Sturchio, N. C., and Kemp, A. J., 1997, The rare earth element geochemistry of acid-sulphate and acid-sulphate-chloride geothermal systems from Yellowstone National Park, Wyoming, USA: Geochimica et Cosmochimica Acta, v. 61, p. 695-706.

Lottermoser, B. G., 1989, Rare earth element study of exhalites within the Willyama Supergroup, Broken Hill Block, Australia: Mineralium Deposita, v. 24, p. 92-99.

Lottermoser, B. G., 1990, Rare-earth element and heavy-metal behavior associated with the epithermal gold deposit on Lihir Island, Papua New Guinea: Journal of Volcanological and Geothermal Research, v. 40, p. 269-289.

Lottermoser, B. G., 1992, Rare earth elements and hydrothermal ore formation processes: Ore Geology Reviews, v. 7, p. 25-41.

MacLean, W. H., 1988, Rare earth element mobility at constant inter-REE ratios in the alteration zone at the Phelps Dodge massive sulphide deposit, Matagami, Quebec: Mineralium Deposita, v. 23, p. 231-238.

McDaniel, D. K., Hemming, S. R., McLennan, S. M., and Hanson, G. N., 1994, Resetting of neodymium isotopes and redistribution of REEs during sedimentary processes: The Early Proterozoic Chelmsford Formation, Sudbury Basin, Ontario, Canada: Geochimica et Cosmochimica Acta, v. 58, p. 931-941.

McGoldrick, P.J., Dunster, J., and Aheimer, M., 1995. The Lady Loretta zinc-lead-silver deposit: primary dispersion halos, sedimentology, ore textures, stable isotopes, and metal distributions - towards a genetic model. AMIRA/ARC p.384, Final Report, 409-446.

McKay, G. A., 1989, Partitioning of rare earth elements between major silicate minerals and basaltic melts: in B.R. Lipin

and G.A. McKay (eds.), Geochemistry and Mineralogy of Rare Earth Elements, Mineralogical Society of America, Reviews in Mineralogy: , v. 21, p. 45-74.

McLennan, S. M., and Taylor, S. R., 1991, Sedimentary rocks and crustal evolution: tectonic setting and secular trends: Journal of Geology, v. 99, p. 1-21.

Michard, A., 1989, Rare earth element systematics in hydrothermal fluids: Geochimica et Cosmochimica Acta, v. 53, p. 745-750.

Michard, A., and Albarède, F., 1986, The REE content of some hydrothermal fluids: Chemical Geology, v. 55, p. 51-60.

Morgan, J. W., and Wandless, G. A., 1980, Rare earth element distribution in some hydrothermal minerals: evidence for crystallographic control: Geochimica et Cosmochimica Acta, v. 44, p. 973-980.

Ohmoto, H., and Lasaga, A., 1982, Kinetics of reaction between aqueous sulfates and sulfides in hydrothermal systems. Geochim. Et. Cosmochim. Acta, 46, 1727-1745.

Ohmoto, H., Mizukami, M., Drummond, S.E., Eldridge, C.S. Pisutha-Arnold, V. and Lenagh, T.C., 1983, Chemical processes of Kuroko formation *in* Ohmoto, H. and Skinner, B.J. eds., Kuroko and Related Volcanogenetic Massive Sulphide Deposits. Econ. Geol., Mon. 5: 570–604.

Parr, J. M., 1992, Rare-earth element distribution in exhalites associated with Broken Hill-type mineralisation at the Pinnacles deposit, New South Wales, Australia: Chemical Geology, v. 100, p. 73-91.

Quinby-Hunt, M.S., and Wilde, P., 1993. Thermodynamic zonation in the black shale facies based on iron-manganese-vanadium content. Chemical Geology, 113, 297-317.

Quinby-Hunt, M.S., and Wilde, P., 1996. Chemical depositional environments of calcic marine black shales. Economic Geology, 91, 4-13.

Reed, M.H., 1982. Calculation of multicomponent chemical equilibria and reaction processes in systems involving minerals, gases and an aqueous phase. Geochim. Cosmochim. Acta, 46: 513-528.

Schandl, E. S., and Gorton, M. P., 1991, Postore mobilization of rare earth elements at Kidd Creek and other Archean massive sulfide deposits: Economic Geology, v. 86, p. 1546-1553.

Spycher, N.F., and Reed, M.H., 1990. Users guide for the SOLTHERM database. University of Oregon (unpublished)

Stumm, W., and Morgan, 1996. Aquatic chemistry : chemical equilibria and rates in natural waters. 3rd edition, John Wiley and Sons, New York

Sverjensky, D. A., 1984, Europium redox equilibria in aqueous solution: Earth and Planetary Science Letters, v. 67, p. 70-78.

Turner, D. and Cooke, D.R., 1998. Users guide to CHILLPLUS. University of Tasmania (unpublished)

Vander Auwera, J., and Andre, L., 1991, Trace elements (REE) and isotopes (O, C, Sr) to characterize the metasomatic fluid sources: evidence from the skarn deposit (Fe, W, Cu) of Traversella (Ivrea, Italy): Contributions to Mineralogy and Petrology, v. 106, p. 325-339.

Whitford, D. J., Korsch, M. J., Porritt, P. M., and Craven, S. J., 1988, Rare earth element mobility around the volcanogenic polymetallic massive sulfide deposit at Que River, Tasmania, Australia: Chemical Geology, v. 68, p. 105-119.

Wood, S. A., and Williams-Jones, A. E., 1994, The aqueous geochemistry of the rare-earth elements and yttrium 4. Monazite solubility and REE mobility in exhalative massive sulfide-depositing environments: Chemical Geology, v. 115, p. 47-60.